Variable speed limits and signalized access control in an urban road network for improved environmental sustainability

Bassel Othman

THÈSE

Pour obtenir le grade de

DOCTEUR DE L'UNIVERSITÉ GRENOBLE ALPES

Spécialité : AUTOMATIQUE - PRODUCTIQUE

Arrêté ministériel : 25 mai 2016

Présentée par

Bassel OTHMAN

Thèse dirigée par **Carlos CANUDAS DE WIT**,Directeur de Recherche, Université Grenoble Alpes

préparée au sein du **Laboratoire Grenoble Images Parole Signal Automatique**
dans **l'École Doctorale Electronique, Electrotechnique, Automatique, Traitement du Signal (EEATS)**

Limitations de vitesse variables et contrôle d'accès dans un réseau routier urbain pour une meilleure durabilité environnementale

Variable speed limits and signalized access control in an urban road network for improved environmental sustainability

Thèse soutenue publiquement le **7 octobre 2021**,
devant le jury composé de :

Monsieur Olivier SENAME
PROFESSEUR DES UNIVERSITES, GRENOBLE INP, Président
Madame Simona SACONE
PROFESSEUR ASSOCIE, Università Degli Studi di Genova, Rapporteure
Monsieur Dan WORK
PROFESSEUR ASSOCIE, Vanderbilt University, Rapporteur
Monsieur Christos CASSANDRAS
PROFESSEUR, Boston University, Examinateur
Monsieur Bart DE SCHUTTER
PROFESSEUR, DELFT University of Technology, Examinateur
Madame Maria Laura DELLE MONACHE
PROFESSEUR ASSISTANT, University of California, Berkeley, Examinatrice

Remerciements

Je tiens tout d'abord à remercier chaleureusement mes encadrants de thèse et notamment mon directeur Carlos Canudas-de-Wit pour son expertise technique qui a grandement contribué à définir les pistes de résolution des problèmes, et pour le partage de son expérience dans la gestion de projet de recherche. Un grand merci à Domenico Di Domenico pour son suivi très régulier, la motivation qu'il m'a donné, et les efforts fournis pour améliorer mes travaux et la rédaction des papiers. Je tiens également à remercier Giovanni De Nunzio pour sa disponibilité et le temps passé sur ce projet. Ses conseils ont toujours été bienveillants et d'une très grande utilité. Merci pour ces nombreuses discussions qui m'ont fait développer mon esprit critique et m'ont poussé à perpétuellement chercher à améliorer mes travaux et à imaginer des pistes de recherche innovantes.

Thanks to my reviewers Simona Sacone and Dan Work, and to my examiners Olivier Sename, Christos Cassandras, Bart De Schutter, and Maria Laura Delle Monache. The exchanges we had before and during the defense were very enriching.

Merci à Yann Creff et au reste de l'équipe Contrôle, Signal et Système d'IFP Energies nouvelles pour leur bonne humeur au quotidien. En particulier, je remercie mes collègues de bureau, par ordre d'arrivée : Johan, David, Lauriane, Adam et Eduardo.

Je tiens également à remercier l'équipe NECS, commune au GIPSA-lab et à l'INRIA, pour leur accueil pendant une partie de ma thèse. Merci à Stéphane et Nicolas d'avoir partagé leur bureau avec moi pendant cette période. Un grand merci à Martin également de m'avoir épaulé dans cette tâche qui peut à première vue paraître insurmontable : le branchement de la salle de visio-conférence du GIPSA-lab le jour de ma soutenance.

Enfin, je souhaite remercier ma famille pour leur soutien quotidien et indéfectible : mes parents, mon frère et ma soeur. C'est en grande partie à vous que je dois la réussite de cette thèse. Merci également à tous mes amis, notamment Samir, Adrien, Victor, et Hugo pour vos encouragements et pour m'avoir changé les idées de mon sujet de thèse, bien que passionnant !

Résumé de la thèse

Cette thèse aborde le sujet de la gestion écologique du trafic urbain. L'objectif est de réduire la consommation d'énergie et les émissions de polluants, sans détériorer les performances du trafic. Les stratégies d'éco-gestion, fortement valorisées par le développement des véhicules connectés et autonomes, peuvent correspondre au contrôle des véhicules, ou à celui des infrastructures.

Le contrôle des véhicules comprend la planification de mouvement (ou eco-driving), d'itinéraire (ou eco-routing), ainsi que le contrôle coopératif. Plus le niveau de connectivité est élevé, plus les avantages environnementaux de ces algorithmes sont grands. De plus, les véhicules autonomes offrent de nouvelles perspectives en terme de coopération, en raison de leur commande plus précise. En pratique, cela correspond à des véhicules qui coordonnent leurs mouvements en communiquant entre eux et avec l'infrastructure.

Le contrôle des infrastructures correspond à la gestion dynamique d'actionneurs de régulation de flux tels que les limitations de vitesse et les feux de signalisation. Son objectif est de réduire les émissions et consommation totales en influant sur les flux de véhicule. En pratique, de telles approches consistent à collecter les données des véhicules circulant dans le réseau routier (densité de véhicules, flux, vitesse moyenne). Ensuite, des algorithmes sont utilisés pour prédire et optimiser l'état du trafic. Dans ce travail, nous avons choisi de nous concentrer sur le contrôle des infrastructures.

Les contributions de cette thèse à la gestion écologique du trafic peuvent être résumées comme suit.

Dans un premier temps, un modèle de trafic macroscopique adapté au milieu urbain est proposé. Il comprend une méthodologie pour traiter les intersections avec des feux de signalisation. Pour estimer la consommation de carburant, ce modèle de trafic est associé à un modèle macroscopique basé sur un réseau de neurones artificiels (ANN). Ce dernier est calibré à l'aide d'un modèle d'énergie physique microscopique et de données fournies par un simulateur de trafic paramétré avec des données urbaines de Floating Car Data (FCD). Les modèles macroscopiques sont préférés pour le contrôle à grande échelle car ils sont plus rapides lorsque le nombre de véhicules considérés est grand. Ils ont également l'avantage de considérer

l'efficacité énergétique globale, qui est la métrique d'intérêt pour les gestionnaires de réseaux routiers en matière d'éco-gestion du trafic.

Ensuite, des expériences sont menées afin d'évaluer la relation entre congestion et efficacité énergétique, essentiellement en régime permanent. L'impact des limitations de vitesse est analysé pour différents scénarios. Les limitations de vitesse impactent directement la consommation d'énergie et les émissions polluantes car elles affectent les accélérations et les vitesses moyennes sur le réseau.

Enfin, un contrôleur est paramétré afin de comparer l'impact du contrôle dynamique des limitations de vitesse avec le contrôle d'accès à une zone urbaine, à la fois dans une zone contrôlée mais aussi dans la zone périurbaine à sa frontière. Le système est simulé à l'aide du simulateur de trafic SUMO, et un modèle physique de consommation de carburant et d'émissions de NOx est utilisé. Les limitations de vitesse sont contrôlées en boucle fermée grâce à une approche de commande prédictive non linéaire (NMPC), dans laquelle l'évolution du trafic et la consommation de carburant sont prédites à l'aide de modèles macroscopiques. Les résultats révèlent que dans les phases transitoires entre différents niveaux de congestion, le contrôleur en boucle fermée est plus rapide pour décongestionner le réseau, de manière économe en énergie. Cela améliore la durabilité environnementale et les performances de trafic à la fois dans le réseau contrôlé, mais aussi au niveau de ses routes frontalières.

Preface

Abstract

The problem of urban traffic management for improved environmental sustainability is addressed. The objective is to reduce the energy consumption (electricity or fuel), as well as the emission of pollutants, without deteriorating the traffic performance. Traffic eco-management strategies, which are greatly enhanced by the development of connected and automated vehicles, can correspond either to the control of vehicles or infrastructures.

The vehicle-side control includes motion planning (or eco-driving), route planning (or eco-routing), as well as cooperative control designs. The higher the level of connectivity, the larger the environmental benefits of such algorithms. Additionally, autonomous vehicles open the door to vehicles cooperation because of their more precise positioning and control, i.e. vehicles that coordinate their movements by communicating within each others and with the infrastructure. This includes vehicle platooning, cooperative adaptive cruise control (CACC), lane changing and merging control, and cooperative intersection control.

The infrastructure-side control corresponds to the dynamic management of road-based flow regulation actuators such as speed limits and traffic light signals duty cycles and offsets. Its objective is to reduce the total pollutant emissions and energy consumption in the network by influencing the vehicular flow as a whole. In practice, such approaches consist in collecting data from vehicles traveling in the road network (vehicle density, traffic flow, average speed, etc.). Then, algorithms are used to predict and optimize the state of traffic. In this work, we choose to focus on the infrastructure-side control.

The contributions of this work to traffic ecological management may be summarized as follows.

Firstly, a formalization of a macroscopic traffic model adapted to the urban environment is proposed. It includes a methodology for treating intersections with traffic light signals. To estimate the fuel consumption, this traffic model is associated with a macroscopic model based on an artificial neural network (ANN). The latter is calibrated using a microscopic physical energy model and data provided

by a microscopic traffic simulator parameterized in order to be compliant with real-world urban Floating Car Data (FCD). Macroscopic models are preferred for large-scale control because they are much faster to compute when the number of vehicles is large. They also have the advantage of considering the overall energy efficiency, which is the metric of interest for road network managers when it comes to traffic eco-management.

Then, experiments are conducted in order to evaluate the relationship between congestion and vehicles' energy efficiency, especially at steady state. The impact of various speed limits are analyzed for different scenarios. Speed limits directly impact energy consumption and pollutant emissions as they affect the accelerations and average speeds through the network.

Finally, a control design comparing variable speed limits (VSL) and signalized access control is proposed for improved environmental sustainability and traffic performance both in a synthetic urban area and in the peri-urban area at its boundaries. The traffic system is modeled using the microscopic traffic simulator SUMO, and a physical fuel consumption and NOx emission model is used. Speed limits are controlled in closed loop through a nonlinear model predictive control (NMPC) approach, in which the traffic evolution and the fuel consumption are predicted with macroscopic models. The results reveal that in transient phases between different levels of congestion, the closed-loop controller is faster to decongest the network, in an energy-efficient way, resulting in an improvement of the environmental sustainability and the traffic performance both in the controlled network, and at its boundary roads.

Dissertation outline

1 Introduction

After a quick overview of the current situation regarding road traffic and its impact on the environment, this chapter mainly deals with a comprehensive state-of-the-art of the traffic eco-management strategies. It proposes a classification that distinguishes the single vehicles and the traffic vehicular flows approaches.

2 Models to simulate and predict traffic dynamics in an urban environment

This chapter reviews microscopic and macroscopic traffic models. Several microscopic car-following models are compared and calibrated using real-world Floating Car Data (FCD) measured in an urban environment. A macroscopic traffic model,

namely the cell transmission model (CTM), is adapted to an urban environment and calibrated in order predict the dynamics of the microscopic traffic model.

3 Models to simulate and predict pollutant emissions and energy consumption

In this chapter, microscopic and macroscopic approaches to model pollutant emissions and energy consumption are explored. A microscopic physical emission and energy consumption model is introduced to evaluate the performance of the urban traffic system, and a macroscopic model based on an artificial neural network (ANN) is introduced and calibrated for prediction purposes. One main challenge for macroscopic pollutant and energy consumption models is to be able to estimate the output of microscopic models, as they do not consider the individual behavior of vehicles, which plays a major role regarding energy efficiency due to the acceleration of vehicles.

4 Variable speed limits control for enhanced energy efficiency

In this chapter, we propose first to investigate the relationship between energy efficiency and traffic dynamics. Then, online closed-loop control approaches are introduced in order to implement VSLs in a Manhattan grid structure. These approaches consider in a first step macroscopic traffic and energy models, and in a second step macroscopic traffic and energy models are considered to predict and optimize the traffic system whose traffic dynamics and pollutant and energy consumption are determined using microscopic models.

5 Comparative study of urban road traffic fuel consumption optimization via variable speed limits and signalized access control

This chapter proposes to compare the benefits in terms of energy efficiency of VSLs and signalized access control in a Manhattan grid structure composed of an urban and a peri-urban area. The objective function explicitly takes into account the energy efficiency in both areas.

6 Conclusions

In this chapter, the main contributions of the dissertation are summarized, and some future perspectives are discussed.

List of publications

Journal articles

- B. Othman, G. De Nunzio, D. Di Domenico, and C. Canudas-de-Wit. Ecological traffic management: A review of the modeling and control strategies for improving environmental sustainability of road transportation. *Annual Review in Control*, 48:292 – 311, 2019. [198]

- B. Othman, G. De Nunzio, D. Di Domenico, and C. Canudas-de-Wit. Analysis of the impact of variable speed limits on environmental sustainability and traffic performance in urban networks.

Book chapters

- B. Othman, G. De Nunzio, A. Sciarretta, D. Di Domenico, and C. Canudas-de-Wit. Connectivity and Automation as Enablers for Energy-Efficient Driving and Road Traffic Management. *Handbook of Climate Change Mitigation and Adaptation*, 2021. [201]

Conference articles

- B. Othman, G. De Nunzio, D. Di Domenico, and C. Canudas-de-Wit. Variable Speed Limits Control in an Urban Road Network to Reduce Environmental Impact and Travel Time. *American Control Conference (ACC) 2020.* [199]

- B. Othman, G. De Nunzio, D. Di Domenico, and C. Canudas-de-Wit. Urban road traffic fuel consumption optimization via variable speed limits or signalized access control: a comparative study. *Conference on Decision and Control (CDC) 2021.* [200]

Conference posters

- B. Othman, G. De Nunzio, D. Di Domenico, and C. Canudas-de-Wit. Variable Speed Limits Control in an Urban Road Network to Reduce Environmental Impact and Travel Time. *e^3CAV workshop 2019.*

Conference presentations

- B. Othman, G. De Nunzio, D. Di Domenico, and C. Canudas-de-Wit. Variable Speed Limits in an Urban Road Network for Improved Environmental Sustainability. *Symposium on Management of Future Motorway and Urban Traffic Systems (MFTS) 2020.*

Patents

- G. De Nunzio, M. Laraki, B. Othman, L. Thibault. Method for determining the quantity of pollutant emissions emitted by a vehicle on a stretch of a road network. 2021.

Contents

List of Figures

List of Tables

List of Acronyms

ACC Adaptive Cruise Control 19

ANN Artificial Neural Network 14

BLX Berg-Lin-Xi 57

CACC Cooperative Adaptive Cruise Control 16

CAVs Connected and Automated Vehicles 4

CFL Courant–Friedrichs–Lewy 66

CMEM Comprehensive Modal Emissions Model 36, 85

CO_2 carbon dioxide 3

CPF Catalyst Pass Fraction 85

CTM Cell Transmission Model 42, 55

DP Dynamic Programming 14

EVs Electric Vehicles 8

FCD Floating Car Data 31

FIFO First In, First Out 62

GIS Geographic Information System 7

GLOSA Green Light Optimal Speed Advice 15

GPS Global Positioning System 9

HEVs Hybrid Electric Vehicles 8

HVs Human-driven Vehicles 11

I2V Infrastructure-to-Vehicle 4

ICCT International Council of Clean Transportation 141

ICEVs Internal Combustion Engine Vehicles 11

IDM Intelligent Driver Model 48

IEA International Energy Agency ..... xv, 2

ISA Intelligent Speed Adaptation 33

LQ Linear-Quadratic 37

LTM Link Transmission Model 36, 57

LWR Lighthill-Whitham-Richard 55

MILP Mixed Integer Linear Programming 15

MINLP Mixed-Integer NonLinear Programming 132

MPC Model Predictive Control 13

NLP NonLinear Programming 132

NMPC Nonlinear Model Predictive Control 42

NOx Nitrogen Oxide 11

NTSB National Transportation Safety Board 140

OECD Organisation for Economic Co-operation and Development 3

PM Particulate Matter 11

RHODES Real-time Hierarchical Optimized Distributed Effective System ... 35

RL Reinforcement Learning 28

SCATS Sydney Coordinated Adaptive Traffic System 35

SCOOT Split, Cycle and Offset Optimisation Technique 35

SMAPE Symmetric Mean Absolute Percentage Error 116

SoC State of Charge 10

SPaT Signal Phase and Timing 15

SPP Shortest-Path Problem 10

TEE Traffic Energy and Emissions 92, 93

TLS Traffic Light Signal 14

TUC Traffic-responsive Urban Control 35

V2I Vehicle-to-Infrastructure 4

V2V Vehicle-to-Vehicle 4

VLM Variable-Length Model 56

VMT Vehicle-Miles Traveled 3

VSLs Variable Speed Limits 20, 33

List of Symbols

h Function that generates groups of vehicles sharing the same speed and acceleration [–] 94

i Index of cell [–] 56, 90

k Index of discrete time [–] 47

l Length of queue [m] 56

l_{veh} Length of vehicles [m] 47, 68

m_{air} In-cylinder air mass per stroke and displaced volume [kg m^{-3} sr^{-1}] 86

m_{O_2} In-cylinder oxygen mass per stroke and displaced volume [kg m^{-3} sr^{-1}] .. 86

m_{fuel} In-cylinder fuel mass per stroke and displaced volume [g L^{-1} str^{-1}] 88

n Number of cells in the road network [–] 95

n_{clusters} Number of clusters of roads [–] 113

p Index of vehicle [–] 47

s^* Desired distance to leading vehicle [m] 48

s^{out} Supply downstream the network [veh s^{-1}] 64

s^{veh} Distance to the leading vehicle [m] 47

s_0 Minimum gap at complete standstill [m] 48

t Continuous time variable [s] 54

v Traffic average speed [m s^{-1}] 54

v_p^{des} Desired speed of vehicle p [m s^{-1}] 49

v_p^{safe} Safe speed of vehicle p [m s^{-1}] 48

v_0 Speed constant [m s^{-1}] 55

v_{e} Equilibrium speed given by the fundamental diagram (for second-order traffic models) [m s^{-1}] 59

v_{max} Maximum speed [m s^{-1}] 49

v_p^{veh} Speed of vehicle p [m s^{-1}] 47

Chapter 1

Introduction

Contents

1.1 Environmental impact of road traffic

Today, transport is one of the most energy-intensive sectors. In fact, as indicated in [121], and represented in Fig. 1.1, the aggregated data of sixteen countries (Australia, Belgium, Canada, Czech Republic, Finland, France, Germany, Hungary, Italy, Japan, Korea, Luxembourg, New Zealand, Spain, the United Kingdom and the United States) reveal that it accounted for the highest share of worldwide energy consumption in 2017 (36%). For example, passenger cars alone used more energy than the whole residential sector. According to [254], the worldwide transportation sector accounted for 55% of the total liquid fuels consumption, and its share is not expected to decrease for the next two decades because of the increasing travel demand.

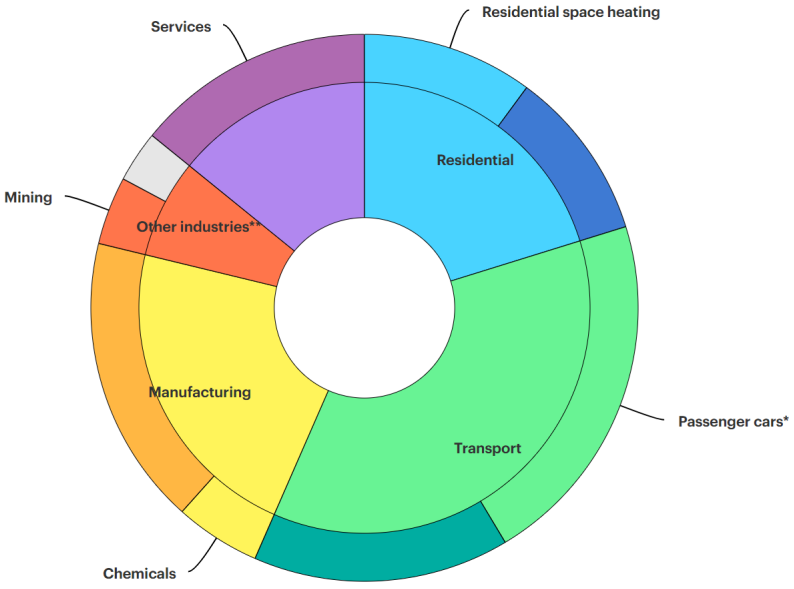

* Passenger cars includes cars, sport utility vehicles and personal trucks.
** Other industries includes agriculture, mining and construction.

Figure 1.1: Largest end-uses of energy by sector in selected International Energy Agency (IEA) countries [121] [©2017 IEA. All rights reserved].

The detailed breakdown of energy consumption in the transport sector can be found in [120] for the same sixteen countries in 2017, and is represented in Fig. 1.2. The international aviation, marine bunkers and pipeline transport are excluded. It appears that the transport sector is largely dominated by road vehicles (88%), especially passenger cars and freight road, that account for 86% of the global

energy consumption. This highlights the potential of cars and trucks control to reduce energy consumption and greenhouse gas emissions.

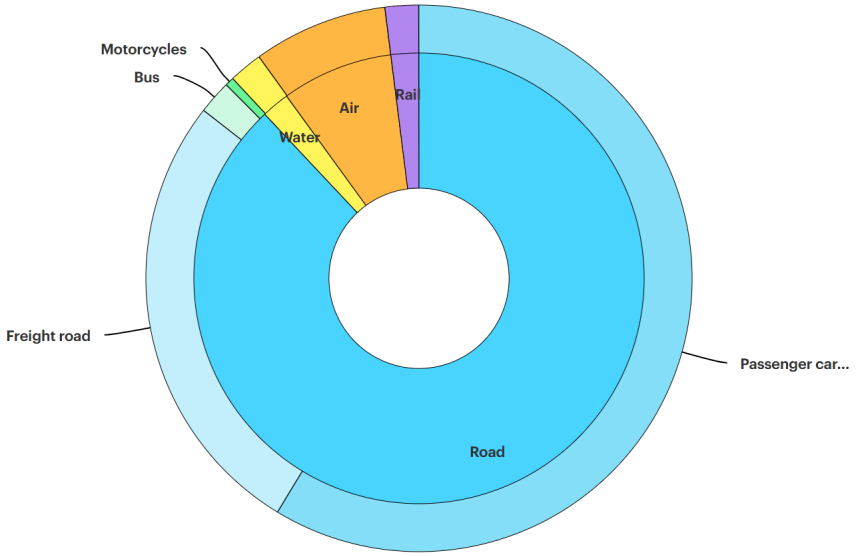

* Passenger cars includes cars, sport utility vehicles and personal trucks.

Figure 1.2: Energy consumption in transport in selected IEA countries [120] [©2017 IEA. All rights reserved].

In the future, projections show that the improved energy efficiency in transportation may lead to a net decline of about 2% in energy use until 2040 in the member countries of the Organisation for Economic Co-operation and Development (OECD), thus outpacing the predicted increase of Vehicle-Miles Traveled (VMT). However, in OECD-Europe, transportation still represents the biggest source of carbon emissions [250], contributing about 25% of the total carbon dioxide (CO_2) emissions, with cars and vans representing more than two thirds of this share [175]. The situation is even more alarming in non-OECD countries, where the transportation energy demand is expected to rise by 64% until 2040, implying an increase of about 15% of energy-related CO_2 emissions [254], which are destined to grow well above the levels imposed by the international climate goals [122]. Population surge and economic growth of the developing countries have been identified as the main causes of the drastic increase of energy demand and pollutant emissions in all sectors [122].

As a result, the current acceleration of environmental degradations and climate change is partly due to the transportation sector. In terms of public health, urban

traffic is blamed for the deterioration of air quality as more and more epidemiological studies have highlighted that mortality and several cardiovascular and respiratory diseases are highly correlated with air pollution [277, 17, 226, 66]. A study conducted in 30 countries revealed that $PM_{2.5}$ concentrations above minimum exposure levels were responsible for 22% of infant deaths [107]. Although traffic related pollutants (NO_2, NO_X, PM_{10}, and $PM_{2.5}$) have been on a downward trend in major cities since 2010 due to the presence of more efficient vehicles in car fleets, pollution levels remain well above the recommended European Limit Value [80].

To improve air quality in urban areas and address these environmental and health issues, the development of new engine technologies can be accompanied by a significant change of individual habits, which can be induced by public authorities [218], and the implementation of innovative intelligent solutions based on connectivity. Such approaches are known as traffic eco-management strategies, i.e. the dynamic control of vehicles and/or road infrastructures in order to reduce air pollution [198].

The benefits of traffic eco-management can be greatly increased thanks to the technological resources offered by Connected and Automated Vehicles (CAVs). Their current development constitutes beyond dispute a significant breakthrough in the movement of people and goods [229]. On the one hand, the number of connected vehicles, i.e. that are able to communicate bidirectionally with other systems in order to process and share a large amount of data, is increasing. Several kinds of connectivity are usually distinguished: Vehicle-to-Infrastructure (V2I), Infrastructure-to-Vehicle (I2V), and Vehicle-to-Vehicle (V2V) communications. On the other hand, research and development of fully automated vehicles, i.e. that are capable of moving safely without human input, are promising as they ensure much shorter reaction times and more precise positioning and control than conventional vehicles. This results in high reliability and ability to anticipate which offer huge potentials for improving safety and comfort, and reducing travel time and fuel consumption. These opportunities are increased through higher CAVs penetration rates as cooperative control possibilities (vehicles acting cooperatively) are enhanced. According to [161], they are expected to represent 20–40 % of the sales by 2030. CAVs widen the scope of possibilities in terms of rerouting, green priority, speed advice at intersections, cooperative control, vehicle platooning, etc. [229, 264].

Therefore, a lot of attention has been drawn worldwide to finding the most effective measures to help reduce the current contribution to greenhouse gas emissions from transportation. Governments, practitioners and researchers seem to agree on the fact that a combination of short-term and long-term strategies must be adopted. In the short-term, policies and regulations encouraging changes in

behavior and travel habits represent a key lever. Attractiveness of alternative means of transportation should be enhanced, a shift to less polluting transport modes should be promoted, and a change in purchasing habits favoring smaller and more energy-efficient cars should be encouraged [38]. In the long-term, the widespread adoption of innovative technological solutions such as electrification, connectivity and automation are expected to enable a significant shift in the future of personal transportation and mobility. The way for such a technological transformation of mobility is already being paved thanks to the diffusion of CAVs, V2V and V2I/I2V cooperation and communication networks, in- and over-roadway sensors, cloud-computing capabilities, etc. [98].

However, the potential energy benefits of these technologies remain uncertain, mostly because of the high level of non-linear dependence between different aspects of an automated transportation system operating with conventional vehicles, as well as possible side-effects of automation [255]. Among the features enabled by the aforementioned technologies that promise to increase energy efficiency and reduce pollutant emissions of transportation, it is worth mentioning eco-driving, eco-routing, platooning, roadway throughput optimization, powertrain electrification, vehicle down-sizing, parking search time reduction, ride-sharing. On the other hand, as for the side-effects that may endanger energy efficiency and emission reduction, it is likely that technology may increase traffic congestion as a consequence of an increased access to mobility, increase travel speeds as a consequence of enhanced safety, increase commute distances as an effect of increased comfort and reduced travel costs, etc. [255].

From a single-vehicle efficiency perspective, research suggests that lightweight, low-speed, autonomous vehicles have the potential to achieve fuel economies an order of magnitude higher than current cars [255]. However, at system-wide level, it is not yet clear whether a high penetration rate of CAVs will have a positive or a negative impact on fuel consumption and CO2 emissions. In fact, [266] explains that some effects of the advent of CAVs will reduce energy consumption (development of platooning and eco-driving, congestion mitigation, vehicle lightweighting and right-sizing, de-emphasized performance, car-sharing, on-demand mobility, and reduced infrastructure footprint), whereas other effects will increase it (travel cost reduction, higher highway speeds, increased vehicle features, and new user groups). Current estimates suggest that the total energy consumption impacts can range from a 90% decrease to a 200% increase in fuel consumption as compared to a projected 2050 baseline energy [33]. The outcomes depend on the direction that will be favored by future policy making.

Such a large variability in the possible outcome of the adoption of the new vehicular and traffic technologies makes it somewhat difficult to focus and prioritize the research efforts to increase energy efficiency of mobility. Nowadays, the

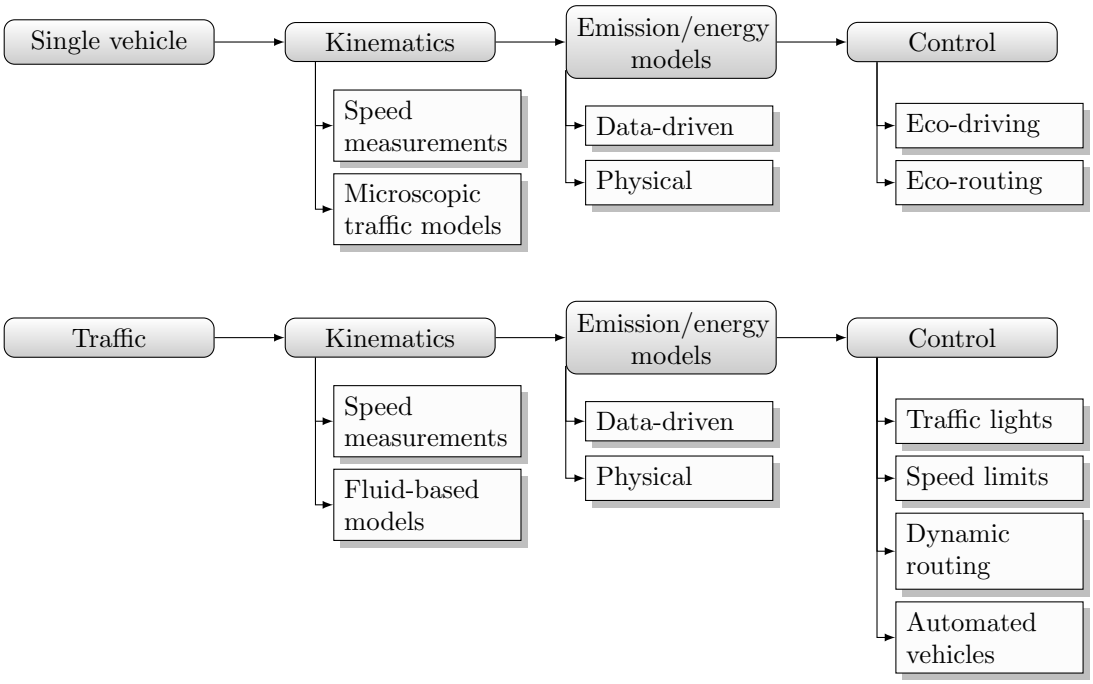

Figure 1.3: Diagram of the global approach for energy consumption and emissions modeling and control for single vehicles and traffic flow.

general trend in research and policy seems to aim to reduce CO_2 emissions by pushing for more efficient vehicles and reducing VMT. This is based on a generally accepted paradigm that congestion mitigation programs should reduce CO_2 emissions. However, it is difficult to prove a clear direct proportionality between congestion and CO_2 emissions [77]. The most reliable approach to improve energy efficiency and reduce pollutant emissions in the design of a traffic regulation measure consists in directly considering these aspects as decision and optimization criteria. Therefore, interest in transportation regulation problems with explicit environmental considerations is growing [272, 265].

Traffic eco-management strategies include the control of vehicles, that modifies their individual speed profiles or route choices, and the control of infrastructures, that influences the vehicular flow as a whole by acting on the typical flow regulation actuators, such as traffic lights, speed limits, etc. The adopted categorization in terms of modeling and control approaches both at vehicle and traffic level for the general problem of reducing environmental impact of road transportation is illustrated in Fig. 1.3.

In the following, a survey of the emission and energy consumption models and control strategies will be presented, both at the scale of single vehicles and road traffic.

1.2 Ecological management of single vehicles

Ecological management strategies adapted to single vehicles aim at optimizing their routes and speed profiles in order to reduce their impact on the environment. Also, vehicles automation opens the door to many strategies for cooperative vehicle control designs. These approaches are usually based on a traffic and an emission and/or energy consumption models in order to predict the behavior of the vehicles under consideration.

1.2.1 Emission and energy consumption models

A microscopic traffic model is used to predict the dynamics of vehicles. Such models describe the behavior of each single vehicle in the traffic flow. They include car-following and cellular automata models to represent the longitudinal dynamics of vehicles. Lane-changing models can also be considered to represent their lateral dynamics [75]. One difficulty associated with these models corresponds to the calibration of the parameters.

Once the microscopic traffic kinematics is determined, it can be associated with a microscopic emission and energy consumption model to predict the behavior of vehicles. Such models estimate the emission and/or energy consumption rates from the vehicles behavior. This can be done using data-driven approaches, including look-up tables [213, 239], regression models [288, 215] and machine learning strategies [5, 193, 123, 284]. Another approach is based on the use of physical models whose parameters have a physical meaning. Such models can be either deterministic [230, 231, 85] or based on random velocity disturbances when a precise knowledge of speed profiles is lacking [35, 132, 278, 83]. A complete review of microscopic emission and energy consumption models is given in Section 3.2.1.

1.2.2 Connected vehicle control designs

The anticipation and prediction potential of connected vehicles opens the door to energy-efficient control approaches. CAVs are even more promising because of their more precise positioning and control. CAVs technology is largely based on the exchange of different types of data between vehicles (V2V) and with the infrastructure (V2I/I2V). Two data types may be differentiated:

- Geographic data (time-invariant) that can be embedded on-board or can be accessible via a Geographic Information System (GIS) server: road network architecture, road elevation and slope, road speed limits, speed bumps, road narrowings, safe speeds on curved roads, etc.

- Traffic data (time-variant) that are provided by other vehicles or by the infrastructure (through sensors, cameras, etc.): traffic information, road closings, state of traffic light signals, weather-related road conditions, etc. Note that in absence of real-time data, historical data can be used to predict traffic slow-downs by systematic evaluation [269].

Based on these data, control strategies can be implemented by vehicles in order to improve their own energy efficiency and reduce their own pollutant emissions, without consideration of the neighboring vehicles' energy consumption ("individual gain" optimization). These strategies are reviewed in this section. Two main approaches can be distinguished:

- eco-routing that consists in route choice optimization,
- eco-driving that corresponds to the optimization of vehicles speed profiles.

They should be used jointly to increase energy efficiency [248]. In practice, CAVs recalculate their most energy-efficient routes, and optimize their future speed profiles in anticipation of surrounding vehicles motion, road slopes and geometry, traffic light signals, etc.

For the sake of completeness, note that fuel cut-off, cylinder deactivation, thermal load management, and power split in Hybrid Electric Vehicles (HEVs) powertrains can be used to minize energy consumption. Also, an energy-efficient driving would include strategic decisions such as vehicle purchase, maintenance, reduction of on-board elements weight, and reduction of the use of air conditioning systems. For example, [146] indicates that during idling condition, the fuel consumption of a conventional gasoline engine vehicle could increase up to 90% because of air-conditioning operation. An overview of the techniques and algorithms to improve energy efficiency of CAVs is proposed by [98].

Note that the modeling and control approaches applied to Electric Vehicles (EVs) and HEVs are much more complex when considering because of their limited range, recharge times, and ability to regenerate energy during deceleration phases [57].

Eco-routing

Route choice is a major factor in vehicles energy consumption. Intuitively, a driver would usually choose the shortest travel distance or the fastest travel time route. However, these are not always the most energy-efficient routes because the shortest route may be partially congested, and the fastest route may be longer and contain high speed limit segments [118]. [143] proposes a model that indicates that the most energy-efficient route could have 25% reduction in fuel consumption over

the fastest route and 23% over the shortest route. As a result, a Swedish study presented by [70] indicates that in 46% of cases the drivers' spontaneous route choices were not the most fuel-efficient routes.

Hence, an energy-efficient driving should integrate an eco-routing algorithm that optimizes the route choice in terms of energy consumption. The eco-routing optimization problem can be formulated as follows

$$p^*(o,d,k) = \underset{p\in\mathcal{P}}{\operatorname{argmin}} \sum_{i\in p} g(i,\theta_k) \tag{1.1a}$$

$$\text{subject to } n_0 = o, \tag{1.1b}$$

$$n_{|p|} = d. \tag{1.1c}$$

where $\mathcal{P}$ is the set of all paths $p = \{n_0, ..., n_d\}$ between origin o and destination d, and p^* is the optimal route. Function g returns the energy consumption associated with the travel on a given segment i. Usually, g depends on the parameters of segment i, that can be time-dependent and are denoted θ_k (road congestion, road type and grade, speed limit, traffic light signals, etc.). These parameters have a great impact on energy consumption. For example, [128] indicates that a vehicle traveling on a 250-meter freeway section with a 6% grade increases its fuel consumption of 86% in comparison with the same section, with identical initial speed, final speed, and trip time, but with a 0% grade.

state vector field

In addition of energy consumption, energy-efficient control strategies also have to pay special attention to travel time and distance. Hence, some eco-routing algorithms formulate the optimization problem with the travel time explicitly appearing either in the constraints [291] or in the objective function [58]. In the case of a bi-objective function, the solution found can be a Pareto-Optimal route [20, 58].

Several formulations of the eco-routing problem can be found in the literature. [142] proposes a comparison of different approaches: one of them averages the observed energy consumption, another one estimates fuel consumption with a regression model, and the last one uses a physical energy model. [70] presents an eco-routing algorithm that classifies the roads of the network into 6 groups, depending on their Global Positioning System (GPS) data. Based on the same data, a fuel consumption factor is calculated for each group. The authors introduce peak and off-peak hours to model the evolution of the traffic during the day. Similarly, [29] proposes to consider not only historical GPS data, but also real-time vehicle velocity trajectories to estimate the energy consumption of each link. [59] presents an innovative eco-routing algorithm especially adapted to EVs in an urban environment, and that considers the impact of onboard accessories and sys-

tems on the electricity consumption. The approach considers historical map data and available average traffic speeds to optimize the route choice. [56] proposes a formulation adapted to HEVs, in which a constraint on the final State of Charge (SoC) is defined. However, the eco-routing optimization is relaxed and solved as a standard Shortest-Path Problem (SPP), the SoC constraints being a-posteriori enforced. [194] presents an approach related to energy-efficient route choice for heavy-duty vehicles, which is quite different from eco-routing strategies as they can only travel on a limited amount of roads. In this work, the approach consists in a precise reconstruction of the characteristics of the road before departure. This kind of tool can be of great interest for fleet managers as it allows them to precisely quantify the fuel cost of different itineraries.

Usually, eco-routing algorithms only take into account the energetic cost of links and not the vehicle behavior at intersections. However, this aspect is crucial in energy consumption estimation. To model the energy consumption at intersections, [58] introduces a transition speed at the interface between two links. Traffic lights at intersections have also to be considered. For example, [241] proposes an eco-routing algorithm based on a signalized traffic network in which the authors use a Markov decision process to model the traffic.

Different methods can be used to solve the eco-routing optimization problem. For example, some authors implement Dijkstra-type algorithms [139], while others use heuristic searches [186] or semi-analytical strategies [56]. To reduce the set of possible solutions, eco-routing algorithms can consider additional constraints on the maximum travel distance.

Anticipating the evolution of traffic is a particularly critical point in the development of eco-routing algorithms. This could be enhanced by implementing cooperative eco-routing approaches, in which the impact on energy efficiency is analyzed at the network level, rather than at the vehicle level only [98].

Eco-driving

In addition of eco-routing algorithms that optimize route choice, it is essential to reduce the occurrences and the intensity of the acceleration phases as they are the ones that consume the most energy. In other words, the optimal speed profile in terms of energy efficiency is a constant speed. However, this instruction is usually impossible to follow in real traffic conditions, especially in an urban environment with traffic light signals, road congestion, pedestrians, cyclists, road grade, different speed limits etc. Hence, the core objective of eco-driving is to predict the traffic evolution and deduce accordingly a speed profile as smooth and energy-efficient as possible along a given route [118]. For example, [280] presents a study that shows that it can be more energy-efficient to have high acceleration and deceleration to catch green lights, rather than idling at red signals and starting

from stops.

Eco-driving approaches, that control both the longitudinal and the lateral dynamics of vehicles, are particularly compatible with autonomous vehicles, as they can accurately track the instructions generated by the eco-driving algorithm [102]. However, it is expected from an eco-driving approach for Human-driven Vehicles (HVs) to return rather an advisory speed profile the user can follow. Another solution is to directly formulate the optimization problem considering the recommended maximal speed of the vehicle as the control input [202, 24].

A key point of eco-driving is the choice of the targeted cruise speed. The objective is to travel at the speed associated with the lowest energy consumption rate, expressed in L/100 km for Internal Combustion Engine Vehicles (ICEVs) and in kWh/100 km for EVs. As indicated by [214], the energy consumption rate is indeed not constant, as

- firstly, the rate decreases with the increase of vehicle speed. The reason is that heat losses are reduced at higher engine speed;
- then, the rate starts increasing at high vehicle speed due to increased friction losses.

As a result, the curve representing fuel consumption rate as a function of vehicle speed shows a U-shape. The optimal speed depends on the vehicle and engine sizing, and on the powertrain type (diesel, gasoline, EVs, HEVs). Fig. 1.4 represents the fuel consumption rate-vehicle speed curve for different passenger cars [285].

Note that vehicles speed profile optimization impacts many other metrics than energy consumption and CO2 emissions. Hence, eco-driving algorithms may have other complementary objectives: reducing pollutant emissions such as Nitrogen Oxide (NOx) and Particulate Matter (PM) emissions, increasing safety, increasing passenger's comfort (by ensuring a low jerk), reducing the travel time, etc.

In the following, a formulation of the eco-driving problem and a discussion about its technical solutions are proposed. The state and control of the vehicle under consideration are respectively denoted $x(t) = \{s(t), v(t), \xi(t)\}$ and $u(t) = \{T_{\mathrm{m}}(t), T_{\mathrm{e}}(t), F_{\mathrm{b}}(t)\}$. The variables $s(t)$, $v(t)$, and $\xi(t)$ are respectively the position, the speed, and the SoC of the vehicle at time t. The variables $T_{\mathrm{m}}(t)$, $T_{\mathrm{e}}(t)$, and $F_{\mathrm{b}}(t)$ denote respectively the electric motor torque, the internal combustion engine torque, and the forces applied by frictional brakes. This formulation is well adapted to HEVs. Note that for ICEVs, ξ and T_{m} should not be considered. Similarly, T_{e} should not be considered with EVs. Based on the vehicle dynamics, f is the state vector field that returns the new vehicle state from its control and previous state. Function g returns the energy consumption rate from the vehicle state and control. In an urban environment, the eco-driving problem can be separated into

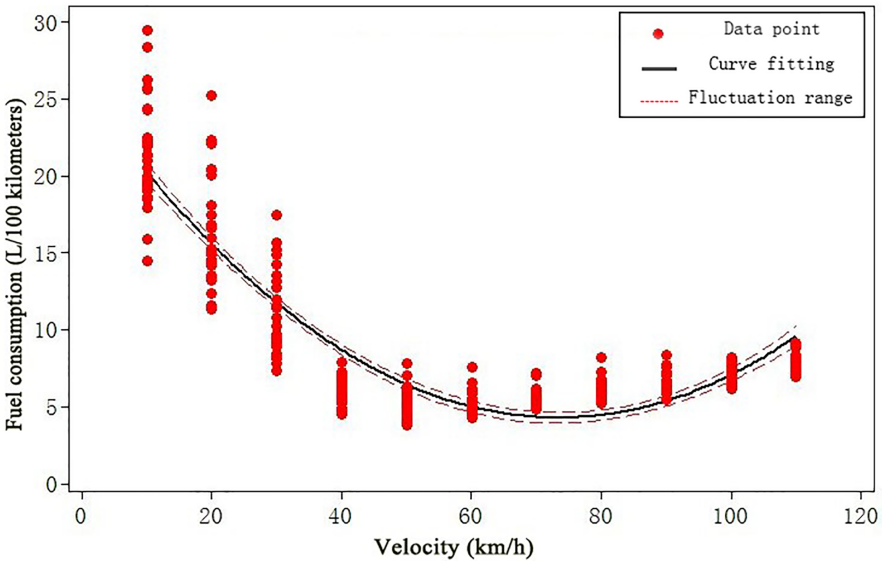

Figure 1.4: Fuel consumption rate as a function of vehicle speed, based on survey reports of different passenger cars [285] [©2018 Yang et al.].

subproblems such that for each single segment of the vehicle's route, the following optimization problem is solved

$$\begin{aligned}
\underset{u}{\text{minimize}} \quad & J = \int_0^{t_\text{f}} g(u, x(t))dt && \text{(1.2a)}\\
\text{subject to} \quad & \dot{x}(t) = f(u, x(t)), && \text{(1.2b)}\\
& 0 \leq s(t) \leq s_\text{f}, && \text{(1.2c)}\\
& v_\text{min}(t, s(t)) \leq v(t) \leq v_\text{max}(t, s(t)), && \text{(1.2d)}\\
& \xi_\text{min} \leq \xi(t) \leq \xi_\text{max}, && \text{(1.2e)}\\
& s(0) = 0, \quad v(0) = v_\text{i}, \quad \xi(0) = \xi_\text{i}, && \text{(1.2f)}\\
& s(t_\text{f}) = s_\text{f}, \quad v(t_\text{f}) = v_\text{f}, \quad \xi(t_\text{f}) = \xi_\text{f}. && \text{(1.2g)}
\end{aligned}$$

[228] presents a complete overview of the eco-driving problem constraints and parameterization. In short, Eq. 1.2c - 1.2e are the state constraints. In particular, Eq. 1.2d represents the fluctuation of traffic speed that can be due to road congestion, speed limits, traffic light signals, etc. Eq. 1.2f and Eq. 1.2g correspond respectively to the initial and the terminal constraints of the segment under consideration.

Two paradigms aiming at solving eco-driving problems can be differentiated: offline optimizations that assume that all road and traffic characteristics and

constraints are known in advance (or at least estimated with increased awareness thanks to connectivity), and online optimizations that use prediction models to perform real-time-capable control, e.g., Model Predictive Control (MPC) approaches [228]. In practice, offline solutions are based on a horizon t_f that corresponds to the travel time of the whole trip. Conversely, online solutions are based on a much shorter horizon t_f, over which the behavior of the preceding and the surrounding vehicles needs to be predicted.

Several approaches can be implemented for offline optimization: dynamic programming [64], Pontryagin's minimum principle [228] or calculating the analytical solution [203]. Online solutions allow to acquire more information in real time about the upcoming route. For example, [112] proposes a method with an on board optimizing controller taking into account the road slope. In the case of connected vehicles, one may also imagine a control design taking into account the prediction of the upcoming traffic conditions and accordingly updating the speed constraints. The main difficulty of online solutions lies in the computation time as they are expected to be compatible with real-time execution.

Some advancements in online eco-driving approaches are presented in [228]. For ICEVs, the authors propose a parametric optimization technique inspired by the analytical solution of a simplified version of the eco-driving optimal control problem. For HEVs, a bi-level algorithm that tries to decouple energy-optimal drive control from hybrid energy-management control is presented.

As indicated previously, eco-driving strategies for EVs and HEVs are promising but they introduce additional challenges because of their limited range, recharge times, and ability to regenerate energy during deceleration phases, which add constraints to the optimization problem. According to [103], even with full regenerative braking, EVs would still benefit from optimized speed profiles that reduce electromechanical energy conversion losses. Concerning ICEVs, the authors show that pulse and glide operation of the engine (chattering optimal control) represent great energy saving potentials, but can be difficult to implement in practice. Finally, the authors indicate that significant energy savings (5%–30% in each scenario) can be achieved by optimizing speed profiles over conventional driving strategies. In particular, energy savings can result from a better utilization of the energy delivered to the wheels, if vehicles are driven with lower and constant speeds, reducing the aerodynamic drag.

One common difficulty in the development of eco-driving systems is the necessity to adequately take into account the presence of preceding vehicles. To overcome this issue, [102] presents an eco-driving control strategy for electric CAVs. The objective is to optimize the speed profiles of CAVs in order to improve their energy efficiency, while guaranteeing safety constraints, i.e. respecting the minimum inter-vehicle distance and maximum speed limits. The controller is set to solve

optimal control problems and return analytical state-constrained solutions under different assumptions. According to the authors, the proposed framework is suitable for online implementations, and significantly improves the energy efficiency without increasing trip time. Similarly, [195] proposes an eco-driving strategy for electric CAVs based on the use of an analytical solution in an MPC framework, which makes it suitable for a real-time use. In this approach, the controller predicts the trajectory of the preceding vehicle under the assumption of constant acceleration. The authors indicate that the algorithm is robust and provides near-optimal speed profiles in terms of energy consumption.

An eco-driving strategy for HEVs, which indicates an energy-optimal speed profile to follow, is proposed in [297]. To reduce the computation time and enable online implementation, an Artificial Neural Network (ANN) is trained to decide which control sequence to apply, and another one is trained to estimate the duration of each control mode in the control sequence. The control sequences include maximal hybrid acceleration, maximal electric acceleration, maximal regenerative braking, maximal hybrid recharge, braking and regenerative braking, optimum hybrid operation, optimum electric operation, and constant speed. These multi-class ANNs are trained in order to return optimal speed profiles from the boundary conditions, and the constraints of the upcoming trip, which can be estimated through connectivity and measurements. In practice, the ANNs are trained using a database provided by the offline resolution of optimal control problems through Dynamic Programming (DP). In fact, DP is an algorithm capable of providing accurate optimal solutions of the problem, but has the disadvantage of a high computational complexity, making real-time implementations of the optimization procedure difficult. The authors indicate that the online ANN-based speed profiles and the offline DP-based speed profiles are reasonably close, both in terms of speed and in terms of energy efficiency. This result highlights the interest of machine learning approaches as they give similar results but have much smaller computation times.

In an urban environment, eco-driving approaches are complex because of the uncertainty of traffic. In particular, it is very difficult to know the Traffic Light Signal (TLS) cycles in advance as some signalized intersections have a variable phase duration depending on the traffic level. If the TLS cycles are unknown by the eco-driving algorithm, [202] proposes a method that considers traffic lights as stop signs in the optimization problem. Naturally, the driver is free not to follow the advised velocity given by the algorithm in the case of green at a traffic light. To take into account the uncertainty on traffic-light cycles, [240] considers a stochastic cycle timing that adds to the red-light duration a random variable. To generate more realistic signal timings, [174] introduces for each intersection a time-varying probability of green based on measured data. In the optimization

process, solutions that pass through time intervals with high green probability are then naturally preferred.

In this sense, the broadcast of Signal Phase and Timing (SPaT) through I2V communication represents a real opportunity in terms of energy efficiency as this reduces the uncertainty about TLS. In the case of known and deterministic TLS cycles, many algorithms can be used to solve the eco-driving problem. For example, [184] presents a method based on dynamic programming, [52] uses Dijkstra's shortest path algorithm, [115] develops a method with model predictive control, [232] implements a genetic algorithm, and [179] proposes to relax the integer constraints of a Mixed Integer Linear Programming (MILP) approach to transform it into an optimal control problem and solve it using the direct adjoining approach. The principle of these algorithms is to add a constraint on the crossing time at intersections. This allows the CAVs to anticipate the future states of TLS and optimize their own speed profile for a timely arrival at a green light. This approach, known as Green Light Optimal Speed Advice (GLOSA), can be enhanced by V2V communication as vehicles would also be aware of the traffic state ahead. In [52], a strategy that optimizes the speed profile of a vehicle is proposed. Its objective is to improve the energy efficiency by catching the green lights along an arterial road. In this work, the authors consider that the information about several successive signalized intersections is available (I2V), but that vehicles do not communicate with each other (no V2V). The authors indicate that the higher the penetration rate, the greater the gains in terms of energy efficiency.

To conclude, it is essential to keep in mind that prior knowledge of in-trip and final trip constraints, such as, inter alia, speed limits, road grade and geometry, state of the road, travel time and distance, and final speed, opens the door to greater energy savings thanks to better anticipation [103]. Eco-driving algorithms' efficiency can also be improved with the consideration of other drivers' aggressiveness, which can be easily addressed when considering CAVs, and with the use of more complex models to predict the state of the surrounding vehicles [195]. Yet, some aspects of the problem, such as the presence of pedestrians or drivers decision making, remain uncertain and hence difficult to predict. This issue can be addressed by the use sensors and cameras. To go further, high CAVs penetration rates offer very good prospects in terms of energy efficiency as they considerably improve the anticipation in CAV driving, car following, and lane selection and merging. A democratization of eco-driving systems would need robust online calculations for all types of powertrains, and the generalization of optimal in-trip advice in all situations, especially in urban areas. This latter is enhanced by the use of I2V communication, which represents a great opportunity to develop green waving, and to approach intersections in an energy-efficient way by anticipating SPaT [228]. According to [98], it is necessary to consider the uncertainty

over the bounds on the predicted vehicle speed. Driver safety, performance improvement, and real-time operation are identified as the main technical challenges for the development of connected CAVs control.

1.2.3 Cooperative vehicle control designs

The first opportunity that is opened up by CAVs consists in the control of vehicles aiming at improving their own energy efficiency, i.e. "individual gain" optimization such as eco-routing and eco-driving approaches presented previously. In this case, CAVs communicate with each other and with the infrastructure, which ensures reliable predictions as the need for guessing is reduced, but vehicles make their decisions individually. As a result, vehicles can appear to be competing in some situations that involve motion conflicts.

Vehicles connectivity and automation offer the possibility to go further and develop vehicles cooperation, i.e. vehicles that communicate (V2V and I2V) and also coordinate their movements. Coordination algorithms enable to mitigate conflict situations and guarantee that decisions are jointly feasible [12]. Such algorithms also open the door to optimal coordinated control, e.g., minimizing the global energy consumption ("common good" optimization). Vehicles cooperation is almost impossible to implement with conventional HVs due to unknown plans of neighboring vehicles and lack of precision to coordinate speed, hence the interest in implementing this kind of approach with CAVs [229].

In practice, cooperation can consist in vehicle platooning, Cooperative Adaptive Cruise Control (CACC), lane changing and merging control, and cooperative intersection control. These points are described and discussed in the following. A key question in vehicles cooperation is the CAVs penetration rate necessary for significant energy efficiency improvement.

Vehicle Platooning

Vehicle platooning consists in the formation of groups of vehicles that travel very closely together. Each platoon is composed of a lead vehicle that controls the speed, and other vehicles that follow the speed setpoint. Vehicle platooning represent a real opportunity in terms of energy efficiency as shorter gaps between the vehicles reduce the aerodynamic drag coefficient. In this sense, the formation of micro-platoons, even of vehicles of different origins and destinations, can reduce energy consumption. Also, reduced distances between the vehicles increase road capacity.

CAVs improve opportunities for vehicle platooning as high speed V2V communication and vehicle automation enable faster reactions resulting in reduced risk of rear-end collision and improved traffic safety. This also allows to reduce the minimum gap between heavy-duty vehicles from about 10 m [27] to 2 m [8],

ensuring higher energy efficiency and road capacity. For example, [32] indicates that an 8-10 meters gap results in an average fuel saving of 8%, while a 3-4 meters gap results in an average fuel saving of 11%. Generally speaking, [177] indicates that the closer the longitudinal spacing, the better the energy efficiency of platoons. For improved energy efficiency, note that the gaps between vehicles could be variable, depending on the road slope [293].

According to [21], three levels of automated platooning can be defined, as follows

1. human-driven platooning with in-platoon resting in which the lead vehicle is handled by a driver and the following vehicles can complete the driving tasks automatically;

2. hybrid platooning in which the following vehicles can be driverless during platooning phases;

3. driverless platooning which involve full autonomous vehicles.

It appears that vehicle platooning is particularly suitable for the movement of heavy duty vehicles, especially on highways as they are traveling at high speed, causing high aerodynamic drag. The opportunity represented by truck platooning in terms of aerodynamic drag reduction is illustrated in Fig. 1.5. Also, trucks usually have to travel long distances on highways and could easily join neighboring trucks to form platoons, even if they have different origins and destinations. The first studies about truck platooning for fuel saving purposes started in the mid-1990s with the European project Chauffeur I [27]. A complete overview of fuel economy in truck platooning can be found in [293].

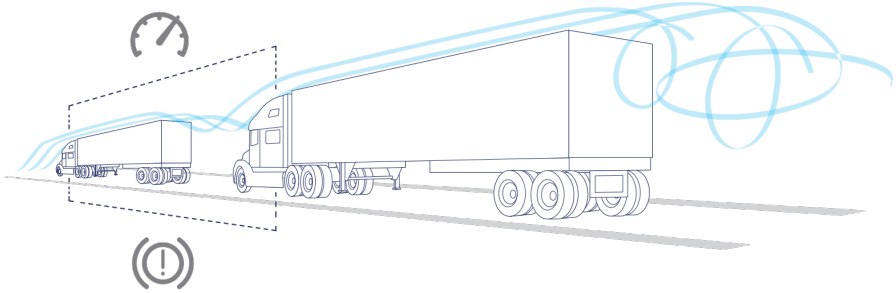

Figure 1.5: Illustration of the reduction of the aerodynamic drag in truck platooning [1] [©Peloton Technology. All rights reserved].

As mentioned above, fuel savings in truck platoons can be maximized through aerodynamic drag coefficient reduction, which is impacted by

- the distance between vehicles, as indicated above;

- the aerodynamic-trailer configuration, e.g., trailer skirts, trailer boat tails [293].

- the position in the platoon. For example, a study conducted with three Class 8 tractor-trailer trucks indicates that the fuel savings of the lead, the second, and the third trucks were respectively 18%, 24%, and 23% [172]. Hence, it seems to be judicious to establish a rotation of the lead vehicle, especially in platoons that are not driverless as it would allow drivers to rest.

Several methods can be used to analyze the aerodynamic drag coefficient evolution and the potential fuel savings: wind tunnel test, road test, track test, and simulation methods. [293] discusses the advantages and disadvantages of each method. This kind of approach is useful for determining the impact of wind direction on fuel savings. For example, [176] indicates that there is still an interest in vehicle platooning under crosswind conditions in terms of energy savings.

In practice, the implementation of vehicle platooning poses some issues. [229] indicates that the development of truck platooning has resulted in significant challenges, e.g., platoon string stability (avoid the amplification of disturbances from the platoon leader to the downstream vehicles.), communication needs, control design, and formation scheduling. For example, platoons on highways may prevent other vehicles from changing lanes or merging into the highway at on-ramps. This phenomenon is accentuated by longer platoon sizes, especially for high traffic densities. This can be solved by dedicating lanes to CAVs and platooning vehicles [190], or by developing adapted algorithms based on V2V communication that allow platoons to change lanes, and to yield gaps for merging vehicles [271]. Another key point for real-world development of vehicle platooning is to ensure algorithms of suitable complexity, especially in case of large number of vehicles platooning. Some researchers have worked in this direction. For example, [258] proposes to formulate the problem of controlling a large number of trucks in a coordinated manner by using clusters. Similarly, [257] presents a heuristic approach based on an iterative algorithm. A crucial point in CAVS platooning consists in the communication needs. In fact, an interruption in the communication with a small distance between vehicles can pose serious safety problems in the case of emergency braking of the lead vehicle. Hence, it is safer to keep large gaps ahead of the platoon leader [234].

Today, truck platooning technology has matured and major manufacturers could penetrate the market in the near future [229]. In 2016, a European project, namely the EU Truck Platooning Challenge, gave rise to the first cross border truck platooning initiative in the world. Six truck platoons (one of each brand: DAF, Daimler, IVECO, MAN, Scania and Volvo) departed from different European cities to arrive in Rotterdam at the same time. [2] presents the main results

of the project and the essential points for further development of real-world truck platooning: involvement of the end users (shippers and haulers), clear segmentations showing where platooning can be operational, high definition maps, reliable real-time traffic information, etc.

For improved energy efficiency, vehicle platooning should be combined with complementary strategies, such as the ones presented in Section 1.2.2: eco-routing, eco-driving, vehicle choice, maintenance, reduction of weight, reduction of the use of air condition systems, etc. [258] proposes a centralized approach aiming at forming and controlling truck platoons. The strategy consists in

1. determining the shortest path for each truck according to their origins and destinations;
2. establishing possible platoon configurations;
3. optimizing the speed profiles of each platoon.

Cooperative Adaptive Cruise Control

Similarly, CACC research has been strongly progressing over the past few years. CACC is basically an enhanced Adaptive Cruise Control (ACC) system which, in addition to using range sensors to adjust the distance from the vehicle ahead, anticipates the motion of neighboring vehicles with a much quicker response through V2V and/or I2V communication. For example, [182] indicates that the communication delay to relay a message from the first to the fourth vehicle can be about only 0.1 seconds with CACC, against more than 5 seconds with autonomous ACC, as they have to witness speed or direction changes of the vehicle in their direct line of sight to react and adapt their own behavior. An illustration of vehicles performing CACC is given in Fig.1.6.

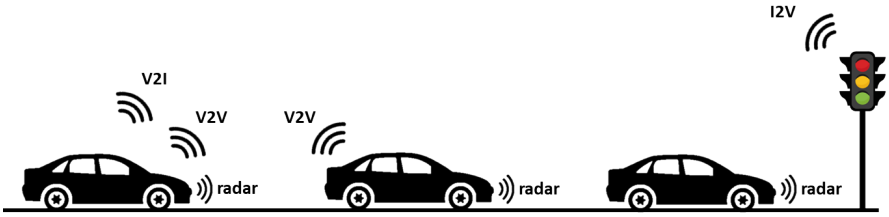

Figure 1.6: Illustration of vehicles forming a CACC string.

The fundamental difference between vehicle platooning and CACC is that a platoon is necessarily composed of a lead vehicle, that other vehicles are following as precisely as possible. In other words, vehicle platooning consists in a hierarchical control structure, while CACC structures allow communication between all

vehicles [229]. Usually, vehicle platooning is based on a constant-distance gap, i.e. a constant distance that does not depend on the speed, while CACC considers a constant-time-gap, i.e. a distance proportional to vehicles speed [234].

The motivations of CACC are very similar to those of vehicle platooning: improving traffic flow, safety, comfort, convenience, customer satisfaction, and decreasing fuel consumption. According to [191], the use of high-speed communication in CACC systems could reduce the average gap between vehicles from 1.4 seconds to 0.6 seconds, which should result in an increase in energy efficiency and in highway lane capacity. In [165], the 100% CACC and the 100% ACC are compared. The results reveal that in the CACC scenario, the fuel consumption rate can be reduced by half, and the capacity can increase up to 49%, depending on the traffic demand. Similarly, [144] proposes to investigate the benefits of a control approach based on cooperation between electric vehicles performing eco-driving. The energy efficiency and string compactness are compared with two scenarios: an ACC strategy, and an eco-driving strategy without cooperation. The results indicate that the cooperating eco-driving control framework outperforms the other control strategies regarding both criteria. Safety can be improved in CACC systems by developing collision warning or mitigation systems, but CACC alone is not primarily a safety system [234].

CAVs are designed to communicate both with the infrastructure (V2I/I2V), and with other vehicles (V2V). According to [234], two major uses of V2I/I2V communication in CACC systems are the implementation of

- Variable Speed Limits (VSLs), aiming at reducing congestion at bottleneck locations by lowering upstream vehicle speeds;
- arterial coordinated start, that coordinates the start of vehicles waiting at a red traffic signal when the signal turns green. In urban areas, arterial coordinated start is particularly promising because of its simplicity and potential huge impact on intersections throughput [160].

In CACC systems, V2V communication consists in sharing at least the vehicle location, speed, acceleration, intentions, and performance limitations. This communication can be used simply to develop more performing ACC, but it also opens the door to much more complex CACC systems, in which vehicles are able to anticipate their decisions by communicating with vehicles that are beyond their direct line of sight. This would greatly contribute to stabilizing the responses of the CACC-equipped vehicles. As with vehicle platooning, V2V CACC is especially promising on highways.

In practice, several string formation and dissolution strategies for improved energy efficiency can be implemented, with differing connectivity architectures and collaboration levels. These strategies can be based on, inter alia, classical

controllers, receding horizon controllers, constrained optimization based on Pontryagin's Minimum Principle [67]. An overview of these approaches is proposed by [234]. The simplest approach for string formation consists in ad-hoc clustering, in which vehicles do not deliberately seek out other CACC-equipped vehicles. In this case, the higher the CACC-equipped vehicles penetration rate, the more efficient this approach is as there are statistically more CACC-equipped vehicles following each other. The interest of ad-hoc vehicles clustering is negligible at low market penetration rates.

CACC string formation strategies can also rely on more developed local coordination methods. The idea is to instruct equipped vehicles that are close to each other to speed up or slow down in order to form a cluster. A still openly debated point is whether or not the benefits of clustering are greater than the losses due to coordination, e.g., acceleration or deceleration and lane changes. This issue is addressed in the COMPANION project led by Scania [151]. It appears that the amount of fuel saved by a truck catching up a platoon ahead depends on the initial distance to the platoon and the distance to the destination. Hence, as for ad-hoc vehicle clustering, local coordination strategies are more energy-efficient at high penetration rates. The main challenges to local coordination consist in determining the vehicles' positions with a great precision, while considering the traffic conditions, road slopes, etc. This kind of approach gives rise to privacy concerns as they may need to broadcast identifying information about the vehicle to catch up. Finally, it is clear that full autonomous vehicles, i.e. CAVs, represent a geat opportunity for local coordination implementation as they prevent drivers from having to change lanes to join a cluster.

Another vehicle clustering strategy consists in global coordination, i.e. an approach that coordinates vehicles with similar origins and destinations in order to form a cluster before they enter the highway [145]. Ideally, vehicles' routes and speed profiles are adjusted to arrive at the same time at the highway entry points. This poses a significant challenge because of the uncertainty of road traffic, and requires long-range communication. In practice, it is likely that this kind of approach will make CACC-equipped vehicles wait before enough vehicles have gathered to cluster together and enter the highway. Through this approach, the main issue is the waiting time before departure, which is difficult to get accepted, especially for short trips. Nevertheless, global coordination strategies can be a good alternative at low penetration rates, when ad-hoc clustering and local coordination approaches are inefficient.

CACC string dissolution strategies also require special attention in order to avoid creating new traffic problems. According to [234], a vehicle can leave a CACC string by making a lane change without decelerating, or by braking first to deactivate the CACC function. In the future, research on CACC string dissolution

approaches needs to be further investigated, especially in unusual cases, such as when multiple consecutive vehicles leave at the same exit. This would require a very high precision, which could be provided by CAVs.

The potential benefits of CACC have already been investigated and quantified through simulations [256] and real-world experiments [182]. In real traffic conditions, [182] indicates that CACC is able to reduce gap variability, and to handle unequipped vehicles cutting in and out. The authors also demonstrate that CACC has a shorter response time and a better string stability than ACC. This confirms the potential for a CACC system to attenuate disturbances, and improve highway capacity and traffic flow stability.

Despite the fact that CACC offers interesting prospects in terms of energy efficiency, very little research has been done to explicitly improve the ecological aspect of the problem. In [273], an approach aiming at minimizing the platoon-wide energy consumption and pollutant emissions at different stages (sequence determination, gap closing and opening, platoon cruising with gap regulation, and platoon joining and splitting) of the CACC system operation is proposed. In comparison with an existing CACC system, the results show that an eco-CACC alternative may reduce the global energy consumption by 1.45% during the formation of a platoon, and by 2.17% during platoon joining phases. As indicated previously in Section 1.2.3, the benefits of vehicle clustering are much higher [172] in comparison with a scenario in which no cooperative control is implemented.

Note that several incentive strategies can be imagined to develop CACC in the future, e.g., transfer payments from the following vehicles to the lead vehicle as they do not all equally benefit from clustering [234], use of managed lanes with pricing strategies [216], etc.

As with vehicle platooning, a limit must be placed on the length of CACC clusters for many reasons, e.g., safety, performance limitations, and integration with conventional vehicles. The main reason for this limit lies in the need to provide sufficient lane-changing gaps for unequipped vehicles. According to [234], the range of the wireless V2V communication system is not the limiting factor anymore as it reaches more than 300 m.

CACC systems raises the question of vehicles clustering within a string. In fact, the simplest approach is to add vehicles in the rear as they arrive. For safety reasons, the heaviest vehicles should be at the front, especially if there are trucks in the string. However, this complicates the string formation and dissolution problems, and may reduce passengers comfort in light-duty vehicles. Another option is to group vehicles by destination. This would reduce the number of maneuvers during the string formation and dissolution, thereby ensuring smoother speed profiles, improved energy efficiency, and traffic flow [234].

Finally, CACC offers huge opportunities in terms of energy efficiency, through-

put, safety, and customer comfort. This can even be enhanced by the development of CAVs, which are fully autonomous. CACC is also compatible with semi-autonomous vehicles, in which the driver needs to control the steering but not the speed of the vehicle, for example. However, this scenario would be less efficient because of human factors such as drivers' reaction time and lack of precision. Drivers would also need a thorough understanding of how CACC works. V2V CACC seems to produce the greatest benefits on highways, while V2I/I2V CACC opens the door to new alternatives in urban environments, especially at intersections. In the future, several challenges regarding CACC string formation and dissolution will have to be met for a large-scale development of CACC. According to [62], the first step in the deployment of CACC systems is to establish efficient and robust communications under highly dynamic environments. Additional issues would also need to be addressed. These include, inter alia, the legal aspects of crashes caused by failure of the system, users' privacy and security, technology certification, and users' training in the case of vehicles that are not fully autonomous. According to [98], future developments of CACC systems should pay special attention to vehicle and string stability with sufficient robustness margins.

Lane Change and Merge

Lane change and merge (into a highway from an on-ramp or exiting to an-off ramp) represent a complex problem, which can be explained by its combinatorial nature and the lack of information about the average speed on the different lanes [229]. Some examples of lane change and merge maneuvers are shown in Fig. 1.7. CAVs offer promising prospects for overcoming the difficulties related to this problem by using V2V communication to anticipate the intention of neighboring vehicles and estimate the traffic speed in each lane. The knowledge of the lanes state in advance could greatly improve eco-routing and eco-driving algorithms for CAVs by making much more judicious and smooth lane changes. For example, [131] proposes a control framework aiming at improving the energy efficiency and the travel time. In this approach, the authors anticipate the behavior of surrounding vehicles to change lane and adjust their speed. Note that in case of lane reductions and moving bottlenecks in congested situations, the speed of the bottleneck and the speed limit play an important role in terms of energy efficiency, traffic flow rate, average speed, and traffic safety [150].

In addition to the benefits brought to individual vehicles, anticipative lane selection and merging could also have a positive impact at a larger scale, by improving the overall energy efficiency through reduced risks of phantom jam, and smoother velocity trajectories, as indicated by [220]. These global benefits could be even greater if the vehicles cooperated, i.e. considered the impact of their decisions on their neighboring vehicles, and behaved in a way that optimizes the

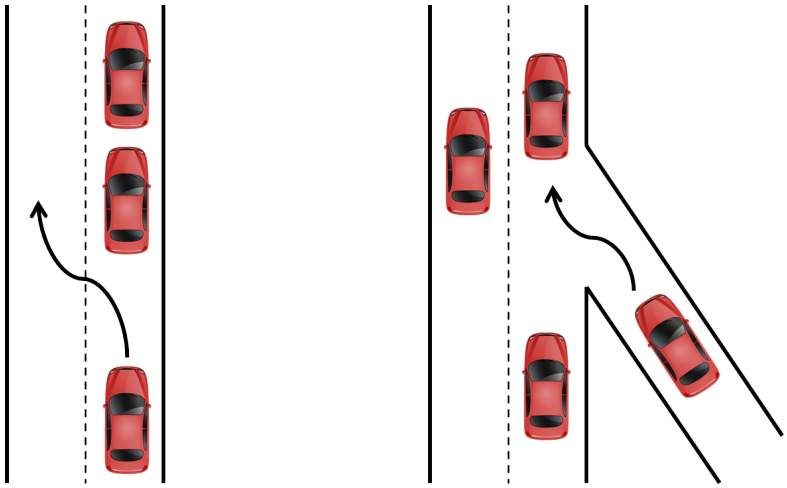

Figure 1.7: Examples of lane change and merge maneuvers.

"common good". In this sense, the vehicles would not act as independent entities, but as elements of a whole whose objective is the overall minimization of energy consumption [229]. This cooperative lane change and merge problem, with "common good" considerations, can be addressed in two different ways:

- by implementing a collaborative distributed control, in which vehicles optimize their own behavior and share their intentions [189, 166];
- by implementing a centralized control, in which the problem is solved at once for a group of cooperative vehicles.

In [68], the authors propose to compare these two approaches in a multi-lane environment. The results indicate that both approaches outperform the classic non-collaborative decentralized controller, i.e. when every vehicle optimizes its behavior to improve its "individual gain". It appears that the centralized algorithm returns the best solutions but its computation time is less suitable for real-time implementation.

In practice, several cooperative lane change and merge strategies can be established. An approach based on cooperative V2V negotiation is presented in [169]. In the same vein, the method presented in [156] consists in the use of transferable utility games, in which gaps in traffic are created in exchange for monetary compensation. In other words, vehicles can pay to change lane faster and reduce their travel time. The problem is solved using Nash bargaining theory, and the results reveal that this kind of approach can help reach win-win situations.

Only a few studies have evaluated the energy savings of cooperative lane change and merge. One of them is presented in [16]. The authors propose a cooperative

strategy that considers vehicles in current and target lanes during lane changing phases. This approach is compared with the traffic model MOBIL, and traffic simulations reveal that the cooperative approach improves merge time and rate, wait time, fuel consumption, average velocity, and flow at the cost of a slightly increased travel time. Similarly, [244] proposes an extended CACC approach adapted to CAVs, which also ensures lane changes. The authors indicate that the system improves traffic flow, and is also supposed to reduce fuel consumption and CO2 emissions.

Just like for other cooperative vehicle control strategies, the V2V communication delay represents a major issue in cooperative lane change and merge approaches. Most of the works on this topic neglect this aspect of the problem. In [11], a cooperative lane change protocol that integrates the impact of V2V communication delay is proposed. The algorithm considers bounding boxes around the vehicles in order to determine the risk of collision. Experiments through physical test drive and simulation reveal that V2V communication systems with 10 Hz update rate are appropriate [114].

According to [219], efficient cooperative lane change and merge systems should perfectly integrate both vehicle-based radar data and GPS data transmitted through V2V communication. To enhance such systems, vehicles could also use the support of I2V communication. The authors also advocate the implementation of dynamic role assignment during lane change maneuvers, rather than fixed roles established prior to the maneuvers.

Cooperative Intersection Control

In urban areas, signalized intersections have a major impact on the energy consumption of vehicles due to braking, idling, and starting from stops. Currently, many TLS timings are scheduled offline, and are then deployed as fix timetables, that can vary over time, e.g., peak hours/rest of the day, week days/weekend days, etc. To reduce idling and improve throughput at intersections, loop-detectors can be installed, in order to trigger rules to override the pre-optimized timetables, or even to optimize the SPaT of the intersection under consideration online (cf. Section 1.3.2). For this reason, the states of traffic light signals generally cannot be known in advance with certainty. In such a scenario, it is possible to use historical data in order to estimate the probability of a green or a red over a future horizon [23].

CAVs offer promising opportunities to improve the energy efficiency at intersections [229]. In fact, their connectivity and automation features can be used to control them at intersections in a cooperative way, i.e. in a “common good” approach. As explained in Section 1.2.3, this can be achieved by CACC systems that improve the throughput by allowing coordinated vehicles starts, thanks to

I2V communication.

In the near future, it is conceivable that some urban areas may only be accessed by CAVs. In these zones where the penetration rate of CAVs would be 100%, traffic light signals as we know them today would not be needed anymore. For example, [39] proposes a framework that optimizes the speed profiles of two vehicles approaching an unsignalized intersection. The study aims at optimizing the travel time and smoothing the CAVs speed profiles for improved passengers' comfort, while ensuring safety constraints. The authors also investigate the effect of the range of the V2V communication devices, and indicate that increasing it up to a specific value is beneficial, but the optimal speed profiles do not change after this point. In [155], a cooperative framework that allocates priority at autonomous intersections based on transferable utility games is proposed. In this approach, vehicles can pay for intersection priority. In other words, winners (time buyers) pay losers (time sellers) in each game. Such strategies are promising as they takee into account the value of vehicles' time, and losers are compensated. The authors also indicate that the approach is robust to adversarial behavior. Similarly, [181] presents an approach based on a polling policy, and [242] proposes to generalize the classical queuing theory to develop slot-based intersections, similar to those commonly used in aerial traffic. The simulation results reveal that such autonomous intersections could double capacity and significantly reduce delays, compared to conventional intersections ruled by traffic light signals. According to [117], reservation-based intersection control systems could improve the energy efficiency by 50%. In fact, the energy consumption and the number of stops are greatly reduced in such systems [72, 71]. [71] indicates that the number of stops can be reduced 100 times, and the improvement in energy efficiency could reach 20%. [4] proposes an illustration, given in Fig. 1.8, of such an autonomous intersection, in which vehicles negotiate the "right of way" using V2V communication.

Figure 1.8: Cooperative intersection [4] [Published with permission of Elsevier].

More generally, a systematic literature review of intelligent intersection management systems for CAVs is proposed in [185]. The authors indicate that some works on this topic consider rule-based methodologies (40%), while others consider optimization methodologies (45%), and hybrid methodologies (11%). Currently, few works are based on machine learning approaches (4%). The authors also explain that the vast majority (93%) of the articles reviewed consider a CAVs penetration rate of 100%. To be more realistic, autonomous intersections should be compliant with mixed traffic (CAVs and conventional HVs), pedestrians, and cyclists. According to the authors, a promising research direction to achieve this objective is to use the feature of CAVs to collect environmental data and share them through V2V communication. Pedestrians and cyclists could also be spotted by fixed cameras or sensors installed at intersections, and their presence could be indicated to approaching vehicles through I2V communication. To go further, additional analysis and artificial intelligence open the door to pedestrians and cyclists intention prediction [45]. Continental is currently working on the development of smarter and safer mobility in cities. An illustration of the company's strategy to anticipate the presence of pedestrians and cyclists is given in Fig. 1.9.

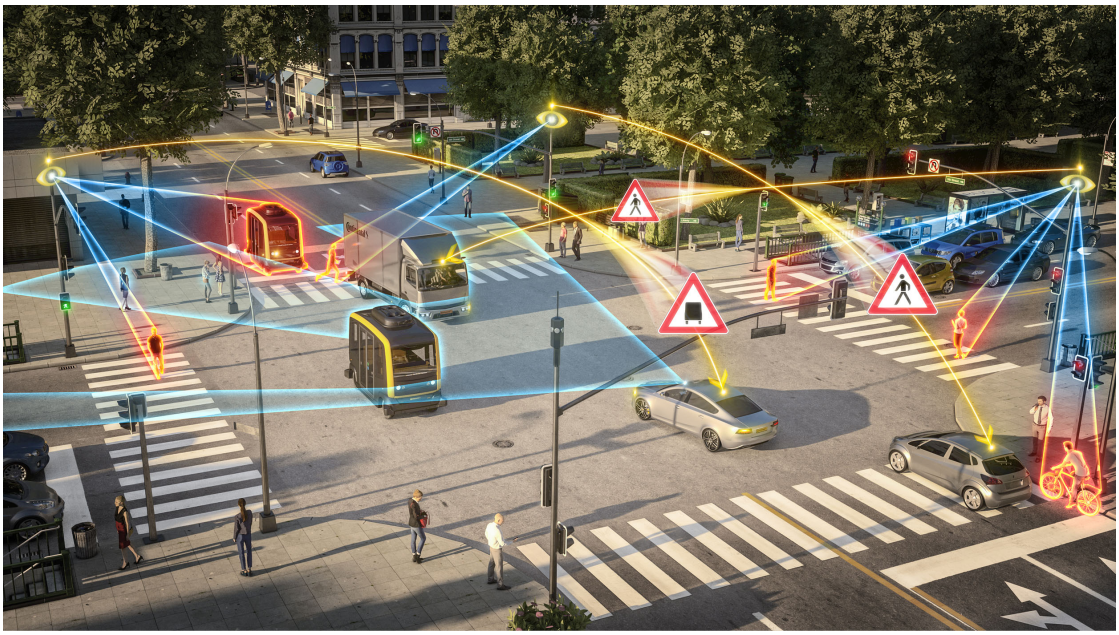

Figure 1.9: Strategy to increase safety by communicating hidden dangers to approaching vehicles and pedestrians at an intersection [45] [©2019 Continental. All rights reserved].

To go further, intelligent intersection management systems for CAVs can be used in conjunction with CACC systems for increased energy efficiency. According

to [127], this kind of approach could shorten the average travel time by 30% and reduce the fuel consumption by around 23% with respect to signalized intersections, in high traffic demand scenarios. Note that such approaches slightly sacrifice the energy efficiency to form platoons, which can be challenging in urban areas.

Traffic Harmonization

CAV technology is a great opportunity to improve traffic fluidity, safety, and energy efficiency. CAVs can optimize their behavior in order to improve their own benefits ("individual gain" optimization), or the global benefits of a group of cooperating CAVs ("common good" optimization).

A key point in CAV research is the management of mixed traffic (CAVs with conventional HVs), as the penetration rate of CAVs will certainly take time before it reaches 100% [161]. In mixed-traffic situations, coordinated and smoother motion of CAVs could also improve the energy efficiency of the surrounding non-automated vehicles, even at low penetration levels [229].

In mixed-traffic conditions, HVs have a strong influence on traffic flow as they increase the spread of shock waves in the downstream direction, causing stop-and-go waves [63]. As indicated in [90], CAVs can be designed to explicitly stabilize the traffic flow and actively dampen stop-and-go waves, which are particularly energy consuming. Such approaches based on Reinforcement Learning (RL) strategies are presented in [263]. On highways, stop-and-go waves may appear due to the presence of bottlenecks. In this kind of situation, [89] proposes to optimize the speed profiles of the CAVs upstream of the bottleneck in order to hedge against the backward shockwaves and smooth the traffic. According to the authors, the resulting speed harmonization greatly improves the energy efficiency (between 12% and 16%, depending on the traffic demand) and reduces environmental impacts. Similarly, [152] presents an approach that optimizes the speed profiles of CAVs in order to use them as moving bottlenecks. The authors indicate that this approach is especially beneficial when the density is low and medium, but its impact is limited in highly congested situations. The study conducted in [63] considers delays due to V2V communication, and confirms the robustness and the efficiency of such approaches to dampen down traffic waves. In [237], the potential benefits of traffic stabilization are quantified through field experiments with 20 to 21 HVs and 1 CAV ($\sim$ 5% of the vehicle fleet) traveling along a circular ring road, as represented in Fig. 1.10. Vehicle velocity and acceleration data are collected, and emissions are estimated using the MOVES model. The results reveal that the presence of a stabilizing CAV may improve the energy efficiency by 15%. The potential benefits on pollutant emissions are even greater (up to 73% reduction for nitrogen oxides). These results are promising, but it is essential to keep in mind that this approach represents a very much tamed scenario, and that less significant

impacts are expected when the density of vehicle is lower, or when there are several lanes, as the stop-and-go waves would be rarer and of lower intensity.

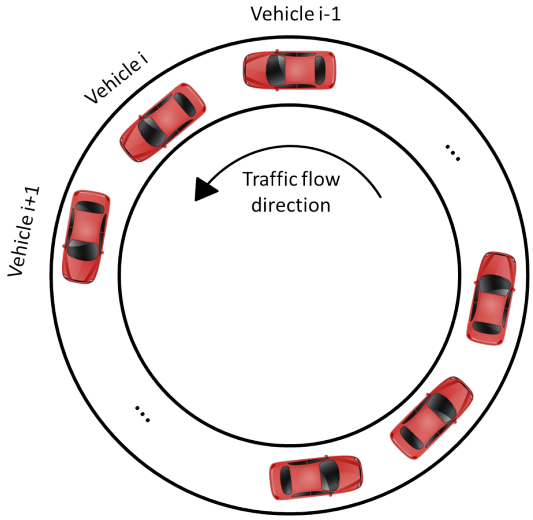

Figure 1.10: Vehicles traveling along a circular ring road.

The effectiveness of the harmonizing effect of CAVs varies according to traffic conditions and CAVs penetration rate. In [294], this phenomenon is analyzed under mixed-traffic conditions in an urban environment. The authors propose a control strategy for vehicles crossing signal-free intersections, described as follows:

- speed profiles are optimized for the CAVs in order to cross the merging zone in a limited time while minimizing the acceleration and comply with safety requirements;
- HVs are subject to priority rules.

The average fuel consumption is measured for different CAVs penetration rates, and different traffic conditions, and is compared with the energy consumption under TLS control, i.e. conventional signalized intersections. In the scenario proposed by the authors, the interest of CAVs in terms of energy efficiency appears to be obvious because the energy consumption decreases as the penetration rate increases. However, the strategy seems to lose its usefulness under heavy congestion. The authors indicate that the limit below which the approach is beneficial is the critical flow rate, which depends on the road capacity, the speed limit, the number of lanes, etc.

To go further, CAVs cooperation too can have a positive effect on traffic-flow performance and energy efficiency. For example, [256] studies the impact of

CACC for a highway-merging scenario from four to three lanes. The simulation results indicate that CACC can have a positive impact on traffic throughput, and can increase highway capacity near lane drops. This is particularly true in conditions with high-traffic volume and high penetration rate of CAVs performing CACC. The authors indicate that a low penetration rate could even lead to a degradation of traffic-flow performance. The impact of CACC on energy efficiency in a complex multi-lane mixed-traffic stream is analyzed in [165]. As indicated previously, the fuel consumption rate of the 100% CACC is reduced by 50% and the capacity could be increased by 49%, compared to the 100% ACC scenario. At 40% penetration rate, the capacity can still be increased by 15% to 19% when adapted control strategies are implemented. The study presented by [165] was performed at a simple freeway merging area, but it can easily be extended to more complex scenarios such as complete freeway or arterial corridors.

Note that other CAV-based strategies than CACC can also improve the overall energy efficiency under mixed-traffic conditions. For example, [268] analyzes the energetic impact in an urban environment of a speed advisory system that optimizes CAVs' speed limits in order to reduce idling at red lights. It appears that this approach not only improves the energy efficiency of CAVs equipped with this speed advisory system, but also benefits HVs and decreases their fuel consumption, with a compromise in average traffic flow and travel time. The authors indicate that the global fuel consumption decreases with the increment of CAVs penetration rate. The reason is that HVs are more likely to follow a smoother-moving CAV.

In conclusion, CAVs and their many cooperative strategies have a positive impact on the overall energy efficiency under mixed-traffic conditions. Their impact varies according to traffic congestion and CAVs penetration rate. In order to improve their impact on energy efficiency, CAVs could cooperate, and coordinate several strategies such as, inter alia, CACC, cooperative lane change and merge, autonomous intersection, and speed harmonization.

1.3 Ecological management of traffic flows

From a network-wide road traffic management perspective, the optimal control of single vehicles can be associated with the control of traffic flows. The main advantage of this type of control is that it allows for a much more macroscopic approach and ensures that the implemented strategy provides for the "common good" at the network level.

When it comes to the control of road infrastructures, microscopic traffic models and emission and energy consumption models may not be appropriate because the individual speed profiles of vehicles are generally not available. In fact, such

measurements represent a huge amount of data which is very difficult to obtain and process. Even if such data were available, the use of microscopic models for control approaches would pose the problem of numerical complexity as the computational load of such models increases sharply with the number of vehicles. Hence, ecological management strategies of traffic flows generally use macroscopic traffic models coupled with emission and energy consumption models to predict and optimize the behavior of road infrastructures, i.e. speed limits, TLS, etc.

1.3.1 Emission and energy consumption models

Macroscopic emission and energy consumption models use aggregate network or link-based traffic data (vehicle density, traffic flow, average speed) to estimate the environmental impact of traffic flows. The traffic data can be either measured by fixed sensors or Floating Car Data (FCD), or predicted using macroscopic fluid-based models, which are much faster than microscopic car-following models. In fact, the latter have enormous computation times at a network level because of the large number of simulated vehicles. Yet, is is essential to keep in mind that macroscopic traffic modeling is not able to reflect differences in microscopic drivers' behavior (e.g. sudden deceleration, merging, lane changing). When traffic is congested, these can result in shock waves causing traffic breakdown, that a macroscopic traffic model cannot depict [138].

Once the macroscopic traffic kinematics is determined, it can be associated with a microscopic emission and energy consumption model, in a mesoscopic framework. As a result, the average pollutant emission and/or energy consumption rates can be multiplied by the flow of vehicles to estimate the global environmental impact. In such a mesoscopic framework, these rates can be provided by emission and energy consumption models based on the average speed and the fleet composition [192]. Some models also consider additional parameters such as the slope, the driving conditions (highways, urban roads, stop-and-go traffic), the volume-to-capacity ratio (number of vehicles divided by the capacity of the link), etc. [29, 105, 187]. To go further, it is possible to consider an emission and energy consumption model that approximates vehicles' acceleration from macroscopic traffic data [288, 124], or that uses machine learning approaches.

As a result, such mesoscopic frameworks consist in coupling a macroscopic traffic model to a microscopic emission and energy consumption model that returns the average emission rate per vehicle. In this sense, they are referred to as meta-models in the following. In practice, many associations of models are possible. For complexity reasons, some are more suitable than others. In order to go large scale, the objective is to find a balance between accuracy and computation time, which depends mainly on the use of the framework (e.g. compatibility with control methods). For example, a question is whether the additional complexity

introduced by more precise traffic models significantly improves the accuracy in depicting the traffic behaviors that impact energy efficiency. Note that a microscopic approach to describe large-scale emissions and energy consumption would provide the best estimations but it would involve a lot of data that can be difficult to obtain and process, the need to precisely calibrate the model, and a sharp increase in computation times. However, this approach can be useful for offline validation purposes.

A complete review of macroscopic emission and energy consumption models is given in Section 3.3.1.

1.3.2 Road infrastructure control designs

In Sections 1.2.2 and 1.2.3, the CAVs control strategies, either for the optimization of their "individual gain" or the "common good", are based on V2V and/or I2V communications. In this section, we review the main infrastructure control strategies to reduce the environmental impact on a large spatial scale and for a large number of vehicles. Such approaches are based on V2I communication. In practice, they consist in collecting data from vehicles traveling in the road network (vehicle density, traffic flow, average speed, etc.), which is greatly simplified with the current development of connected vehicles. Then, the infrastructure actuators are controlled in order to optimize some metrics (global energy consumption, pollutant emissions, traffic throughput, average travel time, etc.). Usually, these actuators are speed limits and TLS duty cycles and offsets, but they can also include for example dynamic routing, which consists in redistributing the traffic demand over the network in a more efficient way by controlling the split ratios at intersections and bifurcations [198].

The objective of road infrastructure ecological management is to determine via an optimization method, at each control time step, the control inputs that minimize the traffic emissions and energy consumption. Note that some approaches do not explicitly minimize emissions or energy consumption. Instead, they tend to mitigate congestion and eliminate shock waves through density homogenization, vehicles interdistance equalization, etc. These methods are likely to indirectly reduce emissions and energy consumption as they reduce the number of accelerations and decelerations [19]. However, it is important to make careful analyses about the effect of congestion reduction on emissions and energy consumption. In fact, their relationship depends on many factors such as the speed of traffic [77].

For optimal CAVs control and maximum energy efficiency, the control of infrastructures, which is based on V2I communication, should be coordinated with the control of CAVs, which is based on V2V and I2V communications. In the following, the control strategies are classified according to the employed actuator. Their implementations are discussed both in highway and urban environments.

Variable Speed Limits

One main possibility in the control of road infrastructures is Variable Speed Limits (VSLs), which consists in imposing variable location-dependent speed limits across the road network. A general overview of the theoretical background and the main strategies of variable speed limits frameworks is proposed in [138].

Many VSLs approaches can be found in the literature. Some of them aim at improving safety [149, 279, 224], increasing road capacity and traffic flow [82, 100, 109], reducing pollution [290], and improving the energy efficiency [199]. Usually, all these approaches consist in harmonizing the traffic speed. Their control frameworks can therefore have a positive impact on several of these metrics [69], and multi-criteria optimization may not always be necessary [137]. VSLs strategies can be of particular interest in cases of poor visibility, especially under foggy conditions [295].

Most VSLs approaches are designed to control a highway environment. Some of them do not aim at explicitly reducing emissions and energy consumption (e.g. SPECIALIST method that eliminates shock waves [109]). An increasingly common approach is to use reinforcement learning methods to optimize speed limits. In [267], the authors propose to follow this approach to minimize the travel time. Other works are explicitly oriented towards energy efficiency improvement. Generally, they implement a multi-objective optimization that minimizes also the travel time so that unrealistic solutions like speed limits equal to zero are avoided. For example, [299] formulates a VSLs problem as a convex quadratic optimization problem in order to minimize the global energy consumption, which is derived from the average speed-based COPERT model. [162] proposes a VSLs control strategy based on the vehicular trajectory that minimizes the fuel consumption of a single vehicle under certain traffic conditions. Another framework is proposed in [290] to control VSLs on highways.

Some approaches have been designed to be compliant in urban environments. For example, [246] and [204] propose frameworks to evaluate the impact of various speed limits on emissions, energy consumption, and traffic congestion, without seeking to optimize speed limits. In [204], the authors use the microscopic traffic model DRACULA and a data-based emission and energy consumption model. A case study is conducted in Ghentbrugge, a neighborhood of the city of Ghent, Belgium. Similarly, [167] proposes to study the effect of speed limits in an urban network by implementing Intelligent Speed Adaptation (ISA). This system suggests, or imposes, speed limits to the driver through in-vehicle electronic devices. Note that ISA only informs road users of the speed limits, but does not calculate it independently for each vehicle. In other words, it is just a communication device. In this study, the authors consider the speed limits as inputs of the simulation, i.e. they can vary with locations but are fixed over the simulation time period, and

are not optimized. Microscopic traffic models, such as DRACULA, highly increase computation times and are therefore very difficult to use in practice for control purposes. However, they are particularly adapted to evaluate the impact of various speed limits in offline frameworks. A few works propose approaches that are based on microscopic traffic models to perform VSL, but they are largely limited by the number of vehicles under consideration. For example, [137] presents an approach to maximize mobility, safety and environmental benefit.

In several works, the authors seek to dynamically optimize speed limits. Some of them do not consider explicitly the environmental aspect, such as [243] which aims at harmonizing the speed within the urban network and maximizing the outflows. Usually, ecological management strategies are based on multi-criteria objective functions in order to improve both the energy efficiency and the traffic performance, and avoid trivial solutions, e.g., minimum or maximum speed limits everywhere. [199] proposes to optimize the weighted sum of energy consumption and total distance traveled by road users, [55] minimizes the energy consumption and the total time spent by vehicles by implementing a method based on shock waves theory, and [51] considers the weighted sum of the energy consumption, the total time spent, the instantaneous travel time, and the total travel distance in a single road section. In [55], the authors propose a method based on shock waves theory to control speed limits in an urban area and optimize the energy consumption and the travel time. A hybrid approach proposed in [259] aims at controlling speed limits for mixed urban and highway networks in order to minimize travel time.

In most of the works presented above, the authors implement MPC strategies. Such approaches are valuable as MPC is compatible with the uncertainties of the traffic models, and it can handle non-linear and non-convex optimization. However, special attention must be paid to the computation time to make it tractable for real-time operation, especially when the control inputs are very numerous. To address this issue, MPC approaches can be parameterized to reduce the number of control inputs. In such frameworks, the number of parameters to optimize is smaller than the number of control inputs and the set of possible solutions is hence smaller. This results in faster computation times but also a loss of performance. For computation time issues, parameterized MPC is more suitable for real-time application than conventional MPC, but it still may be too slow, depending on the considered system, the parameterization, and the control time step. Finally, multi-start optimization algorithms can be implemented to improve the performance of the controller [199, 290].

Finally, machine learning strategies represent a promising opportunity for VSLs implementation as they could greatly reduce computation times. For example, an RL approach aimed at optimizing the total network throughput, the delay time,

and the emissions is proposed in [296]. In this work, the authors propose a case study conducted on the Sioux Falls network.

As mentioned previously, the efficiency of V2I communication-based VSLs approaches can be enhanced when coordinated with cooperative strategies based on V2V and I2V communications. For instance, CACC systems can be subject to VSLs control strategies for improved traffic fluidity and energy efficiency [234].

Traffic Light Signals Adaptive Control

In Section 1.2.3, we reviewed the use of V2V and/or I2V communication to control intersections, that can even be unsignalized when the penetration rate of CAVs reaches 100%. In this section, we address the use of V2I communication in order to control the TLS, i.e. control their cycle time, split time and offset, and improve the overall energy efficiency of the vehicles (HVs and CAVs) traveling in the network. Note that instead of using V2I communication (for HVs that are not connected for example), one may imagine a system with fixed sensors in order to count and locate vehicles. These sensors include loop detectors, proximity sensors, or cameras associated with image classification systems [133].

In this sense, many studies consider the control of TLS in order to maximize the bandwidth [93] and minimize the travel time [130, 106], without special consideration for pollutant emission and energy consumption. Several strategies aim at performing this function: Split, Cycle and Offset Optimisation Technique (SCOOT) [119], Sydney Coordinated Adaptive Traffic System (SCATS) [171], Real-time Hierarchical Optimized Distributed Effective System (RHODES) [183], Traffic-responsive Urban Control (TUC) [65], max-pressure [262], TRANSYT-7F, Synchro, PASSER, TSOP, etc. [93]. In [95], the authors formulate the signal timing control problem as a real-time convex optimization problem whose objective function is the weighted sum of the total travel distance, the density balancing and a regularization term that penalizes abrupt changes in the control dynamics. The density balancing term aims at homogenizing the density over the network. The algorithm is split into subproblems whose sizes are independent of the network size, thus allowing for scalability. Approaches based on machine learning techniques are more and more common for TLS control. For example, [276] proposes to use Knowledge Compilation theory to train an ANN. The controller selects the state of the TLS by observing the presence of vehicles in different regions of the incoming roads. In order to compensate for the lack of data and to take into account the unpredictable behavior of road users, some works propose approaches based on stochastic methods to control TLS [40, 78]. In practice, the main objective of the approaches reviewed in this paragraph, which do not explicitly consider the environmental impact, consists in reducing congestion by improving the throughput and reducing the delay. However, this can have a positive impact on the energy

consumption and pollutant emissions.

In addition, few TLS control strategies in urban areas explicitly consider the reduction of energy consumption. For example, [104] expresses the signal timing optimization as a MILP problem optimizing both the delays and the emissions. The authors consider the Link Transmission Model (LTM) and emissions are calculated as a function of the density of the links. Similarly, [197] proposes a meta-model that considers the analytical approximations of the travel time and the fuel consumption to solve the urban signal timing optimization using a simulation-based optimization algorithm. It is also more and more common to use RL methods to control TLS in an urban network. For example, [136] presents a framework that considers the microscopic dynamics of vehicles. The authors propose to approximate the energy consumption metric by the average number of vehicles stops, assuming that this performance index can be directly related to ecological issues. A more precise approach can be found in [238]. The authors propose to simulate the traffic dynamics through a microscopic traffic model, namely VISSIM, and to calculate the emissions by using the Comprehensive Modal Emissions Model (CMEM) emission and energy consumption model. A signal timings optimization is then conducted using VISGAOST, an optimization program based on the stochastic nature of genetic algorithms. Although the authors propose a case study on a road network composed of two suburban arteries, an online optimization based on this method is not possible because of lengthy calculation times. However, such methods can be implemented for offline optimizations.

It is very common to use MPC to implement TLS control frameworks. For example, [158] uses this approach in an urban traffic network. The authors consider a dynamic fluid-based meta-model associating the S traffic model and VT-micro to characterize emissions. The approach aims at reducing both congestion and emissions as the objective function considers the weighted sum of the travel time and the total emissions. A similar approach based on a gradient-based optimization approach is proposed in [125]. The authors consider an extension of the S traffic model. The optimization criteria is the weighted sum of the travel time, the total emissions, and the absolute difference of two temporally successive control inputs, in order to avoid abrupt variations.

On highways, the equivalent strategy, known as ramp metering, consists in regulating the traffic flow entering the highway at on-ramps. Many ramp metering strategies do not explicitly optimize emissions and energy consumption, but they aim at reaching a desired density. That is the case of ALINEA method, presented in [205], which uses a feedback law and the traffic density measured downstream from the merge area. Similarly, [212] presents an approach to balance the vehicle density on the freeway by formulating the optimization problem as a non-cooperative Nash game.

Some authors express the ramp metering control approach as an optimization problem aiming at explicitly reducing emissions and energy consumption. For example, [47] presents a multi-objective optimization based on a constrained Linear-Quadratic (LQ) control, minimizing both the travel time and the traffic emissions on freeways. [207] formulates the ramp metering control problem as a multi-objective nonlinear constrained optimization problem considering the same objective function. These metrics are calculated considering both the traffic in the on-ramp and in the mainstream. The emissions are calculated using an average speed-based model based on COPERT. The nonlinear optimization problem is solved with a specific version of the feasible direction algorithm: the derivative backpropagation method RPROP. A specific feature of this work is that the authors consider two classes of vehicles (cars and trucks) individually controlled by the optimization process. An overview of ramp metering algorithms can be found in [206].

For optimal energy efficiency and improved throughput, both V2V/I2V and V2I communication-based approaches should be coordinated, i.e. a bi-directional CAV-infrastructure communication should be proposed [282, 54, 94]. For example, [282] presents an approach that combines TLS control and eco-driving in a 100% CAVs environment. The objective of this study is to optimize the TLS timing and the vehicles' arrival time at the intersection in order to reduce the total travel time and the overall energy consumption. The results reveal a significant improvement of energy efficiency and traffic performance, both under constant and varying traffic demand conditions. As mentioned in Section 1.2.3, the communication range has a significant impact on the performance of such approaches: a wider communication range gives better results. In this study, it seems that the better results are obtained with a communication range of about 800m. The TLS cycle length is also of major importance, and the ideal length is 60s, according to the authors. In the same vein, [54] presents a strategy based on the same control actuators (traffic light offsets and recommended speeds) in order to maximize bandwidth along an arterial, which corresponds mainly to improved energy efficiency, lower idling time and number of stops. According to the authors, the impact on travel time mainly depends on the speed advisory. The results of this study show that this kind of approach outperforms other existing strategies, especially in comparison with TLS control and eco-driving when they are not simultaneously controlled. Also, the approach is particularly efficient under free-flow traffic conditions, and energy consumption is reduced without increasing travel time. TLS control can also be coordinated with CACC-enabled strategies. As indicated in Section 1.2.3, this could consist in arterial coordinated start, that coordinates the start of vehicles waiting at a red traffic signal when the signal turns green [160, 234]. To go further, one may also imagine a framework in which the TLS offsets are optimized in order

to minimize the idling of CACC strings [164].

It is also possible to coordinate two control strategies that are both based on V2I communication. For example, [53] introduces a strategy that maximizes bandwidth along an arterial through TLS control and VSL. Here again, the objective is to improve the energy efficiency and reduce the travel time, and the authors indicate a potential dramatic reduction of energy consumption without increasing the travel time. Similarly, [168] and [289] propose approaches that control both TLS and VSLs to reduce energy consumption.

To improve the efficiency of TLS control strategies, the behavior of vehicles, especially HVs, should be considered and predicted. The coordination of multiple intersections, as in bandwidth maximization approaches, also opens the door to further improvement of both the energy efficiency and the traffic performance [282]. Also, such systems need to be robust and adaptable to any type of intersection and network in order to be deployable on a large scale [54]. Finally, it would be interesting to analyze the system response to a traffic demand much higher than the network capacity [53].

Coordinated speed limits and traffic light signals control

To improve the results of road-based control, it is possible to coordinate road-based actuators such as speed limits and signal timing control.

For freeways control, [110] proposes a method to optimize the total travel distance, without considering emissions and energy consumption. The authors develop an MPC framework, in which the control inputs are speed limits and ramp metering. Other authors have used coordinated speed limits and signal timing control to reduce emissions and energy consumption. For example, [289] optimizes the travel time, the fuel consumption, and NO_X emissions via MPC. A very similar approach is presented in [168]. The authors also use MPC to control both ramp metering and speed limits on a highway section, and the objective function is the weighted sum of travel time and total emissions. A specific feature of this work is that multiple classes of vehicles are considered.

A problem to study in an urban environment is bandwidth maximization along an artery. Assuming that all the traffic lights have a common cycle, the problem of bandwidth maximization consist in maximizing the vehicle throughput along the artery under study, by traffic lights offset control. Usually, the actuators are only the traffic light signals offset, like presented in [178] in which the authors express a nonlinear optimization problem and convert it to a MILP. The bandwidth maximization problem optimizes the flow of vehicles but does not explicitly reduce the emissions and energy consumption. Therefore, [53] proposes to formulate an optimization problem in which the objective function contains also terms approximating the travel time and the energy consumption. None of the bandwidth

maximization strategies presented is based on a traffic model. Hence, they work best in steady-state under-saturated traffic conditions.

Dynamic routing

Another solution to reduce emissions and energy consumption is to use dynamic routing. This method consists in redistributing the traffic demand over the network in a more efficient way by controlling the split ratios. In practice, the controller predicts the optimal routes for the main traffic flow directions, and the associated recommendations are communicated to the road users by the mean of in-vehicle devices, radio, or variable message signs [252].

In the literature, the control objective of dynamic routing problems is usually to reach system-optimum or user-equilibrium. The system-optimum corresponds to the minimum travel time and the user-equilibrium is characterized by a density distribution for which all used routes between the same origin-destination pair have the same travel time [283].

Dynamic routing could also be used to directly reduce emissions and energy consumption. For example, [173] proposes a real-time en-route diversion control strategy that minimizes the travel time, total emissions and fuel consumption. The route recommendation provided by variable message signs is considered as the control variable. The split ratios are calculated from the route recommendation considering a drivers' compliance rate which is supposed to be known. The route diversion control uses MPC based on a parallel Tabu Search algorithm.

Emission pricing can also be used as a dynamic routing method aiming at influencing route selection in order to reduce emissions and energy consumption. This method can be static or dynamic. Dynamic road pricing studies based on emissions and energy consumption are reviewed in [272].

1.4 Summary

CAVs offer huge opportunities in terms of energy efficiency, pollutant emissions, throughput, safety, and comfort improvement because of the possibilities regarding the certainty of predictions of their behavior and the precision of their powertrain control. A first approach to reduce their energy consumption consists in the development of simple rule-based control strategies. However, these are usually not sufficient and optimization-based strategies appear to be necessary. Such strategies involve the need of precise and reliable energy consumption models, accurate traffic models for prediction purposes, performing optimization algorithms, as well as fast and long-range communication devices.

One first layer in the optimal control of CAVs corresponds to route planning

(or eco-routing) and motion planning (or eco-driving) strategies based on V2V and I2V communications. In this case, the vehicles are performing "individual gain" optimization. These approaches are more efficient when the CAVs penetration rate is high, because the predictions are more reliable and the need for guessing is reduced. Overall, the more knowledge a CAV has about its in-trip and final trip constraints before its departure, the more effective this kind of approach is. Some uncertainties remain regarding the consideration and the prediction of HVs' aggressiveness.

Another layer in the optimal control of CAVs is the development of cooperative strategies between CAVs in order to improve the overall energy efficiency. These approaches are also based on V2V and I2V communications, but vehicles are here considering the impact of their decisions on the behavior and the energy consumption of other vehicles, i.e. vehicles are performing a "common good" optimization. These control strategies include vehicle platooning, CACC, lane change and merge, and cooperative intersection control. For an optimal control, these cooperative strategies should perfectly integrate both vehicle-based radar data and GPS data transmitted through V2V communication. Also, CAVs can have a harmonizing effect on the speed of the surrounding traffic, especially in case of cooperating CAVs. This harmonization appears to have a beneficial impact on the global energy consumption, but it is difficult to estimate because it depends on the CAVs penetration rate, on traffic congestion, and on the network architecture.

Finally, one last layer consists in the control of infrastructures, especially TLS and VSL, which are based on V2I communication. These approaches are compatible with HVs, but the potential gains are greater with CAVs because they are more precise and have much shorter reaction times.

Based on the works reviewed in this chapter, the orders of magnitude of the gains in energy efficiency offered by the different control strategies are summarized in Table 1.1. These values are to be taken in perspective as the proposed control strategies are highly dependent on traffic conditions, CAVs penetration rate, network architecture, etc. It is essential to note that coordinating complementary control strategies seems particularly promising to improve the overall energy efficiency. In this sense, coordinated VSLs and TLS approaches for example could reduce the energy consumption by up to 40%. Some directions have already been investigated in the literature:

- cooperative intersection control and CACC [127];
- VSLs and CACC [234];
- TLS control and eco-driving [282, 54];
- TLS control and VSLs [53].

- eco-driving and cooperation [144]

Table 1.1: Potential energy efficiency improvement of the control strategies presented in this chapter.

Control strategy			Potential energy efficiency improvement
CAVs control	Connected control	Eco-routing	10% – 15%
		Eco-driving	15% – 40%
	Cooperative control	Car following	20%
		Cooperative intersection	20% – 50%
		Harmonization effect	15%
Infrastructure control	Variable speed limits control		15%
	Traffic light signals control		15%

1.5 Main contributions of the dissertation

The areas covered in this work are depicted in green in Fig.1.11. The main contributions to traffic ecological management lie in the modeling and control strategies, and may be summarized as follows.

Firstly, a complete formalization of a macroscopic traffic model adapted to the urban environment is proposed. It includes a methodology for treating signalized intersections. To estimate the fuel consumption, this traffic model is associated with a macroscopic energy consumption model based on an ANN. The latter is calibrated using a microscopic physical energy model and data provided by a microscopic traffic simulator which is parameterized in order to be compliant with real-world urban FCD. The choice to use an ANN-based model is essentially justified by its performance at low average speeds. Macroscopic models are preferred for large-scale control because they are much faster to compute when the number of vehicles under consideration is large. They also have the advantage of considering the overall energy efficiency of traffic flows, which is the metric of interest for road network managers when it comes to traffic eco-management.

Then, experiments are conducted in order to evaluate the relationship between congestion and vehicles' energy efficiency, especially at steady state. The impact

of various speed limits on the macroscopic traffic variables (density, average speed, flow) is analyzed for different categories of road and traffic demand levels. Speed limits directly impact energy consumption and pollutant emissions as they affect the accelerations and average speeds through the network.

Finally, a parameterized model predictive control design comparing VSLs and signalized access control is proposed for improved environmental sustainability and traffic performance both in a synthetic urban area and in the peri-urban area at its boundaries. The traffic system is modeled using the microscopic traffic simulator SUMO, and a physical fuel consumption and NOx emission model is used to assess the vehicles' energy efficiency. Speed limits are controlled in closed loop through a Nonlinear Model Predictive Control (NMPC) approach, in which the traffic evolution and the future fuel consumption are respectively predicted with a macroscopic traffic model, namely the Cell Transmission Model (CTM), and the calibrated ANN. The results reveal that in transient phases between different levels of congestion, the closed-loop controller is faster to decongest the network, in an energy-efficient way, resulting in an improvement of the environmental sustainability and the traffic performance both in the controlled network, and at its boundary roads. Moreover, for the chosen set of parameters, it appears that the VSLs strategy leads to smoother density variations than the signalized access control, resulting in a more energy-efficient approach.

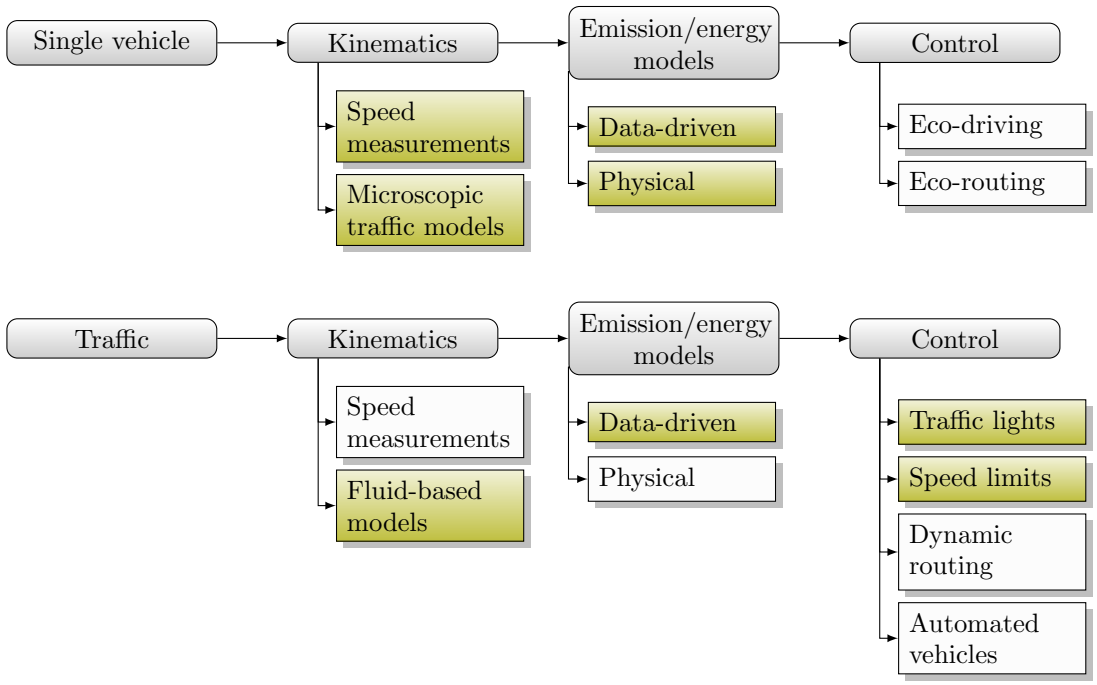

Figure 1.11: Diagram of the global approach for energy consumption and emissions modeling and control for single vehicles and traffic flow. The areas covered in this work are depicted in green.

Chapter 2

Models to simulate and predict traffic dynamics in an urban environment

Contents

2.1 Foreword

The first step of traffic eco-management strategies lies in the modeling of traffic dynamics. This step is crucial as it requires traffic models that are able to capture realistic traffic phenomena such as shock waves, physical queues and queue spillbacks [84].

In this chapter, we will introduce a microscopic traffic model, which is used to represent the dynamics of the vehicles in the road network. The model is calibrated with real-world FCD measured in an urban environment. A macroscopic traffic model will also be introduced. This latter is useful for prediction purposes as its computational burden is much lower.

The main challenges faced in this chapter correspond to the choice and the calibration of the microscopic model in order to be representative of real-world drivers' behavior, and the calibration of the macroscopic model so as to be able to depict the traffic dynamics of the microscopic model.

2.2 Microscopic models for traffic systems simulations

Vehicle movement data can be measured with sensors. In this sense, a solution that has been widely democratized is the use of road users' smartphone devices [247]. Methodologies can then be adopted to express the operation variables of vehicles from such data [253].

In order to implement control strategies, or to simulate a traffic system, it is necessary to introduce a microscopic traffic model. Such models describe the behavior of each single vehicle in the traffic flow. They usually correspond to car-following models that represent the longitudinal dynamics of vehicles. Lane-changing models can also be considered to represent their lateral dynamics [75]. One difficulty associated with these models corresponds to the calibration of the parameters.

2.2.1 State-of-the-art

Car-following approaches

Most of the microscopic traffic models correspond to car-following approaches, which were introduced in the 50s [86, 30]. Such models aim at describing the longitudinal dynamics of vehicles by characterizing at every time step all vehicles' position and speed. The drivers' decision to accelerate or to brake depends on their own speed and on the position and speed of the leading vehicle immediately

ahead. The acceleration $a_p^{\text{veh}}(k)$ of a vehicle p at time step k is defined as a function of the speed of the leading vehicle $v_{p-1}^{\text{veh}}(k)$, the speed difference $\Delta v^{\text{veh}}(k)$ and gap $s^{\text{veh}}(k)$ between the leading and the following vehicles, as well as some constant parameters denoted θ [22].

$$a_p^{\text{veh}}(k) = \frac{v_p^{\text{veh}}(k+1) - v_p^{\text{veh}}(k)}{\delta_t} = f(v_{p-1}^{\text{veh}}(k), \Delta v^{\text{veh}}(k), s^{\text{veh}}(k), \theta) \tag{2.1}$$

where δ_t denotes the time step duration.

In this work, we assume that all vehicles are identical, and their length is denoted l_{veh}. An illustration of the notations is proposed in Fig. 2.1, in which a following vehicle in $x_p^{\text{veh}}(k)$ is traveling at speed $v_p^{\text{veh}}(k)$ behind a leading vehicle in $x_{p-1}^{\text{veh}}(k)$, traveling at a speed $v_{p-1}^{\text{veh}}(k)$.

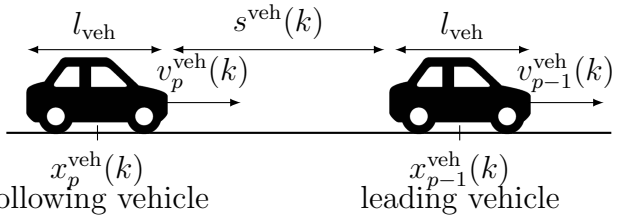

Figure 2.1: Representation of the car-following model paramaters.

The variables $\Delta v^{\text{veh}}(k)$ and $s^{\text{veh}}(k)$ are defined as

$$\Delta v^{\text{veh}}(k) = v_p^{\text{veh}}(k) - v_{p-1}^{\text{veh}}(k) \tag{2.2}$$

$$s^{\text{veh}}(k) = x_{p-1}^{\text{veh}}(k) - x_p^{\text{veh}}(k) - l_{\text{veh}} \tag{2.3}$$

In the literature, some works go further and consider as additional inputs of the model the speed of a group of several leading vehicles instead of one single leader [116].

Most car-following approaches can be categorized into the following strategies [75]:

- Stimulus–response models, which are mainly based on the speed difference between the leader and the following vehicles [87]. Such models may lack precision and realism in certain free-flow situations with large distance headway.

- Safety-distance or collision-avoidance models, which assume that drivers react to the headway distance instead of the speed difference [148].

- Reference-signal models, which introduce signals that the drivers are supposed to track. These can for example correspond to the desired speed or space headway [251].

- Psycho-physical models, which include human factors and aim at characterizing the impact of human perception on car-following models [25]. This is due to the fact that drivers' behavior is not always optimal, they do not continuously react to stimuli, they have different driving styles, etc.

It is essential to bear in mind that the use of a microscopic traffic model, especially in order to estimate emissions and energy consumption, requires a precise calibration of model parameters. An example of methodology to perform such a parameters calibration can be found in [126]. The authors emphasize on its benefits in terms of speed and acceleration estimation.

In the following, we focus on three car-following models that are widespread in the literature [22], namely Krauss, the Intelligent Driver Model (IDM), and Wiedemann.

Krauss model

The default model of the microscopic traffic simulator SUMO [170] is an extension of the Krauß car-following model introduced in [141]. It consists in letting vehicles drive as fast as possible while ensuring safety conditions, i.e. vehicles adjust their speed in order to always be able to avoid a collision if the leading vehicle starts braking. At time step k, the safe speed v_p^{safe} of the following vehicle in $x_p^{\text{veh}}(k)$ is defined as follows

$$v_p^{\text{safe}}(k) = v_{p-1}^{\text{veh}}(k) + \frac{s^{\text{veh}}(k) - s^*(v_p^{\text{veh}}(k))}{\frac{v_{p-1}^{\text{veh}}(k)+v_p^{\text{veh}}(k)}{2b_{\max}} + \tau} \tag{2.4}$$

Parameters $b_{\max}$ and τ denote respectively the vehicles maximum deceleration and the drivers' reaction time. The desired dynamical distance, or desired gap, s^* corresponds to the gap when following other vehicles under steady-state traffic conditions. In Krauss approaches, it is usually defined as

$$s^*(v_p^{\text{veh}}(k)) = v_p^{\text{veh}}(k)\tau + s_0 \tag{2.5}$$

where s_0 denotes the minimum gap at complete standstill, which corresponds to the minimum distance between vehicles, i.e. the distance between vehicles in dense jam situations.

In order to take into account the constraints regarding the maximum speed allowed $v_{\max}$, the vehicles' acceleration capabilities, and the safe speed, the desired

speed $v_p^{\text{des}}(k)$ of the following vehicle is defined as

$$v_p^{\text{des}}(k) = \min\left\{v_{\max}, v_p^{\text{veh}}(k) + a_{\max}\delta_t, v_p^{\text{safe}}(k)\right\} \tag{2.6}$$

where $a_{\max}$ denotes the maximum acceleration. Note that the maximum speed allowed $v_{\max}$ characterizes the speed limits, but also the environmental constraints, e.g. red traffic light signals.

Finally, the speed of the following vehicle is updated as follows

$$v_p^{\text{veh}}(k+1) = \max\left\{0, v_p^{\text{des}}(k) - \eta\right\} \tag{2.7}$$

where η is a random perturbation that is introduced to allow for deviations from optimal driving.

The SUMO-extended Krauß model proposes to slightly modify this model in order to handle different deceleration capabilities among the vehicles, and to adapt the safe speed calculation when using the Euler-position update rule.

Intelligent driver model

The IDM was introduced in [251]. At time step k, the IDM calculates the acceleration $a_p^{\text{veh}}(k)$ of the following vehicle using the following ordinary differential equation

$$a_p^{\text{veh}}(k) = \frac{v_p^{\text{veh}}(k+1) - v_p^{\text{veh}}(k)}{\delta_t} = a\left[1 - \left(\frac{v_p^{\text{veh}}(k)}{v_{\max}}\right)^{\delta} - \left(\frac{s^*(v_p^{\text{veh}}(k), \Delta v^{\text{veh}}(k))}{s^{\text{veh}}(k)}\right)^2\right] \tag{2.8}$$

where δ denotes the acceleration exponent. The IDM defines the desired dynamical distance s^* as

$$s^*(v_p^{\text{veh}}(k), \Delta v^{\text{veh}}(k)) = s_0 + \max\left\{0, v_p^{\text{veh}}(k)\tau + \frac{v_p^{\text{veh}}(k)\Delta v^{\text{veh}}(k)}{2\sqrt{a_{\max}b}}\right\} \tag{2.9}$$

where s_0, τ, $a_{\max}$, and b are IDM parameters denoting respectively the minimum gap at complete standstill, the time headway, the maximum acceleration, and the comfortable deceleration.

Wiedmann model

The Wiedemann model [275] is a psycho-physical car-following model used in the microscopic traffic simulator VISSIM [73]. It distinguishes four driving situations

1. free-flow

2. approaching slower vehicles
3. car-following near steady-state equilibrium
4. critical situations requiring braking action

The thresholds between each situation can be characterized by the distance and speed differences between the leading and the following vehicle. In each situation, different acceleration functions (described in Eq. 2.1) are considered. In practice, this corresponds to different reactions from the drivers to the stimuli generated by the leading vehicle, depending on the situation [298].

2.2.2 Comparison and ability to capture stop-and-go waves

In the literature, several works have compared the performances of car-following models [260, 196]. They have for example highlighted the importance of using models that take into account the drivers' reaction time. In this work, many car-following models can be used to simulate the traffic dynamics. We decide to conduct a comparative study under stationary conditions of the three car-following models discussed above (cf. Section 2.2.1), without claiming to select the best model.

To be in a stationary situation, we propose to consider a 300-meter single-lane ring road with a 50 km/h speed limit, as represented in Fig. 2.2. Simulations are run in SUMO traffic simulator [170], with a density of vehicles varying from 2% to 93% of the maximum density ρ^{M}. In each simulation the speed profile of one vehicle is measured at a frequency of 1 Hz. The speed profiles generated with IDM, Krauss, and Wiedemann models are compared in Fig. 2.3

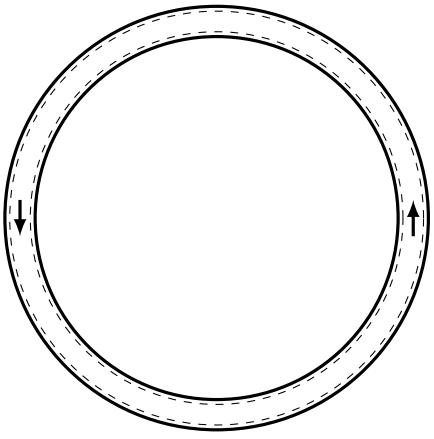

Figure 2.2: 300-meter single-lane ring road with a 50 km/h speed limit. The vehicles' speed profiles are measured at a frequency of 1 Hz.

(a) 2% of the maximum density. (b) 12% of the maximum density. (c) 23% of the maximum density.

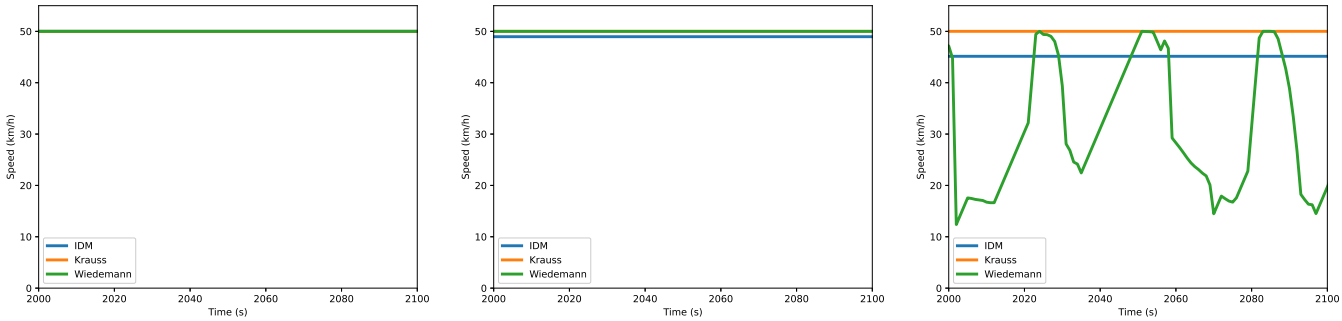

(d) 35% of the maximum density. (e) 47% of the maximum density. (f) 58% of the maximum density.

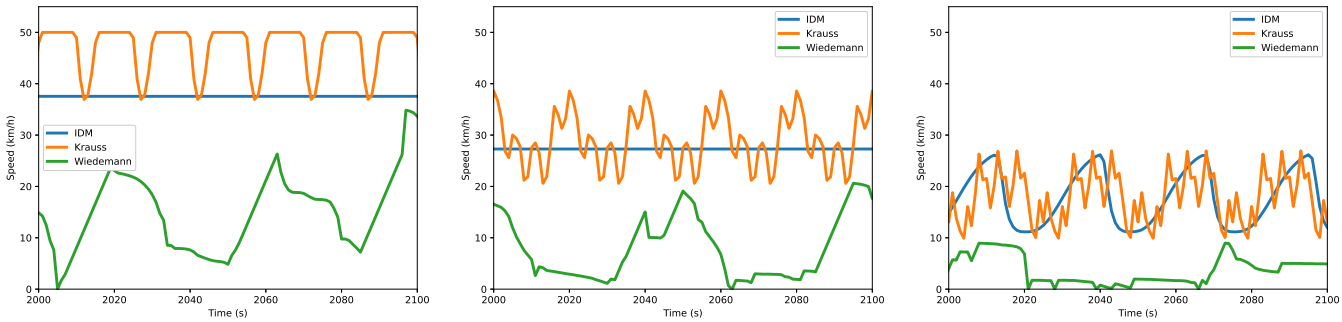

(g) 70% of the maximum density. (h) 82% of the maximum density. (i) 93% of the maximum density.

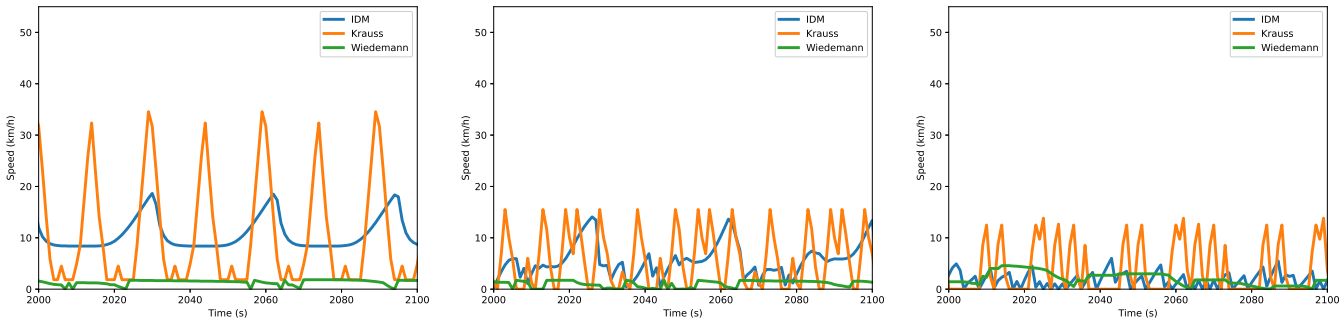

Figure 2.3: Speed profiles generated with IDM, Krauss, and Wiedemann car-following models on a 300-meter single-lane ring road with a 50 km/h speed limit, for various densities (from 2% to 93% of the maximum density ρ^{M}).

Simulations based on the IDM highlight several phases. First, for densities between 2% and 47% of the maximum density (Fig. 2.3a–2.3e), an increase of the density results in a decrease of the speed. In these cases, the speed remains constant. At a certain point (58% of the maximum density in Fig. 2.3f), the stop-and-go phenomenon appears, resulting in oscillating speed profiles. Finally, for densities higher than 82% of the maximum density (Fig. 2.3h–2.3i), the regularity of the oscillations is lost and the variations of the speed profile seem chaotic.

With the Krauss model, the oscillations appear sooner (35% of the maximum density in Fig. 2.3d), and they become almost immediately chaotic. Yet, the average speed is very close to the one observed with IDM, whatever the density level. This highlights the similarity between these two models.

The simulations based on Wiedemann model return very different results from the other two models because of its psycho-physical nature. The vehicles slow down strongly from a density of 23% of the maximum density (Fig. 2.3c), and the average speed is much lower than the other two models, whatever the density level.

Any of these car-following models could be retained for the rest of this work. The IDM is chosen because of its ability to simulate different situations (lower speed without oscillations – regular stop-and-go waves – chaotic stop-and-go waves). An additional motivation for retaining the IDM is given in Section. 4.2.1 regarding the impact of the car-following model on the energy consumption curves. Note that the simulations in this section have been carried out with the parameters calibrated in Section 2.2.3 and SUMO default parameters. These parameters could be adapted to make the models more realistic and representative of a more or less aggressive driving style. This reinforces the idea that any model could have been chosen for the rest of the study.

2.2.3 Calibration of the car-following model

In order to calibrate the microscopic traffic simulator based on the IDM as accurately as possible, we use real-world driving data, collected in France. The motivation of using experimental data to calibrate the model's parameters lies in the fact that several values can be found in the literature, especially on highways or in urban areas [135]. These data are used to calibrate the maximum acceleration and comfortable deceleration parameters of IDM, i.e. $a_{\max}$ and b respectively. The accelerations and decelerations of 648 journeys made in French cities are recorded with the drivers' smartphones at a frequency of 1 Hz, resulting in 30682 data points. The measured accelerations and decelerations are shown in Fig. 2.4 in the form of a box plot. It appears that the maximum acceleration is close to 10 $\mathrm{m.s^{-2}}$ and the maximum deceleration is about -7.5 $\mathrm{m.s^{-2}}$. However, these points can be associated with unusual driving behaviors, other means of transportation (e.g., motorbikes), or even measurement errors because they are much higher than clas-

sical observed maximum accelerations. In order to reduce the influence of outliers, we decide to remove the 1% highest accelerations and the 1% highest decelerations. These boundaries are represented by the dashed red lines in Fig. 2.4. We deduce $a_{\max} = 2.4$ m.s^{-2} and $b = 2.8$ m.s^{-2}, which are of the same order of magnitude as the SUMO parameters (respectively $a_{\max} = 2.6$ m.s^{-2} and $b = 4.5$ m.s^{-2}), and are also consistent with maximum acceleration values deduced from real data and given in the literature [26, 43, 153].

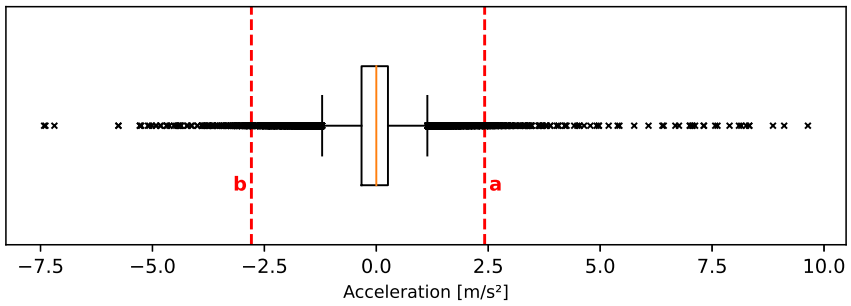

Figure 2.4: Real-world acceleration data of 648 journeys made in French cities and measured at a frequency of 1 Hz, resulting in 30682 data points. $a_{\max}$ and b delineate respectively the 1% highest accelerations and 1% highest decelerations.

Note that the calibration of the comfortable deceleration b is not of primary importance in the sense that vehicles can always perform emergency brakings (up to 9 m.s^{-2}) in order to avoid crashes, to stop at a red TLS, etc. Also, the impact of b on vehicles' energy consumption and pollutant emission is smaller than the one of $a_{\max}$, as vehicles' energy efficiency mostly depends on acceleration phases.

The other IDM parameters are set to standard values, namely $s_0 = 2$ m, $\delta = 4$, and $\tau = 1$ s [251]. The desired speed $v_{\max}$ corresponds to the speed limit, which is denoted V. Its maximum value in an urban area is considered to be 50 km/h. The descriptions and values of IDM parameters considered in this article are summarized in Table 2.1.

It is essential to note that the IDM has some shortcomings to capture real-world phenomena, such as the fact that the maximum vehicles' acceleration remains constant under all traffic conditions. According to [61], the exceeding of the real vehicle deceleration in case of emergency braking is another drawback. Also, the minimum desired gap can be not enough to guarantee safety in critical situations such as accidents for example. Finally, the IDM being a collision free model, it can lead to non-realistic deceleration to avoid collision. In terms of scalability of the traffic network, SUMO has a limited amount of memory and is restricted by the power of the CPU of the system. In practice, SUMO is able to cope with networks of up to 10,000 edges, which is not an issue in this study [140].

Symbol	Description	Value	Unit
$a_{\max}$	Maximum acceleration	2.4	$\mathrm{m.s}^{-2}$
b	Comfortable deceleration	2.8	$\mathrm{m.s}^{-2}$
s_0	Minimum distance between vehicles	2	m
$v_{\max}$	Desired speed	V	$\mathrm{m.s}^{-1}$
δ	Acceleration exponent	4	–
τ	Time headway	1	s

Table 2.1: Microscopic car-following IDM calibrated parameters.

2.3 Macroscopic models for prediction and control purposes

The macroscopic traffic dynamics can be measured with fixed or vehicle embedded sensors. These latter are based on FCD methods that use the drivers' smartphone devices for example. To complete this information, induction loops and cameras can be used to count the number of vehicles.

When this data is not available, or incomplete, or when it is necessary to predict the evolution of traffic for control purposes, dynamic fluid-based models that describe the evolution of traffic in the network as a fluid in a pipe can be used. Some overviews presenting this kind of models can be found in [74, 76, 261, 116].

Such approaches provide the traffic variables, i.e. the density $\rho(x,t)$, the speed $v(x,t)$, and the flow $\varphi(x,t)$, at given position x and time t. They consider the traffic speed as a function of x and t. Therefore, these models reflect the speed differences along links and provide a dynamic traffic speed.

2.3.1 State-of-the-art

Some macroscopic traffic models are reviewed in the following. They are all based on the following conservation law

$$\frac{\partial}{\partial t}\rho(x,t) + \frac{\partial}{\partial x}(\rho(x,t)v(x,t)) = 0 \tag{2.10}$$

Some of these models are continuous and others are spatially and temporally discretized. A distinction is made between first and higher-order models.

First-order models

- *Lighthill-Whitham-Richard model*

[154] and [223] assume that v depends only on ρ. Hence, the flow can be expressed as a function Φ of only ρ as

$$\varphi = \rho v(\rho) = \Phi(\rho) \tag{2.11}$$

The conservation law presented in (2.10) can then be expressed as

$$\frac{\partial}{\partial t}\rho + \frac{\partial}{\partial x}\Phi(\rho) = 0 \tag{2.12}$$

where Φ is a strictly concave C^1 function defined on $[0,\, \rho^{\mathrm{M}}]$ and satisfying

$$\Phi(0) = \Phi(\rho^{\mathrm{M}}) = 0 \tag{2.13}$$

The relationship $\varphi = \Phi(\rho)$ is called the fundamental diagram. The most common fundamental diagrams are listed in Table 2.2 [84]. The parameters w, φ^{M}, and v_0 denote respectively the backward wave speed, the maximum traffic flow, and a positive constant.

Fundamental Diagram	Expression
Greenshields [97]	$\Phi(\rho) = \rho v_{\max}\left(1 - \left(\frac{\rho}{\rho^{\mathrm{M}}}\right)^{p}\right), \quad p \in \mathbb{N}$
Greenberg [96]	$\Phi(\rho) = \rho v_0 \ln\left(\frac{\rho^{\mathrm{M}}}{\rho}\right)$
Underwood	$\Phi(\rho) = \rho v_{\max} \exp\left(-\frac{\rho}{\rho^{\mathrm{M}}}\right)$
California	$\Phi(\rho) = \rho v_0 \left(\frac{1}{\rho} - \frac{1}{\rho^{\mathrm{M}}}\right)$
Trapezoidal [48]	$\Phi(\rho) = \min\left\{\rho v_{\max}, \varphi^{\mathrm{M}}, (\rho^{\mathrm{M}} - \rho)w\right\}$
Triangular [188]	$\Phi(\rho) = \min\left\{\rho v_{\max}, (\rho^{\mathrm{M}} - \rho)w\right\}$

Table 2.2: List of most common fundamental diagrams.

• *Cell transmission model*

The Cell Transmission Model (CTM) [48] is a temporally and spatially discretized version of the Lighthill-Whitham-Richard (LWR) model based on the triangular or the trapezoidal fundamental diagram. The model is defined as

$$\begin{cases} \rho_i(k+1) = \rho_i(k) + \frac{\delta_t}{\delta_x}(\varphi_i^{\mathrm{in}}(k) - \varphi_{i+1}^{\mathrm{in}}(k)) \\ \\ \varphi_i^{\mathrm{in}}(k) = \min\left\{\rho_{i-1}(k)v_{\max},\, \varphi^{\mathrm{M}},\, w(\rho^{\mathrm{M}} - \rho_i(k))\right\} \end{cases} \tag{2.14}$$

where i and δ_x denote respectively the cell index and the discrete-space cell length. The variable $\varphi_i^{\text{in}}(k)$ is the traffic flow entering cell i during $[k\delta_t,\ (k+1)\delta_t]$.

- *Variable-length model*

In order to depict density evolution and track the congestion front, [36] proposes the Variable-Length Model (VLM) for highway traffic modeling. Illustrations are given on a closed ring road and on an urban road with traffic lights in [37].

The VLM is also a discrete version of the LWR model based on the triangular fundamental diagram. The idea is to model any road section with only two lumped cells that are variable in length: an upstream cell in free flow and a downstream congested cell. Consider a road section of length L, then the length of the free and the congested cells will respectively be $L-l$ and l.

The main advantage of the VLM is that it is based on only three state variables: density in the upstream free cell ρ_{f}, density in the downstream congested cell ρ_{c}, and position of the congestion front l. The model reads

$$\begin{cases} \dot{\rho}_{\text{f}} = [\varphi\text{in} - \Phi(\rho_{\text{f}})]\frac{1}{L-l} \\ \dot{\rho}_{\text{c}} = [\Phi(\rho_{\text{c}}) - \varphi_{\text{out}}]\frac{1}{l} \\ \dot{l} = \frac{\Phi(\rho_{\text{f}})-\Phi(\rho_{\text{c}})}{\rho_{\text{c}}-\rho_{\text{f}}} \end{cases} \tag{2.15}$$

where the interface flows $\Phi(\rho_{\text{f}})$ and $\Phi(\rho_{\text{c}})$, which correspond to the demand of the free cell and the supply of the congested cell respectively, can be expressed as

$$\begin{aligned} \Phi(\rho_{\text{f}}) &= \rho_{\text{f}} v_{\max} \\ \Phi(\rho_{\text{c}}) &= w(\rho^{\text{M}} - \rho_{\text{c}}) \end{aligned} \tag{2.16}$$

φ_{in} and φ_{out} are the inflow and outflow at the boundaries of the section of length L. They are defined as

$$\begin{aligned} \varphi_{\text{in}} &= \min\{D_{\text{in}},\ s_{\text{f}}\} \\ \varphi_{\text{out}} &= \min\{D_c,\ S_{\text{out}}\} \end{aligned} \tag{2.17}$$

where D_{in} and S_{out} are respectively the input demand and the output supply. D_c and s_{f} are

$$\begin{aligned} D_c &= \min\{\rho_{\text{c}} v_{\max},\ v_{\max}\rho^{\text{cr}}(v_{\max})\} \\ s_{\text{f}} &= \min\left\{w(\rho^{\text{M}} - \rho_{\text{f}}),\ v_{\max}\rho^{\text{cr}}(v_{\max})\right\} \end{aligned} \tag{2.18}$$

where $\rho^{\text{cr}}(v_{\max})$ is the critical density relative to $v_{\max}$. It is defined as

$$\rho^{\text{cr}}(v_{\max}) = \frac{w\rho^{\text{M}}}{v_{\max} + w} \tag{2.19}$$

[51] proposes to adapt the VLM to the urban environment by considering a binary variable α multiplying the boundary flows in (2.17) to model the behavior of traffic lights, as

$$\alpha = \begin{cases} 1 & \text{, if the traffic light is green} \\ 0 & \text{, otherwise} \end{cases} \tag{2.20}$$

• *Link transmission model*

[286] proposes the Link Transmission Model (LTM), which is a discrete version of the LWR model based on the triangular fundamental diagram, with only one cell per road. Therefore, computation times are reduced.

The LTM introduces the notion of cumulative vehicle counts. $N_{\text{up}}^{\text{tot}}(k\delta_t)$ and $N_{\text{down}}^{\text{tot}}(k\delta_t)$ are respectively the cumulative entering and exiting vehicle count of a given link at $k\delta_t$, based on given split ratios at intersections.

The maximum number of vehicles that can be sent by this link to the next one during time interval $[k\delta_t,\, (k+1)\delta_t]$ is

$$S_{\text{boundary}}(k) = N_{\text{up}}^{\text{tot}}\left((k+1)\delta_t - \frac{L}{v_{\max}}\right) - N_{\text{down}}^{\text{tot}}(k\delta_t) \tag{2.21}$$

The maximum number of vehicles that can leave the considered link during the time interval $[k\delta_t,\, (k+1)\delta_t]$ is

$$S_{\text{link}}(k) = \rho^{\text{M}} L \delta_t \tag{2.22}$$

The number of vehicles sent by the link to the next one is then simply

$$S(k) = \min\left\{S_{\text{boundary}}(k),\, S_{\text{link}}(k)\right\} \tag{2.23}$$

In the same way, the number of vehicles $R(k)$ received by the link is expressed as

$$\begin{cases} R(k) = \min\left\{R_{\text{boundary}}(k),\, R_{\text{link}}(k)\right\} \\ R_{\text{boundary}}(k) = N_{\text{down}}^{\text{tot}}\left((k+1)\delta_t - \frac{L}{w}\right) + \rho^{\text{M}} L - N_{\text{up}}^{\text{tot}}(k\delta_t) \\ R_{\text{link}}(k) = \rho^{\text{M}} L \delta_t \end{cases} \tag{2.24}$$

• *Queue models*

Queue models are interested in the length of the queues at the end of each link i. An example is the Berg-Lin-Xi (BLX) model, presented in [259] and [159]. An extension of the model is proposed in [157]. Like the LTM, the BLX model considers flows between the links.

The queue on link i is composed of N_i^q vehicles. When the traffic light is green, the number of vehicles entering cell i from the upstream cell during time interval $[k\delta_t,\ (k+1)\delta_t]$ is

$$\delta_t \varphi_i^{\text{in}}(k) = \max\left\{0,\ \min\left\{N_{i-1}^q(k) + \delta_t \varphi_{i-1}^{\text{in}}(k), S_i(k), \delta_t \varphi^{\text{M}}\right\}\right\} \tag{2.25}$$

where $S_i(k)$ denotes the available storage of link i at time step k, expressed in number of vehicles.

The queue length and the available storage can be expressed as

$$\begin{cases} N_i^q(k+1) = N_i^q(k) + \delta_t(\varphi_i^{\text{in}}(k) - \varphi_{i+1}^{\text{in}}(k)) \\ \\ S_i(k+1) = S_i(k) + \delta_t(\varphi_{i+1}^{\text{in}}(k) - \varphi_i^{\text{in}}(k)) \end{cases} \tag{2.26}$$

The total number of vehicles in link i at time step k can be determined as

$$N_i(k) = \rho^{\text{M}} L - S_i(k) \tag{2.27}$$

• *Summary*

The LWR model and its discrete variations, presented above, are simple first-order mathematical representations of the traffic inspired by fluid mechanics. They are based on fundamental diagrams that associate φ to ρ. These models are able to capture realistic traffic phenomena such as shock waves, physical queues and queue spillbacks [84].

However, first-order models based on the fundamental diagram are not sufficient to capture unstable traffic variations caused by the inertia of vehicles because they assume that v is always in equilibrium. Consequently, they have limitations in capturing complex traffic phenomena such as stop-and-go waves, capacity drops and phantom jams (formation of clusters of cars with high densities due to the driving style of road users [134]). These must be taken into account in order to best estimate emissions and energy consumption.

Second-order models

Second-order models have been developed in order to capture more realistic traffic behavior in congested areas. They still consider the equation for the conservation of vehicles presented in (2.10) and use the fundamental diagram to determine the steady state of the system, but they have an additional equation for the conservation of momentum.

• *Payne-Whitham model*

An example of a well known second-order model is proposed in [208]. The model has the following form

$$\begin{cases} \partial_t \rho + \partial_x(\rho v) = 0 \\ \partial_t v + v\partial_x v + \frac{1}{\rho}\partial_x(p(\rho)) = \frac{1}{\tau}(v_{\mathrm{e}}(\rho) - v) \end{cases} \tag{2.28}$$

where $v_{\mathrm{e}}(\rho)$ is the equilibrium speed given by the fundamental diagram, and $p(\rho)$ is analogous to the pressure in the fluid dynamics equations and depends on the density [210].

The anticipation term $\frac{1}{\rho}\partial_x(p(\rho))$ models the reaction of vehicles, i.e. acceleration or deceleration, to the variations of ρ. The relaxation term $\frac{1}{\tau}(v_{\mathrm{e}}(\rho)-v)$ models the tendency of vehicles to travel from v towards $v_{\mathrm{e}}(\rho)$ within a time $\tau > 0$ that represents the time needed by the vehicles to adjust their actual speed to $v_{\mathrm{e}}(\rho)$.

The second equation of (2.28) is the acceleration equation. [274] proposes to simplify the model by considering $p(\rho)$ as a constant. Other expressions for this term exist, they are presented in [84], as well as the modeling of an additional viscous term in this equation.

• *Aw-Rascle-Zhang model*

[49] highlights some limitations of the Payne-Whitham model presented above. In particular, the model allows the vehicles to travel with negative speed.

To tackle this problem, [15] and [292] propose the following model

$$\begin{cases} \partial_t \rho + \partial_x(\rho v) = 0 \\ \partial_t(v + p(\rho)) + v\partial_x(v + p(\rho)) = 0 \end{cases} \tag{2.29}$$

where the pressure term p may be defined as

$$p(\rho) = \rho^\gamma, \quad \gamma > 0 \tag{2.30}$$

• *METANET model*

[180] presents the METANET model which is a discrete version of the Payne-Whitham model presented in (2.28). It reads

$$\begin{cases} \rho_i(k+1) = & \rho_i(k) + \frac{\delta_t}{\delta_x}(\varphi_i^{\mathrm{in}}(k) - \varphi_{i+1}^{\mathrm{in}}(k)) \\ v_i(k+1) = & v_i(k) + \frac{\delta_t}{\gamma_1}[v_{\mathrm{e}}(\rho_i(k)) - v_i(k)] \\ & + \frac{\delta_t}{\delta_x} v_i(k)[v_{i-1}(k) - v_i(k)] - \frac{\gamma_2 \delta_t [\rho_{i+1}(k) - \rho_i(k)]}{\gamma_1 \delta_x [\rho_i(k) + \gamma_3]} \end{cases} \tag{2.31}$$

and the authors propose the following fundamental diagram to define the equilibrium speed $v_{\mathrm{e}}(\rho)$

$$v_{\mathrm{e}}(\rho_i) = v_{\max} \exp\left[-\frac{1}{\gamma_4}\left(\frac{\rho_i(k)}{\rho^{\mathrm{cr}}}\right)^{\gamma_4}\right] \tag{2.32}$$

where $\gamma_1 - \gamma_4$ are model coefficients.

METANET was originally introduced to capture traffic phenomena on highways. The proceeding of flows between the segments is fully presented in [180].

Phase transition and higher-order models

Second-order models generally have higher computation times. Phase transition models are a good alternative to the extent that they behave like the classic LWR model when the traffic is free and like a second-order model when the traffic is congested. This allows to capture complex traffic phenomena while keeping reasonable computation times for free-flow traffic.

In [44], the following phase transition model is proposed

- For free flow traffic, the author considers the LWR model, presented in (2.12), with the Greenshields fundamental diagram (cf. Table 2.2, with $p = 1$).
- For congested traffic, v cannot be considered as a function only of the density anymore. In this case, the density-flow points are scattered in a two-dimensional region, based on the following second-order model

$$\begin{cases} \partial_t \rho + \partial_x(\rho v) = 0 \\ \partial_t q + \partial_x((q - Q)v) = 0 \end{cases} \tag{2.33}$$

  where q is the momentum, Q is a parameter of the road considered, and v is expressed as

$$v = \left(1 - \frac{\rho}{\rho^{\mathrm{M}}}\right) \frac{q}{\rho} \tag{2.34}$$

The associated hybrid fundamental diagram is shown in Fig. 2.5.

Finally, higher-order models exist but they are less appropriate for emissions and energy consumption estimation as their computation times are higher. An example of third order model, where the additional equation is for the variance of the speed, can be found in [111]. This method is useful to describe the increase of the speed variance just before traffic jams occur.

Network-wide extension

The traffic models presented above can be extended across a network. The junctions represent a very important part of the extended model. Basically, each junction can be reduced to a combination of simple merge and diverge junctions [84]. A complete overview of macroscopic node models can be found in [245]. The authors present macroscopic node model instances both for signalized and unsignalized intersections.

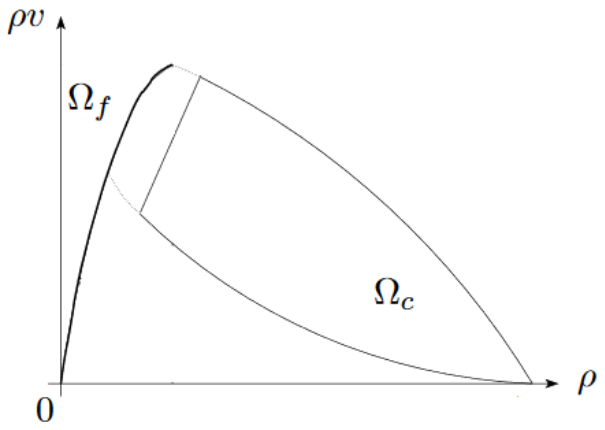

Figure 2.5: Fundamental diagram of the phase transition model, representing the free region Ω_f and the congested region Ω_c [44] [Copyright ©2002 Society for Industrial and Applied Mathematics. Reprinted with permission. All rights reserved].

In the case of the extended CTM, a fundamental diagram is associated with each link, each link being partitioned into uniform cells. An urban version of the CTM is proposed in [281]. The authors use turning ratios assigned to intersections and distinguish two possibilities. First, a cell preceding an intersection can be composed of one traffic light. Such cells have one unique queue, and all the vehicles merge into it. Second, the cell can be divided into sub cells so that each direction has its own traffic light.

Similarly, the LTM can be extended considering the flows sent and received by links [84]. Regarding queue models, [157] considers the case of links with multiple junctions (connected to several upstream and downstream links) and, for control purposes, present the S model, which is basically a simplification of the BLX model, with a time interval equal to the traffic-light cycle.

The network-wide extension approach is similar for second-order traffic models. For example, [84] presents the extension of the Aw-Rascle-Zhang model on a network scale. A more detailed description of this model at junctions can be found in [113].

For control purposes, [51] suggests to simplify the VLM by assuming an average continuous flow through the traffic lights by replacing the binary variable α with $\frac{T_{\text{green}}}{T_{\text{cycle}}}$, where T_{green} and T_{cycle} denote respectively the green phase time and the cycle time of the traffic light. This method is inspired by store-and-forward models, originally suggested by [88]. It allows to describe the urban traffic without using binary variables. Hence, polynomial complexity control methods can be applied to the system, which allows for consideration of large-scale networks. However,

due to this simplification, the effect of offsets between traffic lights of successive intersections is not depicted. Moreover, the oscillations of the system (stop-and-go waves, propagation waves, etc.) are not represented, which is a crucial point for emissions and energy consumption estimation [101, 3].

2.3.2 Urban cell transmission model

In this work, an urban version of the CTM [48], which is a first-order Godunov-type [91] discretization of the LWR model [154, 223], is chosen to predict the evolution of the traffic system. To be compliant with the constraints associated with urban environments, the CTM is extended to consider TLS, and the First In, First Out (FIFO) policy at intersections. In this study, we make the assumption that any type of intersection can be decomposed into simple merges and diverges. We are therefore only interested in the modeling of this type of intersection.

Many other macroscopic traffic models could be used to predict the behavior of the system. In particular, one may consider using second-order macroscopic traffic models, which are more precise than first-order models under certain traffic conditions such as jam waves [180, 111]. Also, they estimate the average traffic speed more precisely. Nevertheless, first-order traffic models have been widely used for traffic control applications in urban areas [249, 243], especially because of their reduced numerical complexity. These models are generally sufficient to estimate traffic evolution in an urban environment. According to [225], nonlinear flow dynamics are of less importance for the description of traffic phenomena in urban networks, which is mainly due to the presence of intersections and TLS. Among first-order models, the CTM [48] clearly remains one of the most prevalent. When the spatial discretization is adequate, the CTM can also capture variations in density and average velocity between adjacent cells, which are crucial for pollutant emissions and energy consumption.

Network characterization

In order to run the CTM in a large scale urban network, it is essential to accurately characterize the network connections, the drivers' behavior at intersections, and the operation of TLS.

We consider an urban road network composed of one-way roads, each road being divided into several cells of same length δ_x. The set of all cells that constitute the network is denoted $\mathcal{R}$. To characterize the connections between cells, each cell $i \in \mathcal{R}$ is associated with two sets $\mathcal{P}_i$ and $\mathcal{N}_i$ containing respectively the upstream and the downstream cells connected to i. We introduce the function $|.|$ that returns the number of elements in a set. Hence, the cells i entering the network verify

Table 2.3: Examples of cells connections.

Cells structure	$\lvert\mathcal{P}_i\rvert$	$\lvert\mathcal{N}_i\rvert$
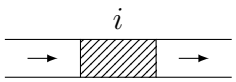	1	1
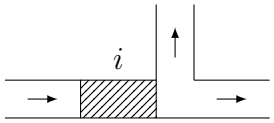	1	2
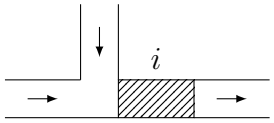	2	1

$|\mathcal{P}_i| = 0$, and the ones exiting the network verify $|\mathcal{N}_i| = 0$. A few illustrating examples are given in Table 2.3.

Based on all the network connections $\{\mathcal{P}_i,\ \mathcal{N}_i \mid i \in \mathcal{R}\}$, we define $\mathcal{C}$ as the set of intersections. An intersection connects cells that verify $\mathcal{P}_i \geq 2$ or $\mathcal{N}_i \geq 2$. To each intersection $c \in \mathcal{C}$ is associated the set of its upstream cells $\mathcal{P}_c$ and its downstream cells $\mathcal{N}_c$.

In order to determine the drivers' behavior at intersections, we introduce split ratios $\beta \in [0, 1]$. For an intersection $c \in \mathcal{C}$, the split ratios represent the fraction of vehicles coming from the upstream cells $i \in \mathcal{P}_c$ that want to go in each of the downstream cells $i \in \mathcal{N}_c$. We assume that they are known and constant over time. They are subject to

$$\forall c \in \mathcal{C}, \sum_{i \in \mathcal{N}_c} \beta_i = 1 \tag{2.35}$$

In this study, we consider that all intersections are regulated by TLS. Hence, each intersection $c \in \mathcal{C}$ has $|\mathcal{P}_c|$ cells regulated by a TLS. In the whole network, the number of cells regulated by a TLS is $\sum_{c \in \mathcal{C}} |\mathcal{P}_c|$. The behavior of the TLS of each of these cells i is defined by a function of time $\alpha_i(k)$ that returns 1 (green) or 0 (red), i.e.

$$\forall c \in \mathcal{C}, \forall i \in \mathcal{P}_c, \alpha_i : [0..T] \to \{0, 1\} \tag{2.36}$$

The functions α_i are fully determined in advance, they must ensure the right of way by verifying at each time step

$$\forall c \in \mathcal{C}, \sum_{i \in \mathcal{P}_c} \alpha_i(k) = 1 \tag{2.37}$$

Note that we define α_i as binary functions as this reflects the phenomenon

of stop-and-go at intersections, which is of particular interest in our study as it has a significant impact on emissions and energy consumption, due to higher accelerations.

Cell transmission model

Based on this network characterization, road traffic is modeled at the network level using the CTM. We define vectors $\rho_k = [\rho_i(k)]_{i\in\mathcal{R}}$ and $V_k = [V_i(k)]_{i\in\mathcal{R}}$ containing respectively the vehicle densities and the speed limits of all the cells at time step k. The system state x_k is defined as

$$x_k = [\rho_{k-1}, \rho_k] \tag{2.38}$$

Note that it includes previous densities ρ_{k-1} because they are used in the macroscopic fuel consumption model (cf. Section 3.3.2).

The flows of vehicles through the network can be determined from the cells demand and supply by applying the Godunov scheme [91]. The demand D_i and supply S_i of cell i are respectively

$$D_i(k) = \min\{V_i(k)\rho_i(k) + d_i(k), \varphi^{\mathrm{M}}(V_i(k))\} \tag{2.39a}$$

$$S_i(k) = \min\{\varphi^{\mathrm{M}}(V_i(k)), \max\{0, w(\rho^{\mathrm{M}} - \rho_i(k))\}\} \tag{2.39b}$$

where φ^{M} and ρ^{M} denote respectively the maximum flow, that depends on the speed limit V_i, and the maximum density. Each cell i is associated with an endogenous traffic demand term $d_i(k)$, which is a modification of the standard CTM that aims to model the generation of vehicles within the network (vehicles leaving homes, parking lots, etc.).

Moreover, the cells entering and exiting the network are considered as vehicle sources and sinks, respectively. As a result, the following parameters are introduced at the network boundaries:

- $d^{\mathrm{in}}(k)$ denotes the demand on all network entering cells (exogenous traffic demand) at time k, i.e. the vehicles from the network upstream that are aiming at entering it;
- $s^{\mathrm{out}}(k)$ denotes the network downstream supply, i.e. the vehicles that can leave the network exiting cells at time k.

Several models can be considered to approximate the fundamental diagram, i.e. the relationship between the vehicles' flow and density at steady state [270]. Some approaches propose to determine its shape in a heuristic way [287]. In the literature, different models have been considered to represent the impact of speed limits on the fundamental diagram [217, 108]. We propose to consider the

trapezoidal fundamental diagram, which was originally considered in [48]. As mentioned in Table 2.2, several other fundamental diagrams can be found in the literature. The main justification of this choice is given in 2.3.3. As illustrated in Fig. 2.6, the trapezoidal fundamental diagram is fully characterized by the speed limit V_i, the backward wave speed w, the maximum vehicle density ρ^{M}, and the maximum flow $\varphi^{\mathrm{M}}(V_i)$.

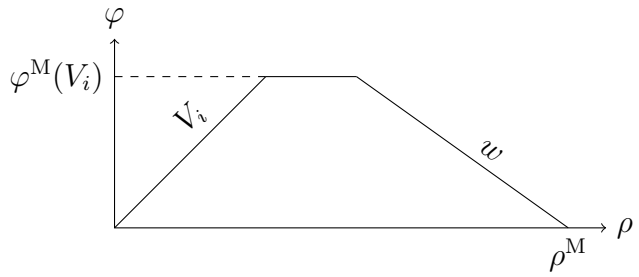

Figure 2.6: Trapezoidal fundamental diagram associated with a speed limit V_i, a backward wave speed w, a maximum vehicle density ρ^{M}, and a maximum flow $\varphi^{\mathrm{M}}(V_i)$.

In case of signalized intersections, the flow of vehicles exiting each cell i of the network at time step k, denoted φ_i^{out}, depends on the number of downstream cells connected to i. It is calculated as indicated in Table 2.4. Note that only the outflows of cells preceding intersections ($|\mathcal{N}_i| \geq 2$) are multiplied by $\alpha_i(k)$ because the other cells are not regulated by TLS.

$\lvert\mathcal{N}_i\rvert$	$\varphi_i^{\mathrm{out}}(k)$
0	$\min\left\{D_i(k), \varphi^{\mathrm{M}}(V_i(k)), s^{\mathrm{out}}(k)\right\}$
1	$\min\left\{D_i(k), \varphi^{\mathrm{M}}(V_i(k)), S_{\mathcal{N}_i}(k)\right\}$
≥ 2	$\alpha_i(k)\min\left\{D_i(k), \varphi^{\mathrm{M}}(V_i(k)), \left\{\frac{S_j(k)}{\beta_j}\right\}_{j\in\mathcal{N}_i}\right\}$

Table 2.4: Outflows of cells in a network.

Similarly, the flow of vehicles entering each cell i of the network at time step k, denoted $\varphi_i^{\mathrm{in}}(k)$, depends on the number of upstream cells connected to i. It is calculated as indicated in Table 2.5.

System dynamics

The dynamics of the system is governed by the function f defined as

$\lvert\mathcal{P}_i\rvert$	$\varphi_i^{\text{in}}(k)$
0	$\min\left\{d^{\text{in}}(k), \varphi^{\text{M}}(V_i(k)), S_i(k)\right\}$
1	$\varphi_{\mathcal{P}_i}^{\text{out}}(k)$
≥ 2	$\beta_i \sum_{j\in\mathcal{P}_i} \varphi_j^{\text{out}}(k)$

Table 2.5: Inflows of cells in a network.

$$x_{k+1} = f(x_k, V_k) \tag{2.40}$$

where

$$f : x_k, V_k \to \begin{pmatrix} \rho_i(k) \\ \rho_i(k) + \frac{\delta_t}{\delta_x}(\varphi_i^{\text{in}}(k) - \varphi_i^{\text{out}}(k)) \end{pmatrix}_{i\in\mathcal{R}} \tag{2.41}$$

In order to guarantee the descriptive ability of the spatiotemporally discrete model and to ensure numerical stability, the Courant–Friedrichs–Lewy (CFL) condition [46] must be verified. It is expressed as

$$\delta_t v_{\max} \leq C\delta_x \tag{2.42}$$

In the literature, some authors suggest to consider the Courant number $C = \frac{1}{2}$ [31, 60]. In our approach, the chosen set of parameters corresponds to $\frac{\delta_t v_{\max}}{\delta_x} \approx \frac{1}{3} < C$.

Based on the fundamental diagram hypotheses and considering that $\varphi = \rho v$, it is possible to estimate the average traffic speed $v_i(k)$ in each cell i at time step k from its density $\rho_i(k)$ and speed limit $V_i(k)$. According to the trapezoidal fundamental diagram proposed by [48],

$$v_i(k) = \min\left\{V_i(k), \frac{\varphi^{\text{M}}(V_i(k))}{\rho_i(k)}, w\frac{\rho^{\text{M}} - \rho_i(k)}{\rho_i(k)}\right\} \tag{2.43}$$

It is essential to keep in mind that, based on the intrinsic definition of the fundamental diagram, this kind of approach determines the speed corresponding to a given density at steady state, and does not always return the precise average speed, because the density does not fully characterize the microscopic behavior of vehicles.

2.3.3 Calibration of the fundamental diagram

The calibration of the macroscopic traffic model is a crucial step in order to ensure accurate predictions of the densities evolution in the controller. According to

[41], calibrating the fundamental diagram by aggregating loop detectors data has several drawbacks. In particular, real traffic systems evolve through equilibrium and transient states, which are difficult to identify. These states can even be mixed in measurements if the sampling period is not adequate. Also, traffic waves cannot be captured at single locations. To go beyond these difficulties, we propose to calibrate the fundamental diagram associated with the IDM set of parameters by modeling in SUMO a synthetic single-lane ring road of 300 m with a TLS. In fact, such networks are particularly suitable for this purpose because they ensure that the system remains in an equilibrium state as the number of vehicles on the road does not change. This facilitates the observation of the fundamental diagram as the transient regimes associated with the variation of the density are not represented. Here, the objective is mainly to understand the impact of the control, i.e. the speed limit, on the fundamental diagram, and to highlight the impact of TLS. Since the parameterization of the microscopic traffic model is identical, we assume that the fundamental diagram thus calibrated is representative of the traffic dynamics in any other network structure.

In order to measure the vehicle density with more precision, a 60-meter long detector upstream of the TLS is introduced instead of using loop detectors. This detector measures the traffic density ρ and the average speed v. The flow of vehicle is a quantity that is supposed to be defined at a point of the road. Yet, to be consistent with the proposed approach, we propose to define it on the whole detector as $\varphi = \rho \times v$. The whole approach is depicted in Fig. 2.7.

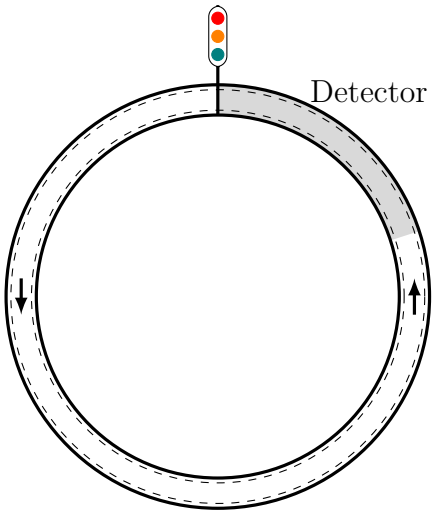

Figure 2.7: 300-meter single-lane ring road with a TLS and a 60-meter long detector measuring traffic density ρ and average speed v at a sampling frequency of 1 Hz.

Two different scenarios are considered to calibrate the fundamental diagram associated with IDM:

- In order to reproduce precisely the shape of the fundamental diagram, we define a scenario (a) in which the TLS is always green (cf. Fig. 2.8a).
- Another scenario (b) is introduced to characterize the impact of a TLS on vehicles' behavior at a macroscopic level. Hence, the TLS alternates between green and red phases in this scenario (cf. Fig. 2.8b).

(a) Scenario (a): TLS always green.

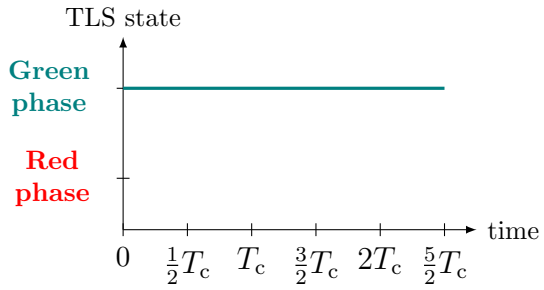

(b) Scenario (b): TLS alternating between green and red phases.

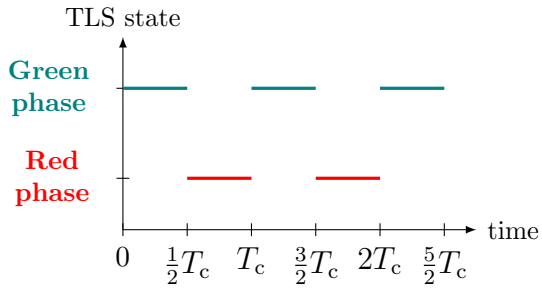

Figure 2.8: Behavior of TLS in scenarios (a) and (b).

In order to cover all density values, several simulations are run for both scenarios, with an increasing number of vehicles on the road, until the maximum density ρ^{M} is reached. It can be calculated from the vehicles' length l_{veh} and the minimum distance between vehicles s_0, as follows

$$\rho^{\mathrm{M}} = \frac{1}{l_{\mathrm{veh}} + s_0} \tag{2.44}$$

In this work, we consider identical vehicles with a length of $l_{\mathrm{veh}} = 5\,\mathrm{m}$, and the IDM parameter s_0 has been set at $2\,\mathrm{m}$ (cf. 2.2.3). This results in a maximum density ρ^{M} equal to about $0.143\ \mathrm{veh.m^{-1}}$.

In scenario (b), we consider a TLS cycle time $T_c = 88\,\mathrm{s}$ (green and red phases of $44\,\mathrm{s}$ each). The detector sampling period is $\frac{1}{8}T_c = 11\,\mathrm{s}$, in order to capture variations within TLS green and red phases. Also, the fact that the detector sampling period is a divisor of green and yellow/red phases duration ensures that points are captured at the maximum flow rate. The scatter plots associated with both scenarios, simulated over a period of $1\,\mathrm{h}$ with a speed limit $V = 50\,\mathrm{km/h}$ are given in Fig. 2.9a & 2.9b.

It appears that scenario (a) (cf. Fig. 2.9a) leads to the classical bell shape of fundamental diagrams [210]. In particular, the IDM set of parameters previously calibrated corresponds to a shape that seems close to [96] or [97] fundamental diagrams. Yet, we decide to approximate the scatter plot with the trapezoidal fundamental diagram introduced in [48] and presented in Section 2.3.2, as it can almost perfectly follow the shape of the scatter plot and it is easy to calibrate, unlike the other approaches. The left slope of the trapezoidal fundamental diagram is set at the road speed limit, i.e. $V = 50\,\text{km/h}$, and the right slope, which is the backward wave speed w, is adjusted to fit the points in the congested area. The calibration gives a value of w equal to 7 m.s^{-1}. Also, based on the scatter points, the value of the maximum flow rate $\varphi^{\text{M}}(V)$ is set at 80% of the ordinate of the two slopes theoretical intersection, i.e. $\varphi^{\text{M}} = 0.8 \times w\rho^{\text{M}}\frac{V}{V+w}$.

Similarly, the same shape of the fundamental diagram and the same value of w and $\varphi^{\text{M}}(V)$ are obtained with scenario (b) (cf. Fig. 2.9b). However, the transient states caused by the TLS lead to more scattered points within the fundamental diagram, which describes an envelope that contains all points. Note that with the CTM, all these transient states are reproduced by the TLS variable α, defined in Section 2.3.2.

To go further, it is essential to calibrate the fundamental diagram for other speed limit values in order to accurately predict the impact of VSLs. For example, the scatter plots associated with both scenarios with a speed limit $V = 20\,\text{km/h}$ are given in Fig. 2.9c & 2.9d. It appears that the same maximum density and backward wave speed values, respectively $\rho^{\text{M}} = 0.143$ veh.m^{-1} and $w = 7$ $m.s^{-1}$, perfectly fit the vehicles' behavior in the congested area. The only difference is the value of the free-flow slope, which is now equal to $V = 20\,\text{km/h}$. Naturally, the value of the maximum flow rate $\varphi^{\text{M}}(V)$ is lower with $V = 20\,\text{km/h}$. However, as can be seen in Fig. 2.9c & 2.9d, considering the value of 80% of the ordinate of the two slopes theoretical intersection is still a realistic approximation of the observed maximum vehicle flow.

To illustrate the impact of the speed limit on the fundamental diagram, the differences between two fundamental diagrams associated with speed limits V_1 and V_2, where $V_1 > V_2$, are summarized in Fig.2.10.

Finally, the descriptions and values of the CTM parameters associated with the previously calibrated IDM set of parameters are summarized in Table 2.6. It is essential to note that even after the fundamental diagram calibration, the relationship between vehicle density ρ and traffic flow φ remains an approximation insofar as it is true only at steady state.

(a) Scenario (a): TLS always green, with $V = 50\,\text{km/h}$.

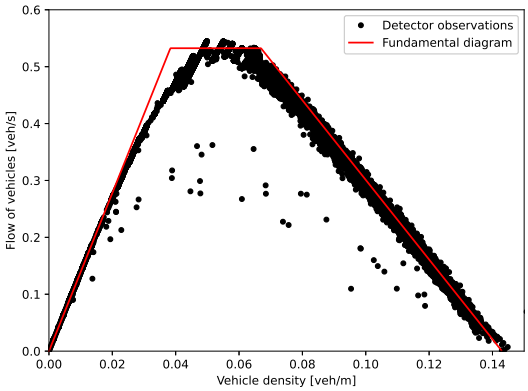

(b) Scenario (b): TLS alternating between green and red phases, with $V = 50\,\text{km/h}$.

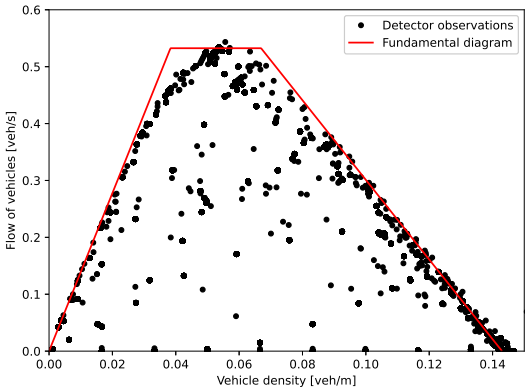

(c) Scenario (a): TLS always green, with $V = 20\,\text{km/h}$.

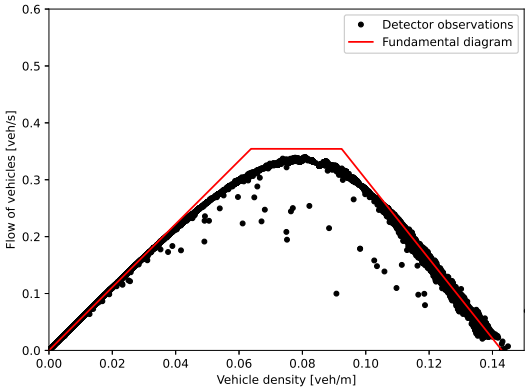

(d) Scenario (b): TLS alternating between green and red phases, with $V = 20\,\text{km/h}$.

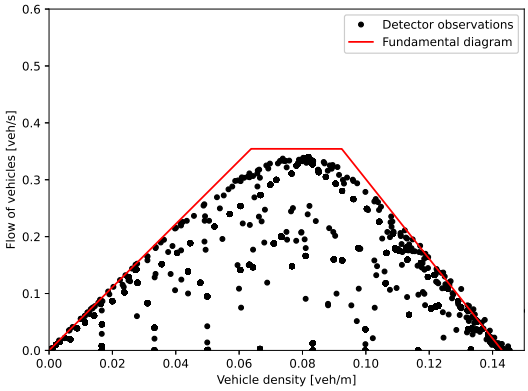

Figure 2.9: Fundamental diagrams in both scenarios, with speed limits of 50 km/h and 20 km/h.

2.4 Comparison of the microscopic and macroscopic models dynamics in a Manhattan grid structure

In this section, we are interested in the comparison between the dynamics of the microscopic and macroscopic traffic models in order to validate the predictions made by the macroscopic one. Its predictive capabilities are tested on a more complex network than the ring road considered in Sections 2.2.2 & 2.3.3 so as

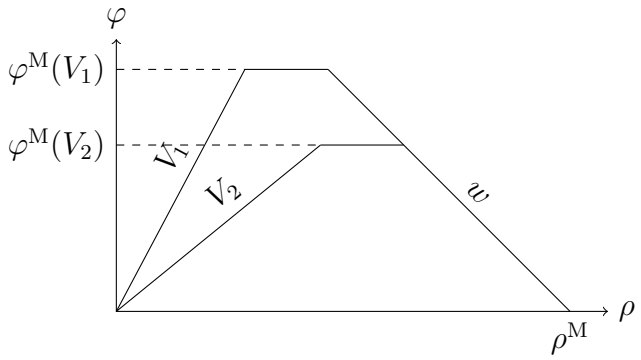

Figure 2.10: Fundamental diagrams associated with speed limits V_1 and V_2, where $V_1 > V_2$.

Symbol	Description	Value	Unit
V	Speed limit (left slope)	V	$\mathrm{m.s^{-1}}$
w	Backward wave speed (right slope)	7	$\mathrm{m.s^{-1}}$
ρ^{M}	Maximum vehicle density	0.143	$\mathrm{veh.m^{-1}}$
$\varphi^{\mathrm{M}}(V)$	Maximum vehicle flow rate	$0.8{\times}w\rho^{\mathrm{M}}\frac{V}{V+w}$	$\mathrm{veh.s^{-1}}$

Table 2.6: Calibrated parameters of the trapezoidal fundamental diagram.

to avoid analyzing steady-state situations only, which are much easier to predict because they perfectly fit the fundamental diagram. To this end, we introduce a Manhattan grid network with TLS at each intersection. Also, peaks are introduced in the traffic demand profile in order to assess the behavior of the model under different congestion levels.

2.4.1 Manhattan grid structure

We consider a Manhattan grid network composed of an urban area (38 roads of 300 meters represented by solid lines in Fig. 2.11) and a peri-urban area (7 roads of 2400 meters represented by dashed lines in Fig. 2.11). The peri-urban area, whose roads can be seen as highway links leading to the urban area, have a speed limit of 70 km/h. The objective of introducing two areas is to analyze the performance of the CTM to predict the dynamics not only in the urban area, but also in a peri-urban area upstream.

As represented in Fig. 2.12, all the roads have the same spatial discretization with cells of 60 m, i.e. 5 cells in the urban roads and 40 cells in the peri-urban roads. At each intersection, both downstream roads have a split ratio of 0.5 and all TLS have cycles of 88 s (44 s green and 44 s red). Also, all TLS are synchronized in

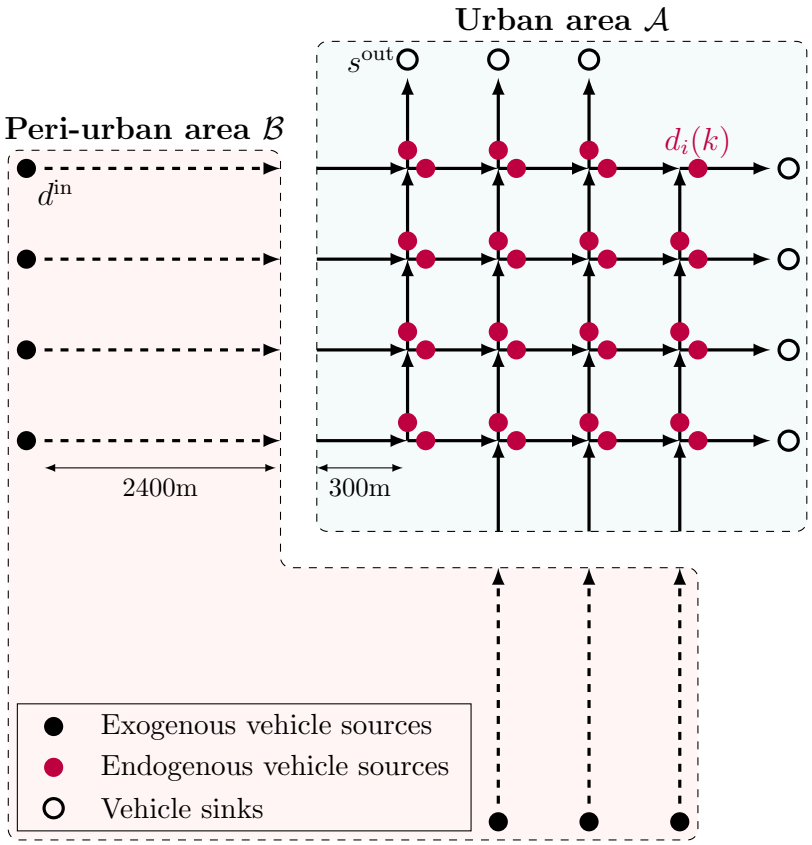

Figure 2.11: Scenario considered to compare the dynamics of the microscopic and macroscopic traffic models. At exogenous sources, vehicles are continuously generated at a rate of $d^{\text{in}} = 0.2$ veh.h^{-1}. At endogenous sources, vehicles are generated between 6 min and 9 min, and between 31 min and 34 min at a rate of $d_i = 0.1$ veh.h^{-1}.

the sense that horizontal (and vertical) roads have the same phases without delay.

2.4.2 Analysis of the prediction performance

Simulations of $T = 1$ h are run with an initial density of 20% of the maximum density. Exogenous sources are considered at the beginning of the peri-urban roads. They generate vehicles at a constant rate of 0.2 veh.h^{-1}. In order to analyze the predictive capabilities of the CTM under different congestion levels, endogenous sources are also considered inside the urban areas. They can be seen as parking lots or residential areas. They generate vehicles between 6 min and 9 min, and between 31 min and 34 min at a rate of 0.1 veh.h^{-1}. Simulations are run with speed limits of 20 km/h and 50 km/h, which are the upper and lower bounds of

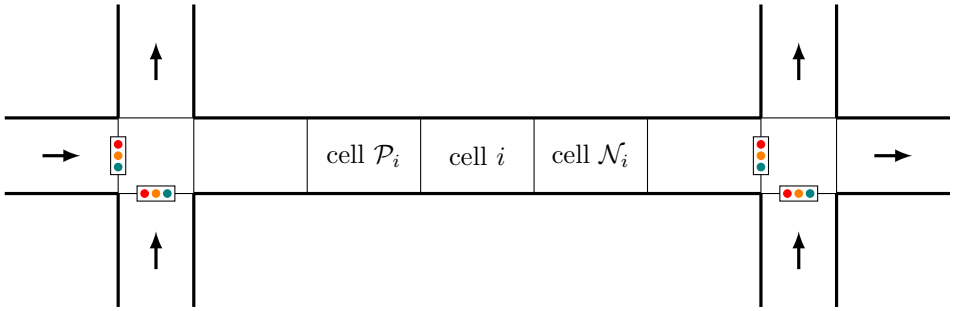

Figure 2.12: TLS positions and spatial discretization of the roads into cells.

the controller presented in Section 4. Tt is therefore essential to evaluate the performance of the prediction on this range.

The actual densities in each cell ρ_i are measured at every time step (of 1 s), and are compared with the densities $\hat{\rho}_i$ predicted along a time horizon of 1 min. The accuracy of the CTM can be analyzed by evaluating an average error on the whole simulation duration T, expressed as a percentage of the maximum density ρ^{M}, as follows

$$\varepsilon_i = \frac{1}{T}\sum_{k=0}^{T}\frac{1}{\Delta_{\mathrm{avg}}}\left|\sum_{e=k-\frac{\Delta_{\mathrm{avg}}}{2}}^{k+\frac{\Delta_{\mathrm{avg}}}{2}}\rho_i(e) - \sum_{e=k-\frac{\Delta_{\mathrm{avg}}}{2}}^{k+\frac{\Delta_{\mathrm{avg}}}{2}}\hat{\rho}_i(e)\right| \times \frac{100\%}{\rho^{\mathrm{M}}} \tag{2.45}$$

In Eq. 2.45, the error ϵ_i at each time step k is defined as a moving average error on a horizon $\Delta_{\mathrm{avg}} = 20\,\mathrm{s}$. This choice is justified by the fact that densities vary much more abruptly in the microscopic simulator SUMO than in the CTM. This is due to the fact that in SUMO, the density is defined as the ratio between the number of vehicles in a cell and the length of cells. Also, it is known that the CTM behaves like a low-pass filter that smooths the densities variation.

The average errors ε_i regarding traffic prediction in each cell i are represented in Fig. 2.13. These errors are evaluated with speed limits of 20 km/h (Fig. 2.13a) and 50 km/h (Fig. 2.13b). It appears that the performance of the traffic predictor is similar for these two speed limits. With 20 km/h, the average error is 5.1% and the maximum error is 8.7%. With 50 km/h, the average error is 4.7% and the maximum error is 8.9%.

In order to better visualize the performance of the prediction, Fig. 2.14 compares the evolution of the time-varying density and average speed given by the microscopic and the macroscopic models in one cell of the network. The chosen cell is preceding a TLS and the speed limit is 50 km/h. Fig. 2.14a represents the evolution in time of the actual density ρ_i in the microscopic traffic simulator (target) and the predicted density $\hat{\rho}_i$ given by the CTM (prediction). For this cell, the

(a) Representation of ε_i with 20 km/h speed limits.

(b) Representation of ε_i with 50 km/h speed limits.

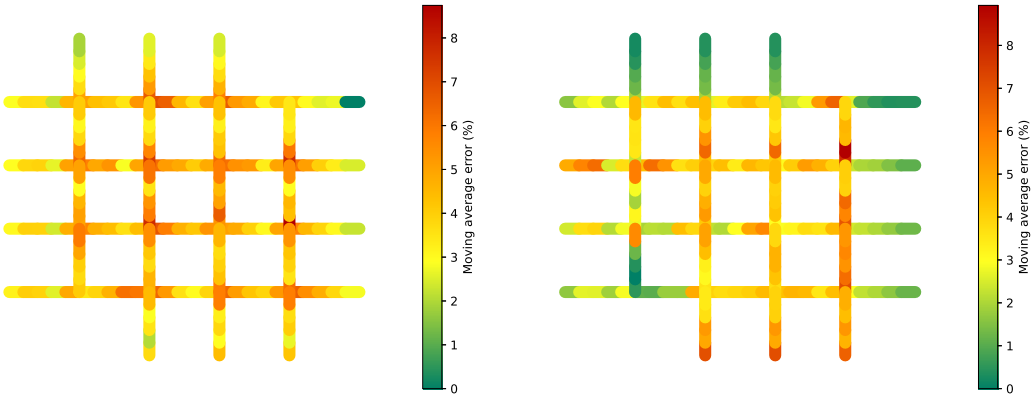

Figure 2.13: Representation of average traffic prediction errors ε_i in each cell i of the network, with 20 km/h and 50 km/h speed limits.

average traffic prediction error ε_i is 4.2%. Similarly, the cell's measured average speed v_i (target) is compared in Fig. 2.14b with its predicted speed $\hat{v}_i$ (prediction), calculated with Eq. 2.43.

The same results are given in Fig. 2.15 for a speed limit of 20 km/h. The average traffic prediction error ε_i is 5.2%. The oscillations observed in Fig. 2.14 & 2.15 with the IDM, especially for the evaluation of the density, are due to the counting of vehicles.

In order to take a more macroscopic view of the prediction performances, we are interested here in the measurement and the prediction of the number of vehicles present in the urban and the peri-urban areas, under 20 km/h and 50 km/h. These results are shown in Fig. 2.16, they all have errors lower than 1%.

In view of these results, we decide to adopt the CTM as macroscopic model to predict the traffic dynamics determined by the microscopic simulator. It is a priori difficult to obtain better results with a first-order model due to their nature based on steady-state situations.

(a) Visualization of the density prediction.

(b) Visualization of the average speed prediction.

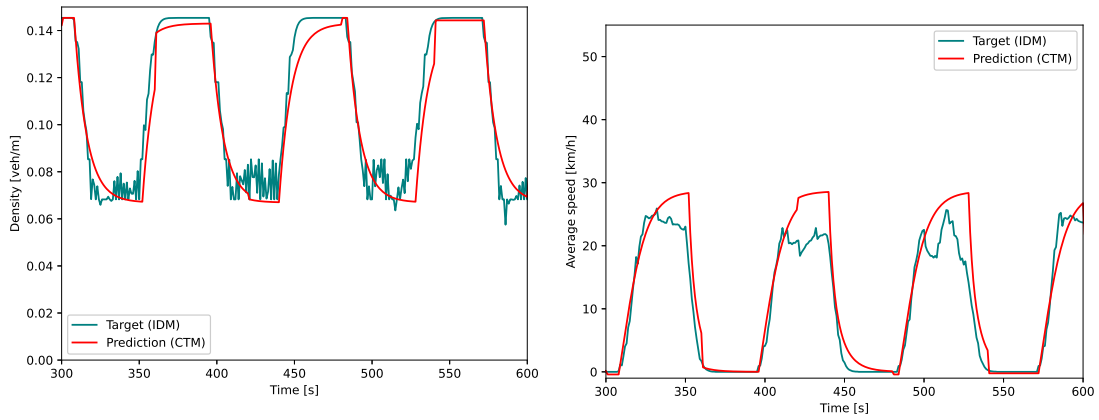

Figure 2.14: Comparison of the actual density ρ_i measured in IDM with the prediction density $\hat{\rho}_i$ given by the CTM in a cell i. The speed limit is 50 km/h and the average traffic prediction error ε_i is 4.2% (left). Comparison of the same cell's average speed v_i measured in IDM with its prediction $\hat{v}_i$ (right).

(a) Visualization of the density prediction.

(b) Visualization of the average speed prediction.

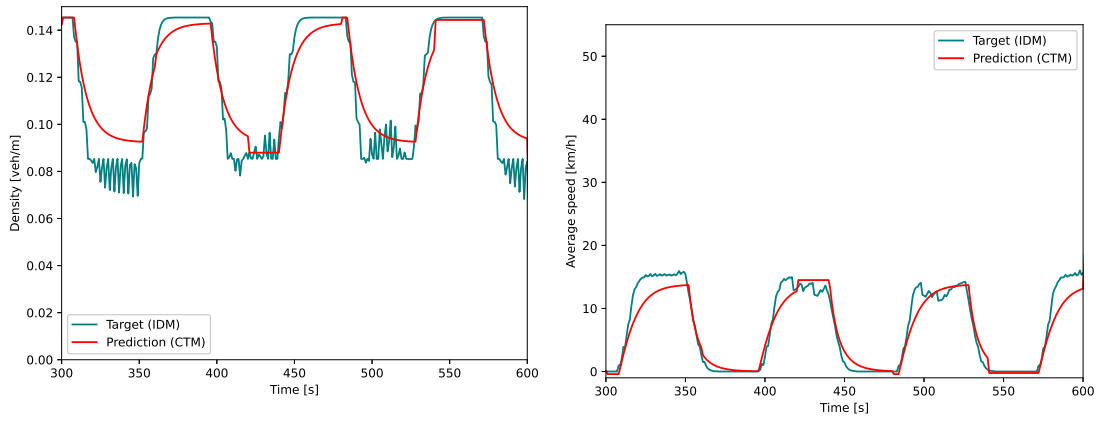

Figure 2.15: Comparison of the actual density ρ_i measured in IDM with the prediction density $\hat{\rho}_i$ given by the CTM in a cell i. The speed limit is 20 km/h and the average traffic prediction error ε_i is 5.2% (left). Comparison of the same cell's average speed v_i measured in IDM with its prediction $\hat{v}_i$ (right).

(a) Number of vehicles in the urban area, with $V = 50\,\mathrm{km/h}$.

(b) Number of vehicles in the peri-urban area, with $V = 50\,\mathrm{km/h}$.

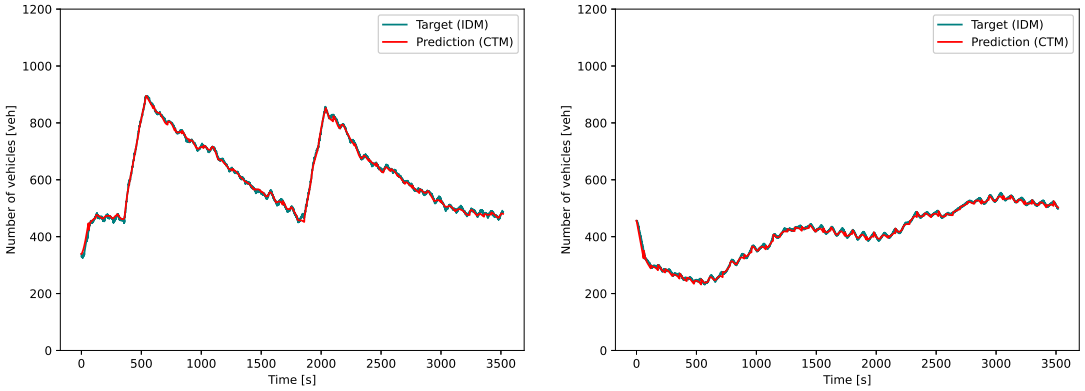

(c) Number of vehicles in the urban area, with $V = 20\,\mathrm{km/h}$.

(d) Number of vehicles in the peri -urban area, with $V = 20\,\mathrm{km/h}$.

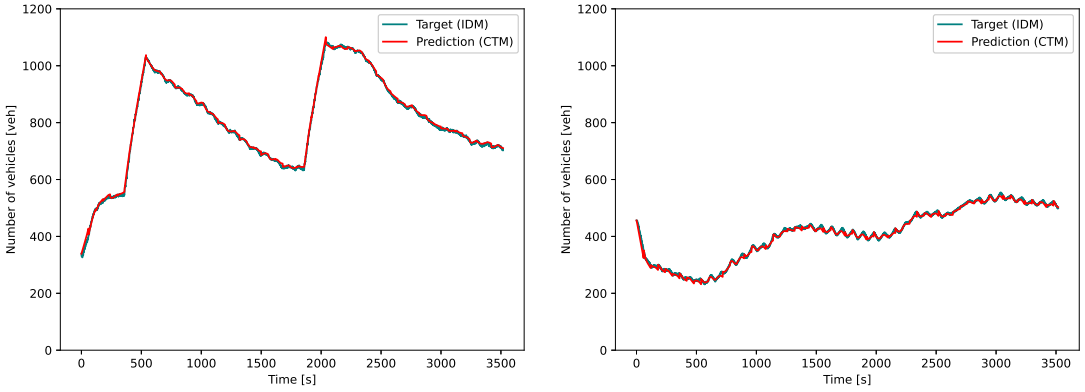

Figure 2.16: Comparison of the actual number of vehicles measured in IDM with the prediction based on the CTM. The vehicles are counted in both the urban and the peri-urban areas, under speed limits of 50 km/h and 20 km/h. The prediction time horizon is 1 min, i.e. the prediction is corrected every 1 min.

Chapter 3

Models to simulate and predict pollutant emissions and energy consumption

Contents

3.1 Foreword

Another crucial step of traffic eco-management strategies lies in the modeling of pollutant emissions and energy consumption. Such models take as inputs the traffic dynamics, which can be described using microscopic data, such as vehicles' speed profiles, or macroscopic data.

In this chapter, both approaches are explored. A microscopic emission and energy consumption model is introduced to evaluate the performance of the urban traffic system, and a macroscopic model is introduced for prediction purposes.

One main challenge for macroscopic pollutant and energy consumption models is to be able to estimate the output of microscopic models, as they do not consider the individual behavior of vehicles, which plays a major role regarding energy efficiency due to the acceleration of vehicles.

3.2 Microscopic models to simulate pollutant emission and energy consumption

Microscopic emission and energy consumption models estimate the rates of pollutant emission and energy consumption (electricity or fuel) from the vehicles' individual dynamics. In this section, the main categories of this kind of models are reviewed in Section 3.2.1, and the physical model considered in the rest of this work is presented in Section 3.2.2.

3.2.1 State-of-the-art

Different models estimating the emission and energy consumption rates (J_y) of a vehicle as a function of its constant parameters (θ) and time-varying operation variables (θ_k) have been investigated in the past. This section presents the data-driven and the physical modeling approaches employed to estimate J_y.

In the proposed formalization, J_y refers to the prediction of the rate of y, which can be calculated per distance traveled by the vehicle (J_y^{spat}) or per time unit (J_y^{temp}), depending on the modeling method. The variable y corresponds either to the emission of a pollutant (CO, NOx, HC, ...) or the energy consumption (fuel or electricity consumption, depending on the vehicle powertrain considered):

$$y \in \{ \text{ fuel or electricity consumption, emission of CO, NOx, HC, ...} \}$$

Such emission and energy consumption models are said microscopic because they consider each vehicle individually. They can be described as

$$J_y = g(\theta_k, \theta) \tag{3.1}$$

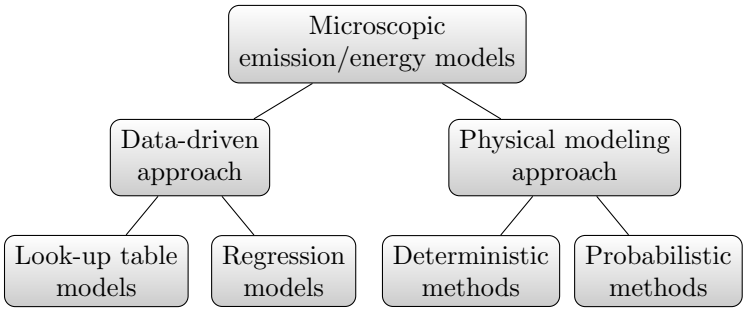

Figure 3.1: Classification of emission and energy consumption models for single vehicles.

where g is a function that relates the model inputs to the output.

The function g can be constructed in different ways. The different approaches detailed in this section to estimate emissions and energy consumption are classified as illustrated in Fig. 3.1.

The first step to determine the emission and energy consumption rates of a vehicle is to determine its operation variables (e.g. speed, acceleration). This aspect has been addressed in Section 2.2. The second step consists in using a microscopic emission and energy consumption model whose inputs are the vehicle operating variables and parameters. This step is presented in detail in the following sections.

In real driving conditions, it is essential to bear in mind that several factors contribute to an increase in energy consumption compared to the certification value. [81] indicates that these factors include, inter alia, certification margins, vehicle's mass and rolling resistance, wind and temperature conditions, additional electric auxiliaries, air conditioning, road grade, and traffic conditions. The impact of these factors are quantified in Table 3.1. According to [81], the actual fuel consumption could be increased, on average, by 24% to 54% in comparison with the official certification value.

Table 3.1: Impact of factors contributing to an increase in energy consumption [81].

Factor	**Description**	**Impacts**	**Global impact**
Certification margins	Vehicle adjustment Homologation margin Protocol design & boundaries	+ 6% + 5% + 4%	+ 15%
Mass	100 kg extra mass		+ 3.2%
Aerodynamics	Real world aerodynamics & side winds		+ 2.2 %
Rolling resistance	Lower energy class Maintenance Winter tyre Wet road	+ 1.7 % + 0.2% + 0.2% + 0.3%	+ 2.4%
Temperature	Annual temperature variation		+ 3.5%
Road grade	0.25% average grade		+ 2.5%
Additional electric auxiliaries	Air conditioning excluded		+ 5%
Air conditioning			+ 5%
Traffic conditions	Congestion level & traffic demand		± 15%
Total			Between + 23.8% and + 53.8%

Data-driven methods

Emission and energy consumption rates can be calculated using data-driven approaches. Basically, they consist in measuring fuel consumption or CO2 emissions and deducing look-up tables, regression models, or machine learning approaches to estimate the energy consumption from the vehicle dynamics. The measurements can be made indoors using a chassis dynamometer, or outdoors during on-road experiments using a portable emissions measurement system (PEMS) [118].

It is generally acknowledged that the impact of vehicular mobility on climate change, i.e. the amount of CO2 emitted by vehicles, is proportional to the fuel consumption. The reason is that the relationship between fuel consumption and CO2 emissions is almost linear [211].

• *Look-up table models*

One old common approach to estimate emission and fuel consumption rates consists in performing chassis dynamometer tests and recording the emissions and fuel consumption in a look-up table, also called emission matrix. Usually, such look-up tables provide J_y from speed and acceleration [213, 239] for a given set of vehicle parameters. These reference emission look-up tables can be used later to instantly estimate emissions and fuel consumption.

Although this method is easy to use, usually the available matrices are sparse, due to measurement difficulties. Moreover, empirical matrix-based prediction concerns only steady-state emissions, and not transient operations [231]. Finally, this method is sensitive to the driving cycle and the quality of on-line measurements. This may lead to large errors.

Another possibility is to determine emission and fuel consumption rates as a function of the vehicle position. [13] proposes to associate to each road a corresponding fuel consumption, based on average measurements. The amount of fuel consumed by a vehicle during a trip is therefore simply approximated by the sum of the average fuel consumption associated with the corresponding roads. This approach is very simple but it cannot distinguish between different types of vehicle, as they are all mixed in the same computed average value. Also, it cannot reflect the evolution of emissions and fuel consumption in case of traffic congestion.

• *Regression models*

Emissions and energy consumption of a single vehicle can also be predicted on a second-by-second basis by using data-based models, such as regression techniques or neural networks. The inputs of these models can typically be the speed, acceleration or power demand, and the outputs are the emission or energy consumption rates prediction.

Regression techniques and neural networks for emission and energy consump-

tion modeling both use the collected data in order to train a model that mimics these data. In regression techniques, it is necessary to identify the model parameters by curve fitting, while in neural networks the weight of the connections between neurons is to be identified.

The use of neural networks to estimate emissions and energy consumption is motivated by the heavy nonlinearity of emissions. There is also a need of high computational efficiency in order to be compatible with second-by-second microscopic traffic models. Such neural network frameworks can be found in [5, 193, 123, 284].

[5] presents non-linear multiple regression models constructed with quadratic and cubic speed-acceleration terms. The data used to determine the coefficients of these models for a given type of vehicle is obtained from dynamometer emission tests, based on the New European Drive Cycle (NEDC) [7]. It is also desirable to use data from vehicles in real urban traffic situations, when available [204]. In fact, it is important to note that emission levels obtained from dynamometer tests can be much lower than those produced in real traffic [209]. For example, a criticism against the NEDC is that its acceleration profile is very smooth and not sufficiently realistic [14].

Based on this technique, the VT-micro model can be formulated in matrix form [288] as

$$\ln(J_y^{\text{temp}}(k)) = \vec{v}(k) M_y \vec{a}(k) \tag{3.2}$$

where M_y denotes the regression coefficients matrix of y for the type of vehicle under consideration, $\vec{v}(k)$ and $\vec{a}(k)$ are respectively the speed and acceleration vectors defined as

$$\begin{aligned} \vec{v}(k) &= \left[1,\ v_p^{\text{veh}}(k),\ v_p^{\text{veh}}(k)^2,\ v_p^{\text{veh}}(k)^3\right] \\ \vec{a}(k) &= \left[1,\ a_p^{\text{veh}}(k),\ a_p^{\text{veh}}(k)^2,\ a_p^{\text{veh}}(k)^3\right]^T \end{aligned} \tag{3.3}$$

Note that the VT-micro model can also be expressed with a regression coefficients matrix for positive accelerations, and another matrix for negative accelerations, depending on the data used to calibrate the model [9]. VT-micro estimates emissions and energy consumption from instantaneous speed and acceleration, i.e. measured at the present time. [215] formulates a regression model, named POLY, which also takes into account the past accelerations and the road grade angle. The model reads

$$\begin{aligned} J_y^{\text{temp}} = \ & \beta_0 + \beta_1 v_p^{\text{veh}}(k) + \beta_2 v_p^{\text{veh}}(k)^2 + \beta_3 v_p^{\text{veh}}(k)^3 \\ & + \beta_4 T^{\text{acc}}(k) + \beta_5 T^{\text{dec}}(k) \\ & + \beta_6 g_a(k) + ... + \beta_{15} g_a(k-9) + \beta_{16} v_p^{\text{veh}}(k) g_a(k) \end{aligned} \tag{3.4}$$

where β_0 to β_{16} are the parameters determined by least-square method for one type of vehicle, $T^{\text{acc}}(k)$ and $T^{\text{dec}}(k)$ are respectively the acceleration and deceleration

duration since their inception up to the current time step k. At each time step, at least one of them is zero. To consider the road grade angle ψ, the function g_a is defined as follows

$$g_a(k) = a_p^{\text{veh}}(k) + g^{\text{grav}} \left[\frac{\psi(k)}{\sqrt{1+\psi^2(k)}} \right] \tag{3.5}$$

where g^{grav} denotes the gravitational constant. POLY is an accurate emission model. However, it may underestimate emissions of higher emitting vehicles as it is built from average measured data [215].

While data-driven models can be developed quickly without prior knowledge on the vehicle or roads, they usually lack a clear physical interpretation and might be too coarse. They may also over-fit the calibration data if the number of variables considered is too large.

Physical modeling approach

An alternative method for estimating emissions and energy consumption is to employ a physical approach that leads to model parameters with physical meaning. Two types of models can be distinguished, the deterministic and probabilistic models, that are both described in the following sections.

- *Deterministic methods*

The emission and energy consumption rates can be determined from the power engine demand P, which can be calculated using the vehicle longitudinal dynamics governed by Newton's second law of motion, as in [228]. For a vehicle p at time step k, it can be expressed as

$$(M + M_{\text{i}}(\gamma(k)))a_p^{\text{veh}}(k) = F_{\text{w}}(k) - F_{\text{a}}(k) - F_{\text{r}}(k) - F_{\text{g}}(k) \tag{3.6}$$

where the resistive forces F_{a}, F_{r}, and F_{g} represent respectively the aerodynamic drag, the rolling resistance force, and the force due to gravity in case of non-negative road grade ψ. The variable F_{w} denotes the wheel force. These forces are illustrated in Fig. 3.2. The variables M and M_{i} denote respectively the vehicle mass and inertial mass. The inertial mass is defined as a function of the gear ratio $\gamma(k)$ associated with gear numbers from 1 to 5, and updated according to a gear law based on the value of the engine speed. The vehicle acceleration $a_p^{\text{veh}}(k)$ is calculated as the discrete derivative of its speed v_p^{veh}.

The resistive forces can be calculated as follows

$$F_{\text{a}}(k) = \frac{1}{2}\rho^{\text{air}} S C_{\text{X}} v_p^{\text{veh}}(k)^2 \tag{3.7a}$$

$$F_{\text{r}}(k) = C_{\text{rr}} M g^{\text{grav}} \tag{3.7b}$$

$$F_{\text{g}}(k) = M g^{\text{grav}} \sin\psi \tag{3.7c}$$

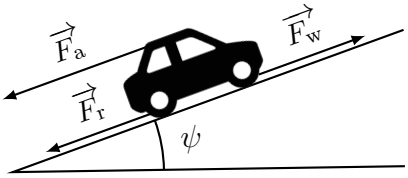

Figure 3.2: Forces applied to a moving vehicle.

where ρ^{air}, C_{X}, C_{rr}, and g^{grav} denote respectively the mass density of air, the aerodynamic drag coefficient, the rolling resistance coefficient, and the gravitational constant.

Based on Eq. 3.6, the wheel force can be positive if $a_p^{\text{veh}}(k) \geq -\frac{F_{\text{a}}(k)+F_{\text{r}}(k)+F_{\text{g}}(k)}{M+M_{\text{i}}(\gamma(k))}$. In this case, the driver is accelerating and a force is applied by the powertrain at the wheels. The wheel force is negative if $a_p^{\text{veh}}(k) < -\frac{F_{\text{a}}(k)+F_{\text{r}}(k)+F_{\text{g}}(k)}{M+M_{\text{i}}(\gamma(k))}$. In this case, the driver is actually braking.

The total tractive power of the vehicle P_{w} is calculated as follows

$$P_{\text{w}} = F_{\text{w}} v_p^{\text{veh}} \tag{3.8}$$

Finally, the power engine demand P can be calculated as follows

$$P = \frac{P_{\text{trac}}}{\eta_{\text{tf}}} + P_{\text{acc}} \tag{3.9}$$

where η_{tf} and P_{acc} denote respectively the efficiency of the transmission and final drive and the engine power demand associated with accessories.

Once the power demand is known, [213] proposes to estimate the emission and energy consumption rates as follows

$$J_y^{\text{temp}} = \begin{cases} a_y + b_y P & \text{, if } P \geq 0 \\ a_y & \text{, if } P < 0 \end{cases} \tag{3.10}$$

where a_y and b_y are the regression coefficients determined for a given y and vehicle type. When y represents the fuel consumption, a_y can be approximated by a linear function of the engine displacement.

[18] proposes to replace the regression coefficients by physical parameters and operation variables to approximate the fuel use rate. The model is defined as

$$J_{\text{fuel}}^{\text{temp}} LHV_{\text{fuel}} \approx \lambda_{\text{air/fuel}} \left(C_{\text{e}} \omega_{\text{e}} d_{\text{e}} + \frac{P}{\eta_{\text{e}}} \right) \tag{3.11}$$

where the engine friction factor C_{e} is the energy used at zero-power output to overcome engine friction. The variables LHV_{fuel}, C_{e}, ω_{e}, e_{e}, η_{e} denote respectively

the fuel lower heating value, the engine friction factor, the engine speed, the engine displacement, and the engine efficiency.

In [10], the authors then propose to calculate the pollutant emission rates as follows

$$J_y^{\text{temp}} = J_{\text{fuel}}^{\text{temp}} \frac{dy}{d(\text{fuel})} CPF_y \tag{3.12}$$

where y refers here only to emissions, $\frac{dy}{d(\text{fuel})}$ corresponds to the grams of engine-out emissions per gram of fuel consumed for pollutant y, and the Catalyst Pass Fraction (CPF) CPF_y can be modeled as

$$CPF_y = 1 - \epsilon_y \exp\left[\left[-b_{\text{CPF}} - c_{\text{CPF}}\left(1 - \frac{1}{\lambda}\right)\right] J_{\text{fuel}}^{\text{temp}}\right] \tag{3.13}$$

The parameters ϵ_y, b_{CPF}, and c_{CPF} denote respectively the maximum catalyst efficiency of y, the stoichiometric CPF coefficient, and the enrichment CPF coefficient.

The Comprehensive Modal Emissions Model (CMEM) is based on (3.12) [231]. It considers different categories of vehicle and different modes of operation (idling, cruising, acceleration, and deceleration). Emission and fuel consumption rates are calculated as a function of the vehicle fleet composition (vehicle categorization based on model year, weight, etc.), operation variables and model-calibrated parameters. The structure of the model is shown in Fig. 3.3. The CMEM predicts emissions well, but may underestimate them for high-emitting vehicles because the model is based on the average data of 300 vehicles (including about 30 high emitters) measured during dynamometer tests, along different driving cycles [222].

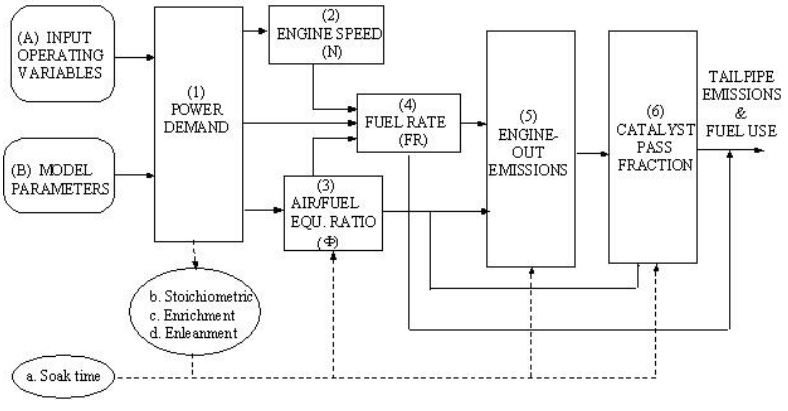

Figure 3.3: Structure of the CMEM [231] [Published with permission of the Center for Environmental Research and Technology].

Another model proposed by [85] estimates emissions from fuel consumption at engine mechanics level. The model relies on the first Law of Thermodynamics and chemical kinetic reaction rate considerations. For NO_x emissions, the model reads

$$\log\left(\frac{d(\text{NOx})}{d(\text{fuel})}\right) = a_0 + a_1 COC + a_2 m_{\text{cyl}} + a_3 m_{O_2} \tag{3.14}$$

where a_0 – a_3 are model coefficients, $\frac{d(\text{NOx})}{d(\text{fuel})}$ is the mass of nitrogen oxides emitted per mass of fuel consumed, COC is the center of combustion (50% energy conversion, from Top Dead Center), and m_{air} and m_{O_2} denote respectively the in-cylinder air and oxygen masses per stroke and displaced volume.

A simplified version of (3.14) is proposed by [247]. The authors propose to express $\log(J_{\text{NOx}})$ as a linear function of the in-cylinder burned gas rate R_{BGR}, as follows

$$\log\left(\frac{d(\text{NOx})}{d(\text{fuel})}\right) = a_4 + a_5 R_{\text{BGR}} \tag{3.15}$$

where a_4, a_5 are model coefficients.

R_{BGR} is expressed as a function of the engine speed and the engine torque for a given type of vehicle, based on the data from the NEDC. The engine conditions are physically determined from the speed of the vehicle and its constant parameters.

The same approach can be considered to estimate the emissions of other pollutants.

• *Probabilistic methods*

The previous models estimate emissions and energy consumption as a function of real vehicle operation variables (e.g. speed and acceleration, power demand, engine mechanics).

However, these data are not always available. One may obtain the velocity through microscopic traffic model simulation. But such models can be difficult to implement, especially on a large spatial scale with a lack of precise knowledge about the traffic situation, and can lead to unrealistically smooth velocity profiles. Hence, probabilistic models, based on random velocity disturbances, have been proposed in the literature.

The general idea of the random velocity disturbances approach is to run the emission and energy consumption models while replacing, for a given route, the actual speed of the vehicle by an approximate second-by-second speed profile $\tilde{v}_p^{\text{veh}}$ built from a deterministic and a stochastic component as

$$\tilde{v}_p^{\text{veh}} = \bar{v} + \eta \tag{3.16}$$

where $\bar{v}$ is the average traffic speed estimated from the road attributes provided by a geographical information system (e.g. speed limit, traffic signs, road grade) and η is a random variation in velocity for the subject vehicle.

It is possible to consider a spatial distribution of speed or acceleration based on driving cycles or statistical distributions [35].

[132] combines Markov chains with deterministic route attributes to generate the speed profile. In this model, η is adjusted according to

$$P(X(k+1) = X_i | X(k) = X_j) = M_{\mathrm{TP}}(i,j) \tag{3.17}$$

where $X(k) = [v_p^{\mathrm{veh}}(k)\ a_p^{\mathrm{veh}}(k)]^T$ is the state vector of the vehicle p at time step k, and the transition probability matrix M_{TP} is built from real data.

Another probabilistic model is the Motor Vehicle Emission Simulator (MOVES), presented by [278]. The aim of this method is to make the velocity trajectory more realistic. Thus, it is assumed that vehicle detector stations provide an estimation of $\bar{v}$. The random variation in velocity is defined as

$$\eta(k) = \tilde{v}_p^{\mathrm{veh}}(k-1) + a_p^{\mathrm{veh}}(k-1) - \bar{v}(k) \tag{3.18}$$

A procedure to determine the acceleration a_p^{veh} is presented in [278].

Probabilistic approaches are a solution in case of lack of information about the vehicle dynamics. By construction, they are less accurate than models based on the actual speed, but can be effectively used to estimate emissions and energy consumption [142]. To improve these methods, traffic prediction models could be integrated to determine $\bar{v}$.

Note that the variability of certain unobserved parameters between vehicles (e.g. temperature, Reid vapor pressure) can affect the emissions and energy consumption. These issues can be addressed by introducing probabilistic correction factors [83].

3.2.2 Physical pollutant and energy consumption model

In this section, a microscopic physical model, similar to the approaches reviewed in Section 3.2.1, is proposed to calculate the energy consumption and NOx emissions of internal combustion engine vehicles one by one, based on their longitudinal dynamics.

Note that even in the presence of lateral maneuvers such as lane changes, considering the longitudinal motion alone is sufficient because the energy associated with transient maneuvers can usually be neglected [230].

As in Eq. 3.6–3.7, Newton's second law of motion is used to determine the wheel force of the vehicle under consideration F_{w}. Then, the wheel torque T_{w} can be calculated as follows

$$T_{\mathrm{w}}(k) = F_{\mathrm{w}}(k) R \tag{3.19}$$

where R denotes the wheel radius.

The engine torque T_e and the engine speed ω_e can be directly calculated using the following relationships

$$T_\mathrm{e}(k) = \frac{T_\mathrm{w}(k)}{\gamma(k)\eta_\mathrm{gb}} \tag{3.20a}$$

$$\omega_\mathrm{e}(k) = \min\left\{\max\left\{\frac{v_p^\mathrm{veh}(k)\gamma(k)}{R}, \omega_\mathrm{min}\right\}, \omega_\mathrm{max}\right\} \tag{3.20b}$$

where η_gb, ω_min, and ω_max denote respectively the gear box efficiency, the minimum engine speed, and maximum engine speed. Based on the engine torque and speed, the fuel consumption rate y^fuel, expressed in liters per second, can be given by fuel consumption maps, such as the one shown in Fig. 3.4a for the same Euro 4 diesel light vehicle.

Based on the original work of [85] and the extension proposed in [247], a new regression model is introduced to calculate NOx emissions. The model returns the NOx emission rate y^NOx, expressed in kilograms per second, based on the fuel consumption rate y^fuel, the burned gas rate R_BGR, and the in-cylinder fuel mass per stroke and displaced volume m_fuel. It reads

$$\log\left(\frac{y^\mathrm{NOx}}{y^\mathrm{fuel}\rho^\mathrm{fuel}}\right) = a_1 + a_2 R_\mathrm{BGR} + a_3 m_\mathrm{fuel} \tag{3.21}$$

where a_1 – a_3 are regression coefficients, R_BGR is obtained from T_e and ω_e using the map given in Fig. 3.4b, and the in-cylinder fuel mass per stroke and displaced volume m_fuel is defined as follows

$$m_\mathrm{fuel} = y^\mathrm{fuel}\rho^\mathrm{fuel} \times 1000 \times 60 \times \frac{2\pi}{60 \times \omega_\mathrm{eng}} \frac{2}{4} \frac{N_\mathrm{cyl}}{d_\mathrm{e}} \tag{3.22}$$

where ρ^fuel and N_cyl denote respectively the fuel density and the number of cylinders. The factor $\frac{2}{4}$ characterizes the fact that the cycle of four-stroke engines consists of two crankshaft revolutions and four piston strokes.

Finally, the total fuel consumption $E^{0\to T}$ and NOx emissions $NOx^{0\to T}$ in the whole network between time steps 0 and T can be calculated as follows

$$E^{0\to T} = \sum_{k=0}^{T}\sum_{p} \delta_t y_p^\mathrm{fuel}(k) \tag{3.23a}$$

$$NOx^{0\to T} = \sum_{k=0}^{T}\sum_{p} \delta_t y_p^\mathrm{NOx}(k) \tag{3.23b}$$

The choice of the values of the parameters introduced above are given in Table 3.2. They correspond to a Euro 4 diesel passenger car, which represented around 27.8% of the French statistical vehicle fleet in 2017 [42].

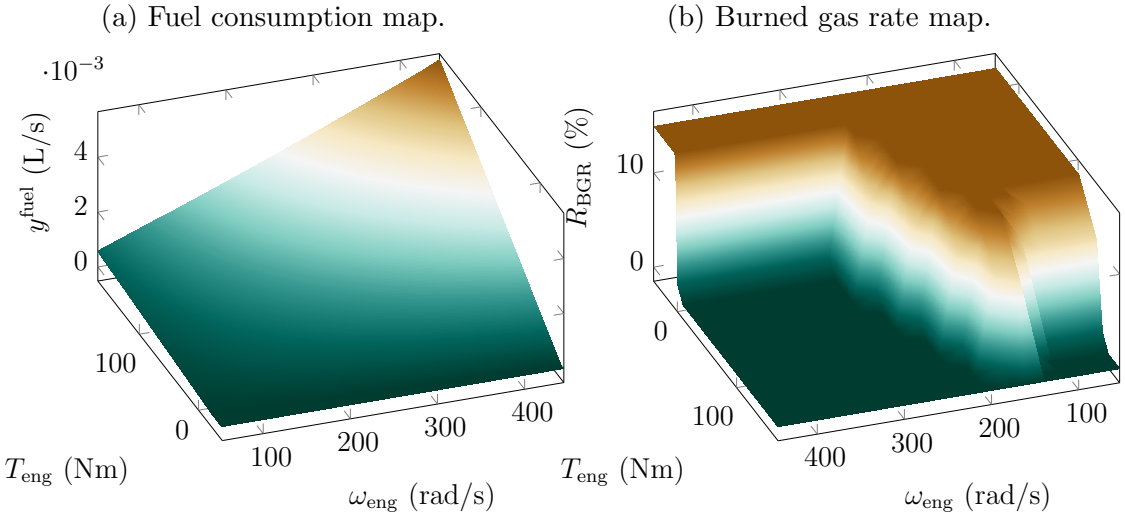

Figure 3.4: Fuel consumption and burned gas rate maps, defined as functions of the engine speed and engine torque.

3.3 Macroscopic models to predict pollutant emission and energy consumption

Macroscopic emission and energy consumption models estimate the rates of pollutant emission and energy consumption (electricity or fuel) from the macroscopic traffic dynamics (vehicle density, flow, average speed). In this section, the main categories of this kind of models are reviewed in Section 3.3.1, and the calibration and validation of a macroscopic model based on an artificial neural network (ANN) is presented in Section 3.3.2.

3.3.1 State-of-the-art

As mentioned in Section 2.3, the macroscopic traffic dynamics can be measured (average speed) or estimated through dynamic fluid-based traffic models. In this section, the meta-models used to calculate emissions and energy consumption from the traffic dynamics are presented. These meta-models consist in a mesoscopic framework as they usually associate macroscopic traffic data with models based on the microscopic functioning of vehicles. Two approaches are considered: meta-models associated with static average speed-based approaches or with dynamic fluid-based models. A discussion on the impact of the spatial and temporal discretizations is also proposed.

Symbol	Description	Value	Unit
C_{rr}	Rolling resistance coefficient	0.007	–
C_{X}	Drag coefficient	0.27	–
M	Vehicle mass	1340	kg
N_{cyl}	Number of cylinders	4	–
R	Wheel radius	0.32	m
S	Vehicle cross-section	1.95	m^2
d_{e}	Engine displacement	1,87	L
g^{grav}	Gravitational acceleration	9.81	m.s^{-2}
η_{gb}	Gear box efficiency	0.95	–
ρ^{air}	Air density	1.22	kg.m^{-3}
ρ^{fuel}	Fuel density	0.845	kg.L^{-1}
ω_{max}	Maximum engine speed	$\frac{4250\times 2\pi}{60}$	rad.s^{-1}
ω_{min}	Minimum engine speed	$\frac{800\times 2\pi}{60}$	rad.s^{-1}

Table 3.2: Microscopic fuel consumption and NOx emission model parameters and variables.

Meta-model associated with static average speed-based approaches

The average speed of the traffic on each link i is defined as

$$\bar{v}(i) = \frac{1}{T}\sum_{k=1}^{T}\frac{1}{N_i(k)}\sum_{j=1}^{N_i(k)} v_j^{\text{veh}}(k) \tag{3.24}$$

where $N_i(k)$ is the number of vehicles on link i at time step k. In the following, the average speed of link i, $\bar{v}(i)$, is referred to as $\bar{v}$ for simplicity.

Emissions and energy consumption can be calculated by considering an average speed-based approach. This is done by a meta-model whose general procedure is illustrated in Fig. 3.5, and operation steps are presented below.

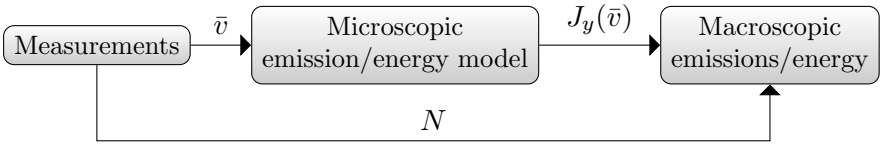

Figure 3.5: Structure of the emission and energy consumption meta-model associated with static average speed-based approaches.

1. The average speed $\bar{v}$ and the number of vehicles N are measured, or estimated.

2. The emission or energy consumption rate of a single vehicle J_y is calculated from $\bar{v}$ using a microscopic emission and energy consumption model (cf. Section 1.2.1).

3. $J_y(\bar{v})$ is then multiplied by N to approximate the total emission or energy consumption rate.

Note that this procedure can be conducted at different scales. The average speed $\bar{v}$ and the number of vehicles associated N can refer to a single link of a network, if the data are available, or to a larger spatial area. Moreover, the duration between two successive measurements usually depend on the measuring devices. These issues are addressed in Section 3.3.1.

This meta-model can be associated either with a data-based or a physical microscopic emission and energy consumption model. These approaches are detailed below. Note that they involve measuring, or estimating, the number of vehicles on the roads under consideration.

Some authors propose to associate the meta-model with a data-based microscopic emission and energy consumption model.

For instance, [29] proposes the following regression-based model in order to estimate the fuel use rate of a single vehicle

$$\ln\left(J_{\text{fuel}}^{\text{spat}}\right) = \beta_0 + \beta_1\bar{v} + \beta_2\bar{v}^2 + \beta_3\bar{v}^3 + \beta_4\bar{v}^4 + \beta_5\psi \tag{3.25}$$

where β_0 to β_5 are the regression coefficients.

Another common approach to estimate emissions and energy consumption on a large spatial scale is to associate this meta-model with a microscopic model based on aggregated data-driven emission or energy consumption factors $J_y(\bar{v}, \theta)$ that depend on the traffic average speed $\bar{v}$ and some vehicle parameters θ.

Let Ω be the set of possible parameters sets. Aggregated factors are usually simply the mean values of experimental measurements and are typically expressed in mass of pollutant emitted (or mass of fuel consumed) per vehicle and per unit distance traveled. Hence, the total emission or energy consumption rate, i.e. the output of the meta-model, of a link i containing N_i^θ vehicles with the set of parameters θ is denoted J_y^i and is given by

$$J_y^i = \sum_{\theta\in\Omega} N_i^\theta J_y(\bar{v}, \theta) \tag{3.26}$$

In practice, detailed information on the fleet composition is not available. Hence, a reference set can be considered, i.e. all the vehicles have the same parameters $\bar{\theta}$, and the emission or energy consumption rate on link i simply becomes:

$$J_y^i = N_i^{\bar{\theta}} J_y(\bar{v}, \bar{\theta}) \tag{3.27}$$

The COPERT (COmputer Programme to calculate Emissions from Road Transport) model [192] developed by the European Environment Agency is based on this method. Several vehicle parameters are included in θ: the vehicle type (passenger car, light commercial vehicle, heavy duty vehicle, L-category vehicle), the fuel type, the engine displacement and its registration date. The sets of parameters of all the vehicles constitute the vehicle fleet composition. An example of emission factors obtained with COPERT for different types of vehicle as a function of the speed is given in Fig. 3.6.

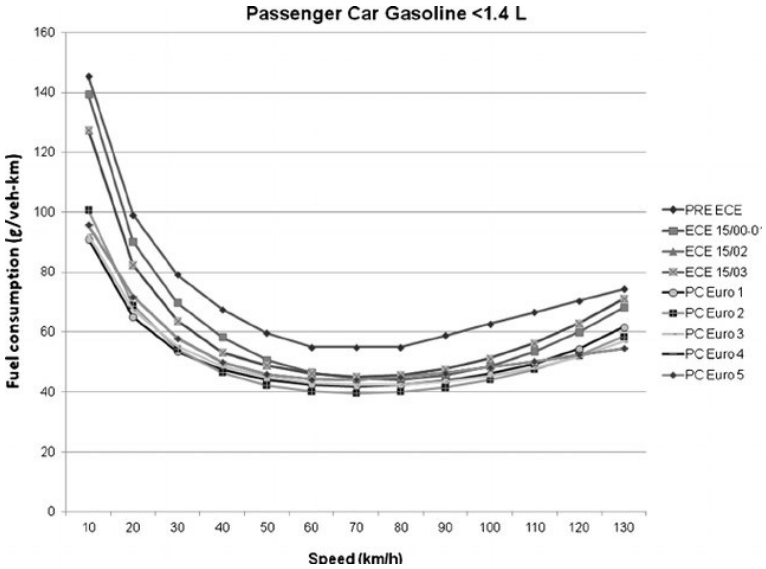

Figure 3.6: Fuel consumption factors of different gasoline passenger cars calculated with COPERT [236] [Published with permission of Networks and Spatial Economics].

[105] proposes the HBEFA (HandBook Emission FActors for road transport) model, which is more precise. This method additionally considers the driving conditions (highways, urban roads, stop-and-go traffic) and the volume-to-capacity ratio (number of vehicles divided by the capacity of the link), which is a dynamic variable, to determine $J_y(\bar{v}, \theta)$.

The accuracy can also be improved by multiplying the emission and energy consumption factor $J_y(\bar{v}, \theta)$ by a congestion correction factor, as does the Traffic

Energy and Emissions (TEE) model. The objective is to represent the effect of congestion on emissions and energy consumption. The congestion correction factor depends on the average speed, the traffic-light timing, the link length, and the traffic density [187]. These variables and parameters are used to estimate the time spent in each traffic situation (cruising, acceleration, deceleration and idling) and thus reflect the speed variability along the considered road link. The corresponding speed profile can then be reconstructed.

One limitation of these aggregated factors models is that the emission and energy consumption factors are not fundamental, as they depend on the driving cycle used during the measurements.

It is also possible to use this meta-model by associating it with a physical emission and energy consumption model.

For example, [129] proposes to use the following microscopic physical model to estimate the energy consumption needed by a vehicle p to travel a section of length L.

$$E = \begin{cases} E^{\mathrm{r}} + (\nu - 1)E^{\mathrm{p}} & \text{, if } E^{\mathrm{p}} \leq 0 \\ E^{\mathrm{r}} & \text{, if } E^{\mathrm{p}} > 0 \end{cases} \tag{3.28}$$

where $\nu \in [0, 1]$ is the downhill potential energy recuperation coefficient. The resistance and the potential energies are respectively given by

$$\begin{aligned} E^{\mathrm{r}} &= \frac{\rho^{\mathrm{air}}}{2} S C_{\mathrm{d}} \bar{v}^2 L + M g^{\mathrm{grav}} C_{\mathrm{rr}} L \cos\psi \\ E^{\mathrm{p}}(i) &= M g^{\mathrm{grav}} L \sin\psi \end{aligned} \tag{3.29}$$

where C_{d} is the Reynolds coefficient.

To model more precisely the speed change at an intersection, [58] introduces a transition speed at the interface between two links of respective average speeds $\bar{v}_{\mathrm{before}}$ and $\bar{v}_{\mathrm{after}}$ defined as

$$v_{\mathrm{transition}} = \mu \frac{\bar{v}_{\mathrm{before}} + \bar{v}_{\mathrm{after}}}{2} \tag{3.30}$$

where $\mu \in [0, 1]$ is a parameter depending on the type of interface (e.g. stop sign, traffic light, turning movement, etc.). This transition speed can be introduced to any model similar to the one presented in (3.28) – (3.29) to better model intersections.

Meta-model associated with dynamic fluid-based models

Emissions and energy consumption can be calculated by considering the fluid-based models dynamics. This is done by another meta-model whose general procedure is illustrated in Fig. 3.7, and operation steps are presented below.

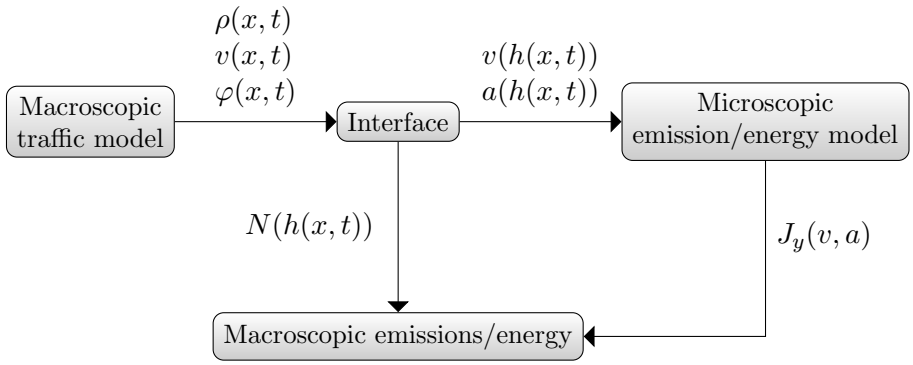

Figure 3.7: Structure of the emission and energy consumption meta-model associated with dynamic fluid-based traffic models.

1. First, a dynamic fluid-based traffic model is chosen (cf. Section 2.3.1). It provides the traffic variables, i.e. $\rho(x,t)$, $v(x,t)$, $\varphi(x,t)$.

2. Then, these variables are processed by an interface to generate groups of vehicles $h(x,t)$ sharing the same speed and acceleration. The interface calculates the speed, acceleration and number of vehicles of each group. They are respectively denoted $v(h(x,t))$, $a(h(x,t))$ and $N(h(x,t))$.

3. A microscopic emission and energy consumption model is chosen (cf. Section 1.2.1). It provides the emission or energy consumption rate $J_y(v,a)$ of a vehicle of group $h(x,t)$ using the outputs $v(h(x,t))$ and $a(h(x,t))$ of the interface.

4. The emission or energy consumption rate $J_y(v,a)$ of a vehicle of group $h(x,t)$ is multiplied by the number of vehicles in the corresponding group $N(h(x,t))$ to provide the total emission or energy consumption rate of group $h(x,t)$.

The procedure presented above is repeated as many times as there are groups. It is important to note that this generation of groups with homogeneous operation variables relies on the spatial and temporal discretizations of the traffic model. This issue is addressed in Section 3.3.1.

The procedure of the interface presented above is detailed in the following [288].

To compute emissions and energy consumption, the employed traffic models are often discrete both in time and in space. Hence, two acceleration components have to be considered: the temporal and the spatio-temporal accelerations:

- The temporal acceleration a^{temp} is experienced by the vehicles that stay within the same cell from one time step to the next one. It reflects the speed

variation within a cell. It is expressed as

$$a_i^{\text{temp}}(k) = \frac{v_i(k+1) - v_i(k)}{\delta_t} \tag{3.31}$$

The number of vehicles N^{temp} subject to this acceleration, i.e. that stay within the cell i during time interval $[k\delta_t,\ (k+1)\delta_t]$ is equal to

$$N_i^{\text{temp}}(k) = \delta_x \rho_i(k) - \varphi_i^{out}(k)\delta_t \tag{3.32}$$

The first term represents the number of vehicles initially in cell i at time step k, and the second term characterizes the number of vehicles that have leaving it. These vehicles constitute a group $h(x,t)$ mentioned above. There are as many groups of this type as there are cells in the spatial discretization of the traffic model.

- The spatio-temporal acceleration a^{spat} is experienced by the vehicles that move from one cell to another one. It reflects the speed difference between adjacent cells. For each cell i, the acceleration $a_{r,i}^{\text{spat}}$ from its upstream cell r is defined as

$$a_{r,i}^{\text{spat}}(k) = \frac{v_i(k) - v_r(k-1)}{\delta_t} \tag{3.33}$$

The number of vehicles N^{spat} subject to this acceleration, i.e. that have moved from the cell r to cell i during time interval $[k\delta_t,\ (k+1)\delta_t]$ is

$$N_{r,i}^{\text{spat}}(k) = \begin{cases} \delta_t \varphi_i^{\text{in}}(k) & \text{if } |\mathcal{P}_i| = 0 \\ \delta_t \varphi_r^{\text{out}}(k) & |\mathcal{P}_i| = 1 \\ \beta_i \delta_t \varphi_r^{\text{out}}(k) & \text{if } |\mathcal{P}_i| = 2 \end{cases} \tag{3.34}$$

These vehicles constitute a group $h(x,t)$ mentioned above. There are as many groups of this type as there are cells interfaces in the spatial discretization of the traffic model.

Ultimately, a generic formulation to calculate the emissions and energy consumption rate in a network made of n cells is

$$\begin{aligned} J_y^{\text{network}}(k) = \ & \textstyle\sum_{i=1}^{n} J_y(a_i^{\text{temp}}(k), v_i(k)) N_i^{\text{temp}}(k) + \\ & \textstyle\sum_{i=1}^{n} \sum_{j=1}^{n} J_y(a_{i,j}^{\text{spat}}(k), v_i(k)) N_{i,j}^{\text{spat}}(k) \end{aligned} \tag{3.35}$$

where $N_{i,j}^{\text{spat}}$ is always zero if there is no connection between cells i and j. The first term of (3.35) refers to the emissions and energy consumption of vehicles staying in the same cell from time step k to $k+1$ (temporal acceleration term),

and the second term refers to those of vehicles moving from one cell to another (spatio-temporal acceleration term).

To estimate emissions and energy consumption more precisely, this calculation can be done by differentiating classes of vehicles. In that case, the function J_y can consider the real parameters θ of the vehicles instead of average values.

This meta-model can be associated either with a data-based or a physical microscopic emission and energy consumption model. Some examples are presented below. Naturally, the meta-model procedure is generic and can be adopted to other models.

Some authors propose to use this meta-model by associating it with a data-based emission and energy consumption model. For example, [288] proposes to integrate the macroscopic traffic second order model METANET with the microscopic data-driven emission and fuel consumption model VT-micro. The resulting meta-model, called VT-macro, is mainly suitable for modeling emissions and energy consumption on highways.

Similarly, [158] suggests to associate the traffic first order S model with VT-micro in an urban network. The authors present a set of possible behaviors for the vehicles (e.g. free, idling, accelerating, decelerating, start-and-stop behavior). Another use of the meta-model in an urban environment can be found in [124], in which the authors propose the same models association.

It is also possible to use this meta-model by associating it with a physical emission and energy consumption model. For example, [51] develops a method based on the VLM and a physical approach to determine energy consumption. This model considers only the spatio-temporal component of acceleration. In each cell, energy consumption is determined from the cell average speed (either free or congested), considering zero temporal acceleration. At the interface of the cells, the energy is calculated based on the following spatio-temporal acceleration

$$a_{i,j}^{\text{spat}} = \min\left\{a, \frac{v_j - v_i}{\delta_t}\right\} \tag{3.36}$$

where the maximum acceleration a is a model parameter. Note that time does not appear in the formulation of [51] because the analysis is performed at steady state.

Spatial and temporal discretizations

The spatial and temporal discretizations of the methods used are a crucial point in emissions and energy consumption estimation: a compromise has to be found between precision and computation time.

- *Spatial discretization*

Concerning the use of the average speed meta-model, measurements of average speed and number of vehicles made on a road level would naturally give better results than measurements made on a larger spatial scale. But this depends mainly on the devices used to monitor the traffic. Some average speed-based meta-models consider a fine spatial discretization in order to be compatible with urban networks (e.g. COPERT Street Level [221]).

When using the meta-model associated with dynamic fluid-based models, the choice of the spatial discretization step size should be given some thought. A balance concerning the number of cells and their length has to be found in order to satisfy the desired accuracy without excessively increasing computation times.

- *Temporal discretization*

Some authors have proposed methods to use the average speed meta-model with high-frequency data inputs, i.e. average speeds and number of vehicles updated at high frequency. For example, [147] proposes a method to adapt the COPERT emission and fuel consumption model to high-frequency data inputs. This kind of approach is more precise. However, it is essential to note that the average speed-based meta-model is static. In other words, even with high frequency data inputs, emissions and energy consumption are calculated for successive average speeds, but do not consider the acceleration of vehicles, yet crucial to fully characterize emissions and energy consumption [6].

Dynamic fluid-based meta-models can consider macroscopic accelerations, and should therefore be more precise. However, the choice of δ_t is particularly critical as it must lead to realistic acceleration values while respecting the CFL condition given in Eq. 2.42.

- *Summary*

In other words, adopting a dynamic fluid-based approach with very long time step size and length of cells is similar to having an average speed-based approach. The difference would be that the data are obtained by simulation instead of being measured.

Finally, the most precise way to calculate emissions and energy consumption at a large spatial scale would be to use a microscopic traffic model and to associate it with a microscopic emission and energy consumption model (cf. Section 1.2.1). In fact, this approach is the only one able to reflect differences in microscopic drivers' behavior (e.g. sudden deceleration, merging, lane changing). When traffic is congested, these can result in shock waves causing traffic breakdown, that a macroscopic traffic model cannot depict [138]. However, microscopic models are not appropriate at large scale because of the enormous computation times generated by the large number of vehicles considered. [227] proposes a statistical approach to process this large amount of data by introducing sampling methods.

The author suggests to estimate emissions and energy consumption only in some relevant locations of the network, and to extend the estimations at larger scales.

3.3.2 Artificial Neural Network-based model

Macroscopic pollutant emission and energy consumption models are particularly adapted to eco-management control strategies based on prediction because of their lower numerical complexity.

As discussed previously in Section 3.3.1, several approaches can be implemented to estimate fuel consumption from the macroscopic traffic variables. A first strategy consists in using emission factors, which are typically defined as a function of the average speed, but can also take additional macroscopic variables as arguments [192, 105]. Such models are particularly efficient to estimate aggregated emission levels, but they do not take into account the dynamic aspect of traffic. To consider traffic dynamics, some works propose to introduce macroscopic accelerations, which are defined as the temporal and spatio-temporal numerical derivatives of the average speed [288]. Yet, such approaches raise the question of model calibration and temporal discretization fineness, which is crucial in the calculation of acceleration. Spatial calibration also plays an essential role because this type of model assumes that all vehicles in the same cell are subject to the same acceleration.

Therefore, we propose in this work to calibrate an ANN-based macroscopic fuel consumption model which is consistent with the parameterization of the problem. In particular, it is expected that this model will be more accurate because of its greater sensitivity to fuel overconsumption at low average speeds. This latter is caused by successive acceleration and deceleration phases, that are not necessarily captured by other macroscopic models. Finally, it is essential to note that despite good performances expected for the following study cases, this ANN-based model may not be adapted to all types of networks and all types of vehicle driving style.

Calibration

The model predicts the fuel consumption rate of vehicles in each cell i, expressed in liters per second per vehicle, from the variables returned by the traffic prediction model, namely the CTM. Because of the granularity of the information provided by the CTM, the macroscopic energy model associates the same fuel consumption rate to all the vehicles of the same cell at a given time.

In practice, the ANN is composed of three hidden layers. It is trained with traffic data obtained through SUMO simulations, and energy consumption data determined from the vehicles' speed profiles using the microscopic physical fuel consumption model. The data are measured at a frequency of 1 Hz, generating

about 3.5 million data. As a result, the ANN predicts the average fuel consumption rate per vehicle of vehicles in cell i at time k, denoted $\hat{y}_i^{\text{fuel}}(k)$. The ANN inputs are listed in Fig.3.8, they include the densities and speeds at current and previous time steps, the speed limit, and the TLS state. In case cell i is not regulated by a TLS, we consider $\forall k, \alpha_i(k) = 1$. The densities and speeds at previous time steps are included in the model inputs as they add information on the dynamics of the system. This partially compensates for the fact that the macroscopic CTM variables do not contain any information on vehicles accelerations. Such approaches have already been proposed in the literature. For example, [288] introduces macroscopic accelerations in the VT-macro model, based on the derivatives of cells' average speeds.

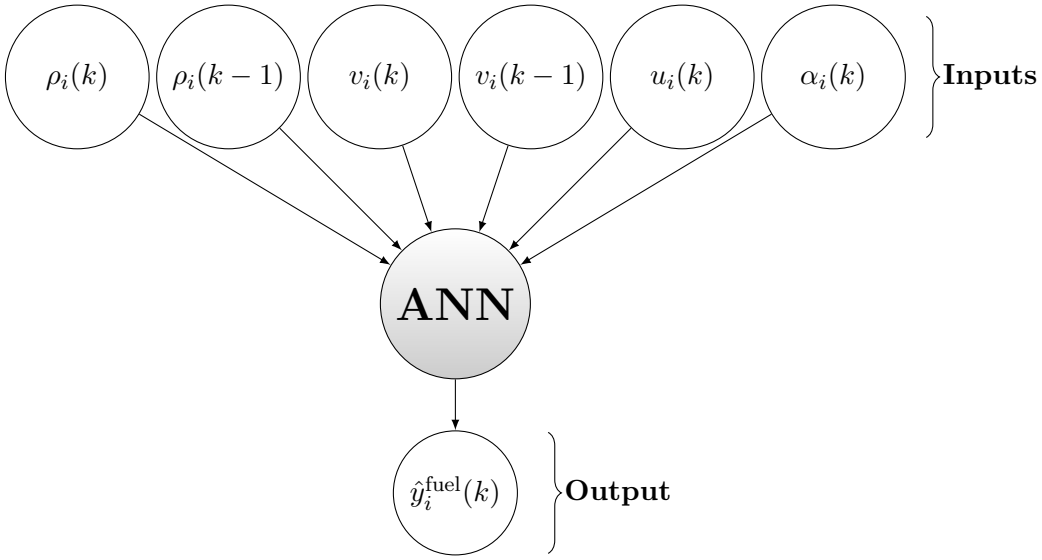

Figure 3.8: Representation of the ANN inputs and output.

As a result, the prediction of the total fuel consumption in the whole network over a prediction time horizon Δ_p (between time steps k and $k + \Delta_p$), expressed in liters, can be calculated as

$$\hat{E}^{k \to k+\Delta_p} = \sum_{e=k}^{k+\Delta_p} \sum_{i \in \mathcal{R}} \delta_x \delta_t \rho_i(e) \hat{y}_i^{\text{fuel}}(k) \tag{3.37}$$

The ANN model is trained using the Manhattan grid network introduced in Fig. 2.11. To generate training data, eight simulations are run with two different initial densities (0% and 70% of the maximum density ρ^{M}), and four different constant speed limits (20 km/h, 30 km/h, 40 km/h, 50 km/h) are considered in the urban area. Note that a constant speed limit of 70 km/h is always considered in

the peri-urban area as its speed limit will not be considered as a control actuator in this work. Measurements of the density, speed, and energy consumption rate are carried out in each cell i with a frequency of 1 Hz. All simulations have the same duration of 15 minutes.

Validation

It is essential to evaluate the performance of the ANN-based macroscopic energy model by running it on new data. To that extent, four simulations of $T = 15\,\text{min}$ are run with initial densities of 30% and 20% of the maximum density in the urban and the peri-urban areas, respectively. The demand is constant over time and equal to 0.2 veh.s^{-1} at each source. The simulations are run with constant speed limits of 20 km/h, 30 km/h, 40 km/h, and 50 km/h. In each simulation, the fuel consumption is calculated using the microscopic energy model, and constitutes the target, which is compared with the output of the ANN-based macroscopic energy model. The results are shown in Fig. 3.9. On average, the error between the target and the prediction is 11.5% (from 4% with 20 km/h speed limits to 16.4% with 50 km/h speed limits). This gap is mainly due to the fact that not all information on vehicles' behavior can be captured using macroscopic traffic variables alone, and that a set of macroscopic variables may correspond to different microscopic situations. However, it appears that the trend of the two curves is similar, which corresponds to the expected result.

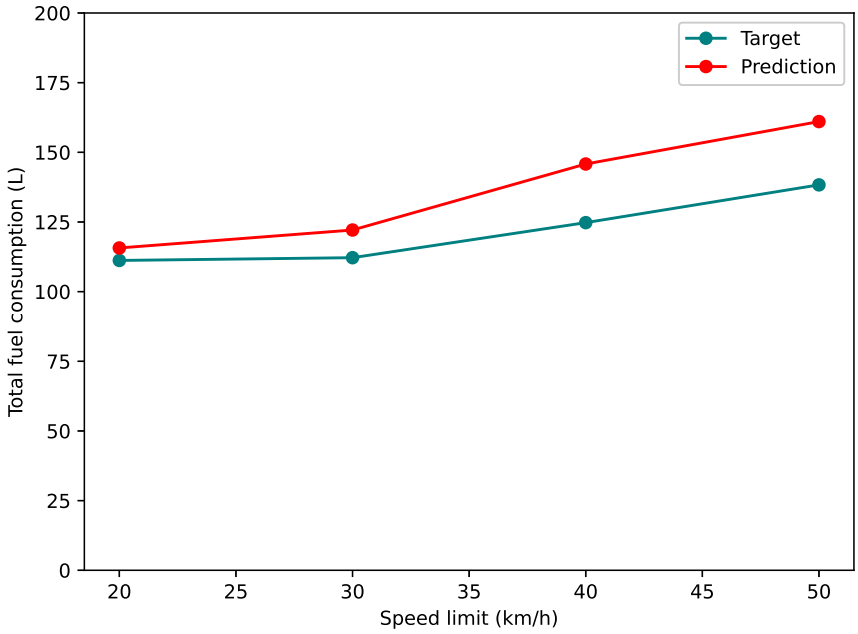

Figure 3.9: Comparison of the actual fuel consumption given by the microscopic model (target) with the corresponding macroscopic energy model output (prediction) in an evaluation scenario.

Chapter 4

Variable speed limits control for enhanced energy efficiency

Contents

4.1 Foreword

In this chapter, we propose first to investigate the relationship between energy efficiency and traffic dynamics. Then, online closed-loop control approaches are introduced in order to implement VSLs in a Manhattan grid structure. These approaches consider in a first step macroscopic traffic and energy models. In a second step, macroscopic traffic and energy models are considered to predict and optimize the traffic system whose traffic dynamics and pollutant and energy consumption are determined using microscopic models.

4.2 Analysis of the relationship between energy efficiency and traffic dynamics

The relationship between energy efficiency and traffic dynamics can be investigated in different ways. In this section, we propose first to analyze the impact of the car-following model on the energy consumption, calculated with the microscopic energy consumption model. Then, the relationship between energy efficiency and traffic dynamics is characterized on the ring road (cf. Fig. 2.7) and in the Manhattan grid network (cf. Fig. 2.11). In particular, the impact of congestion and speed limits is characterized.

4.2.1 Impact of the car-following model on the energy consumption

A comparison between IDM, Krauss, and Wiedemann car-following models based on the speed profiles of the vehicles has been proposed in Section 2.2.2. To go further, we propose in this section to analyze the impact of the choice of the car-following model on the energy consumption curves.

Simulations are run with the physical energy model described in Section 3.2.2. They are performed on the ring road presented in Fig. 2.2 so as to characterize the behavior of the models in a steady-state situation. The speed limit is 50 km/h.

The fuel consumption is normalized by the distance traveled by the vehicles, and the average consumption is represented in Fig. 4.1 as a function of the density, i.e. the number of vehicles on the ring road.

The average fuel consumption is increasing with the density for all models. The fuel consumption curve determined with Wiedemann car-following model reaches much higher levels than the other two models. This was expected in view of the very low speed and the numerous acceleration and deceleration phases of vehicles observed with this model in Fig. 2.3. It is interesting to note that the three phases

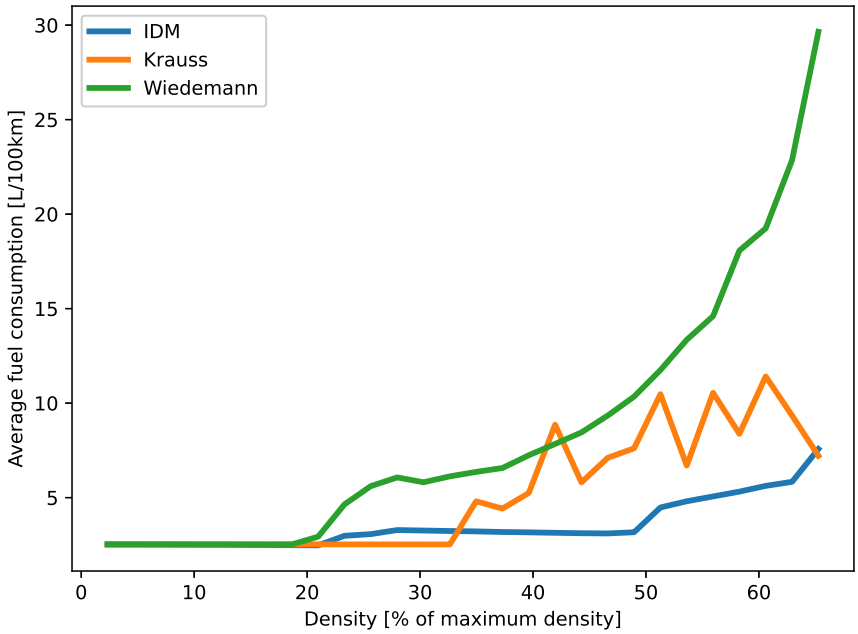

Figure 4.1: Comparison of the fuel consumption curves, expressed in L/100km, as a function of the density for IDM, Krauss, and Wiedemann car-following models.

identified with the IDM in Fig. 2.3 (lower speed without oscillations – regular stop-and-go waves – chaotic stop-and-go waves) appear clearly in Fig. 4.1 with two main steps around 20% and 50% of the maximum density. Also, the IDM is preferred to Krauss model because the curve of this latter is not monotonous, which a priori does not really make physical sense. These elements reassure us in our choice to consider the IDM as car-following model in this work, although each of the 3 models presented could have been taken as reference.

4.2.2 Stationary analysis of the relationship between energy efficiency and traffic dynamics on a ring road

The relationship between energy consumption and traffic dynamics can be further analyzed using the IDM and the physical emission and energy consumption model presented in Section 3.2.2. In particular, we are interested in analyzing the impact of the speed limit and the presence of a TLS for different congestion levels. This study is conducted considering the ring road presented in Fig. 2.7 to reach steady-state conditions, with a TLS that is either always green or that alternates between green and red phases.

The results are given in Fig. 4.2. As mentioned in Section 4.2.1, the average

fuel consumption is always globally increasing with the density. This is due to the fact that thermal vehicles are more energy efficient at 50 km/h than at lower speed limits, because of the u-shaped consumption curve presented in Fig. 1.4. Also, the apparition of stop-and-go waves at higher densities deteriorates the energy efficiency because of successive acceleration and braking phases.

The results also reveal that regardless of the presence of TLS, 50 km/h speed limits are always more energy efficient than 20 km/h for low density values, but that this observation is reversed when the density exceeds a certain threshold. Again, this can be explained by the u-shaped consumption curve and by the fact that accelerations up to 50 km/h naturally consume more energy than accelerations up to 20 km/h.

These results highlight the potential of speed limit control in urban areas to optimize energy consumption. Also, the fact that the fuel consumption curves under 20 km/h and 50 km/h speed limits have different shapes depending on the presence of TLS, and that their intersections do not occur for the same density level (around 50% of the maximum density without TLS, around 60% of the maximum density with TLS) highlights the fact that control must be adapted to each situation.

4.2.3 Quasi-stationary analysis of the relationship between energy efficiency and traffic dynamics in a Manhattan grid structure

To go further, we propose in this section to analyze the relationship between energy efficiency and traffic dynamics in the Manhattan grid structure presented in Fig. 2.11. In particular, we are interested in analyzing the impact of the speed limit in the urban area for different congestion levels. To that extent, simulations of $T = 15$ min are run with an initial density of 20% of the maximum density in the peri-urban area (and different initial densities of 0%, 30%, 60%, and 90% of the maximum density in the urban area). For each initial density level, simulations are run with constant speed limits varying from 20 km/h to 50 km/h, with a step of 5 km/h. The traffic demand at each exogenous source is considered constant over time and equal to $d^{\text{in}} = 0.2$ veh.s^{-1} (the endogenous sources are not considered here). A short simulation time T is chosen in order to limit the decongestion and keep densities of the same order of magnitude within each simulation. The higher the initial density, the longer it takes to decongest the network.

The results are given in Fig. 4.3 & 4.4. On the one hand, the observation of Fig. 4.3a reveals that the TTD in the urban area, which is to be maximized to improve traffic fluidity, is always increasing with the speed limit, whatever the level of congestion. However, it is higher with initial densities of 30% and

(a) Fuel consumption as a function of the density, without TLS.

(b) Fuel consumption as a function of the average speed, without TLS.

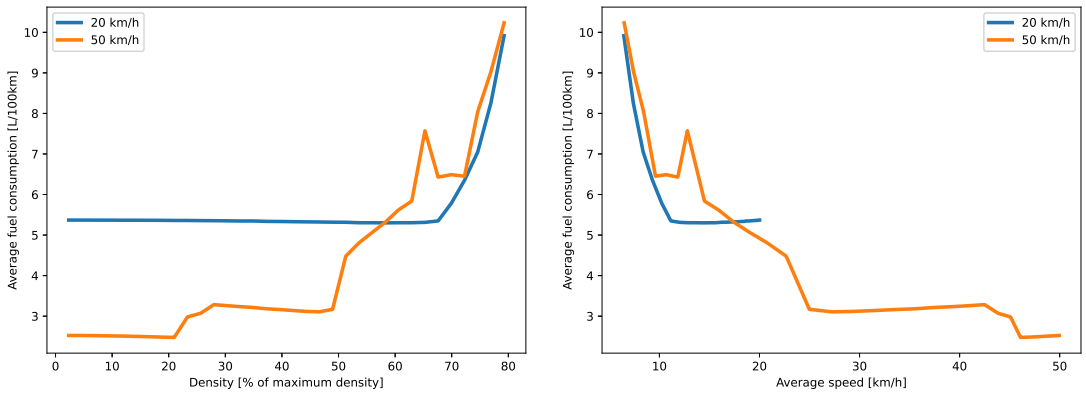

(c) Fuel consumption as a function of the density, with TLS.

(d) Fuel consumption as a function of the average speed, with TLS.

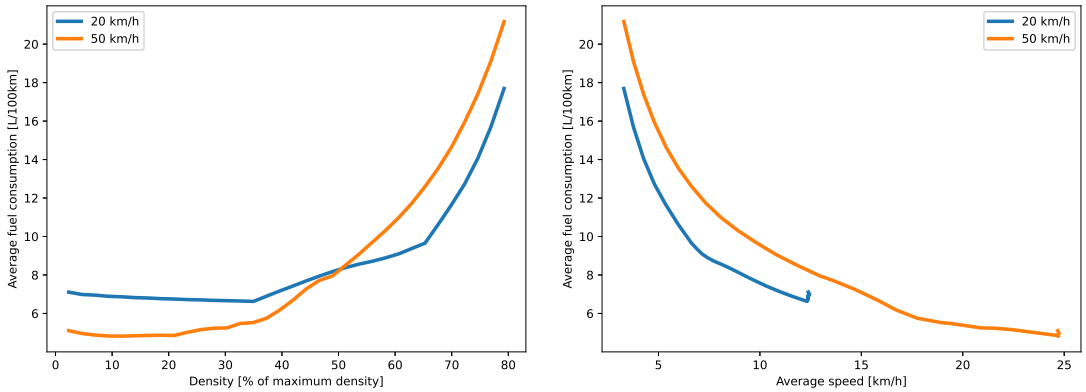

Figure 4.2: Average fuel consumption on the ring road as a function of the density and the average speed. Simulations are run with and without TLS (as described in the scenarios defined in Section 2.3.3), under 20 km/h and 50 km/h speed limits.

60% than 0% and 90%, which suggests that the network TTD is maximized for density values close to the plateau of the trapezoidal fundamental diagram, which corresponds to the critical density. On the other hand, the TTD in the peri-urban area, represented in Fig. 4.3b, seems to be monotonously decreasing with an increasing congestion level in the network, because of the presence of queues that mechanically reduce the flow entering the network. However, it appears that its loss is negligible as long as the density is lower than the critical density.

Concerning the environmental impact, Fig. 4.3c & 4.3d show that the total fuel consumption and NOx emissions in the urban area, calculated using the microscopic model, are monotonously increasing with the speed limit. However, it is

(a) TTD in the urban area.

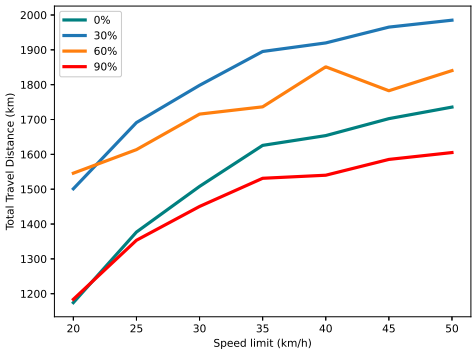

(b) TTD in the peri-urban area.

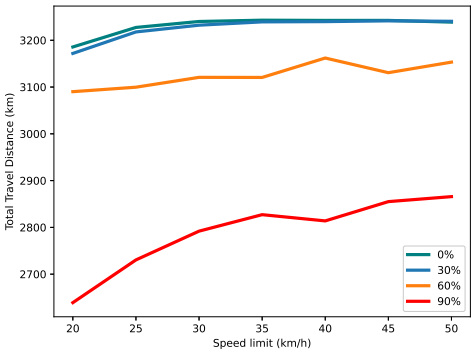

(c) Total fuel consumption in the urban area.

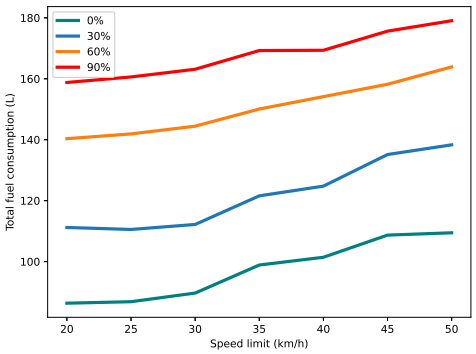

(d) Total NOx emissions in the urban area.

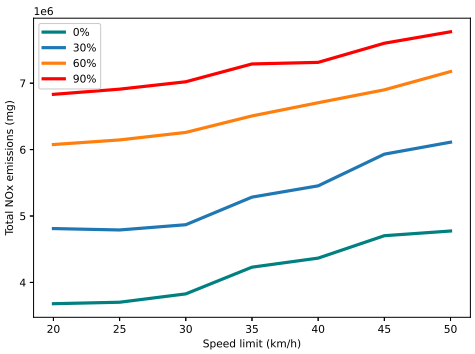

Figure 4.3: TTD, total fuel consumption and NOx emissions for different initial densities (from 0% to 90% of the maximum density ρ^{M}) under different constant speed limits (from 20 km/h to 50 km/h).

(a) Average fuel consumption in the urban area.

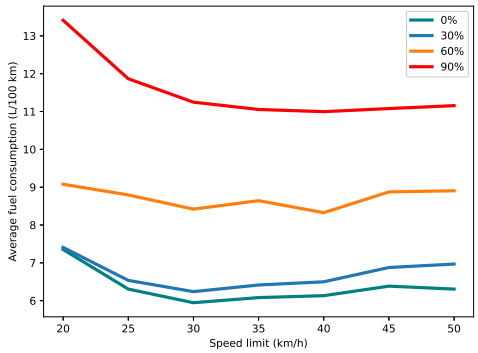

(b) Average NOx emissions in the urban area.

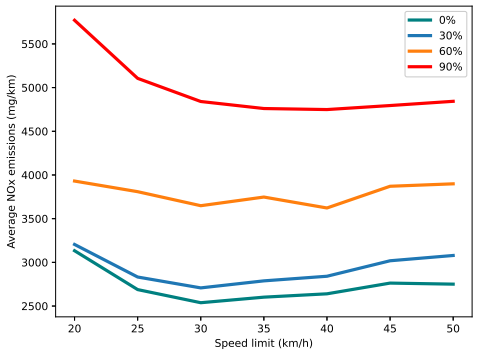

(c) Average fuel consumption in the peri-urban area.

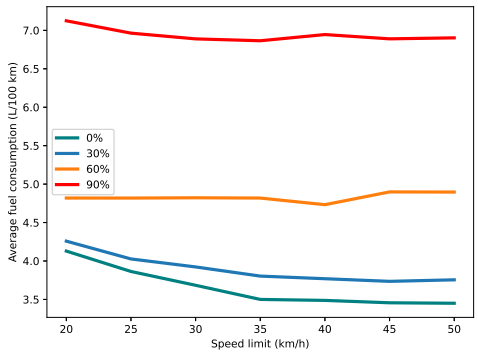

(d) Average NOx emissions in the peri-urban area.

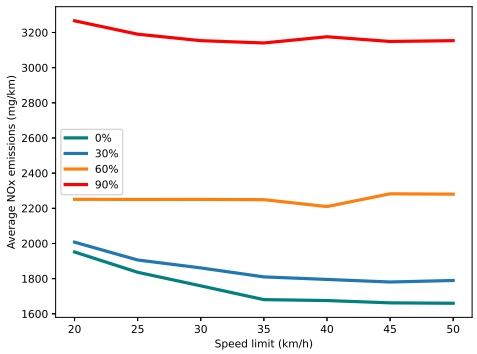

Figure 4.4: Average fuel consumption and NOx emissions for different initial densities (from 0% to 90% of the maximum density ρ^{M}) under different constant speed limits (from 20 km/h to 50 km/h).

difficult to draw a conclusion from these observations in the sense that the TTD in the urban area is also increasing with the speed limit. Hence, it is necessary to define new criteria to be able to compare the different scenarios, such as an objective function that integrates the TTD. In this sense, we define the average fuel consumption $E_{avg}^{0\to T}$ and NOx emissions $NOx_{avg}^{0\to T}$, per vehicle and per distance traveled. Classically, these criteria are respectively expressed in L/100km and in mg/km, and are defined as follows

$$E_{avg}^{0\to T} = \frac{E^{0\to T}}{TTD^{0\to T}} \tag{4.1a}$$

$$NOx_{avg}^{0\to T} = \frac{NOx^{0\to T}}{TTD^{0\to T}} \tag{4.1b}$$

The average fuel consumption and NOx emissions are represented in Fig. 4.4a & 4.4b. These functions seem to be convex, and the position of the minimum appears to depend on the level of congestion.

In the peri-urban area, Fig. 4.4c & 4.4d show that the appearance of queues due to a highly congested urban area can have a major impact on the average fuel consumption and NOx emissions.

As a result, both the environmental and the traffic performance criteria reveal a switch in the system efficiency around the critical density, i.e. the density values close to the plateau of the trapezoidal fundamental diagram that correspond to the maximum flow. Also, there seems to be a trade-off between energy efficiency and traffic performance, and the best compromise lies around the critical density in the network. For a given level of congestion at steady state, the choice of the speed limit characterizes another trade-off between TTD, which is to be maximized, and E_{avg} and NOx_{avg} that are to be minimized. These results are instinctive and allow a priori to validate the approach developed in this study. To go further, the optimal speed limit might be above 50 km/h but this range of speed limits are not analyzed here as it would pose safety issues in an urban environment.

4.3 Variable speed limits control strategy using macroscopic models

In view of the results presented in Section 4.2, it appears that the online closed-loop control of speed limits, is of particular interest as it could maintain the system at desired density levels, and ensure smooth transitions between different levels of congestion. In this section, we propose to analyze the performance of an ecological VSLs approach aimed at reducing the environmental impact and improving the traffic performance using an NMPC framework. In this section, we only consider

macroscopic traffic (CTM) and emission/energy consumption (VT-macro) models, both for simulation and prediction purposes. Simulations are run in a Manhattan grid network.

4.3.1 Control strategy

Model predictive control framework

The closed-loop MPC control framework implemented in this study is given in Fig. 4.5. The block diagram shows the inputs and outputs of the different blocks considered. In practice, the closed-loop controller operates as follows:

1. At each control time step k, i.e. multiple of the control time horizon Δ_c, the current state of the system x_k is measured and provided to the MPC controller.

2. The traffic predictor estimates the evolution of the system state $\hat{x}^{k+1\to k+\Delta_p}$ (here, $\hat{x}^{k+1\to k+\Delta_p} = x^{k+1\to k+\Delta_p}$ because the same models are used for simulation and prediction) on a prediction time horizon Δ_p, i.e. between $k+1$ and $k+\Delta_p$. As indicated in Eq. 2.38, the predicted state is defined as

$$\hat{x}_k = [\hat{\rho}_{k-1}, \hat{\rho}_k] \tag{4.2}$$

   where $\hat{\rho}(k)$ denotes the predicted densities at time step k.

3. The fuel consumption $\hat{E}^{k+1\to k+\Delta_p}$ between time steps $k+1$ and $k+\Delta_p$, expressed in liters, is predicted using a macroscopic fuel consumption model (here again, $\hat{E}^{k+1\to k+\Delta_p} = E^{k+1\to k+\Delta_p}$).

4. An optimizer based on the Broyden-Fletcher-Goldfarb-Shanno (BFGS) algorithm repeats steps 2 and 3 in order to find system inputs, i.e. a trajectory of speed limits $V^{k+1\to k+\Delta_p} = \left[[V_i(e)]_{i\in\mathcal{R}}\right]_{e\in[k+1..k+\Delta_p]}$, minimizing an objective function J along the prediction time horizon Δ_p. Once this optimum trajectory of speed limits is found, its first iteration, i.e. between $k+1$ and $k+\Delta_c$ is applied to the system. Note that to reduce the computational burden of the approach, clusters of roads can be introduced to parameterize the trajectory of speed limits. In practice, all the roads of the same cluster are controlled by the same variable, i.e. they are subject to the same speed limit at any time of the simulation.

The BFGS algorithm, used in the optimizer block, is an iterative method, which is able to solve unconstrained nonlinear optimization problems [34, 79, 92, 233]. It is based on an approximation of the inverse of the second derivative of the

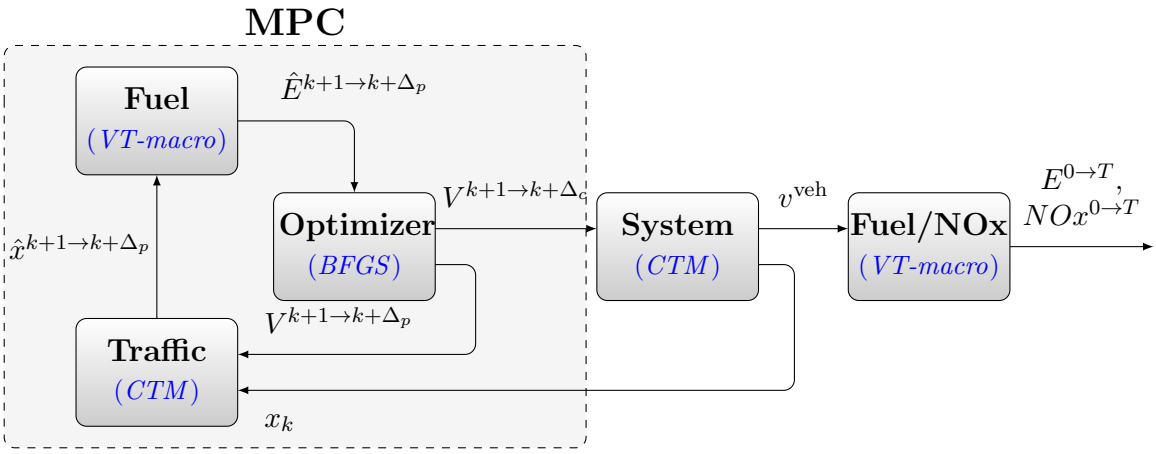

Figure 4.5: Block diagram of the global approach for ecological VSLs strategy using macroscopic models.

objective function, rather than explicitly constructing the Hessian matrix. In practice, this approximation is obtained from gradient evaluations via a secant method. As a result, the computational complexity of the algorithm is only $\mathcal{O}(n^2)$. In the literature, several works have evaluated the numerical performance of this quasi-Newton method, and have demonstrated its global convergence properties on uniformly convex problems, which is not the case in this work [163]. In this work, we are using L-BFGS-B, which is a limited-memory version of the algorithm that is particularly suited to high-dimensional problems. This version also handles bound constraint minimization, which is necessary to remain within the allowable speed limits.

To improve the performance of the solver, the BFGS algorithm is used in a two-phase method that combines a global stepping algorithm with local minimization at each time step. In total, we consider in this work 6 runs of the local minimizer in order to improve the global solution and to reduce the risk of local optimum. As a result, the controller takes an average of 8 min 30 s to run at each control time step, which makes it compatible with off-line approaches only.

For implementation reasons, the prediction time horizon Δ_p should be a multiple of the control time horizon Δ_c. The corresponding proportionality coefficient K is defined as follows

$$\exists K \in \mathbb{N}^*,\ \Delta_p = K\Delta_c \tag{4.3}$$

The operation of the MPC controller of this study is illustrated in Fig. 4.6. In order to simplify the implementation of such a methodology, it is parameterized as follows:

- Between two successive control time steps k and $k + \Delta_c$, the control, i.e.

the speed limits, remain constant. They are continuous and bounded by $V_{\min} = 20\,\text{km/h}$ and $V_{\max} = 50\,\text{km/h}$.

- All the cells of a given road have the same speed limit.

- In order to reduce the degree of freedom of the system, it is possible to go further and group the roads in a few clusters, each cluster then being controlled by a single speed limit variable. A counterpart of this approach is that the solution obtained may be suboptimal. However, it is usually necessary when going large scale because considering n_{clusters} clusters of roads results in an optimization problem with $K \times n_{\text{clusters}}$ variables only at each control time step. In practice, K and n_{clusters} can both be adapted to have convenient computation times. The choice of the value of K should be a compromise between the computational burden and the robustness of the controller. The choice of n_{clusters} mainly depends on the structure of the network.

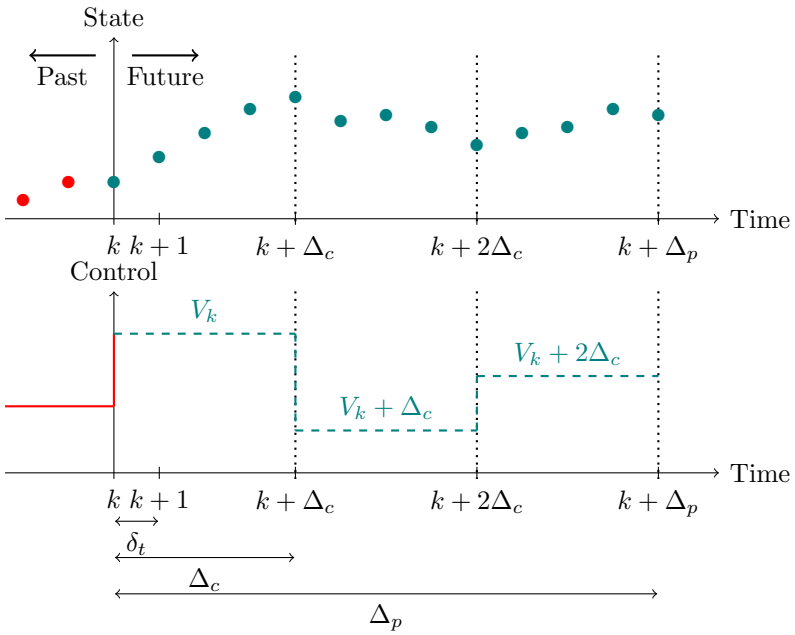

Figure 4.6: Representation of the NMPC framework, for $K = 3$.

As a result, the controller solves the following optimization problem

$$\begin{aligned} \min_{V^{k\to k+\Delta_p}} \quad & J(\hat{x}^{k\to k+\Delta_p}, V^{k\to k+\Delta_p}) \\ \text{s.t.} \quad & \rho_i(e+1) = \rho_i(e) + \tfrac{\delta_t}{\delta_x}\left(\varphi_i^{\text{in}}(e) - \varphi_i^{\text{out}}(e)\right), \forall e \in [k, \dots, k+\Delta_{\text{p}}-1] \\ & V_i(e) \in [20, 50] \text{ km/h}, \forall i \in \mathcal{R}, \forall e \in [0..T] \end{aligned} \tag{4.4}$$

The control horizon is set to $\Delta_c = 5\,\text{min}$, so as to have a compromise between the flexibility of the controller and the comfort of road users. In order to ensure the robustness of the controller, we propose to consider $K = 6$ (i.e. $\Delta_p = 30\,\text{min}$).

Objective function

The choice of the objective function is crucial in traffic eco-management control strategies. Several formulations can be implemented to solve ecological traffic management problems [198]. Usually, this kind of objective function is the weighted sum of an ecological metric, and a traffic efficiency metric. The purpose of this multi-objective optimization, based on metrics that can be antagonistic, is to avoid trivial solutions (for example, reduce the speed limits of the entering roads in order to reduce the number of vehicles in the network, which will naturally reduce the fuel consumption), and find a compromise between energy efficiency and traffic performance. In this study, we consider

$$J(\hat{x}^{k\to k+\Delta_p}, V^{k\to k+\Delta_p}) = \lambda \frac{\hat{E}^{k+1\to k+\Delta_p}}{\sigma_{\text{E}}} - (1-\lambda)\frac{\hat{TTD}^{k+1\to k+\Delta_p}}{\sigma_{\text{TTD}}} \tag{4.5}$$

where σ_{E} and σ_{TTD} are normalization coefficients, and λ is a weighting coefficient. The variables $\hat{E}^{k+1\to k+\Delta_p}$ (in liters) and $\hat{TTD}^{k+1\to k+\Delta_p}$ (in meters) are the spatial (in the whole network) and temporal (over the prediction time horizon Δ_p) integrals of the fuel consumption and the total distance traveled by the vehicles, respectively. They are defined as follows

$$\hat{E}^{k+1\to k+\Delta_p} = \delta_t \sum_{e=k+1}^{k+\Delta_p} \sum_{i\in\mathcal{R}} E_i(x_e, V_e) \tag{4.6a}$$

$$\hat{TTD}^{k+1\to k+\Delta_p} = \delta_t \delta_x \sum_{e=k+1}^{k+\Delta_p} \sum_{i\in\mathcal{R}} \rho_i(e) v_i(e) \tag{4.6b}$$

The average speed in cell i at time step k, denoted $v_i(k)$, is determined with Eq. 2.43. $E_i(x_k, V_k)$ denotes the fuel consumption, in liters per second, in cell i

during time interval $[k\delta_t, (k+1)\delta_t]$. It is calculated using the VT-macro approach [288], described as

$$E_i(x_k, V_k) = E_i^{\text{temp}}(x_k, V_k) + \sum_{r \in \mathcal{P}_i} E_{r,i}^{\text{spat}}(x_k, V_k) \tag{4.7}$$

where the energy consumption quantities on account of macroscopic temporal and spatio-temporal accelerations are respectively

$$E_i^{\text{temp}}(x_k, V_k) = N_i^{\text{temp}}(k)\xi(a_i^{\text{temp}}(k)) \cdot M_{\text{fuel}} \cdot \xi(v_i(k))^T \tag{4.8a}$$

$$E_{r,i}^{\text{spat}}(x_k, V_k) = N_{r,i}^{\text{spat}}(k)\xi(a_{r,i}^{\text{spat}}(k)) \cdot M_{\text{fuel}} \cdot \xi(v_i(k))^T \tag{4.8b}$$

M_{fuel} is the model regression parameters matrix [288, 9]. It can be calibrated for fuel consumption, but also for pollutant emissions (for example, M_{NOx} for NOx emissions). The function ξ is defined as

$$\xi(x) = \begin{bmatrix} 1 & x & x^2 & x^3 \end{bmatrix} \tag{4.9}$$

Note that M_{fuel} can depend on the acceleration, in which case there is a set of parameters $M_{\text{fuel},+}$ calibrated for positive accelerations, and a set of parameters $M_{\text{fuel},-}$ calibrated for negative accelerations.

The exact acceleration values of vehicles cannot be obtained with certainty from the traffic flow models. Thus, we propose to estimate them following the approach presented in [288]. This method considers that each vehicle is subject to either a temporal or a spatio-temporal acceleration. The way to calculate these accelerations a_i^{temp} and $a_{r,i}^{\text{spat}}$, as well as the number of vehicles subject to these accelerations N_i^{temp} and $N_{r,i}^{\text{spat}}$ have been detailed in Eq. 3.31–3.34.

We introduce acceleration lower and upper bounds, respectively denoted $a_{\min}$ and $a_{\max}$, to be realistic and remain in the domain of definition of the energetic model. When $a_i^{\text{temp}}(k)$ or $a_{r,i}^{\text{temp}}(k)$ exceeds $a_{\max}$, (4.8) becomes

$$E_i^{\text{temp}}(k) = N_i^{\text{temp}}(k)\frac{a_i^{\text{temp}}(k)}{a_{\max}}\xi(a_{\max})\ M_{\text{fuel}}\ \xi(v_i(k))^T \tag{4.10a}$$

$$E_{r,i}^{\text{spat}}(k) = N_{r,i}^{\text{spat}}(k)\frac{a_{r,i}^{\text{spat}}(k)}{a_{\max}}\xi(a_{\max})\ M_{\text{fuel}}\ \xi(v_i(k))^T \tag{4.10b}$$

4.3.2 Simulation and results

In this section, we evaluate the control performance by comparing the following cases

- case *ref*: constant speed limit V_{ref} (uncontrolled);
- case *vsl*: VSLs managed by the controller (controlled).

Traffic performance metrics

In order to evaluate the impact of the VSLs strategy on the environment, and on the traffic performance within and at the boundaries of the network, we propose to connect it to a performance evaluation model.

Additional metrics, which are not in the objective function, are introduced and listed in Table 4.1. The variable $Q_i(k)$ denotes the number of vehicles queuing in front of the network entering cell i at time step k. Depending on the value of the weighting coefficient λ, a trade-off is expected between the ecological metrics (E and NOx), and the traffic performance metrics. We propose to set $\lambda = 0.5$.

Simulations are run considering the baseline (*ref*) and the controlled (*vsl*) scenarios. Based on the Symmetric Mean Absolute Percentage Error (SMAPE) approach, we define the relative improvement of each metric X, denoted η_X as

- $\eta_X = -\frac{X_{\text{ref}} - X_{\text{vsl}}}{(X_{\text{ref}} + X_{\text{vsl}})/2}$, if X is to be maximized;
- $\eta_X = \frac{X_{\text{ref}} - X_{\text{vsl}}}{(X_{\text{ref}} + X_{\text{refvsl}})/2}$, if X is to be minimized.

where X_{ref} and X_{vsl} are the values of metric X evaluated in cases *ref* and *vsl*, respectively. All metrics are to be minimized, except TTD and SoD, which are to be maximized.

If $\eta_X > 0$, the control is beneficial for metric X. If $\eta_X < 0$, the control has degraded metric X.

Case study

We propose to consider the Manhattan grid network composed of $n = 40$ identical one-way roads of 300 m each, as represented in Fig. 4.7. The network is composed of 8 entering roads and 8 exiting roads. Four clusters of roads are considered in this network (the roads of one cluster are controlled with the same speed limit variable):

1. the roads entering the network,
2. the roads exiting the network,
3. the horizontal inner roads,
4. the vertical inner roads.

The horizontal and vertical roads are grouped in two different clusters because they have different split ratios.

The duration of simulation is set to $T = 1\,\text{h}$. We consider an initial density of vehicles ρ_0, and a constant traffic demand on each entering road $d = 1200\,\text{veh/h}$, i.e. a global demand on the network of 9600 veh/h.

Table 4.1: Metrics introduced to evaluate the environmental sustainability and traffic performance.

Symbol	Unit	Description	Formula
E	L	Total fuel consumption.	$\hat{E}^{1\to T}$ (cf. 4.6 – 4.10)
NOx	kg	Total NOx emissions.	$\hat{NOx}^{1\to T}$ (cf. 4.6 – 4.10)
E_{veh}	L	Average fuel consumption per vehicle that has been in the network.	$\frac{E}{\delta_x \sum_{i\in\mathcal{R}} \rho_i(0) + \delta_t \sum_{k=1}^{T} \sum_{i\in\{j\,\vert\,\lvert\mathcal{P}_j\rvert=0\}} \varphi_i^{\text{in}}(k)}$
NOx_{veh}	kg	Average NOx emissions per vehicle that has been in the network.	$\frac{NOx}{\delta_x \sum_{i\in\mathcal{R}} \rho_i(0) + \delta_t \sum_{k=1}^{T} \sum_{i\in\{j\,\vert\,\lvert\mathcal{P}_j\rvert=0\}} \varphi_i^{\text{in}}(k)}$
TTD	m	Distance traveled by all vehicles in the network.	$\hat{TTD}^{1\to T}$ (cf. 4.6b)
TTS_{net}	s	Total time spent by all vehicles in the network.	$\delta_t \delta_x \sum_{k=1}^{T} \sum_{i\in\mathcal{R}} \rho_i(k)$
TTS_{queue}	s	Total time spent by vehicles queuing in front of the entering roads of the network (outside the network).	$\delta_t \sum_{k=1}^{T} \sum_{i\in\{j\,\vert\,\lvert\mathcal{P}_j\rvert=0\}} Q_i(k)$
QoS	veh	Total number of vehicles queuing outside the network at the end of the simulation.	$\sum_{i\in\{j\,\vert\,\lvert\mathcal{P}_j\rvert=0\}} Q_i(T)$
SoD	–	Ratio between the number of vehicles that have entered the network and those aiming at entering the network.	$\frac{\delta_t \sum_{k=1}^{T} \sum_{i\in\{j\,\vert\,\lvert\mathcal{P}_j\rvert=0\}} \varphi_i^{\text{in}}(k)}{QoS + \delta_t \sum_{k=1}^{T} \sum_{i\in\{j\,\vert\,\lvert\mathcal{P}_j\rvert=0\}} \varphi_i^{\text{in}}(k)}$

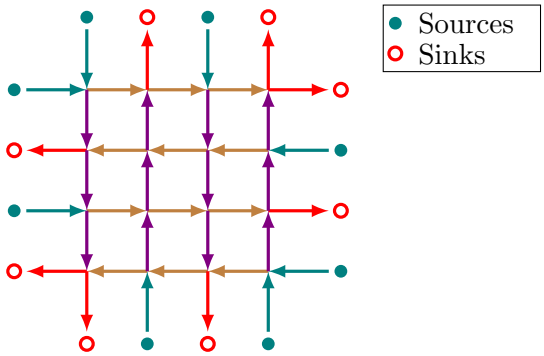

Figure 4.7: Manhattan grid network with 300 m roads composed of 5 cells of 60 m. At sources, vehicles are continuously generated at a rate of 1200 veh/h. Each color represents a cluster of roads, that are controlled by the same speed limit variable.

In order to alter the symmetry of the network, we propose to introduce privileged directions: the split ratios β_i are set to 0.7 for the vertical roads, and 0.3 for the horizontal roads. The TLS at each intersection have cycles of 1 min, without any offset, characterized as follows

- 30 s of green for the horizontal roads;
- 30 s of green for the vertical roads;

In order to find a compromise between the computational burden and the traffic model precision, we propose to consider a discretization of $n_{\text{cells}} = 5$ cells per road.

Results

For environmental reasons, more and more cities have made the choice to generalize the 30 km/h speed limit [28]. Hence, we propose to calculate the metrics improvements with respect to both $V_{\text{ref}} = 50\,\text{km/h}$ and $V_{\text{ref}} = 30\,\text{km/h}$. In each case, simulations are run for an initial density ρ_0 varying from 0 to $0.8\rho^{\text{M}}$ in order to get a broad view of the control performance. The results are given in Fig. 4.8.

For initial densities $\rho_0 \leq 0.7\rho^{\text{M}}$, when compared to the uncontrolled case with $V_{\text{ref}} = 50\,\text{km/h}$ (cf. Fig. 4.8a), the controller improves the ecological metrics ($\eta_{E_{\text{veh}}}$ and $\eta_{NOx_{\text{veh}}}$ are positive), without deteriorating the traffic performance within and at the boundaries of the network. When compared to the case with $V_{\text{ref}} = 30\,\text{km/h}$ (cf. Fig. 4.8b), the solutions proposed by the controller constitute a compromise between the ecological metrics ($\eta_{E_{\text{veh}}}$ and $\eta_{NOx_{\text{veh}}}$ are negative) and the traffic performance metrics, which are improved both within and at the boundaries of the network.

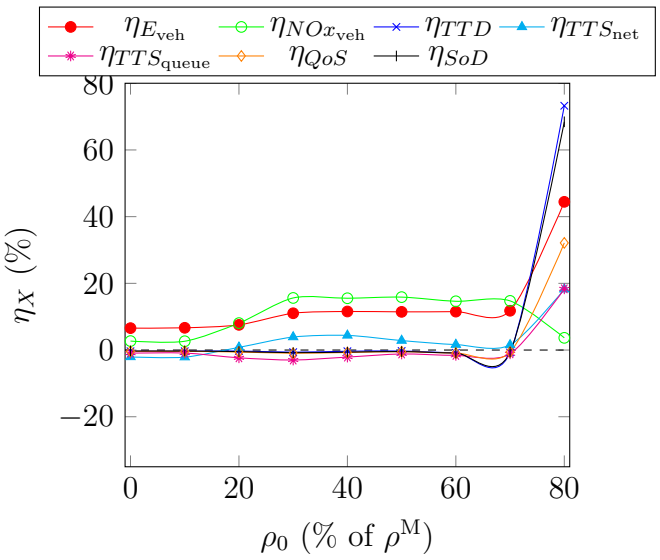

(a) $V_{\text{ref}} = 50\,\text{km/h}$

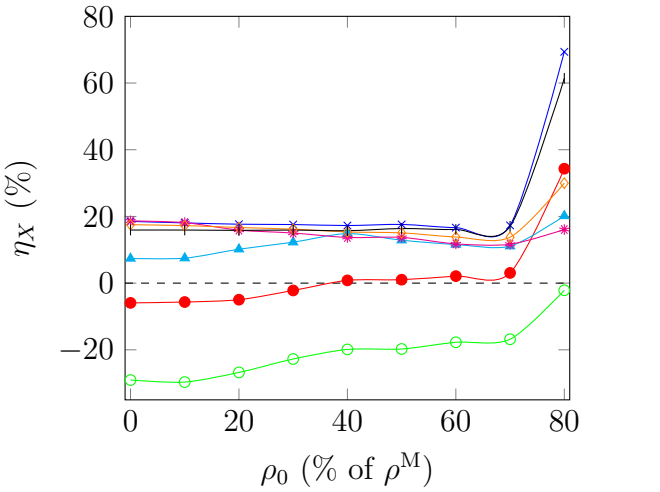

(b) $V_{\text{ref}} = 30\,\text{km/h}$

Figure 4.8: η_X as a function of ρ_0, for $d = 1200\,\text{veh/h}$.

For initial densities $\rho_0 > 0.7\rho^{\mathrm{M}}$, all metrics start to improve significantly, with respect to both $V_{\mathrm{ref}} = 50\,\mathrm{km/h}$ and $V_{\mathrm{ref}} = 30\,\mathrm{km/h}$. The reason is that the NMPC prediction makes the VSLs strategy able to avoid gridlocks, while both uncontrolled cases fail to prevent it.

An illustration of this is given in Fig. 4.9, where after $T = 1\,\mathrm{h}$ of simulation, the uncontrolled case with $V_{\mathrm{ref}} = 50\,\mathrm{km/h}$ gives rise to a gridlock, while the VSLs control is able to maintain traffic fluidity.

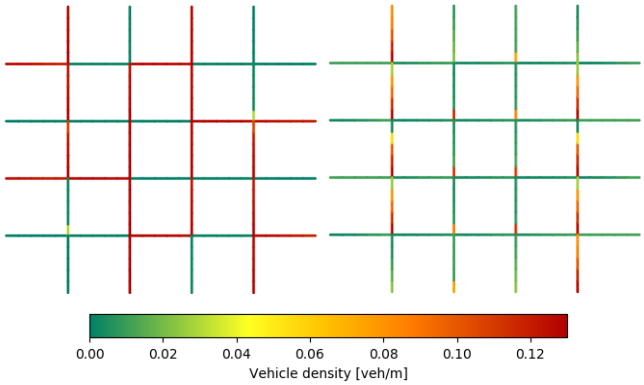

Figure 4.9: Density distribution in the network after one hour of simulation, for $\rho_0 = 0.8\rho^{\mathrm{M}}$, in the uncontrolled $V_{\mathrm{ref}} = 50\,\mathrm{km/h}$ (left) and controlled (right) scenarios.

For the chosen set of parameters, simulation results reveal that the controller improves ecological metrics when compared to the uncontrolled 50 km/h speed limits scenario, and improves traffic performance metrics when compared to the uncontrolled 30 km/h speed limits scenario. The controller is more efficient in congested situations, in particular via gridlock avoidance. This is consistent with VSLs designs applied to highways, which are mostly effective in congested systems [100].

4.4 Variable speed limits control strategy in a microscopic traffic simulator

In this section, we propose to implement the VSLs control strategy introduced in Section 4.3 in a closed-loop framework whose dynamics and calculation of pollutant emissions/fuel consumption are performed by microscopic models. The simulations are run in the Manhattan grid network presented in Fig. 2.11, with the urban and peri-urban areas. Both exogenous and endogenous sources are considered here.

4.4.1 Control strategy

In the proposed framework, the traffic system is modeled using the microscopic traffic simulator SUMO [170], and a physical fuel consumption and NOx emission model is used to assess the vehicles' environmental impact. The speed limits are controlled through the same nonlinear model predictive control (NMPC) approach, in which the traffic evolution and the future fuel consumption are respectively predicted with the CTM and ANN-based model presented in Section 3.3.2. This strategy is summarized in Fig. 4.10.

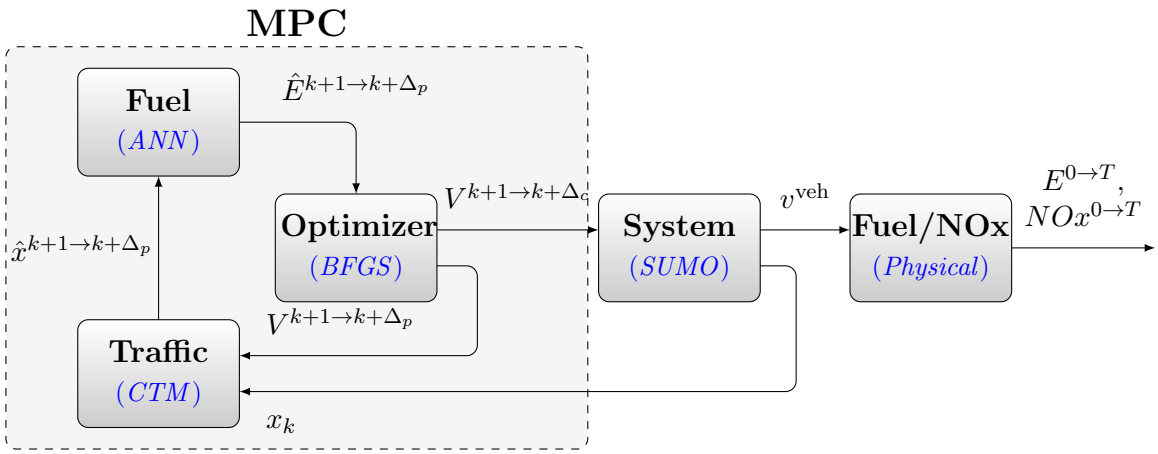

Figure 4.10: Block diagram of the global approach for ecological VSLs strategy modeled in a microscopic traffic simulator and controlled with macroscopic traffic and fuel consumption models.

In the literature, MPC strategies constitute a commonly used methodology to control traffic systems [290, 137, 243]. Yet, [50] highlights shortcomings associated with this framework, which can be summarized as follows

- Although the computing power nowadays allows the use of complex prediction models, it is difficult in practice to have access to the large amount of real data needed to run them, such as dynamic origin-destination matrices.
- The route choice of road users when considering vehicles as individual entities constitute an unpredictable gaming activity.
- Road networks behave chaotically under heavy congestion situations.

To alleviate these issues, the framework of this work is positioned downstream of the traffic assignment problem. In practice, we consider in this study that the

origin-destination matrices and the precise routes of all vehicles are fully determined in advance. They are randomly generated by the traffic simulator to be compliant with the split ratio values at each intersection, which are not controlled.

In this study, we propose to define the objective function as the ratio between the predicted total fuel consumption $\hat{E}^{k+1\to k+\Delta_p}$ and the predicted total travel distance $\hat{TD}^{k+1\to k+\Delta_p}$ between $k+1$ and $k+\Delta_p$. Minimizing this ratio is relevant for optimizing the traffic energy efficiency as it corresponds to the average fuel consumption of a vehicle per unit distance. Usually, it is expressed in liters per 100 kilometers traveled.

In this study, the fuel consumption $\hat{E}^{k+1\to k+\Delta_p}$ is predicted using the ANN-based macroscopic fuel consumption model presented in Section 3.3.2. Our motivations lie in the fact that it is calibrated to mimic the behavior of the microscopic models under consideration. This is also due to the advantages of this kind of model, quickly discussed in Section 3.3.2.

As a result, the objective function J can be expressed as

$$J(\hat{x}^{k\to k+\Delta_p}, V^{k\to k+\Delta_p}) = \frac{\hat{E}^{k+1\to k+\Delta_p}}{\hat{TD}^{k+1\to k+\Delta_p}} \tag{4.11}$$

4.4.2 Simulation and results

We propose to evaluate the controller in a time-varying demand scenario in order to transit between different states of congestion. The scenario is defined as follows:

- The simulation is run in the Manhattan grid network with an urban and a peri-urban area, as described in Fig. 2.11. Both areas are considered in this approach in order to measure the vehicles' speed profiles not only in the controlled urban area, but also in the upstream area. This is essential in order to get a complete picture and evaluate the impact of the controller on energy efficiency and traffic performance at the network boundaries, if queues are appearing for example. Contrary to the approach presented in Section 4.3.2 with alternating directions for each road (cf. Fig. 4.7), a network with privileged directions (upwards and to the right) is considered in order to broaden the range of possibilities and avoid situations in which the controller only needs to avoid gridlocks for example.

- The simulation duration is $T = 1\,\text{h}$. The control time horizon Δ_c is set at $1\,\text{min}$ and the prediction time horizon Δ_p is set at $5\,\text{min}$, i.e. $K = 5$. Note that Δ_c is set longer than the simulation time step $\delta_t = 1\,\text{s}$ in order to make the controller more realistic. The control time horizon Δ_c is shorter than in the approach considering only macroscopic models (cf. Section 4.3) in order to avoid the prediction to drift too much from the dynamics of the system.

- In order to reduce the computational burden, two clusters of roads are considered (the roads of one cluster are controlled with the same speed limit variable). Due to the simple network architecture, the first one is composed of the roads at the interface between the urban and the peri-urban area. The other one is composed of the inner urban roads. The peri-urban area is not controlled but the effect of the control of the urban area on the peri-urban area is investigated in detail. The clusters of the urban area are identified in Fig. 4.11.

- At the peri-urban sources (cf. green dots in Fig. 4.11), vehicles are continuously generated at a rate of $d^{\text{in}} = 0.2$ veh.s^{-1} (exogenous demand). With this kind of network, it is difficult to significantly increase the level of congestion simply by varying the generation rate of these sources. This is mainly due to the presence of TLS at each intersection, and to the fact that all roads have the same capacity. Hence, some additional endogenous sources that generate vehicles intermittently are added in the network (cf. red dots in Fig. 4.11). These sources aim at reaching a congested situation in a short time in order to simulate a peak demand. They have the following demand

$$d_i(k) = \begin{cases} 0.1\,\text{veh/s}, & \text{if } 6\,\text{min} \leq k \leq 9\,\text{min} \\ 0.1\,\text{veh/s}, & \text{if } 31\,\text{min} \leq k \leq 34\,\text{min} \\ 0\,\text{veh/s}, & \text{otherwise} \end{cases} \tag{4.12}$$

Fig. 4.12 represents the optimal speed limits found by the closed-loop control, as well as the evolution of the number of vehicles in the urban area both in the closed-loop control approach and in the baseline scenarios that have constant speed limits of 30 km/h and 50 km/h (these baseline scenarios both have 70 km/h speed limits in the peri-urban area). It appears that in situations of peak demand, the controller is able to decongest the network faster than the baseline scenarios.

Fig. 4.13 compares the metrics measured in the closed-loop control approach and in the baseline scenarios. The ecological metrics, i.e. average fuel consumption and NOx emissions are represented in Fig. 4.13a & 4.13b respectively, and the traffic performance metrics, i.e. the TTD and the number of arrived vehicles, are represented in Fig. 4.13c & 4.13d respectively. These metrics are always measured both in the urban and the peri-urban areas. Peri-urban roads have constant speed limits of 70 km/h in all simulations. For the urban area, the number of arrived vehicles corresponds to those that went in one of the sinks, and for the peri-urban area, the number of arrived vehicles corresponds to those that have entered the urban area by the end of the simulation.

The results indicate that the controller is able to reduce the average fuel consumption in the urban area, which corresponds to the objective function, from

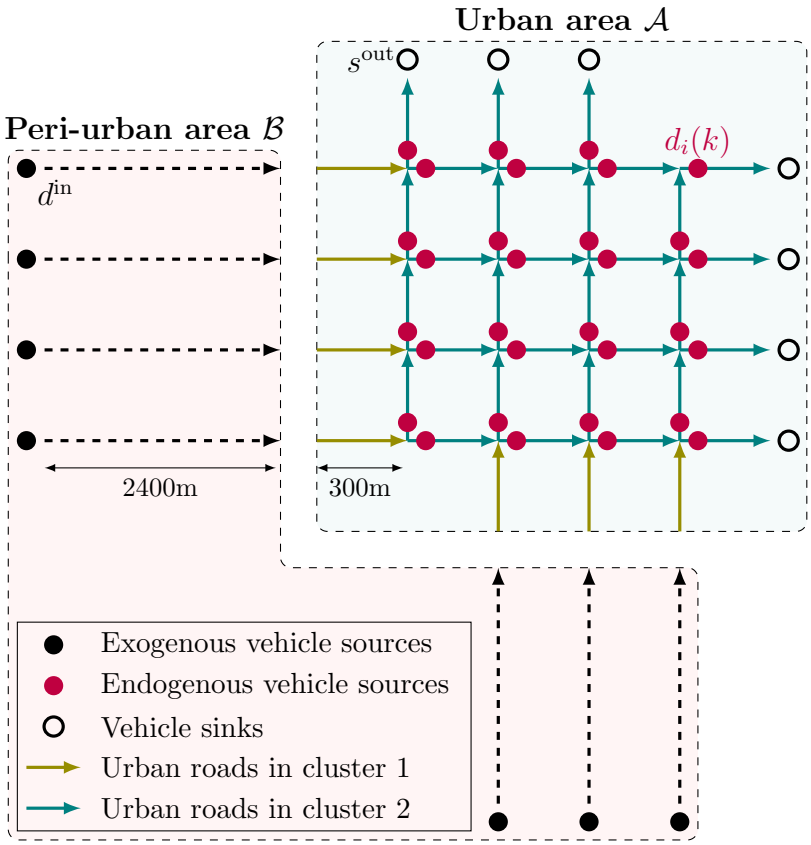

Figure 4.11: Scenario for which the online control approach is performed. Urban roads of the same color are in the same cluster and hence have the same speed limit. At exogenous sources, vehicles are continuously generated at a rate of 0.2 veh.s^{-1}. At endogenous sources, vehicles are generated between 6 min and 9 min, and between 31 min and 34 min at a rate of 0.1 veh.s^{-1}.

7.7 L/100km to 6.5 L/100km, i.e. by approximately 16%. On a macroscopic scale, the total fuel consumption (in both areas) during 1 h is 1167 L in the open-loop 30 km/h approach and 998 L in the closed-loop control approach. This gap corresponds to a total reduction of 451 kilograms of CO2. Thanks to a faster decongestion of the urban area, the lengths of queues in the peri-urban roads are reduced. This results in a reduction of the average fuel consumption on these roads also (respectively 29% and 5% reduction with the 30 km/h and 50 km/h baseline scenarios).

Similarly, the faster decongestion performed by the controller results in a reduction of NOx emissions in both areas. In comparison with the open-loop 30 km/h approach, the controller reduced the average NOx emissions by 14% in the urban area and by 27% in the peri-urban area. In comparison with the open-loop

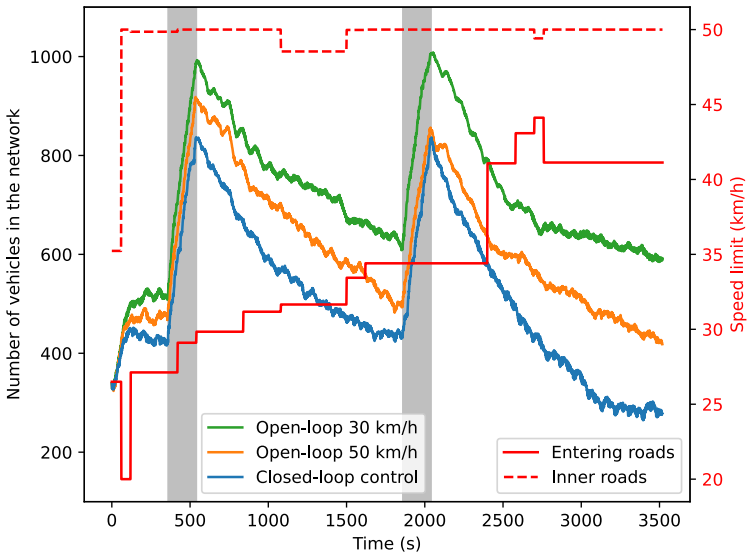

Figure 4.12: Representation of the evolution of the optimal speed limits, and of the number of vehicles in the urban area in the controlled and in the baseline scenarios. The gray zones characterize the phases in which the endogenous sources are generating vehicles.

50 km/h approach, the controller reduced the average NOx emissions by 16% in the urban area and by 7% in the peri-urban area.

In addition to the average fuel consumption and NOx emissions reduction, the controller also improves traffic fluidity. In comparison with the open-loop 30 km/h approach, the controller increases the TTD by 16% in the urban area and by 4% in the peri-urban area. In comparison with the open-loop 50 km/h approach, the controller increases the TTD by 4% in the urban area and by 1% in the peri-urban area. This indicates that, despite a lower number of vehicles present in the urban area at each moment of the simulation (cf. Fig. 4.12), the global flow of vehicles is improved by the controller.

The improvement of traffic fluidity is also highlighted by the number of arrived vehicles. In total, 940 and 259 more vehicles have completed their journeys, i.e. have reached a sink, in the closed-loop control scenario, in comparison with the open-loop 30 km/h and 50 km/h approaches respectively. This indicates that

Note that the controller could be more realistic by limiting the possible speed limits to multiple of 5 km/h, for example. A simulation has been made by rounding the controller outputs in this way. The resulting average fuel consumption is 6.8 L/100km, i.e. a reduction of 12% (instead of 16% with continuous speed limits values) in comparison with the baseline scenarios.

In brief, the developed closed-loop control strategy is particularly efficient in the proposed traffic scenario, which aims at reproducing a high congestion resulting from a peak demand. In fact, it appears that the controller is able to decongest the network much faster than in the baseline scenarios. This results in an improvement of both the ecological and the traffic performance metrics. Most importantly, these metrics are not only improved inside the controlled network, but also at its boundaries, i.e. in the uncontrolled peri-urban area.

It is interesting to note that inside the network, the controller keeps a speed limit close to 50 km/h. This can be interpreted as a way to accelerate the decongestion of the network. Indeed, the analysis conducted in Section 4.2 shows that 50 km/h speed limits constitute a good compromise between average fuel consumption and TTD.

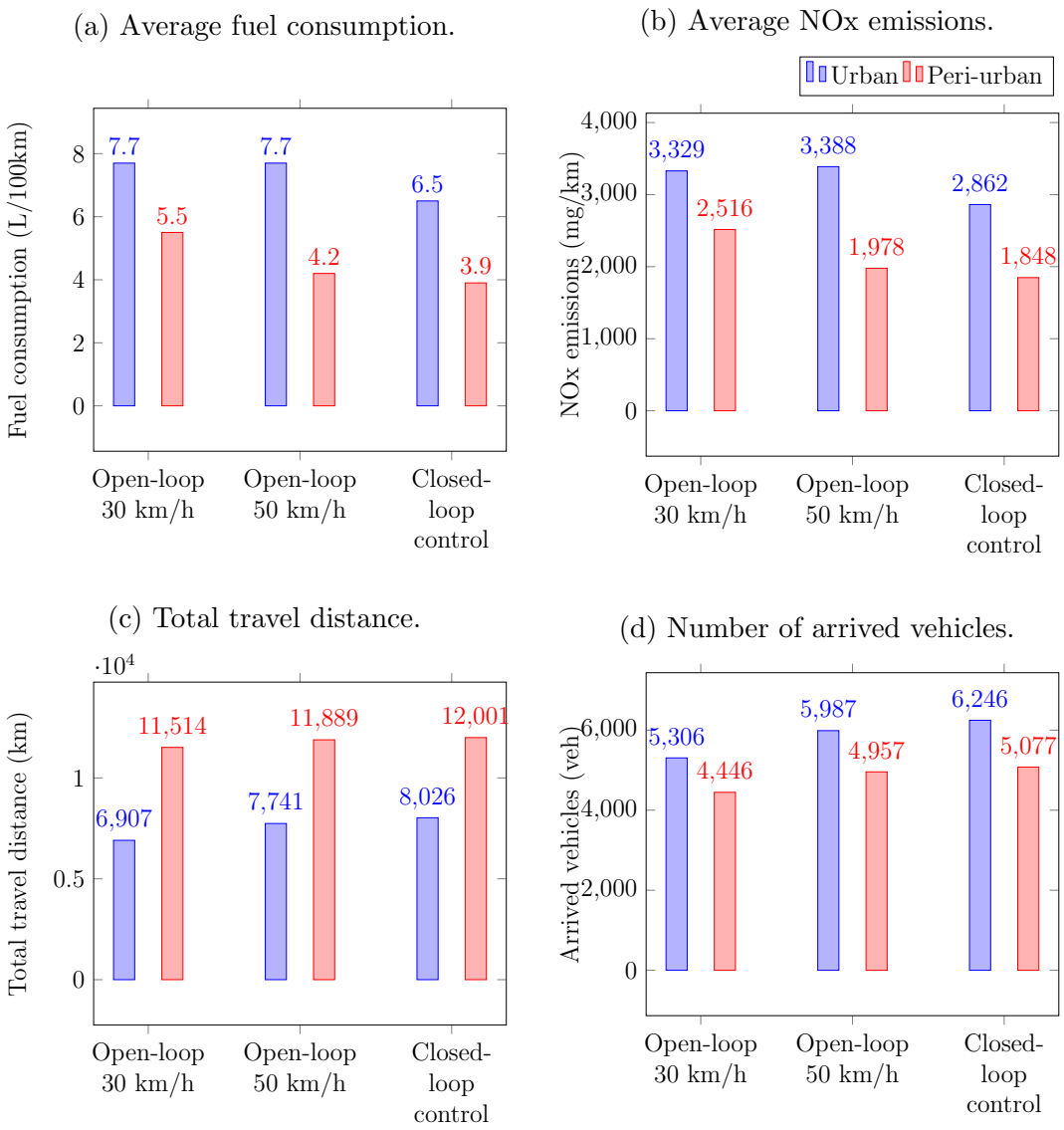

Figure 4.13: Comparison of the ecological and the traffic performance metrics measured when the online VSLs approach is performed, with baseline scenarios that have constant speed limits of 30 km/h and 50 km/h.

Chapter 5

Comparative study of urban road traffic fuel consumption optimization via variable speed limits and signalized access control

Contents

5.1 Foreword

In this chapter, we propose to compare the ecological potential of two control actuators: VSLs performed within an urban area and a signalized access control to this area. This study is conducted in the closed-loop microscopic traffic simulator. The use of signalized access control actuators to optimize the flow of vehicles between different areas of a network is a well-known subject in the literature [99, 235]. These approaches usually focus on developing control systems for efficient congestion management in large-scale urban networks.

The control strategy presented in Chapter 4 is considered as the VSL controller. The same Manhattan grid network composed of an urban and a peri-urban area (Fig. 4.11) with the same demand scenario presented in Chapter 4 are used in the following.

5.2 Optimal control of signalized access control

In this section, we present the signalized access control approach, which consists in regulating the green time of the access control actuators located at the interface between the urban and the peri-rban area, as indicated in Fig. 5.1.

Control framework

The control framework is identical to the one detailed for VSLs in Fig. 4.10. The only difference is that the control variable corresponds to the actuators duty cycle κ instead of the speed limits V_i. The corresponding block diagram is represented in Fig. 5.2. The duty cycle κ takes on continuous values between 0 (closed access) and 1 (open access). It is defined as

$$\kappa = \frac{\Delta_{\text{green}}}{\Delta_{\text{c}}} \tag{5.1}$$

where Δ_{green} and Δ_{c} denote respectively the green and the cycle durations.

As a result, the behavior of the access control actuators is characterized by the green function Θ defined as

$$\Theta(k) = \begin{cases} 1, & \text{if } k \leq \left\lfloor \frac{k}{\Delta_{\text{c}}} \right\rfloor + \kappa\Delta_{\text{c}} \\ 0, & \text{otherwise} \end{cases} \tag{5.2}$$

This modification impacts the flow at the interface between the urban and the peri-urban area. Let us introduce $\mathcal{B}' \subset \mathcal{B}$ as the subset of cells in the peri-urban area that contain the cells at the border with the urban area, i.e. the ones whose outflow is regulated by the access control actuators. The impact of the access control actuators on the flow of vehicles are specified in Fig. 5.1.

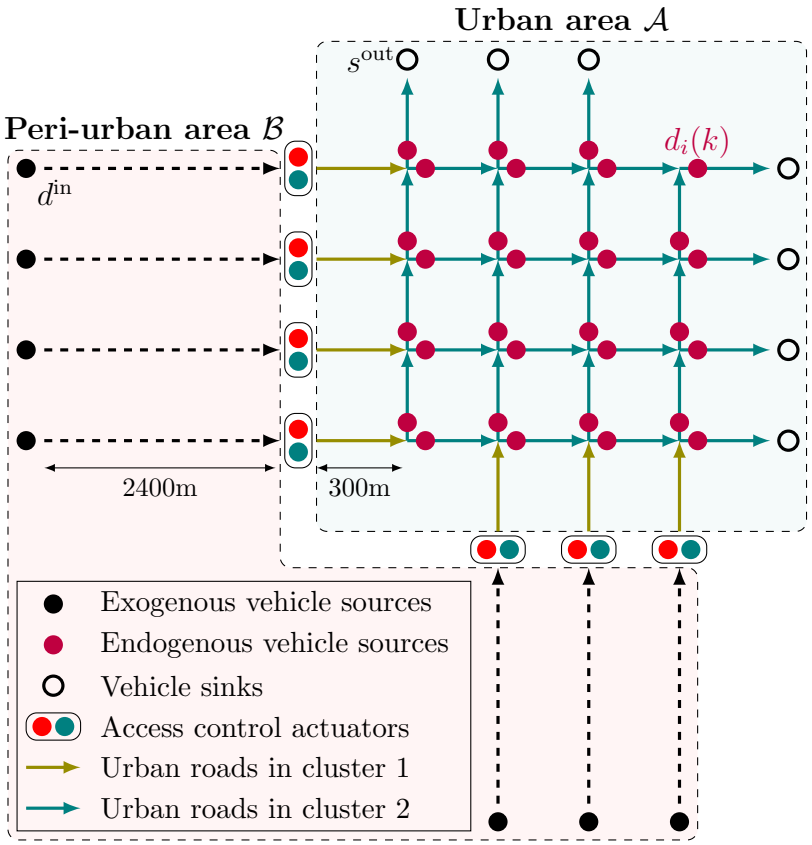

Figure 5.1: Representation of the road network and the signalized access control actuators. The urban area corresponds to the solid line roads and the peri-urban area is represented by the dashed line roads.

Objective function

In this chapter, we propose to use an objective function that explicitly considers the energy efficiency in both areas of the network in order to ensure that the energy efficiency in the peri-urban area is not compromised for the benefit of the urban area. The most natural way to do so is to consider the weighted sum of the average energy consumption in each area, as follows

$$J(\hat{x}^{k\to k+\Delta_p}, \kappa^{k\to k+\Delta_p}) = \lambda \frac{E_{\mathcal{A}}^{k\to k+\Delta_p}}{\sigma_{\mathcal{A}} TTD_{\mathcal{A}}^{k\to k+\Delta_p}} + (1-\lambda)\frac{E_{\mathcal{B}}^{k\to k+\Delta_p}}{\sigma_{\mathcal{B}} TTD_{\mathcal{B}}^{k\to k+\Delta_p}} \tag{5.3}$$

where $\sigma_{\mathcal{A}}$ and $\sigma_{\mathcal{B}}$ are normalization coefficients, and λ is a weighting coefficient. The two terms are normalized because the fuel consumption rates can be very different in both areas due to the presence of TLS and to different speed limits. In this sense, the actuators seek to obtain a compromise of the energy efficiency between

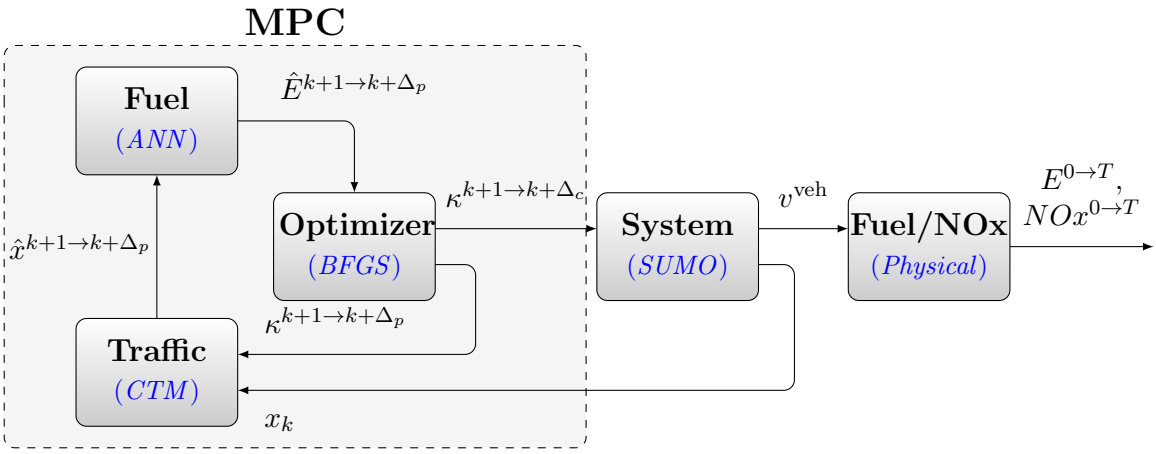

Figure 5.2: Block diagram of the global approach for ecological signalized access control.

both areas. $E_{\mathcal{A}}^{1\to T}$ and $E_{\mathcal{B}}^{1\to T}$ are calculated using the ANN-based macroscopic fuel consumption model presented in Section 3.3.2.

In this approach, the control actuators are the access points between the peri-urban and the urban area, whose behavior is characterized by the duty cycle κ. It appears explicitly in equation 5.2 and in the expressions of flows in Table 5.1. Due to the network symmetry and the fact that the exogenous demands are all equal, we propose to control all the access points with the same control variable. Therefore, the controller solves the following problem at each control iteration k

$$\begin{aligned} \min_{\kappa^{k\to k+\Delta_p}} \quad & J(\hat{x}^{k\to k+\Delta_p}, \kappa^{k\to k+\Delta_p}) \\ \text{s.t.} \quad & \rho_i(e+1) = \rho_i(e) + \tfrac{\delta_t}{\delta_x}\left(\varphi_i^{\text{in}}(e) - \varphi_i^{\text{out}}(e)\right), \forall e \in [k..k+\Delta_{\text{p}}-1] \\ & \kappa(e) \in [0,1], \forall e \in [0..T] \end{aligned} \tag{5.4}$$

The fact that the controller optimizes the duty cycle κ, which takes continuous values between 0 and 1, rather than the binary function Θ leads to a NonLinear Programming (NLP) problem and avoids a Mixed-Integer NonLinear Programming (MINLP) formulation, whose complexity would be much higher.

Table 5.1: Expression of cells outflows and inflows in presence of access control actuators, depending on the number of upstream and downstream connections.

$\lvert\mathcal{N}_i\rvert$	Expression of $\varphi_i^{\text{out}}(k)$
0	$\min\left\{D_i(k), \varphi_i^{\text{M}}, s^{\text{out}}(k)\right\}$
1	If $i \in \mathcal{B}'$: $\Theta(k) \times \min\left\{D_i(k), \varphi_i^{\text{M}}, S_{\mathcal{N}_i}(k)\right\}$ Else: $\min\left\{D_i(k), \varphi_i^{\text{M}}, S_{\mathcal{N}_i}(k)\right\}$
≥ 2	$\alpha_i(k) \min\left\{D_i(k), \varphi_i^{\text{M}}, \left\{\frac{S_j(k)}{\beta_j}\right\}_{j\in\mathcal{N}_i}\right\}$
$\lvert\mathcal{P}_i\rvert$	Expression of $\varphi_i^{\text{in}}(k)$
0	$\min\left\{d^{\text{in}}(k), \varphi_i^{\text{M}}, S_i(k)\right\}$
1	If $\mathcal{P}_i \in \mathcal{B}'$: $g(k) \times \min\left\{D_{\mathcal{P}_i}(k), \varphi_{\mathcal{P}_i}^{\text{M}}, S_i(k)\right\}$ Else: $\min\left\{D_{\mathcal{P}_i}(k), \varphi_{\mathcal{P}_i}^{\text{M}}, S_i(k)\right\}$
≥ 2	$\beta_i \sum_{j\in\mathcal{P}_i} \alpha_j(k) \min\left\{D_j(k), \varphi_j^{\text{M}}, \left\{\frac{S_l(k)}{\beta_l}\right\}_{l\in\mathcal{N}_j}\right\}$

5.3 Comparison between signalized access control and variable speed limits

5.3.1 Case study

Three traffic scenarios are defined

1. *Uncontrolled baseline*: the accesses from the peri-urban to the urban area are permanently open. The speed limits are constantly equal to 70 km/h in the peri-urban area and 50 km/h in the urban area.

2. *Controlled VSL*: the accesses from the peri-urban to the urban area are permanently open. The speed limits are constantly equal to 70 km/h in the peri-urban, but they are dynamically optimized in the urban area, taking continuous values between 20 km/h and 50 km/h.

3. *Controlled with access control*: the accesses from the peri-urban to the urban area are controlled, but the speed limits are constant over the simulation duration (70 km/h in the peri-urban area and 50 km/h in the urban area).

To satisfy the Courant-Friedrichs-Lewy (CFL) [46] condition, the time step duration δ_t is set to 1 s because δ_x is equal to 60 meters. The control and prediction horizons of the NMPC strategy are respectively set at $\Delta_\mathrm{c} = 1\,\mathrm{min}$ and $\Delta_\mathrm{p} = 5\,\mathrm{min}$. The weighting coefficient λ is set to 0.7 in order to privilege the environmental sustainability in the urban area because it is supposed to be denser with more traffic.

In the urban area, all roads are one-way, of equal length and capacity. At each intersection, both downstream roads have the same split ratio $\beta_i = 0.5$.

We consider a simulation of duration $T = 1\,\mathrm{h}$ during which the exogenous demand is set at $d^\mathrm{in} = 0.2\,\mathrm{veh/s}$ and the intermittent endogenous vehicle sources have the following demand

$$d_i(k) = \begin{cases} 0.1\,\mathrm{veh/s}, & \text{if } 6\,\mathrm{min} \leq k \leq 9\,\mathrm{min} \\ 0.1\,\mathrm{veh/s}, & \text{if } 31\,\mathrm{min} \leq k \leq 34\,\mathrm{min} \\ 0\,\mathrm{veh/s}, & \text{otherwise} \end{cases} \tag{5.5}$$

5.3.2 Simulation results

The results of the three scenarios defined in Section 5.3.1 are summarized in Fig. 5.3. The fuel consumption, the $\mathrm{NO_X}$ emissions, and the TTD are calculated using the data of the microscopic traffic simulator SUMO and the physical energy and $\mathrm{NO_X}$ models.

The average fuel consumption and $\mathrm{NO_X}$ emissions presented in Fig. 5.3a & 5.3b indicate that the VSL controller is able to improve the energy efficiency both in the urban (18%) and in the peri-urban (14%) areas. Similar results are observed with $\mathrm{NO_X}$ emissions, which are reduced by 18% in the urban area and by 13% in the peri-urban area. However, the access control approach only allows to improve the environmental sustainability in the urban area (fuel consumption reduced by 7% and $\mathrm{NO_X}$ emissions reduced by 6%) in exchange for a deterioration of the performances in the peri-urban area (fuel consumption increased by 21% and $\mathrm{NO_X}$ emissions increased by 19%).

Fig. 5.3c reveals that the impact of both controllers on the TTD is lower, which is conceivable because it is not explicitly the optimization criterion. The VSL controller improves it both in the urban (5%) and in the peri-urban (1%) areas. The access control approach deteriorates it in the urban area (2%) and does not affect it in the peri-urban area.

As a result, the VSL controller is more appropriate in this study because it gives better results in both areas in terms of energy efficiency, pollutant emissions, and traffic performance. In practice, both controllers aim at reducing the inflow in the urban area during peak times because the congestion deteriorates the energy efficiency. The difference is that the control of accesses is much more discriminating

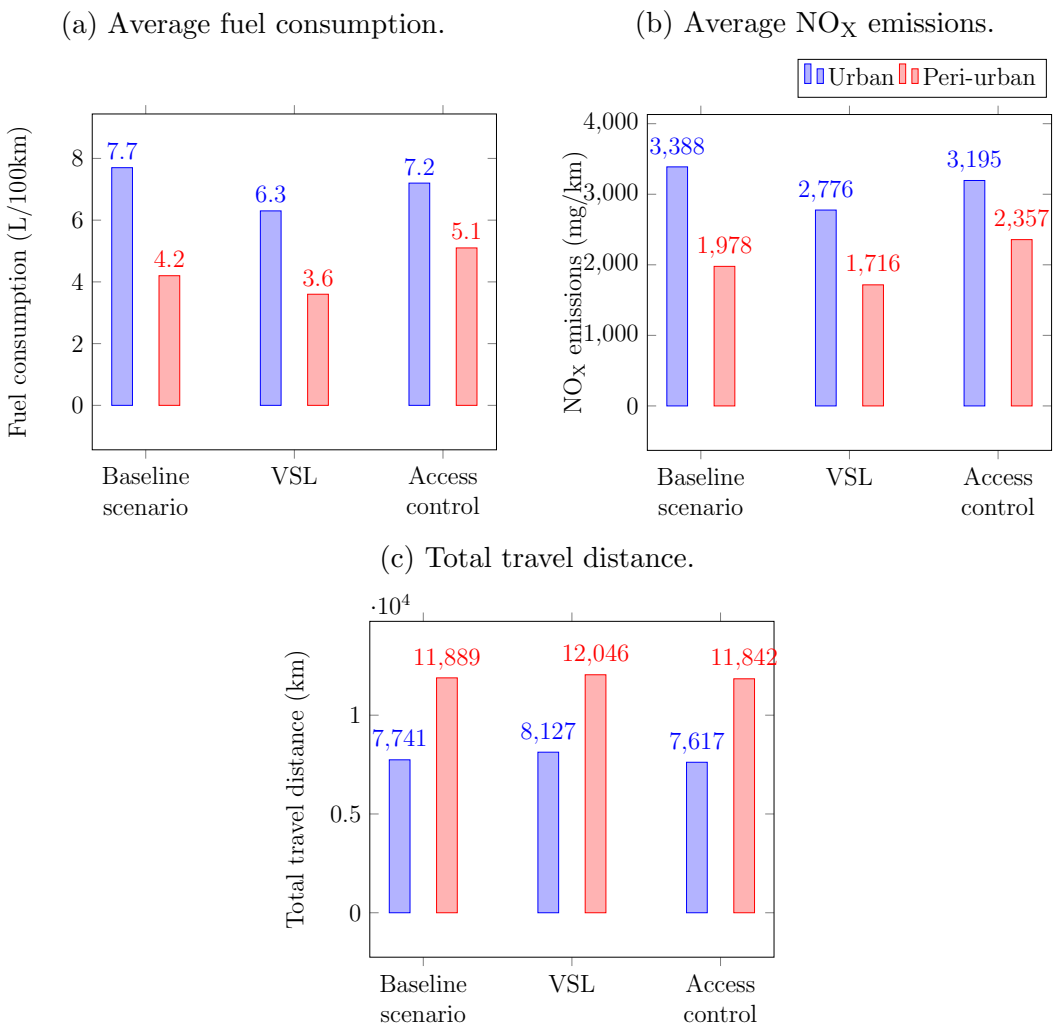

Figure 5.3: Comparison of the energy efficiency, the pollutant emission level, and the traffic performance in the baseline scenario, the VSLs approach, and the access control approach.

towards vehicles in the peri-urban area as it forces them to stop and start, which is very energy consuming. On the other hand, the VSL controller leads to smoother variations of the densities in the peri-urban area, which improves the potential of fuel consumption reduction.

Chapter 6

Conclusions

Contents

6.1 Review of the contributions

Several microscopic car-following models can be considered in a traffic simulator. Based on the generated speed profiles and energy consumption curves under different levels of congestion, the IDM is chosen in this work. It is calibrated to be compliant with urban accelerations captured by real-world FCD. A macroscopic traffic model, namely the CTM, is calibrated to predict the dynamics in the microscopic simulator. The results indicate an average error of 5% on density prediction. An ANN is calibrated to predict the fuel consumption from macroscopic traffic data. The average error on fuel consumption prediction is 11.5% in comparison with the reference calculated with a microscopic physical energy model.

The analysis of the relationship between energy efficiency and traffic dynamics highlights the negative impact of congestion and queuing on fuel consumption. However, reducing the speed limit in congested situations has been shown to have a positive impact on the average vehicle fuel consumption, expressed in L/100 km. Additionally, the impact of the presence of a TLS has been investigated. The results indicate that it plays a role in the optimal speed limit regarding energy efficiency and NO_X emissions. More generally, this observation emphasizes taking into account the details of the road infrastructure to develop a control approach. Finally, while the TTD is optimal at critical density, the energy efficiency is optimal for any density value below the critical density.

The implementation of closed-loop VSLs shows that they have great potential in terms of avoiding gridlocks, regulating flows between different areas of a road network, which can result in a significant reduction in fuel consumption and emissions, as well as a smoother and more efficient road traffic. In the proposed scenarios, the closed-loop control strategy not only improves the environmental sustainability and traffic performance in the controlled network, but also improves these metrics at the network boundaries, i.e. in the uncontrolled peri-urban area. These benefits are mainly due to a faster decongestion of the network. It seems that VSLs in an urban road network is most effective during transient phases between different levels of density, such as demand peaks that lead to congestion. Additionally, a comparison of the effect on energy efficiency of VSLs and signalized access control in a synthetic two-region network of intermediate size reveals that the VSL approach is more efficient. In fact, it reduces the global fuel consumption up to 18% in the urban area, against 7% for the access control which also decreases the performance in the peri-urban area. The reason is that VSL leads to smoother density variations, which are more energy-efficient.

6.2 Outlook

The use of macroscopic models to predict the evolution of traffic and energy consumption is inherently critical as the behavior of vehicles cannot be determined with certainty using macroscopic traffic variables only. In this sense, machine learning techniques, such as the ANN used in this work, are promising because such models can be trained in various situations with inputs of different types. However, the risk of overfitting associated with these approaches is significant. Typically, it is not guaranteed that the ANN calibrated in this work will perform as well with other network structures, driver behaviors, time and spatial discretizations, etc. In the near future, the quick development of connected vehicles will considerably increase the available data. In addition to this, computing capabilities have recently been greatly improved. Macroscopic models should consequently be more and more efficient and robust for a wide range of scenarios.

The VSLs control strategy proposed in this dissertation is of interest in scenarios corresponding to heavy congestion, and more particularly in scenarios in which traffic transits between different levels of congestion. In this sense, the applicability of this kind of controller in urban areas is similar to the one observed in highways. Furthermore, with the proposed set of parameters, VSLs are more promising than signalized access control in urban areas. However, this is conditioned by the formal compliance with speed limits, which is not guaranteed as long as no monitoring measures are put in place, or as long as CAVs are not yet widely deployed.

To go further, the macroscopic control approaches proposed in this work can be combined with microscopic strategies (eco-driving, eco-routing, vehicle platooning, CACC, cooperative lane change and merge, cooperative intersection control, etc.) to improve the energy efficiency. This is particularly useful in situations where macroscopic control is of less interest, such as during phases of low congestion. A natural extension of this work is the implementation of a real road network with a more complex architecture. Typically, this would be accompanied by a new cluster definition for the VSLs approach, with more than 2 clusters. In this work, analyzes of the controller performance with more than 2 clusters was an issue because of local optima. Other possible extensions correspond to the addition of driver uncertainty, the impact of other means of transport such as buses, bicycles and pedestrians, as well as the analysis of the compliance with speed limits.

In this work, we consider that the speed limits take continuous values between 20 km/h and 50 km/h. In order to facilitate the implementation of this strategy if the controlled vehicles are not autonomous, the possible values should be limited to multiples of 10 km/h for example. From the road network management perspective, implementing macroscopic control approaches represents a significant investment. Yet, this kind of approaches may call into question the choice of

fixed speed limits, and be an element of consideration, with the safety and noise pollution aspects.

6.3 Insights on the urban mobility in the future

The current situation regarding pollutant emissions and energy consumption of road transportation in urban areas is alarming both for environmental and health reasons. Traffic eco-management strategies appear to be a promising lever in the long-term to reduce the environmental impact of transportation. These approaches are mainly based on the communication between vehicles and infrastructures. To go further, autonomous vehicles represent a great opportunity to improve the performance of these techniques because of their more precise and predictable behavior. In this sense, CAVs are considered the next major technological advance in the mobility sector. They have a crucial role to play in road safety, as well as traffic fluidity and energy efficiency improvement.

Today the technology of CAVs is mature and could be rapidly developed in countries with an adequate road infrastructure. However, just as with the first driverless elevators in the 1940s, people are concerned and still have a lot of resistance in trusting CAVs. One reason is certainly that we all have this psychological bias that makes us believe that we are better at certain tasks than we actually are. For example, surveys show that 74% of people believe they are above average drivers. Yet, according to the National Transportation Safety Board (NTSB), 94% of the 60 million people killed on the road during the 20th century are due to human errors. Furthermore, recent studies on CAVs allow us to draw unequivocal conclusions about their safety. For example, a study conducted with Waymo vehicles in 2019, based on 6.1 million miles of automated driving, reveals that among the 18 accidents recorded, none was serious enough to expect serious injuries. More importantly, all 8 significant accidents recorded involved an error of a human driver of another vehicle that was driving the wrong side of the road, running a red traffic light, over the speed limit, etc. In a context of increasingly multi-modal urban mobility (pedestrians, bicycles, scooters), autonomous vehicles open up new perspectives and solutions to the ban on vehicles in cities.

A likely scenario for the future urban mobility is based on the combination of different solutions such as CAVs, extended public transportation services, attractive network architectures for bikes and pedestrians, etc. Such scenarios, that aims at improving energy efficiency, air quality, road safety, and traffic throughput, would be accompanied by measures by public authorities to encourage people to adapt their behavior. With the fast development of connected vehicles, such multi-modal cities would promote demand-driven traffic control, and more particularly the cooperation of complementary traffic eco-management strategies.

When it comes to designing the cities of the future, a main and recurring idea is generally to adopt a low-carbon and non-polluting mobility. In this sense, the development of EVs should accelerate in the coming years. This is due to supportive regulatory frameworks in several countries, an increased number of models, and ever more competitive price of batteries. According to the IEA, there were 10 million EVs in the world at the end of 2020. In 2020, their registrations increased by 41% and represented 4.6% of total sales share. In the Sustainable Development Scenario, it is expected that around 230 million EVs will be on the world's roads in 2030, representing a stock share of 12%.

In urban areas, EVs have the main advantage of having a motorization that does not emit pollutants, which is a major drawback of ICEVs during acceleration phases. Moreover, they emit very few fine particles due to braking because of their regenerative braking feature, which consists in turning into energy some of the deceleration's kinetic energy to charge the batteries. Regarding air pollution, their only negative point could come from a faster wear of the tires because of the heavy batteries that compose them.

Today, a very important point regarding the large-scale development of EVs corresponds to the production and recycling of their batteries. Despite this, EVs are still much cleaner than ICEVs over their lifetime, according to the International Council of Clean Transportation (ICCT). Typically, an EV produces half of the greenhouse gas emission of an average European ICEV. In countries with very low-carbon electricity, such as Norway or France, the life-cycle emissions of an EV are less than 30% of an ICEV. As a result, battery manufacturing life-cycle emissions debt is rather quickly paid off (typically less than 2 years compared to driving an ICEV). Yet, it appears that battery manufacturing emissions can vary by a factor of up to 10, which highlights the need for additional investigation on this topic.

Besides these points, the main difference between EVs and ICEVs is associated with the eco-routing paradigm, as the limited range, recharge times, and ability to regenerate energy during deceleration phases need to be taken into account when dealing with EVs. As a result, traffic eco-management strategies are very similar for ICEVs and EVs.

Chapter 7

Résumé substantiel

Contents

7.1 Introduction

Les véhicules autonomes offrent de grandes opportunités en termes d'amélioration de l'efficacité énergétique, des émissions de polluants, de la fluidité du trafic, de la sécurité routière et du confort en raison de l'aspect prédictif de leur comportement. Certaines règles de contrôle simples peuvent être implémentées afin de réduire leur consommation énergétique. Cependant, celles-ci ne sont généralement pas suffisantes et des méthodes d'optimisation semblent alors nécessaires. De telles stratégies nécessitent des modèles de trafic et de consommation d'énergie précis et fiables, d'algorithmes d'optimisation performants, ainsi que de dispositifs de communication longue distance rapides.

Une première approche d'optimisation de l'efficacité énergétique des véhicules autonomes porte sur des stratégies de recherche d'itinéraire (*eco-routing*) et d'optimisation des profils de vitesse (*eco-driving*), basées non seulement sur la communication entre les véhicules, mais également sur la communication avec l'infrastructure routière. Les véhicules effectuent alors une optimisation du "gain individuel" visant à réduire leur propre consommation. Ces approches sont plus efficaces lorsque le taux de pénétration des véhicules autonomes est élevé car les prédictions deviennent plus fiables. Globalement, plus les contraintes du voyage sont connues avant le départ, plus ce type d'approche est efficace.

Une deuxième approche correspond au développement de stratégies coopératives entre les véhicules autonomes afin d'améliorer l'efficacité énergétique globale. Ces approches sont également basées sur les communications entre les véhicules et avec l'infrastructure, mais les véhicules envisagent ici l'impact de leurs décisions sur le comportement et la consommation d'énergie des autres véhicules également, ils effectuent donc une optimisation du "bien commun". Ces stratégies de contrôle comprennent par exemple le peloton de véhicules, le CACC, le changement de voies coopératif et le contrôle coopératif des intersections. Par ailleurs, les véhicules autonomes peuvent avoir un effet d'harmonisation sur la vitesse du trafic environnant, en particulier dans les cas de coopération. Cette harmonisation semble avoir un impact bénéfique sur la consommation énergétique globale, mais elle est difficile à estimer car elle dépend du taux de pénétration, de la congestion du trafic et de l'architecture du réseau.

Enfin, une dernière approche visant à optimiser l'efficacité énergétique correspond non pas au contrôle des véhicules, mais à celui des infrastructures routières. Ce potentiel a été exploré en milieu autoroutier avec des limitations de vitesse variables ou des approches de type *ramp metering*. En milieu urbain, de telles approches, n'ont été que très rarement évaluées avec une considération explicite de la consommation énergétique dans le problème d'optimisation. En ville, cette approche pourrait se traduire en pratique par la mise en place de limitations de vitesse variables, ou d'un contrôle des feux de signalisation.

Dans ce manuscrit, nous nous intéressons à l'évaluation du potentiel de cette troisième approche car cela constitue un vide dans la littérature scientifique. Toutefois, il est essentiel de noter que la coordination de stratégies de contrôle complémentaires semble particulièrement prometteuse pour améliorer l'efficacité énergétique globale des véhicules. Ainsi, les contributions de la thèse peuvent être résumées comme indiqué ci-dessous.

D'abord, la formalisation complète d'un modèle de trafic macroscopique adapté au milieu urbain est proposée. Elle comprend une méthodologie pour le traitement des intersections. Pour estimer la consommation de carburant, ce modèle de trafic est associé à un modèle de consommation d'énergie macroscopique basé sur un réseau de neurones. Ce dernier est calibré à l'aide d'un modèle d'énergie physique microscopique et de données fournies par un simulateur de trafic microscopique préalablement paramétré à partir de données réelles. L'utilisation d'un réseau de neurones est essentiellement justifiée par ses bonnes performances lorsque la vitesse moyenne du trafic routier est faible. Les modèles macroscopiques sont préférés pour le contrôle à grande échelle en raison de leur faible complexité. Ils ont également l'avantage de considérer l'efficacité énergétique globale, qui est la métrique d'intérêt pour les gestionnaires de réseaux routiers lorsqu'il est question d'efficacité énergétique.

Ensuite, des simulations sont menées afin d'évaluer la relation entre la congestion et l'efficacité énergétique des véhicules, notamment en régime permanent. L'impact des différentes limitations de vitesse sur le trafic (densité, vitesse moyenne, débit) est analysé pour différents niveaux de demande du trafic. Les limitations de vitesse ont un impact direct sur la consommation d'énergie ainsi que sur les émissions polluantes car elles affectent les accélérations et les vitesses moyennes sur l'ensemble du réseau.

Enfin, un contrôleur en boucle fermée est introduit afin d'analyser et de comparer l'impact de limitations de vitesse variables et de contrôle d'accès à une zone urbaine en termes de durabilité environnementale et de fluidité du trafic. L'impact du contrôleur est évalué dans la zone urbaine contrôlée, mais aussi dans la zone péri-urbaine qui la borde. Les résultats révèlent que dans les phases transitoires entre différents niveaux de congestion, le contrôleur permet de décongestionner le réseau plus rapidement, réduisant ainsi la consommation de carburant et les émissions de polluant, et assurant un trafic plus fluide dans les zones urbaine et péri-urbaine. De plus, pour les paramètres considérés, les limitations de vitesse variables conduisent à des variations de densité plus douces qu'avec le contrôle d'accès, se traduisant par des économies d'énergie.

7.2 Modèles pour la simulation et la prédiction de la dynamique du trafic routier en milieu urbain

La première étape des stratégies de gestion écologique du trafic correspond à la modélisation de la dynamique du trafic. Cette étape est cruciale car elle nécessite des modèles de trafic capables de capturer des phénomènes de trafic complexes comme l'apparition d'ondes de choc ou la dynamique des files d'attente.

Pour ce faire, nous utilisons dans ces travaux un modèle de trafic microscopique. Après comparaison de plusieurs modèles, nous décidons de conserver le *Intelligent Driver Model* car il donne lieu à des niveaux de consommation de carburant cohérents pour différentes densités de véhicules. Les paramètres du modèle sont calibrés avec des données d'accélération réelles mesurées en milieu urbain.

Un modèle de trafic macroscopique de premier ordre est également introduit. Cette famille de modèle a l'avantage de présenter une complexité bien plus faible et indépendante du nombre de véhicules dans le système, car les variables d'état sont les densités dans les différentes cellules du réseau. Toutefois, ces modèles sont en contrepartie moins précis. Ces caractéristiques sont idéales pour prédire la dynamique réelle du système (simulée avec le modèle microscopique) dans un contrôleur en boucle fermée, afin d'ajuster les actionneurs du réseau le plus efficacement possible. En particulier, nous utilisons dans ces travaux le *Cell Transmission Model*. Ce modèle repose sur l'hypothèse du diagramme fondamental, qui définit une relation entre flux et densité de véhicules. Nous considérons le diagramme fondamental trapézoïdal présenté en Fig. 7.1.

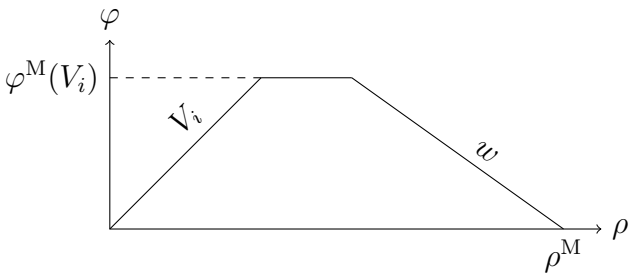

Figure 7.1: Diagramme fondamental trapézoïdal associé à une limitation de vitesse V_i, une vitesse de propagation d'onde w, une densité de véhicules maximum ρ^{M}, et un flux de véhicules maximum $\varphi^{\mathrm{M}}(V_i)$.

Ce diagramme fondamental a été calibré afin de prédire au mieux la dynamique du modèle de trafic microscopique. Comme nous pouvons le voir sur la Fig. 7.2 qui montre la densité de véhicules ainsi que la vitesse moyenne du trafic calculées

dans une cellule avec les modèles microscopique et macroscopique, il apparaît que la prédiction est très bonne puisque l'erreur est inférieure à 5%.

(a) Prédiction de la densité. (b) Prédiction de la vitesse moyenne.

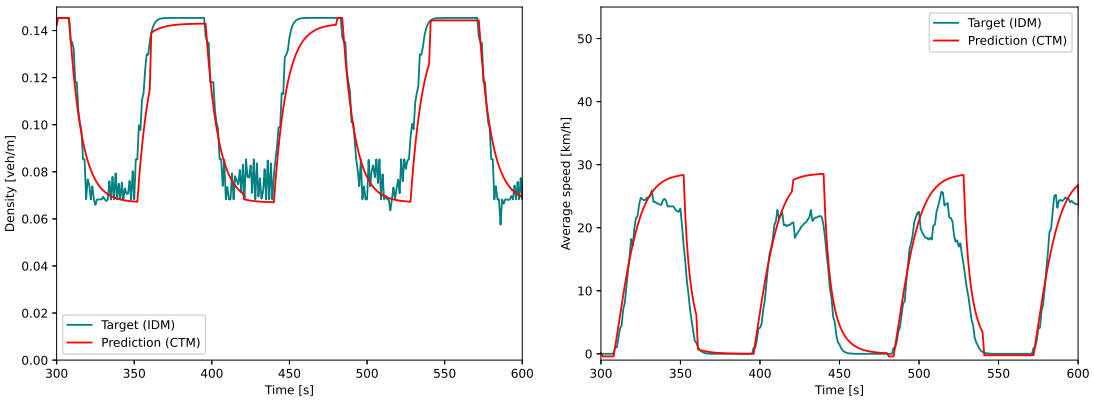

Figure 7.2: Comparaison de la densité réelle ρ_i mesurée avec IDM avec la densité prédite $\hat{\rho}_i$ donnée par le CTM dans la cellule i. La vitesse limite est 50 km/h et nous observons une erreur moyenne ε_i de 4.2% (gauche). Comparaison de la vitesse moyenne v_i dans la même cellule mesurée avec IDM avec sa prédiction $\hat{v}_i$ (droite).

Les principaux défis rencontrés dans ce chapitre correspondent au choix et à la calibration du modèle microscopique afin d'être représentatif du comportement réel des conducteurs, ainsi qu'à la calibration du modèle macroscopique afin de pouvoir prédire la dynamique du modèle microscopique.

7.3 Modèles pour la simulation et la prédiction des émissions de polluant et de la consommation énergétique

Une autre étape cruciale des stratégies de gestion écologique du trafic correspond à la modélisation des émissions de polluants et de la consommation d'énergie. De tels modèles prennent en entrée la dynamique du trafic, qui peut être décrite à l'aide de données microscopiques, telles que les profils de vitesse des véhicules, ou de données macroscopiques comme les densités et flux de véhicules ainsi que les vitesses moyennes.

Dans notre approche, un modèle microscopique de consommation et d'émission de polluants est associé au modèle de trafic microscopique précédemment décrit

(a) Cartographie du taux de consommation de carburant.

(b) Cartographie du BGR.

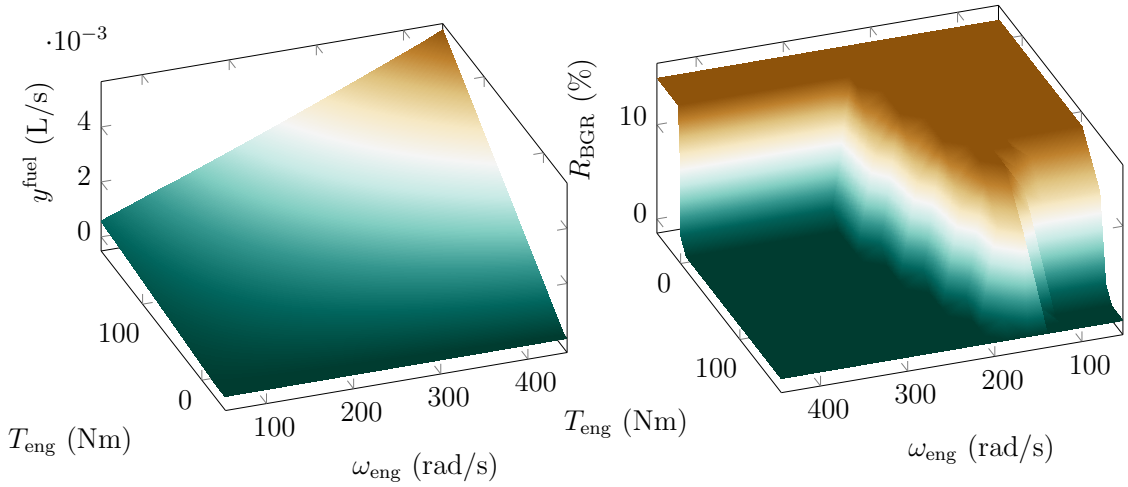

Figure 7.3: Cartographies de consommation de carburant et de BGR, définies comme des fonctions des couples et régimes moteur.

afin d'évaluer l'impact environnemental du système. A partir du principe fondamental de la dynamique et des paramètres des véhicules considérés, les couples T_{eng} et régimes Ω_{eng} moteur sont calculés pour chaque véhicule à chaque instant. Il est alors possible de calculer le taux de consommation de carburant y^{fuel} associé en utilisant une cartographie comme celle donnée Fig. 7.3a. De même, le taux d'émission de NOx peut être calculé en utilisant la relation suivante : $\log\left(\frac{y^{\text{NOx}}}{y^{\text{fuel}}\rho^{\text{fuel}}}\right) = a_1 + a_2 R_{\text{BGR}} + a_3 m_{\text{fuel}}$
où $a_1 - a_3$ sont des coefficients de régression, R_{BGR} est obtenu avec la cartographie en Fig. 7.3b, et m_{fuel} représente la masse de carburant dans le cylindre par course du piston et volume déplacé.

Ensuite, la consommation de carburant et les émissions de NOx réelles entre les instants 0 et T peuvent alors être calculées comme indiqué ci-dessous :

$$E^{0\to T} = \sum_{k=0}^{T} \sum_{p} \delta_t y_p^{\text{fuel}}(k) \tag{7.1a}$$

$$NOx^{0\to T} = \sum_{k=0}^{T} \sum_{p} \delta_t y_p^{\text{NOx}}(k) \tag{7.1b}$$

Un modèle macroscopique de consommation est également introduit à des fins prédictives. Nous calibrons un réseau de neurones qui prend en entrée les variables

macroscopiques indiquées Fig. 7.4. Ce modèle prédit le taux de consommation des véhicules dans une cellule i, plutôt que de calculer le taux de consommation de chaque véhicule indépendamment. C'est ce qui lui permet d'être plus efficace et de s'affranchir de l'impact du nombre de véhicules dans le système sur la complexité de la prédiction. En moyenne, l'erreur avec ce modèle est de 11.5%, ce qui représente un bon résultat dans le sens où cette approche n'a pas toute l'information en entrée puisqu'elle se contente de l'information macroscopique.

En effet, un état macroscopique du système peut en réalité correspondre à une infinité d'états microscopiques. C'est essentiellement là que réside toute la difficulté lorsqu'il est question de prédire la sortie du modèle microscopique à l'aide de modèles macroscopiques : le comportement individuel des véhicules, qui joue un rôle majeur dans l'efficacité énergétique en raison des accélérations, ne peut pas être pris en compte.

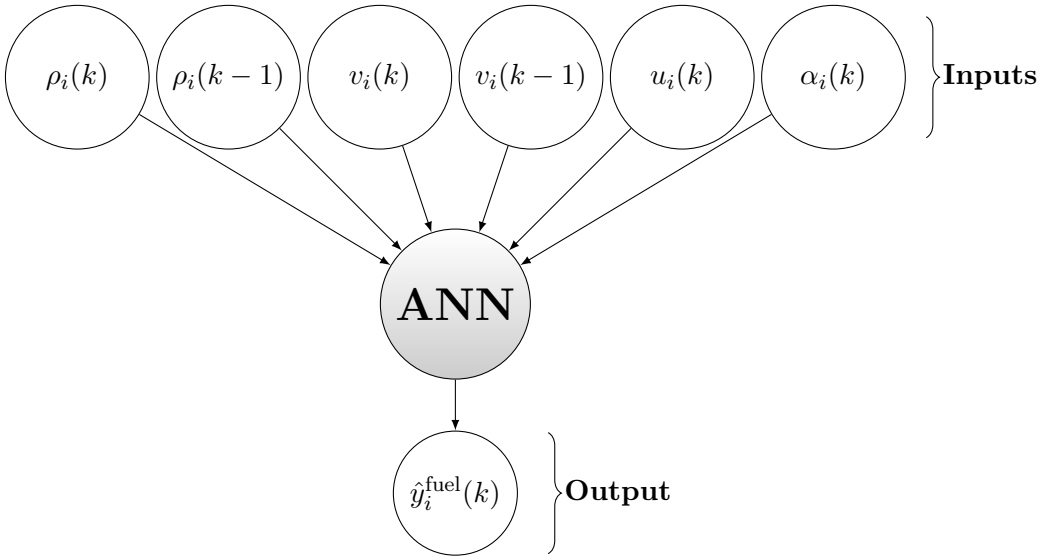

Figure 7.4: Représentation des entrées et sortie du réseau de neurones du modèle de consommation macroscopique.

7.4 Relation entre dynamique et efficacité énergétique du trafic

Afin de quantifier l'impact du niveau de congestion et de la limitation de vitesse sur l'efficacité énergétique des véhicules, nous proposons de simuler un flux de véhicules sur un anneau constitué d'une voie et d'un feu de signalisation (cf. Fig. 7.5). Cette approche présente l'avantage de donner lieu à un état quasi-stationnaire du trafic.

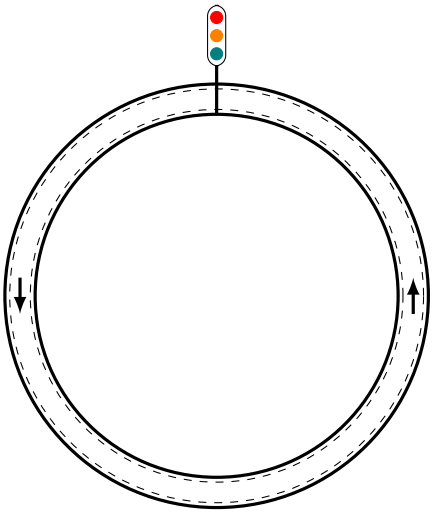

Figure 7.5: Anneau de 300 mètres constitué d'une unique voie et d'un feu de signalisation.

Plusieurs simulations sont alors réalisées, pour différentes densités et limitations de vitesse. Les résultats sont présentés en Fig. 7.6.

Deux phases apparaissent clairement :

- Pour les faibles densités, une grande limitation de vitesse est moins consommatrice en énergie car les moteurs des véhicules se rapprochent de leur fonctionnement optimal.
- Au-delà d'une certaine densité, une congestion se forme et des phénomènes de *stop-and-go* apparaissent, une limitation de vitesse plus faible devient moins consommatrice en énergie car cela réduit les accélérations.

Encore une fois, ces résultats obtenus à partir de simulations très simplistes décrivent le comportement des véhicules en régime permanent uniquement. Toutefois, cela permet de souligner l'impact des limitations de vitesse sur la consommation des véhicules, et montre qu'il n'existe a priori pas une limitation de vitesse optimale, mais que cela dépend des conditions de trafic.

7.5 Optimisation de l'efficacité énergétique par limitations de vitesse variables et contrôle d'accès

Un contrôleur basé sur une approche de *Nonlinear Model Predictive Control* est implémenté afin d'optimiser l'efficacité énergétique des véhicules dans une zone

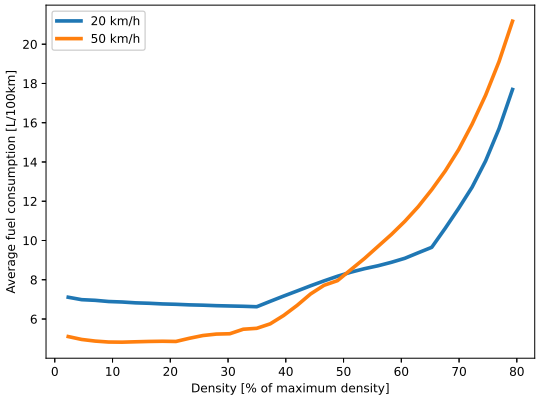

Figure 7.6: Consommation de carburant en fonction de la densité.

urbaine. Ce contrôleur est constitué des modèles introduits précédement comme indiqué dans la Fig. 7.7.

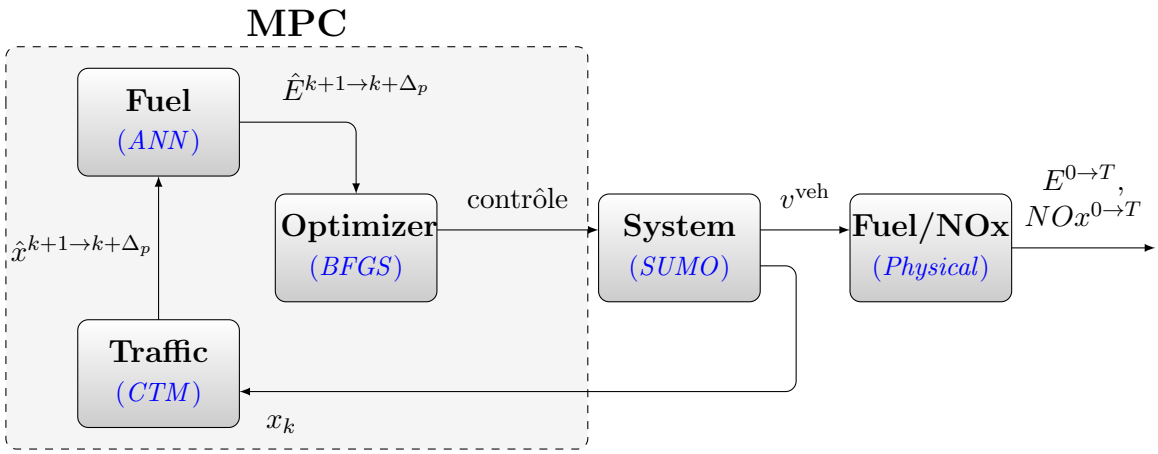

Figure 7.7: Schéma-bloc de l'approche de gestion écologique du trafic routier en milieu urbain.

Le contrôleur est évalué dans le scénario décrit en Fig. 7.8. Nous considérons une zone péri-urbaine et une zone urbaine avec 7 points de passage de la première vers la deuxième. Les véhicules sont générés au niveau des sources de véhicules exogènes en amont de la zone péri-urbaine. Les sources de véhicules endogènes génèrent également des véhicules de manière intermittente afin de simuler des pics dans la demande de trafic qui correspondent par exemple aux heures de pointe. Les puits de véhicules se situent en aval de la zone urbaine.

Les outils de contrôle du trafic considérés dans cette approche se situent dans la zone urbaine uniquement, mais l'impact du contrôle sur la zone péri-urbaine est

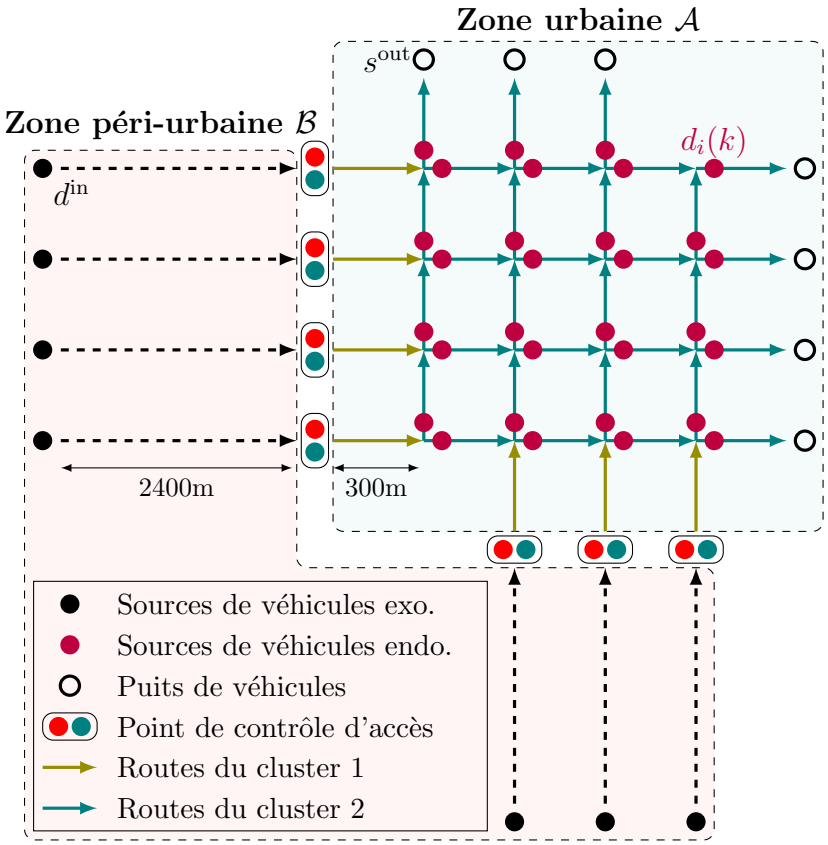

Figure 7.8: Réseau routier constitué d'une zone urbaine et d'une zone péri-urbaine.

également pris en compte. Ainsi, la fonction objectif considérée par le contrôleur est une somme pondérée des efficacités énergétiques dans les deux zones :

$$J(\hat{x}^{k\to k+\Delta_p}, \kappa^{k\to k+\Delta_p}) = \lambda \frac{E_{\mathcal{A}}^{k\to k+\Delta_p}}{\sigma_{\mathcal{A}} TTD_{\mathcal{A}}^{k\to k+\Delta_p}} + (1-\lambda)\frac{E_{\mathcal{B}}^{k\to k+\Delta_p}}{\sigma_{\mathcal{B}} TTD_{\mathcal{B}}^{k\to k+\Delta_p}}$$

En pratique, nous comparons les stratégies suivantes :

- Limitations de vitesse variables dans la zone urbaine entre 20 km/h et 50 km/h.
- Contrôle d'accès entre les zones peri-urbaine et urbaine.
- Scénario de référence sans contrôleur.

Les résultats obtenus sont décrits dans la Fig. 7.9. Sur le plan de la consommation et des émissions, ils indiquent que le contrôle des limitations de vitesse de vitesse est bien plus intéressant que le contrôle d'accès. En effet, pour le scénario

(a) Consommation de carburant moyenne.

(b) Émissions de NO_X moyennes.

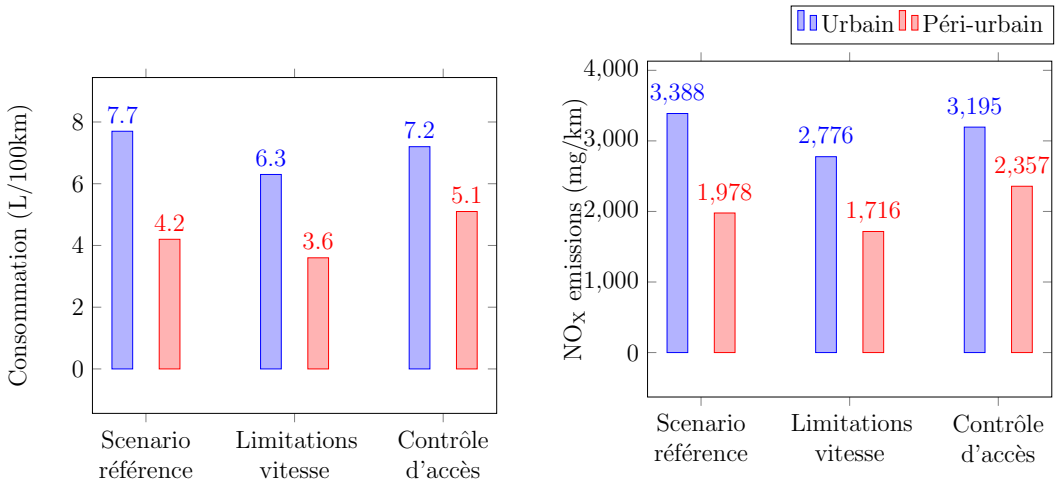

(c) Distance totale parcourue.

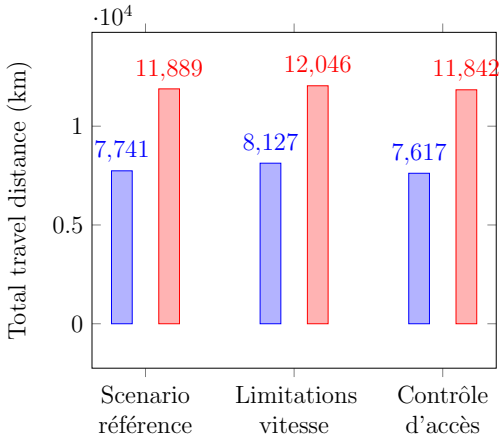

Figure 7.9: Consommation de carburant, émissions de NOx, et fluidité du trafic pour chacune des trois stratégies de contrôle.

considéré, le premier améliore les résultats significativement dans les zones tandis que le deuxième les améliore dans la zone urbaine au détriment de la zone péri-urbaine. Les limitations de vitesse variables permettent par ailleurs de fluidifier le trafic routier.

Malgré le fait que chacun des deux contrôleurs imaginés cherchent essentiellement à réguler le flux de véhicules entrant dans la zone urbaine, les meilleures performances des limitations de vitesse variables s'expliquent par le fait que le contrôle d'accès est beaucoup plus discriminant envers les véhicules en zone péri-urbaine car il les oblige à s'arrêter puis à repartir, ce qui est très énergivore. En

d'autres termes, les limitations de vitesse variables conduisent à des variations de densité plus douces en zone péri-urbaine, ce qui améliore le potentiel de réduction de la consommation de carburant.

7.6 Conclusion

Les principaux résultats et contributions des travaux réalisés dans cette thèse peuvent résumés comme suit.

Un modèle de trafic microscopique, l'IDM, a été sélectionné à partir des courbes de consommation d'énergie simulées sous différents niveaux de congestion. Il a été calibré pour être représentatif d'accélérations réelles mesurées en milieu urbain. Un modèle de trafic macroscopique, le CTM, est calibré pour prédire la dynamique du simulateur microscopique. Les résultats indiquent une erreur moyenne de 5% sur la prédiction de densité. Un réseau de neurones est calibré pour prédire la consommation de carburant à partir de données de trafic macroscopiques. L'erreur moyenne sur la consommation prédite est de 11,5% par rapport à la référence calculée avec un modèle d'énergie physique microscopique.

L'analyse du lien entre efficacité énergétique et dynamique du trafic met en évidence l'impact négatif des embouteillages sur la consommation de carburant. Cependant, il a été démontré que la réduction de la limitation de vitesse dans des situations de congestion pouvait permettre de réduire cette surconsommation, mais qu'elle pouvait au contraire dégrader l'efficacité énergétique lorsqu'elle était réduite alors que la circulation est fluide. Par ailleurs, l'analyse de l'impact de la présence d'un feu de signalisation dans cette étude met l'accent sur l'importance de la prise en compte du détail de l'infrastructure routière pour développer une démarche de contrôle. Enfin, alors que la fluidité du trafic est optimale à densité critique, l'efficacité énergétique est quant à elle optimale pour toute valeur de densité inférieure à la densité critique.

Les limitations de vitesse variables ont démontré avoir un grand potentiel en milieu urbain pour éviter les embouteillages et réguler les flux entre les différentes zones, ce qui peut significativement réduire la consommation de carburant et les émissions tout en fluidifiant le trafic. Dans les scénarios proposés, la stratégie de contrôle en boucle fermée améliore non seulement les performances dans la zone contrôlée, mais également dans sa zone frontalière. Ces bénéfices sont principalement dus à une décongestion plus rapide du réseau. Il semble que les limitations de vitesse variables soient plus efficaces pendant les phases transitoires entre différents niveaux de densité. Une comparaison avec le contrôle d'accès a mis en évidence la plus-value apportée par les limitations de vitesse variables dans les scénarios considérés. La raison principale est qu'elles conduisent à des variations de densité plus douces, qui sont plus économes en énergie.

Bibliography

[1] Peloton technology. `https://peloton-tech.com/how-it-works`. Accessed: 2020-08-14.

[2] L. Aarts and G. Feddes. European truck platooning challenge. In *International Symposium on Heavy Vehicle Transport Technology*, 2016.

[3] K. Aboudolas, M. Papageorgiou, and E. Kosmatopoulos. Store-and-forward based methods for the signal control problem in large-scale congested urban road networks. *Transportation Research Part C: Emerging Technologies*, 17(2):163 – 174, 2009.

[4] M. Ahmane, A. Abbas-Turki, F. Perronnet, J. Wu, A. El Moudni, J. Buisson, and R. Zeo. Modeling and controlling an isolated urban intersection based on cooperative vehicles. *Transportation Research Part C: Emerging Technologies*, 28:44–62, 2013.

[5] K. Ahn. Microscopic fuel consumption and emission modeling. Master's thesis, Virginia Tech, 1998.

[6] K. Ahn and H. Rakha. The effects of route choice decisions on vehicle energy consumption and emissions. *Transportation Research Part D: Transport and Environment*, 13(3):151 – 167, 2008.

[7] K. Ahn, H. Rakha, and A. Trani. Microframework for modeling of high-emitting vehicles. *Transportation Research Record*, 1880:39–49, 2004.

[8] A. Al Alam, A. Gattami, and K. H. Johansson. An experimental study on the fuel reduction potential of heavy duty vehicle platooning. In *13th International IEEE Conference on Intelligent Transportation Systems*, pages 306–311. IEEE, 2010.

[9] M. Alsabaan, K. Naik, T. Khalifa, and A. Nayak. Applying vehicular networks for reduced vehicle fuel consumption and co2 emissions. In *Intelligent Transportation Systems*. IntechOpen, 2012.

[10] F. An, M. Barth, J. Norbeck, and M. Ross. Development of comprehensive modal emissions model: Operating under hot-stabilized conditions. *Transportation Research Record: Journal of the Transportation Research Board*, (1587):52–62, 1997.

[11] H. An and J.-i. Jung. Design of a cooperative lane change protocol for a connected and automated vehicle based on an estimation of the communication delay. *Sensors*, 18(10):3499, 2018.

[12] H. Andersen, X. Shen, Y. H. Eng, D. Rus, and M. H. Ang Jr. Connected cooperative control of autonomous vehicles during unexpected road situations. *Mechanical Engineering*, 139(12):S3–S7, 2017.

[13] O. Andersen, C. S. Jensen, K. Torp, and B. Yang. Ecotour: Reducing the environmental footprint of vehicles using eco-routes. In *Mobile Data Management (MDM), 2013 IEEE 14th International Conference on*, volume 1, pages 338–340. IEEE, 2013.

[14] M. Andre and C. Pronello. Relative influence of acceleration and speed on emissions under actual driving conditions. *International Journal of Vehicle Design*, 18(3–4):340–353, 1997.

[15] A. Aw and M. Rascle. Resurrection of" second order" models of traffic flow. *SIAM Journal on Applied Mathematics*, 60(3):916–938, 2000.

[16] T. Awal, M. Murshed, and M. Ali. An efficient cooperative lane-changing algorithm for sensor-and communication-enabled automated vehicles. In *2015 IEEE Intelligent Vehicles Symposium (IV)*, pages 1328–1333. IEEE, 2015.

[17] K. Balakrishnan, S. Dey, T. Gupta, R. Dhaliwal, M. Brauer, A. J. Cohen, J. D. Stanaway, G. Beig, T. K. Joshi, A. N. Aggarwal, et al. The impact of air pollution on deaths, disease burden, and life expectancy across the states of india: the global burden of disease study 2017. *The Lancet Planetary Health*, 3(1):e26–e39, 2019.

[18] M. Barth, F. An, J. Norbeck, and M. Ross. Modal emissions modeling: A physical approach. *Transportation Research Record: Journal of the Transportation Research Board*, (1520):81–88, 1996.

[19] M. Barth and K. Boriboonsomsin. Real-world carbon dioxide impacts of traffic congestion. *Transportation Research Record: Journal of the Transportation Research Board*, (2058):163–171, 2008.

[20] D. P. Bertsekas. *Dynamic programming and optimal control*, volume 1. Athena scientific Belmont, MA, 1995.

[21] A. K. Bhoopalam, N. Agatz, and R. Zuidwijk. Planning of truck platoons: A literature review and directions for future research. *Transportation Research Part B: Methodological*, 107:212–228, 2018.

[22] L. Bieker-Walz, M. Behrisch, M. Junghans, and K. Gimm. Evaluation of car-following-models at controlled intersections. 2017.

[23] R. Bodenheimer, A. Brauer, D. Eckhoff, and R. German. Enabling glosa for adaptive traffic lights. In *2014 IEEE Vehicular Networking Conference (VNC)*, pages 167–174. IEEE, 2014.

[24] T. Boehme, F. Held, C. Rollinger, H. Rabba, M. Schultalbers, and B. Lampe. Application of an optimal control problem to a trip-based energy management for electric vehicles. *SAE International Journal of Alternative Powertrains*, 2:115–126, 2013.

[25] E. R. Boer. Car following from the driver's perspective. *Transportation Research Part F: Traffic Psychology and Behaviour*, 2(4):201–206, 1999.

[26] P. Bokare and A. Maurya. Acceleration-deceleration behaviour of various vehicle types. *Transportation research procedia*, 25:4733–4749, 2017.

[27] C. Bonnet and H. Fritz. Fuel consumption reduction in a platoon: Experimental results with two electronically coupled trucks at close spacing. Technical report, SAE Technical Paper, 2000.

[28] J. Bordarie. Public policy of urban mobility: Impact of the history and practices on young drivers' social representation of 30 km/h. *Journal of Nonprofit & Public Sector Marketing*, 29(2):211–234, 2017.

[29] K. Boriboonsomsin, M. J. Barth, W. Zhu, and A. Vu. Eco-routing navigation system based on multisource historical and real-time traffic information. *IEEE Transactions on Intelligent Transportation Systems*, 13(4):1694–1704, 2012.

[30] M. Brackstone and M. McDonald. Car-following: a historical review. *Transportation Research Part F: Traffic Psychology and Behaviour*, 2(4):181–196, 1999.

[31] G. Bretti, R. Natalini, and B. Piccoli. Numerical approximations of a traffic flow model on networks. *NHM*, 1(1):57–84, 2006.

[32] F. Browand, J. McArthur, and C. Radovich. Fuel saving achieved in the field test of two tandem trucks. *UC Berkeley: California Partners for Advanced Transportation Technology*, 2004.

[33] A. Brown, J. Gonder, and B. Repac. An analysis of possible energy impacts of automated vehicles. In G. Meyer and S. Beiker, editors, *Road vehicle automation*, Lecture notes in mobility, pages 137–153. Springer, Cham, 2014.

[34] C. G. Broyden. The convergence of a class of double-rank minimization algorithms 1. general considerations. *IMA Journal of Applied Mathematics*, 6(1):76–90, 1970.

[35] W. Burghout. *Hybrid microscopic-mesoscopic traffic simulation*. PhD thesis, KTH, 2004.

[36] C. Canudas-de-Wit. Best-effort highway traffic congestion control via variable speed limits. In *Decision and Control and European Control Conference (CDC-ECC), 2011 50th IEEE Conference on*, pages 5959–5964. IEEE, 2011.

[37] C. Canudas-de-Wit and A. Ferrara. A variable-length cell transmission model for road traffic systems. *Transportation Research Part C: Emerging Technologies*, 97:428 – 455, 2018.

[38] L. Chapman. Transport and climate change: a review. *Journal of Transport Geography*, 15(5):354–367, 2007.

[39] A. C. Charalampidis and D. Gillet. Speed profile optimization for vehicles crossing an intersection under a safety constraint. In *2014 European Control Conference (ECC)*, pages 2894–2901. IEEE, 2014.

[40] R. Chen and C. G. Cassandras. Stochastic flow models with delays, blocking and applications to multi-intersection traffic light control. *Discrete Event Dynamic Systems*, 30(1):125–153, 2020.

[41] N. Chiabaut, C. Buisson, and L. Leclercq. Fundamental diagram estimation through passing rate measurements in congestion. *IEEE Transactions on Intelligent Transportation Systems*, 10(2):355–359, 2009.

[42] CITEPA. Gaz à effet de serre et polluants atmosphériques. Bilan des émissions en France de 1990 à 2018. Technical report, 2020.

[43] B. Ciuffo, V. Punzo, and M. Montanino. Global sensitivity analysis techniques to simplify the calibration of traffic simulation models. methodology and application to the idm car-following model. *IET Intelligent Transport Systems*, 8(5):479–489, 2014.

[44] R. M. Colombo. Hyperbolic phase transitions in traffic flow. *SIAM Journal on Applied Mathematics*, 63(2):708–721, 2002.

[45] Continental. Continental launches smart city mobility and transportation hub for safer and smarter cities. `https://www.continental.com/en-us/press-/press-releases/smart-city-mobility-205048`, 2019.

[46] R. Courant, K. Friedrichs, and H. Lewy. On the partial difference equations of mathematical physics. *IBM journal of Research and Development*, 11(2):215–234, 1967.

[47] A. Csikós, T. Luspay, and I. Varga. Modeling and optimal control of travel times and traffic emission on freeways. *IFAC Proceedings Volumes*, 44(1):13058 – 13063, 2011. 18th IFAC World Congress.

[48] C. F. Daganzo. The cell transmission model: A dynamic representation of highway traffic consistent with the hydrodynamic theory. *Transportation Research Part B: Methodological*, 28(4):269–287, 1994.

[49] C. F. Daganzo. Requiem for second-order fluid approximations of traffic flow. *Transportation Research Part B: Methodological*, 29(4):277–286, 1995.

[50] C. F. Daganzo. Urban gridlock: Macroscopic modeling and mitigation approaches. *Transportation Research Part B: Methodological*, 41(1):49–62, 2007.

[51] G. De Nunzio, C. Canudas-de-Wit, and P. Moulin. Urban traffic eco-driving: A macroscopic steady-state analysis. In *Control Conference (ECC), 2014 European*, pages 2581–2587. IEEE, 2014.

[52] G. De Nunzio, C. Canudas-de-Wit, P. Moulin, and D. Di Domenico. Eco-driving in urban traffic networks using traffic signals information. *International Journal of Robust and Nonlinear Control*, 26(6):1307–1324, 2016.

[53] G. De Nunzio, G. Gomes, C. Canudas-de-Wit, R. Horowitz, and P. Moulin. Arterial bandwidth maximization via signal offsets and variable speed limits control. In *Decision and Control (CDC), 2015 IEEE 54th Annual Conference on*, pages 5142–5148. IEEE, 2015.

[54] G. De Nunzio, G. Gomes, C. Canudas-de-Wit, R. Horowitz, and P. Moulin. Speed advisory and signal offsets control for arterial bandwidth maximization and energy consumption reduction. *IEEE Transactions on Control Systems Technology*, 25(3):875–887, 2017.

[55] G. De Nunzio and P.-O. Gutman. An application of shock wave theory to urban traffic control via dynamic speed advisory. In *hEART 2017: 6th Symposium of the European Association for Research in Transportation*, 2017.

[56] G. De Nunzio, A. Sciarretta, I. Ben Gharbia, and L. L. Ojeda. A constrained eco-routing strategy for hybrid electric vehicles based on semi-analytical energy management. In *2018 21st International Conference on Intelligent Transportation Systems (ITSC)*, pages 355–361, 2018.

[57] G. De Nunzio and L. Thibault. Energy-optimal driving range prediction for electric vehicles. In *2017 IEEE Intelligent Vehicles Symposium (IV)*, pages 1608–1613, 2017.

[58] G. De Nunzio, L. Thibault, and A. Sciarretta. Bi-objective eco-routing in large urban road networks. In *2017 IEEE 20th International Conference on Intelligent Transportation Systems (ITSC)*, pages 1–7, 2017.

[59] G. De Nunzio, L. Thibault, and A. Sciarretta. Model-based eco-routing strategy for electric vehicles in large urban networks. In *Comprehensive energy management–eco routing & velocity profiles*, pages 81–99. Springer, 2017.

[60] M. L. Delle Monache. *Traffic flow modeling by conservation laws*. PhD thesis, 2014.

[61] O. Derbel, T. Peter, H. Zebiri, B. Mourllion, and M. Basset. Modified intelligent driver model for driver safety and traffic stability improvement. *IFAC Proceedings Volumes*, 46(21):744–749, 2013.

[62] K. C. Dey, L. Yan, X. Wang, Y. Wang, H. Shen, M. Chowdhury, L. Yu, C. Qiu, and V. Soundararaj. A review of communication, driver characteristics, and controls aspects of cooperative adaptive cruise control (cacc). *IEEE Transactions on Intelligent Transportation Systems*, 17(2):491–509, 2015.

[63] M. Di Vaio, G. Fiengo, A. Petrillo, A. Salvi, S. Santini, and M. Tufo. Cooperative shock waves mitigation in mixed traffic flow environment. *IEEE Transactions on Intelligent Transportation Systems*, 20(12):4339–4353, 2019.

[64] W. Dib, A. Chasse, D. Di Domenico, P. Moulin, and A. Sciarretta. Evaluation of the energy efficiency of a fleet of electric vehicle for eco-driving application. *Oil & Gas Science and Technology–Revue d'IFP Energies nouvelles*, 67(4):589–599, 2012.

[65] V. Dinopoulou, C. Diakaki, and M. Papageorgiou. Applications of the urban traffic control strategy tuc. *European Journal of Operational Research*, 175(3):1652 – 1665, 2006.

[66] D. W. Dockery and C. A. Pope. Acute respiratory effects of particulate air pollution. *Annual review of public health*, 15(1):107–132, 1994.

[67] A. Dollar, A. Sciarretta, and A. Vahidi. Information and collaboration levels in vehicular strings: A comparative study. *IFAC Proceedings Volumes*, 2020.

[68] A. Dollar, A. Sciarretta, and A. Vahidi. Multi-agent control of lane-switching automated vehicles for energy efficiency. In *2020 American Control Conference (ACC)*, pages 422–429. IEEE, 2020.

[69] S. Du and S. Razavi. Variable speed limit for freeway work zone with capacity drop using discrete-time sliding mode control. *Journal of Computing in Civil Engineering*, 33(2):04019001, 2019.

[70] E. Ericsson, H. Larsson, and K. Brundell-Freij. Optimizing route choice for lowest fuel consumption–potential effects of a new driver support tool. *Transportation Research Part C: Emerging Technologies*, 14(6):369–383, 2006.

[71] S. A. Fayazi and A. Vahidi. Mixed-integer linear programming for optimal scheduling of autonomous vehicle intersection crossing. *IEEE Transactions on Intelligent Vehicles*, 3(3):287–299, 2018.

[72] S. A. Fayazi, A. Vahidi, and A. Luckow. Optimal scheduling of autonomous vehicle arrivals at intelligent intersections via milp. In *2017 American control conference (ACC)*, pages 4920–4925. IEEE, 2017.

[73] M. Fellendorf and P. Vortisch. Microscopic traffic flow simulator vissim. In *Fundamentals of traffic simulation*, pages 63–93. Springer, 2010.

[74] A. Ferrara, S. Sacone, and S. Siri. First-order macroscopic traffic models. In *Freeway traffic modelling and control*, chapter 3. Springer, 2018.

[75] A. Ferrara, S. Sacone, and S. Siri. Microscopic and mesoscopic traffic models. In *Freeway traffic modelling and control*, chapter 5. Springer, 2018.

[76] A. Ferrara, S. Sacone, and S. Siri. Second-order macroscopic traffic models. In *Freeway traffic modelling and control*, chapter 4. Springer, 2018.

[77] C. Fiori, V. Arcidiacono, G. Fontaras, D. Komnos, M. Makridis, V. Marzano, K. Mattas, C. Thiel, and B. Ciuffo. Less congestion implies less energy consumption: Is it really true? Technical report, 2018.

[78] J. L. Fleck, C. G. Cassandras, and Y. Geng. Adaptive quasi-dynamic traffic light control. *IEEE Transactions on Control Systems Technology*, 24(3):830–842, 2015.

[79] R. Fletcher. A new approach to variable metric algorithms. *The computer journal*, 13(3):317–322, 1970.

[80] A. Font, L. Guiseppin, M. Blangiardo, V. Ghersi, and G. W. Fuller. A tale of two cities: is air pollution improving in paris and london? *Environmental Pollution*, 249:1–12, 2019.

[81] G. Fontaras, N.-G. Zacharof, and B. Ciuffo. Fuel consumption and co2 emissions from passenger cars in europe–laboratory versus real-world emissions. *Progress in Energy and Combustion Science*, 60:97–131, 2017.

[82] J. R. D. Frejo, I. Papamichail, M. Papageorgiou, and B. De Schutter. Macroscopic modeling of variable speed limits on freeways. *Transportation research part C: emerging technologies*, 100:15–33, 2019.

[83] H. C. Frey and J. Zheng. Probabilistic analysis of driving cycle-based highway vehicle emission factors. *Environmental Science & Technology*, 36(23):5184–5191, 2002.

[84] M. Garavello, K. Han, and B. Piccoli. *Models for Vehicular Traffic on Networks*. American Institute of Mathematical Sciences, 2016.

[85] U. Gärtner, G. Hohenberg, H. Daudel, and H. Oelschlegel. Development and application of a semi-empirical nox model to various hd diesel engines. In *Thermo-and Fluid Dynamic Processes in Diesel Engines 2*, pages 285–312. Springer, 2004.

[86] D. C. Gazis, R. Herman, and R. B. Potts. Car-following theory of steady-state traffic flow. *Operations research*, 7(4):499–505, 1959.

[87] D. C. Gazis, R. Herman, and R. W. Rothery. Nonlinear follow-the-leader models of traffic flow. *Operations research*, 9(4):545–567, 1961.

[88] D. C. Gazis and R. B. Potts. The oversaturated intersection. Technical report, 1963.

[89] A. Ghiasi, X. Li, and J. Ma. A mixed traffic speed harmonization model with connected autonomous vehicles. *Transportation Research Part C: Emerging Technologies*, 104:210–233, 2019.

[90] V. Giammarino, S. Baldi, P. Frasca, and M. L. D. Monache. Traffic flow on a ring with a single autonomous vehicle: An interconnected stability perspective. *IEEE Transactions on Intelligent Transportation Systems*, pages 1–11, 2020.

[91] S. Godunov. A difference scheme for numerical computation of discontinuous solution of hyperbolic equation. *Math. Sbornik*, 47:271–306, 1959.

[92] D. Goldfarb. A family of variable-metric methods derived by variational means. *Mathematics of computation*, 24(109):23–26, 1970.

[93] G. Gomes. Bandwidth maximization using vehicle arrival functions. *IEEE Transactions on Intelligent Transportation Systems*, 16(4):1977–1988, 2015.

[94] N. J. Goodall, B. L. Smith, and B. Park. Traffic signal control with connected vehicles. *Transportation Research Record*, 2381(1):65–72, 2013.

[95] P. Grandinetti, C. Canudas-de Wit, and F. Garin. Distributed optimal traffic lights design for large-scale urban networks. *IEEE Transactions on Control Systems Technology*, (99):1–14, 2018.

[96] H. Greenberg. An analysis of traffic flow. *Operations Research*, 7(1):79–85, 1959.

[97] B. Greenshields, W. Channing, H. Miller, et al. A study of traffic capacity. In *Highway research board proceedings*, volume 1935. National Research Council (USA), Highway Research Board, 1935.

[98] J. Guanetti, Y. Kim, and F. Borrelli. Control of connected and automated vehicles: State of the art and future challenges. *Annual Reviews in Control*, 45:18–40, 2018.

[99] J. Haddad and N. Geroliminis. On the stability of traffic perimeter control in two-region urban cities. *Transportation Research Part B: Methodological*, 46(9):1159–1176, 2012.

[100] M. Hadiuzzaman and T. Z. Qiu. Cell transmission model based variable speed limit control for freeways. *Canadian Journal of Civil Engineering*, 40(1):46–56, 2013.

[101] R. Hall. *Handbook of transportation science*, volume 23. Springer Science & Business Media, 2012.

[102] J. Han, A. Sciarretta, L. L. Ojeda, G. De Nunzio, and L. Thibault. Safe-and eco-driving control for connected and automated electric vehicles using analytical state-constrained optimal solution. *IEEE Transactions on Intelligent Vehicles*, 3(2):163–172, 2018.

[103] J. Han, A. Vahidi, and A. Sciarretta. Fundamentals of energy efficient driving for combustion engine and electric vehicles: An optimal control perspective. *Automatica*, 103:558 – 572, 2019.

[104] K. Han, H. Liu, V. V. Gayah, T. L. Friesz, and T. Yao. A robust optimization approach for dynamic traffic signal control with emission considerations. *Transportation Research Part C: Emerging Technologies*, 70:3–26, 2016.

[105] S. Hausberger. Emission factors from the model phem for the hbefa version 3. 2009.

[106] Q. He, K. L. Head, and J. Ding. Pamscod: Platoon-based arterial multimodal signal control with online data. *Transportation Research Part C: Emerging Technologies*, 20(1):164–184, 2012.

[107] S. Heft-Neal, J. Burney, E. Bendavid, and M. Burke. Robust relationship between air quality and infant mortality in africa. *Nature*, 559(7713):254–258, 2018.

[108] A. Hegyi, B. De Schutter, H. Hellendoorn, and T. Van Den Boom. Optimal coordination of ramp metering and variable speed control-an mpc approach. In *Proceedings of the 2002 American Control Conference (IEEE Cat. No. CH37301)*, volume 5, pages 3600–3605. IEEE, 2002.

[109] A. Hegyi, S. P. Hoogendoorn, M. Schreuder, H. Stoelhorst, and F. Viti. Specialist: A dynamic speed limit control algorithm based on shock wave theory. In *2008 11th International IEEE Conference on Intelligent Transportation Systems*, pages 827–832, 2008.

[110] A. Hegyi, B. D. Schutter, and H. Hellendoorn. Model predictive control for optimal coordination of ramp metering and variable speed limits. *Transportation Research Part C: Emerging Technologies*, 13(3):185 – 209, 2005.

[111] D. Helbing. Improved fluid-dynamic model for vehicular traffic. *Physical Review E*, 51(4):3164, 1995.

[112] E. Hellström, M. Ivarsson, J. Åslund, and L. Nielsen. Look-ahead control for heavy trucks to minimize trip time and fuel consumption. *Control Engineering Practice*, 17(2):245–254, 2009.

[113] M. Herty and M. Rascle. Coupling conditions for a class of second-order models for traffic flow. *SIAM Journal on Mathematical Analysis*, 38(2):595–616, 2006.

[114] D. Heß, R. Lattarulo, J. Pérez, J. Schindler, T. Hesse, and F. Köster. Fast maneuver planning for cooperative automated vehicles. In *2018 21st International Conference on Intelligent Transportation Systems (ITSC)*, pages 1625–1632. IEEE, 2018.

[115] B. HomChaudhuri, A. Vahidi, and P. Pisu. Fast model predictive control-based fuel efficient control strategy for a group of connected vehicles in urban road conditions. *IEEE Transactions on Control Systems Technology*, 25(2):760–767, 2017.

[116] S. P. Hoogendoorn and P. H. Bovy. State-of-the-art of vehicular traffic flow modelling. *Proceedings of the Institution of Mechanical Engineers, Part I: Journal of Systems and Control Engineering*, 215(4):283–303, 2001.

[117] S. Huang, A. W. Sadek, and Y. Zhao. Assessing the mobility and environmental benefits of reservation-based intelligent intersections using an integrated simulator. *IEEE Transactions on Intelligent Transportation Systems*, 13(3):1201–1214, 2012.

[118] Y. Huang, E. C. Ng, J. L. Zhou, N. C. Surawski, E. F. Chan, and G. Hong. Eco-driving technology for sustainable road transport: A review. *Renewable and Sustainable Energy Reviews*, 93:596–609, 2018.

[119] P. Hunt, D. Robertson, R. Bretherton, and R. Winton. Scoot-a traffic responsive method of coordinating signals. Technical report, 1981.

[120] IEA. Energy consumption in transport in selected iea countries. `https://www.iea.org/data-and-statistics/charts/energy-consumption-in-transport-in-selected-iea-countries-2017`, 2017.

[121] IEA. Largest end-uses of energy by sector in selected iea countries. `https://www.iea.org/data-and-statistics/charts/largest-end-uses-of-energy-by-sector-in-selected-iea-countries-2017`, 2017.

[122] International Energy Agency. World energy outlook 2018, 2018.

[123] S. Jafarmadar. A comparative analysis of two neural network predictions for performance and emissions in a biodiesel fuelled diesel engine. 2015.

[124] A. Jamshidnejad, I. Papamichail, M. Papageorgiou, and B. De Schutter. A mesoscopic integrated urban traffic flow-emission model. *Transportation Research Part C: Emerging Technologies*, 75:45–83, 2017.

[125] A. Jamshidnejad, I. Papamichail, M. Papageorgiou, and B. De Schutter. Sustainable model-predictive control in urban traffic networks: Efficient solution based on general smoothening methods. *IEEE Transactions on Control Systems Technology*, 26(3):813–827, 2018.

[126] L. Jie, H. V. Zuylen, Y. Chen, F. Viti, and I. Wilmink. Calibration of a microscopic simulation model for emission calculation. *Transportation Research Part C: Emerging Technologies*, 31:172 – 184, 2013.

[127] Q. Jin, G. Wu, K. Boriboonsomsin, and M. Barth. Platoon-based multi-agent intersection management for connected vehicle. In *16th International IEEE Conference on Intelligent Transportation Systems (ITSC 2013)*, pages 1462–1467. IEEE, 2013.

[128] Q. Jin, G. Wu, K. Boriboonsomsin, and M. J. Barth. Power-based optimal longitudinal control for a connected eco-driving system. *IEEE Transactions on Intelligent Transportation Systems*, 17(10):2900–2910, 2016.

[129] T. Jurik, A. Cela, R. Hamouche, R. Natowicz, A. Reama, S. Niculescu, and J. Julien. Energy optimal real-time navigation system. *IEEE Intelligent Transportation Systems Magazine*, 6(3):66–79, 2014.

[130] M. A. S. Kamal, J.-i. Imura, T. Hayakawa, A. Ohata, and K. Aihara. Traffic signal control of a road network using milp in the mpc framework. *International journal of intelligent transportation systems research*, 13(2):107–118, 2015.

[131] M. A. S. Kamal, S. Taguchi, and T. Yoshimura. Efficient driving on multilane roads under a connected vehicle environment. *IEEE Transactions on Intelligent Transportation Systems*, 17(9):2541–2551, 2016.

[132] D. Karbowski, N. Kim, and A. Rousseau. Route-based online energy management of a phev and sensitivity to trip prediction. In *Vehicle Power and Propulsion Conference (VPPC), 2014 IEEE*, pages 1–6. IEEE, 2014.

[133] P. Kataria and A. Rani. Real-time traffic light management system with manual control. In *2019 3rd International Conference on Recent Developments in Control, Automation & Power Engineering (RDCAPE)*, pages 419–424. IEEE, 2019.

[134] B. S. Kerner and P. Konhäuser. Cluster effect in initially homogeneous traffic flow. *Physical Review E*, 48(4):R2335, 1993.

[135] A. Kesting, M. Treiber, and D. Helbing. Enhanced intelligent driver model to access the impact of driving strategies on traffic capacity. *Philosophical Transactions of the Royal Society A: Mathematical, Physical and Engineering Sciences*, 368(1928):4585–4605, 2010.

[136] M. A. Khamis and W. Gomaa. Enhanced multiagent multi-objective reinforcement learning for urban traffic light control. In *2012 11th International Conference on Machine Learning and Applications*, volume 1, pages 586–591. IEEE, 2012.

[137] B. Khondaker and L. Kattan. Variable speed limit: a microscopic analysis in a connected vehicle environment. *Transportation Research Part C: Emerging Technologies*, 58:146 – 159, 2015.

[138] B. Khondaker and L. Kattan. Variable speed limit: an overview. *Transportation Letters*, 7(5):264–278, 2015.

[139] S. Kluge, C. Santa, S. Dangl, S. Wild, M. Brokate, K. Reif, and F. Busch. On the computation of the energy-optimal route dependent on the traffic load in ingolstadt. *Transportation Research Part C: Emerging Technologies*, 36:97 – 115, 2013.

[140] G. Kotusevski and K. Hawick. A review of traffic simulation software. 2009.

[141] S. Krauß. *Microscopic modeling of traffic flow: Investigation of collision free vehicle dynamics*. PhD thesis, 1998.

[142] M. Kubička, J. Klusáček, A. Sciarretta, A. Cela, H. Mounier, L. Thibault, and S.-I. Niculescu. Performance of current eco-routing methods. In *Intelligent Vehicles Symposium (IV), 2016 IEEE*, pages 472–477. IEEE, 2016.

[143] Y. Kuo. Using simulated annealing to minimize fuel consumption for the time-dependent vehicle routing problem. *Computers & Industrial Engineering*, 59(1):157–165, 2010.

[144] V. K. Lakshmanan, A. Sciarretta, and O. E. Ganaoui-Mourlan. Cooperative eco-driving of electric vehicle platoons for energy efficiency and string stability. *IFAC-PapersOnLine*, 54(2):133–139, 2021. 16th IFAC Symposium on Control in Transportation Systems CTS 2021.

[145] J. Larson, K.-Y. Liang, and K. H. Johansson. A distributed framework for coordinated heavy-duty vehicle platooning. *IEEE Transactions on Intelligent Transportation Systems*, 16(1):419–429, 2014.

[146] J. Lee, J. Kim, J. Park, and C. Bae. Effect of the air-conditioning system on the fuel economy in a gasoline engine vehicle. *Proceedings of the Institution of Mechanical Engineers, Part D: Journal of Automobile Engineering*, 227(1):66–77, 2013.

[147] D. Lejri, A. Can, N. Schiper, and L. Leclercq. Accounting for traffic speed dynamics when calculating copert and phem pollutant emissions at the urban scale. *Transportation Research Part D: Transport and Environment*, 63:588 – 603, 2018.

[148] W. Leutzbach. *Introduction to the theory of traffic flow*, volume 47. Springer, 1988.

[149] M. Levin, R. Chen, C.-F. Liao, and T. Zhang. Improving intersection safety through variable speed limits for connected vehicles (no. cts 19-12). Technical report, Roadway Safety Institute, 2019.

[150] X. Li and J.-Q. Sun. Studies of vehicle lane-changing dynamics and its effect on traffic efficiency, safety and environmental impact. *Physica A: Statistical Mechanics and its Applications*, 467:41 – 58, 2017.

[151] K.-Y. Liang, J. Mårtensson, and K. H. Johansson. When is it fuel efficient for a heavy duty vehicle to catch up with a platoon? *IFAC Proceedings Volumes*, 46(21):738–743, 2013.

[152] T. Liard, R. Stern, and M.-L. Delle Monache. Optimal driving strategies for traffic control with autonomous vehicles. In *The 21rst IFAC World Congress*, July 2020.

[153] M. Liebner, M. Baumann, F. Klanner, and C. Stiller. Driver intent inference at urban intersections using the intelligent driver model. In *2012 IEEE Intelligent Vehicles Symposium*, pages 1162–1167. IEEE, 2012.

[154] M. J. Lighthill and G. B. Whitham. On kinematic waves ii. a theory of traffic flow on long crowded roads. *Proceedings of the Royal Society London A*, 229(1178):317–345, 1955.

[155] D. Lin and S. E. Jabari. Pay for intersection priority: A free market mechanism for connected vehicles. *arXiv preprint arXiv:2001.01813*, 2020.

[156] D. Lin, L. Li, and S. E. Jabari. Pay to change lanes: A cooperative lane-changing strategy for connected/automated driving. *Transportation Research Part C: Emerging Technologies*, 105:550–564, 2019.

[157] S. Lin, B. De Schutter, Y. Xi, and H. Hellendoorn. Efficient network-wide model-based predictive control for urban traffic networks. *Transportation Research Part C: Emerging Technologies*, 24:122–140, 2012.

[158] S. Lin, B. De Schutter, Y. Xi, and H. Hellendoorn. Integrated urban traffic control for the reduction of travel delays and emissions. *IEEE Transactions on Intelligent Transportation Systems*, 14(4):1609–1619, Dec 2013.

[159] S. Lin and Y. Xi. An efficient model for urban traffic network control. *IFAC Proceedings Volumes*, 41(2):14066–14071, 2008.

[160] J. Lioris, R. Pedarsani, F. Y. Tascikaraoglu, and P. Varaiya. Doubling throughput in urban roads by platooning. *IFAC-PapersOnLine*, 49(3):49–54, 2016.

[161] T. Litman. *Autonomous vehicle implementation predictions*. Victoria Transport Policy Institute Victoria, Canada, 2017.

[162] B. Liu, D. Ghosal, C.-N. Chuah, and H. M. Zhang. Reducing greenhouse effects via fuel consumption-aware variable speed limit (fc-vsl). *IEEE Transactions on Vehicular Technology*, 61(1):111–122, 2011.

[163] D. C. Liu and J. Nocedal. On the limited memory bfgs method for large scale optimization. *Mathematical programming*, 45(1):503–528, 1989.

[164] H. Liu, X.-Y. Lu, and S. E. Shladover. Traffic signal control by leveraging cooperative adaptive cruise control (cacc) vehicle platooning capabilities. *Transportation research part C: emerging technologies*, 104:390–407, 2019.

[165] H. Liu, S. E. Shladover, X.-Y. Lu, and X. Kan. Freeway vehicle fuel efficiency improvement via cooperative adaptive cruise control. *Journal of Intelligent Transportation Systems*, pages 1–13, 2020.

[166] P. Liu, U. Ozguner, and Y. Zhang. Distributed mpc for cooperative highway driving and energy-economy validation via microscopic simulations. *Transportation Research Part C: Emerging Technologies*, 77:80–95, 2017.

[167] R. Liu and J. Tate. Network effects of intelligent speed adaptation systems. *Transportation*, 31(3):297–325, 2004.

[168] S. Liu, H. Hellendoorn, and B. De Schutter. Model predictive control for freeway networks based on multi-class traffic flow and emission models. *IEEE Transactions on Intelligent Transportation Systems*, 18(2):306–320, 2017.

[169] A. Lombard, F. Perronnet, A. Abbas-Turki, and A. El Moudni. On the cooperative automatic lane change: Speed synchronization and automatic "courtesy". In *Design, Automation & Test in Europe Conference & Exhibition (DATE), 2017*, pages 1655–1658. IEEE, 2017.

[170] P. A. Lopez, M. Behrisch, L. Bieker-Walz, J. Erdmann, Y.-P. Flötteröd, R. Hilbrich, L. Lücken, J. Rummel, P. Wagner, and E. Wießner. Microscopic traffic simulation using sumo. In *The 21st IEEE International Conference on Intelligent Transportation Systems*. IEEE, 2018.

[171] P. Lowrie et al. The sydney co-ordinated adaptive traffic system (scats) – principles, methodology, algorithms. In *Proceedings of the International Conference on Road Traffic Signaling, London, UK*, 1982.

[172] X.-Y. Lu and S. E. Shladover. Automated truck platoon control. Technical report, Institute of Transportation Studies, UC Berkeley, 2011.

[173] L. Luo, Y.-E. Ge, F. Zhang, and X. J. Ban. Real-time route diversion control in a model predictive control framework with multiple objectives: Traffic efficiency, emission reduction and fuel economy. *Transportation Research Part D: Transport and Environment*, 48:332–356, 2016.

[174] G. Mahler and A. Vahidi. Reducing idling at red lights based on probabilistic prediction of traffic signal timings. In *American Control Conference (ACC), 2012*, pages 6557–6562. IEEE, 2012.

[175] N. Mandl and M. Pinterits. Annual european union greenhouse gas inventory 1990–2016 and inventory report 2018, 2018.

[176] B. Marcu and F. Browand. Aerodynamic forces experienced by a 3-vehicle platoon in a crosswind. Technical report, SAE Technical Paper, 1999.

[177] B. McAuliffe, M. Croken, M. Ahmadi-Baloutaki, and A. Raeesi. Fuel-economy testing of a three-vehicle truck platooning system. *UC Berkeley*, 2017.

[178] N. Mehr, M. Sanselme, N. Orr, R. Horowitz, and G. Gomes. Offset selection for bandwidth maximization on multiple routes. In *2018 Annual American Control Conference (ACC)*, pages 6366–6371. IEEE, 2018.

[179] X. Meng and C. G. Cassandras. Optimal control of autonomous vehicles approaching a traffic light. *arXiv preprint arXiv:1802.09600*, 2018.

[180] A. Messmer and M. Papageorgiou. Metanet: a macroscopic simulation program for motorway networks. *Traffic Engineering & Control*, 31:466–470, 1990.

[181] D. Miculescu and S. Karaman. Polling-systems-based autonomous vehicle coordination in traffic intersections with no traffic signals. *IEEE Transactions on Automatic Control*, 65(2):680–694, 2019.

[182] V. Milanés, S. E. Shladover, J. Spring, C. Nowakowski, H. Kawazoe, and M. Nakamura. Cooperative adaptive cruise control in real traffic situations. *IEEE Transactions on intelligent transportation systems*, 15(1):296–305, 2013.

[183] P. Mirchandani and L. Head. A real-time traffic signal control system: architecture, algorithms, and analysis. *Transportation Research Part C: Emerging Technologies*, 9(6):415 – 432, 2001.

[184] M. Miyatake, M. Kuriyama, and Y. Takeda. Theoretical study on eco-driving technique for an electric vehicle considering traffic signals. In *Power Electronics and Drive Systems (PEDS), 2011 IEEE Ninth International Conference on*, pages 733–738. IEEE, 2011.

[185] E. Namazi, J. Li, and C. Lu. Intelligent intersection management systems considering autonomous vehicles: a systematic literature review. *IEEE Access*, 7:91946–91965, 2019.

[186] G. Nannicini, D. Delling, D. Schultes, and L. Liberti. Bidirectional a* search on time-dependent road networks. *Networks*, 59(2):240–251, 2012.

[187] E. Negrenti. The 'corrected average speed' approach in enea's tee model: an innovative solution for the evaluation of the energetic and environmental impacts of urban transport policies. *Science of the total environment*, 235(1-3):411–413, 1999.

[188] G. F. Newell. A simplified theory of kinematic waves in highway traffic, part i: General theory. *Transportation Research Part B: Methodological*, 27(4):281–287, 1993.

[189] J. Nie, J. Zhang, W. Ding, X. Wan, X. Chen, and B. Ran. Decentralized cooperative lane-changing decision-making for connected autonomous vehicles. *IEEE Access*, 4:9413–9420, 2016.

[190] H. Noorvand, G. Karnati, and B. S. Underwood. Autonomous vehicles: assessment of the implications of truck positioning on flexible pavement performance and design. *Transportation Research Record*, 2640(1):21–28, 2017.

[191] C. Nowakowski, J. O'Connell, S. E. Shladover, and D. Cody. Cooperative adaptive cruise control: Driver acceptance of following gap settings less than one second. In *Proceedings of the Human Factors and Ergonomics Society Annual Meeting*, volume 54, pages 2033–2037. SAGE Publications Sage CA: Los Angeles, CA, 2010.

[192] L. Ntziachristos, D. Gkatzoflias, C. Kouridis, and Z. Samaras. Copert: A european road transport emission inventory model. pages 491–504, 2009.

[193] O. Obodeh and C. Ajuwa. Evaluation of artificial neural network performance in predicting diesel engine nox emissions. *European Journal of Scientific Research*, 33(4):642–653, 2009.

[194] L. L. Ojeda, A. Chasse, and R. Goussault. Fuel consumption prediction for heavy-duty vehicles using digital maps. In *2017 IEEE 20th International Conference on Intelligent Transportation Systems (ITSC)*, pages 1–7, 2017.

[195] L. L. Ojeda, J. Han, A. Sciarretta, G. De Nunzio, and L. Thibault. A real-time eco-driving strategy for automated electric vehicles. In *2017 IEEE 56th Annual Conference on Decision and Control (CDC)*, pages 2768–2774, 2017.

[196] J. J. Olstam and A. Tapani. *Comparison of Car-following models*, volume 960. Swedish National Road and Transport Research Institute Linköping, 2004.

[197] C. Osorio and K. Nanduri. Energy-efficient urban traffic management: a microscopic simulation-based approach. *Transportation Science*, 49(3):637–651, 2015.

[198] B. Othman, G. De Nunzio, D. Di Domenico, and C. Canudas-de-Wit. Ecological traffic management: A review of the modeling and control strategies for improving environmental sustainability of road transportation. *Annual Reviews in Control*, 48:292 – 311, 2019.

[199] B. Othman, G. De Nunzio, D. Di Domenico, and C. Canudas-de-Wit. Variable speed limits control in an urban road network to reduce environmental impact of traffic. In *2020 Annual American Control Conference (ACC)*, pages 1179–1184. IEEE, 2020.

[200] B. Othman, G. De Nunzio, D. Domenico, and C. Canudas-De-Wit. Urban road traffic fuel consumption optimization via variable speed limits or signalized access control: A comparative study. In *IEEE Conference on Decision and Control (CDC) 2021*, 2021.

[201] B. Othman, G. de Nunzio, A. Sciarretta, D. Di Domenico, and C. C. de Wit. *Connectivity and Automation as Enablers for Energy-Efficient Driving and Road Traffic Management*. Springer New York, 2021.

[202] E. Ozatay, S. Onori, J. Wollaeger, Ü. Özgüner, G. Rizzoni, D. Filev, J. Michelini, and S. D. Cairano. Cloud-based velocity profile optimization for everyday driving: A dynamic-programming-based solution. *IEEE Transactions on Intelligent Transportation Systems*, 15:2491–2505, 2014.

[203] E. Ozatay, U. Ozguner, J. Michelini, and D. Filev. Analytical solution to the minimum energy consumption based velocity profile optimization problem with variable road grade. *IFAC Proceedings Volumes*, 47(3):7541–7546, 2014.

[204] L. I. Panis, S. Broekx, and R. Liu. Modelling instantaneous traffic emission and the influence of traffic speed limits. *Science of the Total Environment*, 371(1-3):270–285, 2006.

[205] M. Papageorgiou, H. Hadj-Salem, J.-M. Blosseville, et al. Alinea: A local feedback control law for on-ramp metering. *Transportation Research Record*, 1320(1):58–67, 1991.

[206] M. Papageorgiou and A. Kotsialos. Freeway ramp metering: An overview. *IEEE transactions on intelligent transportation systems*, 3(4):271–281, 2002.

[207] C. Pasquale, I. Papamichail, C. Roncoli, S. Sacone, S. Siri, and M. Papageorgiou. Two-class freeway traffic regulation to reduce congestion and emissions via nonlinear optimal control. *Transportation Research Part C: Emerging Technologies*, 55:85–99, 2015.

[208] H. Payne. Models of freeway traffic and control. In *Mathematical Models of Public Systems*. Simul. Counc. Proc., 1971.

[209] L. Pelkmans and P. Debal. Comparison of on-road emissions with emissions measured on chassis dynamometer test cycles. *Transportation Research Part D: Transport and Environment*, 11(4):233 – 241, 2006.

[210] B. Piccoli and A. Tosin. A review of continuum mathematical models of vehicular traffic. *Encyclopedia of Complexity and Systems Science*, pages 9727–9749, 2009.

[211] G. Pinto and M. T. Oliver-Hoyo. Using the relationship between vehicle fuel consumption and co2 emissions to illustrate chemical principles. *Journal of Chemical Education*, 85(2):218, 2008.

[212] D. Pisarski and C. Canudas-de-Wit. Nash game-based distributed control design for balancing traffic density over freeway networks. *IEEE Transactions on Control of Network Systems*, 3(2):149–161, 2016.

[213] K. Post, J. Kent, J. Tomlin, and N. Carruthers. Fuel consumption and emission modelling by power demand and a comparison with other models. *Transportation Research Part A: General*, 18(3):191–213, 1984.

[214] W. W. Pulkrabek. Engineering Fundamentals of the Internal Combustion Engine, 2nd Ed. *Journal of Engineering for Gas Turbines and Power*, 126(1):198–198, 2004.

[215] Y. G. Qi, H. H. Teng, and L. Yu. Microscale emission models incorporating acceleration and deceleration. *Journal of Transportation Engineering*, 130(3):348–359, 2004.

[216] S. F. Qom, Y. Xiao, and M. Hadi. Evaluation of cooperative adaptive cruise control (cacc) vehicles on managed lanes utilizing macroscopic and mesoscopic simulation. In *Transportation Research Board 95th Annual Meeting*, number 16-6384, 2016.

[217] X. Qu, L. Li, Z. Yi, P. Mao, and M. Yang. Traffic flow modeling of freeway variable speed limit control based on the big data of driving behavior. *Journal of Advanced Transportation*, 2020, 2020.

[218] S. Quarmby, G. Santos, and M. Mathias. Air quality strategies and technologies: A rapid review of the international evidence. *Sustainability*, 11(10):2757, 2019.

[219] K. Raboy, J. Ma, E. Leslie, and F. Zhou. A proof-of-concept field experiment on cooperative lane change maneuvers using a prototype connected automated vehicle testing platform. *Journal of Intelligent Transportation Systems*, pages 1–16, 2020.

[220] K. Raboy, J. Ma, J. Stark, F. Zhou, K. Rush, and E. Leslie. Cooperative control for lane change maneuvers with connected automated vehicles: A field experiment. Technical report, 2017.

[221] N. K. Rai, A. Vyas, and S. K. Singh. Street level modeling of pollutants for residential areas. *International Journal of Engineering Research and Application*, 7(10):52–57, 2017.

[222] H. Rakha, K. Ahn, and A. Trani. Comparison of mobile5a, mobile6, vt-micro, and cmem models for estimating hot-stabilized light-duty gasoline vehicle emissions. *Canadian Journal of Civil Engineering*, 30:1010–1021, 2003.

[223] P. I. Richards. Shock waves on the highway. *Operations Research*, 4(1):42–51, 1956.

[224] M. Robinson et al. Examples of variable speed limit applications. 2000.

[225] H. H. Salem, J. Chrisoulakis, M. Papageorgiou, N. Elloumi, and P. Papadakos. The use of metacor tool for integrated urban and interurban traffic control. evaluation in corridor peripherique, paris. In *Proceedings of VNIS'94-1994 Vehicle Navigation and Information Systems Conference*, pages 645–650. IEEE, 1994.

[226] J. M. Samet, F. Dominici, F. C. Curriero, I. Coursac, and S. L. Zeger. Fine particulate air pollution and mortality in 20 us cities, 1987–1994. *New England journal of medicine*, 343(24):1742–1749, 2000.

[227] N. Schiper. *Traffic data sampling for air pollution estimation at different urban scales*. PhD thesis, Université de Lyon, 2017.

[228] A. Sciarretta, G. D. Nunzio, and L. L. Ojeda. Optimal ecodriving control: Energy-efficient driving of road vehicles as an optimal control problem. *IEEE Control Systems Magazine*, 35(5):71–90, 2015.

[229] A. Sciarretta and A. Vahidi. *Energy Saving Potentials of CAVs*, pages 1–31. Springer International Publishing, Cham, 2020.

[230] A. Sciarretta and A. Vahidi. *Fundamentals of Vehicle Modeling*, pages 33–62. Springer International Publishing, Cham, 2020.

[231] G. Scora and M. Barth. Comprehensive modal emissions model (cmem), version 3.01. *User guide. Centre for Environmental Research and Technology. University of California, Riverside*, 1070, 2006.

[232] M. Seredynski, W. Mazurczyk, and D. Khadraoui. Multi-segment green light optimal speed advisory. In *Parallel and Distributed Processing Symposium Workshops & PhD Forum (IPDPSW), 2013 IEEE 27th International*, pages 459–465. IEEE, 2013.

[233] D. F. Shanno. Conditioning of quasi-newton methods for function minimization. *Mathematics of computation*, 24(111):647–656, 1970.

[234] S. E. Shladover, C. Nowakowski, X.-Y. Lu, and R. Ferlis. Cooperative adaptive cruise control: Definitions and operating concepts. *Transportation Research Record*, 2489(1):145–152, 2015.

[235] I. I. Sirmatel and N. Geroliminis. Stabilization of city-scale road traffic networks via macroscopic fundamental diagram-based model predictive perimeter control. *Control Engineering Practice*, 109:104750, 2021.

[236] N. Sobrino, A. Monzón, and S. Hernandez. Reduced carbon and energy footprint in highway operations: The highway energy assessment (hera) methodology. *Netw Spat Econ*, 16:1–20, 2014.

[237] R. E. Stern, Y. Chen, M. Churchill, F. Wu, M. L. D. Monache, B. Piccoli, B. Seibold, J. Sprinkle, and D. B. Work. Quantifying air quality benefits resulting from few autonomous vehicles stabilizing traffic. *Transportation Research Part D: Transport and Environment*, 67:351 – 365, 2019.

[238] A. Stevanovic, J. Stevanovic, K. Zhang, and S. Batterman. Optimizing traffic control to reduce fuel consumption and vehicular emissions: Integrated approach with vissim, cmem, and visgaost. *Transportation Research Record*, 2128(1):105–113, 2009.

[239] P. Sturm, G. Kirchweger, S. Hausberger, and R. Almbauer. Instantaneous emission data and their use in estimating road traffic emissions. *International Journal of Vehicle Design*, 20, 1998.

[240] C. Sun, J. Guanetti, F. Borrelli, and S. Moura. Robust eco-driving control of autonomous vehicles connected to traffic lights. *arXiv preprint arXiv:1802.05815*, 2018.

[241] J. Sun and H. X. Liu. Stochastic eco-routing in a signalized traffic network. *Transportation Research Part C: Emerging Technologies*, 59:32 – 47, 2015. Special Issue on International Symposium on Transportation and Traffic Theory.

[242] R. Tachet, P. Santi, S. Sobolevsky, L. I. Reyes-Castro, E. Frazzoli, D. Helbing, and C. Ratti. Revisiting street intersections using slot-based systems. *PloS one*, 11(3):e0149607, 2016.

[243] M. Tajali and A. Hajbabaie. Dynamic speed harmonization in urban street networks. *Computer-Aided Civil and Infrastructure Engineering*, 03 2018.

[244] E. Talavera, A. Díaz-Álvarez, F. Jiménez, and J. E. Naranjo. Impact on congestion and fuel consumption of a cooperative adaptive cruise control system with lane-level position estimation. *Energies*, 11(1):194, 2018.

[245] C. M. Tampère, R. Corthout, D. Cattrysse, and L. H. Immers. A generic class of first order node models for dynamic macroscopic simulation of traffic flows. *Transportation Research Part B: Methodological*, 45(1):289 – 309, 2011.

[246] M. Taylor. Network modeling of the traffic, environmental and energy effects of lower urban speed limits. *Road and Transport Research*, 9:48–57, 12 2000.

[247] L. Thibault, P. Degeilh, O. Lepreux, L. Voise, G. Alix, and G. Corde. A new gps-based method to estimate real driving emissions. In *2016 IEEE 19th International Conference on Intelligent Transportation Systems (ITSC)*, pages 1628–1633, 2016.

[248] L. Thibault, G. D. Nunzio, and A. Sciarretta. A unified approach for electric vehicles range maximization via eco-routing, eco-driving, and energy consumption prediction. *IEEE Transactions on Intelligent Vehicles*, 3:463–475, 2018.

[249] E. Thonhofer, T. Palau, A. Kuhn, S. Jakubek, and M. Kozek. Macroscopic traffic model for large scale urban traffic network design. *Simulation Modelling Practice and Theory*, 80:32–49, 2018.

[250] Transport & Environment. Co2 emissions from cars: the facts, 2018.

[251] M. Treiber, A. Hennecke, and D. Helbing. Congested traffic states in empirical observations and microscopic simulations. *Physical review E*, 62(2):1805, 2000.

[252] M. Treiber and A. Kesting. Model-based traffic flow optimization. In *Traffic Flow Dynamics*, chapter 21. Springer, 2013.

[253] M. Treiber and A. Kesting. Trajectory and floating-car data. In *Traffic Flow Dynamics*, chapter 2. Springer, 2013.

[254] U.S. Energy Information Administration. International energy outlook, 2017.

[255] U.S. Energy Information Administration. Study of the potential energy consumption impacts of connected and automated vehicles, 2017.

[256] B. Van Arem, C. J. Van Driel, and R. Visser. The impact of cooperative adaptive cruise control on traffic-flow characteristics. *IEEE Transactions on intelligent transportation systems*, 7(4):429–436, 2006.

[257] S. Van de Hoef. *Fuel-efficient centralized coordination of truck platooning*. PhD thesis, KTH Royal Institute of Technology, 2016.

[258] S. Van De Hoef, K. H. Johansson, and D. V. Dimarogonas. Fuel-optimal centralized coordination of truck platooning based on shortest paths. In *2015 American Control Conference (ACC)*, pages 3740–3745. IEEE, 2015.

[259] M. Van den Berg, A. Hegyi, B. De Schutter, and H. Hellendoorn. Integrated traffic control for mixed urban and freeway networks: A model predictive control approach. *European Journal of Transport and Infrastructure Research EJTIR, 7 (3)*, 2007.

[260] C. Van Hinsbergen, W. Schakel, V. Knoop, J. van Lint, and S. Hoogendoorn. A general framework for calibrating and comparing car-following models. *Transportmetrica A: Transport Science*, 11(5):420–440, 2015.

[261] F. van Wageningen-Kessels, H. van Lint, K. Vuik, and S. Hoogendoorn. Genealogy of traffic flow models. *EURO Journal on Transportation and Logistics*, 4(4):445–473, 2015.

[262] P. Varaiya. The max-pressure controller for arbitrary networks of signalized intersections. In *Advances in Dynamic Network Modeling in Complex Transportation Systems*, pages 27–66. Springer, 2013.

[263] E. Vinitsky, A. Kreidieh, L. Le Flem, N. Kheterpal, K. Jang, C. Wu, F. Wu, R. Liaw, E. Liang, and A. M. Bayen. Benchmarks for reinforcement learning in mixed-autonomy traffic. In *Conference on Robot Learning*, pages 399–409, 2018.

[264] J. D. Vreeswijk, M. Mahmod, and B. van Arem. Energy efficient traffic management and control-the ecomove approach and expected benefits. In *13th International IEEE Conference on Intelligent Transportation Systems*, pages 955–961. IEEE, 2010.

[265] J. D. Vreeswijk, M. Mahmod, and B. van Arem. Energy efficient traffic management and control - the ecomove approach and expected benefits. In *13th International IEEE Conference on Intelligent Transportation Systems*, pages 955–961. 2013.

[266] Z. Wadud, D. MacKenzie, and P. Leiby. Help or hindrance? the travel, energy and carbon impacts of highly automated vehicles. *Transportation Research Part A: Policy and Practice*, 86:1–18, 2016.

[267] E. Walraven, M. T. Spaan, and B. Bakker. Traffic flow optimization: a reinforcement learning approach. *Engineering Applications of Artificial Intelligence*, 52:203 – 212, 2016.

[268] N. Wan, A. Vahidi, and A. Luckow. Optimal speed advisory for connected vehicles in arterial roads and the impact on mixed traffic. *Transportation Research Part C: Emerging Technologies*, 69:548–563, 2016.

[269] N. Wan, C. Zhang, and A. Vahidi. Probabilistic anticipation and control in autonomous car following. *IEEE Transactions on Control Systems Technology*, 27(1):30–38, 2017.

[270] D. Wang, X. Ma, D. Ma, and S. Jin. A novel speed–density relationship model based on the energy conservation concept. *IEEE Transactions on Intelligent Transportation Systems*, 18(5):1179–1189, 2016.

[271] M. Wang, S. van Maarseveen, R. Happee, O. Tool, and B. van Arem. Benefits and risks of truck platooning on freeway operations near entrance ramp. *Transportation Research Record*, 2673(8):588–602, 2019.

[272] Y. Wang, W. Y. Szeto, K. Han, and T. L. Friesz. Dynamic traffic assignment: A review of the methodological advances for environmentally sustainable road transportation applications. *Transportation Research Part B: Methodological*, 111:370–394, 2018.

[273] Z. Wang, G. Wu, P. Hao, K. Boriboonsomsin, and M. Barth. Developing a platoon-wide eco-cooperative adaptive cruise control (cacc) system. In *2017 IEEE Intelligent Vehicles Symposium (IV)*, pages 1256–1261. IEEE, 2017.

[274] G. B. Whitham. *Linear and nonlinear waves*. John Wiley & Sons, 1974.

[275] R. Wiedemann. Simulation des strassenverkehrsflusses. 1974.

[276] S. Wollenstein-Betech, C. Muise, C. G. Cassandras, I. C. Paschalidis, and Y. Khazaeni. Explainability of intelligent transportation systems using knowledge compilation: a traffic light controller case. In *2020 IEEE 23rd International Conference on Intelligent Transportation Systems (ITSC)*, pages 1–6. IEEE, 2020.

[277] World Health Organization. Ambient air pollution: a global assessment of exposure and burden of disease, 2016.

[278] G. Wu, K. Boriboonsomsin, and M. J. Barth. Development and evaluation of an intelligent energy-management strategy for plug-in hybrid electric vehicles. *IEEE Trans. Intelligent Transportation Systems*, 15(3):1091–1100, 2014.

[279] Y. Wu, M. Abdel-Aty, L. Wang, and M. S. Rahman. Improving flow and safety in low visibility conditions by applying connected vehicles and variable speed limits technologies. Technical report, 2019.

[280] H. Xia, K. Boriboonsomsin, and M. Barth. Dynamic eco-driving for signalized arterial corridors and its indirect network-wide energy/emissions benefits. *Journal of Intelligent Transportation Systems*, 17(1):31–41, 2013.

[281] B. Xie, M. Xu, J. Härri, and Y. Chen. A traffic light extension to cell transmission model for estimating urban traffic jam. In *PIMRC*, pages 2566–2570, 2013.

[282] B. Xu, X. J. Ban, Y. Bian, W. Li, J. Wang, S. E. Li, and K. Li. Cooperative method of traffic signal optimization and speed control of connected vehicles at isolated intersections. *IEEE Transactions on Intelligent Transportation Systems*, 20(4):1390–1403, 2018.

[283] T. D. Xu, L. J. Sun, Z. R. Peng, and Y. Hao. Integrated route guidance and ramp metering consistent with drivers' en-route diversion behaviour. *IET Intelligent Transport Systems*, 5(4):267–276, 2011.

[284] Z. Xu, Y. Kang, and W. Lv. Analysis and prediction of vehicle exhaust emission using ann. In *2017 36th Chinese Control Conference (CCC)*, pages 4029–4033. IEEE, 2017.

[285] L. Yang, X. Hu, and L. Fang. Carbon emissions tax policy of urban road traffic and its application in panjin, china. *PloS one*, 13(5), 2018.

[286] I. Yperman. The link transmission model for dynamic network loading. 2007.

[287] H. Yu, J. Kong, Y. Ren, and C. Yin. On the urban link fundamental diagram based on velocity-weighted flow and queue length. *Symmetry*, 12(11):1852, 2020.

[288] S. Zegeye, B. De Schutter, J. Hellendoorn, E. Breunesse, and A. Hegyi. Integrated macroscopic traffic flow, emission, and fuel consumption model for control purposes. *Transportation Research Part C: Emerging Technologies*, 31:158–171, 2013.

[289] S. K. Zegeye. Model-based traffic control for sustainable mobility. 2011.

[290] S. K. Zegeye, B. De Schutter, J. Hellendoorn, E. A. Breunesse, and A. Hegyi. A predictive traffic controller for sustainable mobility using parameterized control policies. *IEEE Transactions on Intelligent Transportation Systems*, 13(3):1420–1429, 2012.

[291] W. Zeng, T. Miwa, and T. Morikawa. Prediction of vehicle co2 emission and its application to eco-routing navigation. *Transportation Research Part C: Emerging Technologies*, 68:194–214, 2016.

[292] H. M. Zhang. A non-equilibrium traffic model devoid of gas-like behavior. *Transportation Research Part B: Methodological*, 36(3):275–290, 2002.

[293] L. Zhang, F. Chen, X. Ma, and X. Pan. Fuel economy in truck platooning: A literature overview and directions for future research. *Journal of Advanced Transportation*, 2020, 2020.

[294] Y. Zhang and C. G. Cassandras. The penetration effect of connected automated vehicles in urban traffic: an energy impact study. In *2018 IEEE Conference on Control Technology and Applications (CCTA)*, pages 620–625. IEEE, 2018.

[295] X. Zhao, W. Xu, J. Ma, H. Li, Y. Chen, and J. Rong. Effects of connected vehicle-based variable speed limit under different foggy conditions based on simulated driving. *Accident Analysis & Prevention*, 128:206–216, 2019.

[296] F. Zhu and S. V. Ukkusuri. Accounting for dynamic speed limit control in a stochastic traffic environment: A reinforcement learning approach. *Transportation Research Part C: Emerging Technologies*, 41:30 – 47, 2014.

[297] J. Zhu, C. Ngo, and A. Sciarretta. Real-time optimal eco-driving for hybrid-electric vehicles. *IFAC-PapersOnLine*, 52(5):562 – 567, 2019. 9th IFAC Symposium on Advances in Automotive Control AAC 2019.

[298] M. Zhu, X. Wang, A. Tarko, et al. Modeling car-following behavior on urban expressways in shanghai: A naturalistic driving study. *Transportation research part C: emerging technologies*, 93:425–445, 2018.

[299] Y. Zu, C. Liu, R. Dai, A. Sharma, and J. Dong. Real-time energy-efficient traffic control via convex optimization. *Transportation Research Part C: Emerging Technologies*, 92:119 – 136, 2018.